Titre: Title:	Modelling of Wind Energy Converters for Slow and Fast Transients
Auteur: Author:	Luis Daniel Bellomo
Date:	2011
Type:	Mémoire ou thèse / Dissertation or Thesis
Référence: Citation:	Bellomo, L. D. (2011). Modelling of Wind Energy Converters for Slow and Fast Transients [Thèse de doctorat, École Polytechnique de Montréal]. PolyPublie. https://publications.polymtl.ca/574/

UNIVERSITÉ DE MONTRÉAL

MODELLING OF WIND ENERGY CONVERTERS FOR SLOW AND FAST TRANSIENTS

LUIS DANIEL BELLOMO
DÉPARTEMENT DE GÉNIE ÉLECTRIQUE
ÉCOLE POLYTECHNIQUE DE MONTRÉAL

THÈSE PRÉSENTÉE EN VUE DE L'OBTENTION
DU DIPLÔME DE PHILOSOPHIAE DOCTOR (Ph.D.)
(GÉNIE ÉLECTRIQUE)

AVRIL 2011

UNIVERSITÉ DE MONTÉAL
ÉCOLE POLYTECHNIQUE DE MONTRÉAL

Cette thèse intitulée

MODELLING OF WIND ENERGY CONVERTERS FOR SLOW AND FAST TRANSIENTS

présentée par: BELLOMO Luis Daniel
en vue de l'obtention du diplôme de : Philosophiae Doctor
a été dûment accepté par le jury d'examen constitué de :

M. KOCAR Ilhan, Ph.D., président
M. MAHSEREDJIAN Jean, Ph.D., membre et directeur de recherche
M. OLIVIER Guy, Ph.D., membre et codirecteur de recherche
M. SAAD Omar, M.Sc.A., membre
M.GAGNON Richard, Ph.D., membre

ACKNOWLEDGMENTS

I wish to thank my director, Professor Jean Mahseredjian for his constant human and technical supports. I have also appreciated the various presentations on this project in different seminars organized by Jean.

I also wish to thank to my co-director, Professor Guy Olivier and every professor at École Polytechnique de Montréal for their teachings, help, hospitality and friendship.

I am dedicating this work to my parents, Antonio and Nuncia, my wife Adriana and my daughter Malena.

RÉSUMÉ

Pour améliorer la précision des études de l'impact de la génération éolienne sur les réseaux électriques, il est nécessaire développer des outils de simulation plus rapides et précis et utiliser des modèles de plus en plus sophistiqués. Les simulations sont généralement et traditionnellement effectuées de façon indépendante pour les phénomènes transitoires rapides et lents. Pour les transitoires lents, l'approche classique est basée sur l'utilisation de méthodes de solution simplifiées avec des approximations. Ces méthodes se classent dans la catégorie des transitoires électromécaniques. Les modèles plus sophistiqués sont basés sur la simulation détaillée de tous les composants d'une éolienne. Ces modèles appartiennent à la catégorie des transitoires électromagnétiques (EMT pour Electromagnetic Transients). Il est cependant très compliqué d'effectuer des simulations détaillées pour des périodes de simulation longues à cause des restrictions de temps de calcul. Cela est particulièrement vrai dans les grandes simulations d'intégration des éoliennes au réseau électrique. L'objectif et l'innovation de cette thèse est la simulation d'éoliennes avec une méthode de type EMT et un logiciel de type EMTP (Electromagnetic Transients Program) en appliquant des techniques de modélisation rapides et la combinaison avec des modèles détaillés. Ainsi les phénomènes lents et rapides peuvent être simulés dans un seul environnement de type EMTP. Un second objectif est la contribution de plusieurs modèles d'éoliennes pour les phénomènes rapides et lents.

Cette thèse présente trois types de modèles, deux modèles à valeur moyenne et un modèle détaillé, dans le même environnement du logiciel EMTP-RV et en utilisant les mêmes méthodes numériques. Le développement des modèles de type détaillé sert principalement de référence pour la validation et la démonstration de précision pour les modèles à valeur moyenne.

Les modèles à valeur moyenne sont à deux niveaux de précision. Au premier niveau l'objectif est d'obtenir des résultats suffisamment précis pour des études sur les

transitoires électromécaniques et au deuxième niveau les modèles servent à augmenter la précision et éliminer des limitations.

Les techniques de modélisation présentées sont validées en utilisant des techniques de simulation comparatives basées sur les logiciels EMTP-RV et PSS/E. PSS/E est utilisé pour la simulation des phénomènes transitoires électromécaniques seulement. La thèse contribue aussi ce type de modèle avec des analyses comparatives et des explications sur les limitations.

De façon générale le développement de modèles d'éoliennes est une tâche complexe et une contribution importante de cette thèse est l'élaboration de plusieurs types de modèles complets avec des améliorations au niveau des techniques d'initialisation, des composants des modèles, des contrôles, des méthodes d'agrégation et des aspects pratiques d'intégration. Le traitement dans deux environnements (PSS/E et EMTP-RV) différents constitue un travail complexe. Les modèles serviront aussi à des travaux de recherche futurs sur l'intégration des parcs d'éoliennes dans les réseaux électriques et sur les systèmes contrôle-commande.

Les modèles développés dans cette thèse servent à étudier des phénomènes transitoires de réseau sur une large gamme de fréquences pour des problèmes d'intégration des éoliennes dans les réseaux: surtensions, défauts, contrôle de fréquence, îlotage et qualité d'onde.

ABSTRACT

To improve the accuracy of wind generator grid impact studies, it is needed to develop faster and sophisticated models using various simulation tools. The simulations are usually carried out independently for fast and slow transients. Traditional slow transient analysis methods are based on simplified solution methods with various approximations. These methods fall into the category of electromechanical transients. More sophisticated models are based on the detailed simulation of all wind generator components. Such models fall into the category of electromagnetic transients (EMT). It is, however, complicated to run detailed simulations for long simulation periods due to computer time restrictions. This is especially true in large grid integration simulations. The objective and innovation of this thesis is the simulation of wind generators in EMTP-type (Electromagnetic Transients Program) programs using faster modeling techniques with small integration time-steps and the capability to combine with detailed models. This way fast and slow transients are solved in the same environment and with acceptable computational speed. Another objective of this thesis is the contribution of wind generator models for wind farm integration studies.

This thesis presents the integration of three types of models, two mean value type models and one detailed EMTP-type (Electromagnetic Transients Program type), in the same EMTP-RV (software of EMTP-type) environment and with the same numerical methods. The mean value type models are distinguished by their precision levels. At the first level the model is demonstrated to contribute to significant reduction of computing time while limiting the loss of accuracy. At the second level the model provides precision improvement over the first level while still limiting computational efforts.

The presented modeling techniques are validated using comparative simulation techniques based on EMTP-RV and PSS/E. PSS/E is only used for the simulation of electromechanical transients.

Since the development of wind generator models is a complex task on its own, this thesis also contributes by developing various comprehensive models with appropriate

improvements in several aspects, such as initialization techniques, aggregation, controls, model components and the complicated establishment of validation and comparison of models in two different environments, namely PSS/E and EMTP-RV. The contributed models will be also used in future research works related to wind generation integration into power systems and related controls.

The contributed models are of wideband type and are used for studying power system integration problems, such as overvoltags, undervoltages, frequency deviation, power quality and islanding.

Table of Contents

List of figures

List of tables

CHAPTER 1. INTRODUCTION

1.1 Overview

The study of wind generators is performed for various purposes in power systems. When wind parks are integrated into a power grid it is required to perform various studies such as network stability, protection, short-circuit, overvoltage and undervoltage conditions and power quality analysis. In addition it may be necessary to study lightning transients, switching transients and temporary overvoltage conditions.

Under normal operation conditions, the current and voltage waveforms of a wind generator are nearly sinusoidal and the system is in steady-state. The complete network and wind park interconnected system may be however, submitted to various internal and external perturbations. Internal perturbations are commonly changes in settings and switching of various configuration and control devices. External perturbations are typically faults on transmission lines or cables and lightning effects. In wind parks external perturbations are also caused by changes in wind conditions and related reactions of the wind turbine. Transients can be generated in the wind park or in the power grid. A new or a previously existing steady-state may be reached after system transients have been damped out or eliminated by protection devices. In some cases the action of protection devices may cause topological changes and/or setting changes. Such changes may result into new operating conditions or complete isolation of a wind park.

The commonly used tools for studying wind parks and power grids fall into two categories: electromechanical transients and electromagnetic transients.

1.2 Electromechanical transients

Electromechanical transients are studied for assessing the capability of a power system to reach stable steady-state after a disturbance. Such studies are also called power system stability studies (stability-type) and require the modeling of various

control systems including machine exciters, frequency controls and stabilizers. Control systems are usually represented through block-diagrams.

The study of electromechanical transients is conducted for lower frequency transients, typically oscillations below 10 Hz. Due to the lower frequency range, such transients can be studied with simplified models. A widely used software package in the industry is PSS/E [1]. This software is used in this thesis. The basic assumptions in such a package are: balanced network conditions, absence of harmonics and absence of nonlinearities in power devices. The balanced network assumptions allow modeling the grid using only its positive sequence representation. The control systems are represented for both power grid synchronous machines and wind generators. Due to the slower transient assumptions many details in the modeling of devices, such as synchronous machines or wind generator asynchronous machines are ignored or approximated. The simulation waveforms are computed in RMS quantities (phasors). The numerical integration time-step is typically close to 8 ms for a fundamental frequency of 60 Hz. The study interval (time scale) can go up to minutes.

Software packages, such as PSS/E are used to study the power system stability under various perturbations assuming nominal frequency phasors in the network. Such packages are also called stability-type packages.

Before starting any dynamic (transient) analysis, it is required to compute the steady-state operating conditions of the network. This is done by setting power and voltage constraints on all grid busses including the bus at the interconnection point with the wind park. The wind park is set to control power (active and reactive) and voltage. Then a load-flow solution is performed for finding all phasors in the complete network. In PSS/E the dynamic simulation starts from the load-flow solution after initializing all state variables.

1.3 Electromagnetic transients

The electromagnetic transients are of wideband nature and require detailed modeling techniques. The objective is to study wind generators and power grids with all

possible details. Electromagnetic transients are studied with EMTP-type (electromagnetic transients program) software packages [2][3][4]. The software package used in this thesis is EMTP-RV [2][3]. Such software allows to study:

- unbalanced multiphase networks
- harmonics
- nonlinear models
- power electronics
- control systems (block-diagram approach)

In fact there are no assumptions on the studied system conditions and often the challenge is the gathering of data. The wind generator or wind energy converter (WEC) is modeled using the actual representation of its power electronics based converters. All nonlinearities, such as transformer saturation and surge arresters can be represented. It is a circuit level simulation approach.

In EMTP-type methods it is possible to study both slow and fast transients. The waveforms are computed in actual quantities imitating oscilloscope measurements. The typical numerical integration time-steps are in the order of microseconds. It is usually not possible to exceed $250\,\mu s$ without significant loss of accuracy. In the case of power electronics and due to the more stringent precision requirements, it is necessary to use much smaller time-steps, such as $20\,\mu s$ or even below $10\,\mu s$. The time scales of studies do not usually exceed a few seconds (up to 10 s, for example).

In addition to small time-steps and the time-domain solution of all equations, packages such as EMTP-RV apply an iterative process for solving nonlinear equations due to nonlinear components, such as surge arresters and transformer saturation branches. Although fast convergence methods are employed, it is required to iterate from two to three times per time-point solution, which imposes further burdens on the computational speed of a simulation. The iterative procedure is required for accurate and simultaneous solutions of nonlinear component equations with the linear network equations.

EMTP-type studies are also started from a steady-state solution. The main program blocks of EMT-RV are shown in Figure 1. After grabbing the network netlist from the graphical user interface (GUI), EMTP-RV must first perform a load-flow solution. This is a nonlinear problem. The provided constraints are in the form of equations, such as active power equality (control) and voltage equality (control). Once the load-flow solution converges, it is needed to perform a steady-state solution in which all constraints are replaced by lumped circuit equivalents. This process is needed for initializing the following time-domain solution in which all network models are given electrical circuit equivalents or equivalent functions. The steady-state phasor solution is used to compute the time-domain solution at the time-point t=0. It is also used to initialize the numerical integration technique.

In EMTP-RV it is possible to initialize complex systems and start the time-domain simulation in quasi perfect steady-state. EMTP-RV also provides means for initializing control systems.

The precise initialization of the simulated network is of major importance. If the studied network is not initialized it will start from 0-state and the time-domain steady-state solution will be reached only after the decay of all transients. In other words the complete system will first respond with its natural frequencies. In some cases it is possible to reach undesirable steady-state conditions. Moreover, the lack of initialization procedures has a tremendous impact on the computing time of the study.

There is however, a major difficulty with the automatic initialization of power electronics components. This is the case in wind generators with power electronics converters. Since the switching patterns are not easy to predict and since the overall system becomes nonlinear, in most cases the best approach is to initialize only the linear network and start the power electronics based components from black. The waste in computing time can be currently minimized, but not eliminated. Some specific methods must be researched for the case of wind generators.

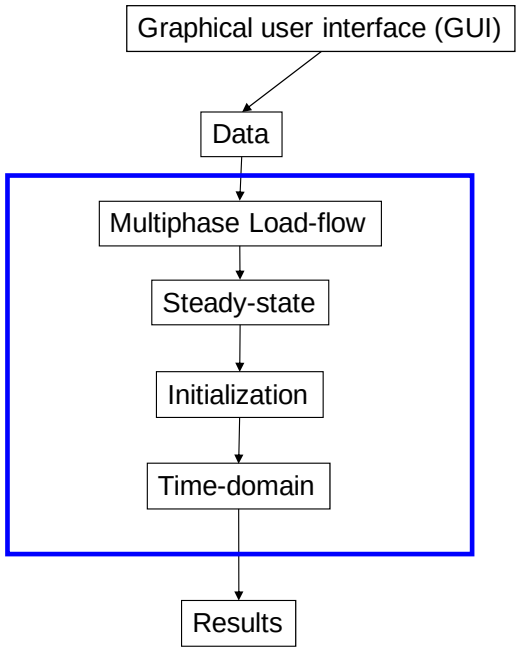

Figure 1: Main solution modules of EMTP-RV

Although it is now possible to use EMTP-RV [4] for very accurate stability type studies, its computer requirements are often unaffordable specially when performing a large number of scenario analysis. That is why stability-type packages are still commonly used for assessing wind park interconnection problems in power grids. Usually power system utilities conduct EMTP-type studies for verification purposes and for reduced time scales.

1.4 Differences between stability-type and EMTP-type simulators

Stability-type methods can be mainly used to evaluate the performance of wind parks (several WECs) using an aggregation model of a number of WECs, for slow transients or slow dynamics. The objective is to evaluate the performance of a wind park connected to the grid for electromechanical transients. These are oscillations below 10 Hz. The network equations are solved in steady-state using phasors at the fundamental frequency. The synchronous machine equations and the WEC equations are usually solved in time-domain using block-diagrams.

The significant drawback in stability-type methods is the reduced precision. The case of wind generators is particularly more complex and encounters several limitations when using simplified modeling approaches. This is mainly due to the presence of power electronics based converters and related controls. The larger time-step usage causes errors in the determination of some control parameters and the simplified representation of the converter remains inadequate for imitating its transient behaviour.

As explained earlier, stability-type methods (PSS/E) are based on the positive-sequence assumption, which means that the network is assumed to be balanced. This is not necessarily correct since in addition to unbalanced conditions due to untransposed lines, there could be unbalanced load conditions. Another important issue is that nonlinear power devices, such as transformer saturations and surge arresters, cannot be solved in stability type methods. Arrester models, for example, are important for the correct evaluation of overvoltages and related protection systems.

On the other hand, the main limitations with EMTP-type methods are usually lack of data for precise component models and computing time. The reduction of computing time in EMTP-type methods is an important research topic.

To conclude, it can be said that ultimately speaking, all simulations must be conducted with EMTP-type methods for increased precision and studies for a wideband of frequencies within the same environment and in a unified GUI and data approach. This thesis proposes solutions towards this direction.

1.5 Real-time simulation methods

In addition to offline EMTP-type methods, there is a family of methods capable to perform real-time simulations [5]. This means that the assembled network equations are solved synchronously with the real-time clock. If an event is observed during a given real-time interval, then it is simulated using the same computer time. Moreover, intermediate events or waveform samples are also occurring in synchronism with an external real-time clock. This means that such real-time simulators can be interfaced with external physical control systems and even power devices. The most important

current application is the interfacing with control devices for testing WEC controls in network conditions. This is an ultimate validation tool for the real control blocks of the WEC.

It is obvious that real-time simulation methods offer dramatic advantages in computational speed. They also offer the possibility to perform parametric simulations for sensitivity analysis. The real-time computation process, however, currently imposes significant restrictions on the mathematical solution process. Such restrictions result in reduced precision. The current drawbacks as compared to offline EMTP-type methods are: one time-step delay based solution for nonlinear components, simplifications in models to accommodate real-time performance and availability on commonly used computer environments with commonly used operating systems. The setup time of real-time simulators is also usually more complicated.

It is understandable that real-time methods will continue to improve in precision and performance and the gap between offline and real-time methods will be reduced in the upcoming years. This is accompanied by increased needs in network studies. In some cases the growth of simulation and analysis needs is faster than the improvement pace in simulation tools.

The methods presented in this thesis are for off-line simulation tools, but they also have an important impact on real-time simulation methods. This is explained by the fact that due to similarities in solution methods, many improvements in offline methods can be readily transposed into real-time methods.

1.6 Basic concepts of a wind turbine

The wind turbine converts the kinetic energy of wind to mechanical power applied to the generator. The power extracted from a wind turbine may be represented by the well known equation:

$$P_w = \frac{\rho}{2} \pi r^2 V_w^3 C_p \tag{1.1}$$

In this equation:

P_w is extracted wind power (W)

ρ is the air density (kg/m^3)

r is the blade radius (m)

V_w is the wind speed (m/s)

C_p is the performance coefficient (pu)

The performance coefficient C_p is a function of tip-speed ratio and blade pitch angle. The blade pitch angle is a controlled variable. The tip-speed ration λ is given by:

$$\lambda = \frac{r\,\Omega_{turbine}}{V_w} \tag{1.2}$$

where λ is in pu and $\Omega_{turbine}$ is the turbine rotational speed in rad/s.

The only parameter that can be controlled is the pitch angle and consequently C_p. The performance coefficient curves may be represented as a function of the wind speed when the rotational speed and the pitch angle are kept constant. In this condition, from the peak of C_p, the curves decrease when the tip-speed ratio increases (see equation (1.2) and Figure 2).

Wind turbines are designed to support winds between 10 to 15.0 m/s with a power shutdown when the wind speed exceeds 25 m/s.

Equation (1.1) allows calculating the mechanical torque submitted to the wind generator rotating machine. The remaining sophistication is related to the machine controls and application of power electronics. The various wind generator technologies are discussed in the following sections.

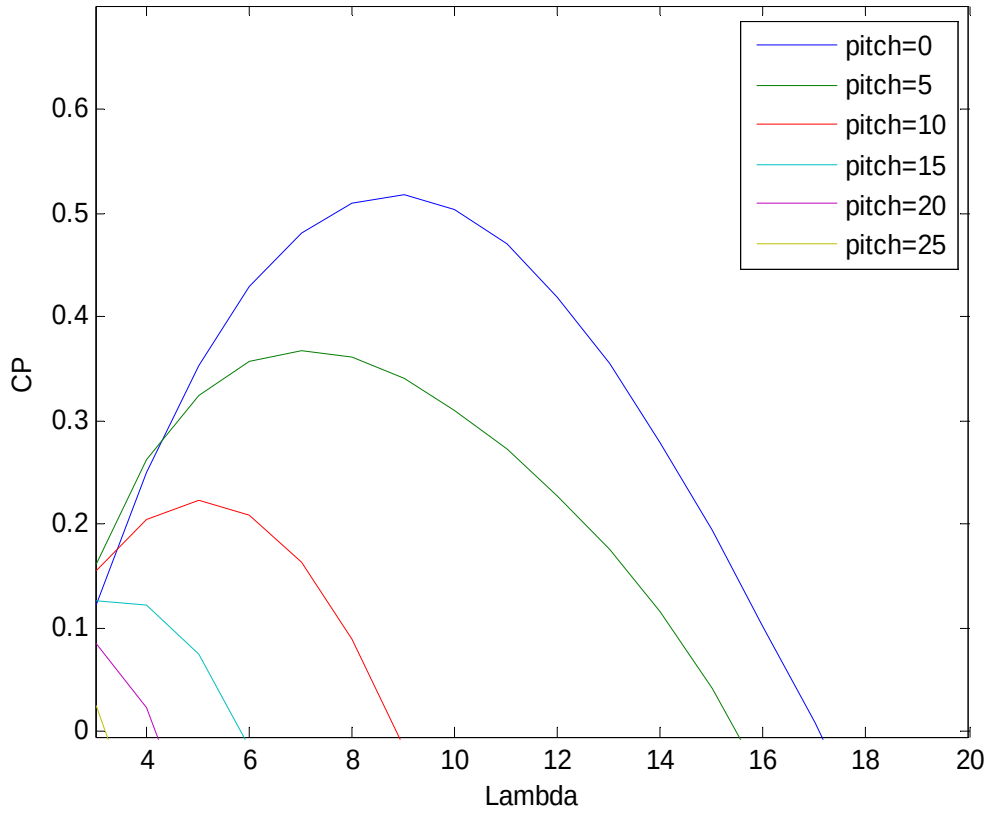

Figure 2 : C_p **coefficient as a function of** λ **and pitch angle in degrees**

1.7 Wind generator technologies

There are currently three main types of WEC technologies:

- Constant speed turbines based on conventional induction generator
- Variables speed turbines: doubly-fed induction generator (DFIG)
- Gearless turbines: slow speed conventional generator connected to the grid by a back-to-back frequency converter (full converter WEC, FCG)

The permanent magnet generator, which requires no excitation, is usually used instead of the conventional synchronous generator in the third type of WEC.

1.7.1 Conventional induction generator

In this case from a mechanical stand point the machine operates at constant speed. In this way, the asynchronous generator must be considered as a system that provides power at constant fixed speed. The overall topology is shown in Figure 3. A transformer is used to connect to the grid.

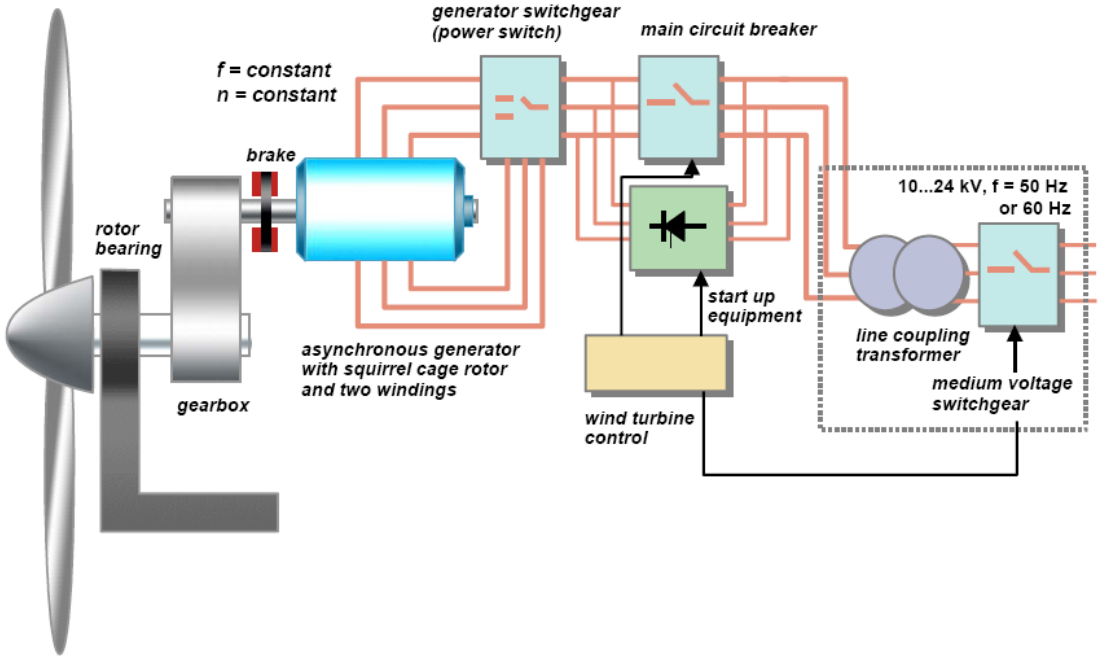

Figure 3 : Conventional induction generator

A soft starter may be used with the objective to minimise the voltage impact during the machine startup. Once the unit is connected to the grid it runs as a super synchronous induction generator. Since the frequency applied to the stator is almost constant due to the grid frequency, the created magnetic flux rotates at constant speed. The turbine speed is not always following the wind speed and thus it is not possible to extract the maximum wind power. In some constant speed generator applications, the stator has two separate windings with different number of poles. At high wind speeds it is possible to use the winding with the lower number of poles. At lower wind speeds the winding with the higher number of poles is switched on for the lowers synchronous speed. This scheme is for optimizing the extracted power from the wind.

During its operation the induction generator (as the induction motor) absorbs reactive power from the system. The reactive power sustains the rotating magnetic field in the air gap between the rotor and the stator. Utilities request manufacturers to provide shunt compensation to keep the power factor close to unity.

In wind farms based on conventional induction generators connected to the distribution grid, a common practice is to disconnect the generators from the grid when a fault occurs. This practice was used due to the fact that if the machine is not disconnected after a fault, the mechanical torque applied during the fault condition may exceed the pullout torque and become unstable.

1.7.2 Doubly fed induction generator (DFIG)

DFIG is the more common variable speed wind turbine technology available today (see Figure 4.) The principle of the DFIG is that rotor windings are connected to the grid via slip rings and a back-to-back voltage source converter that controls both the rotor and the grid currents. A transformer is used to connect to the grid. The power captured by the wind turbine is converted into electrical power by the DFIG and transmitted to the grid through the stator and rotor windings.

The back-to-back converter is divided into two components: the rotor-side converter and the grid-side converter. Both converters are voltage source converters using forced commutated power electronics devices (IGBTs) to synthesize an AC voltage from a DC voltage source represented by a capacitor.

The back-to-back converter is a bi-directional frequency converter. The grid-side converter works at the grid frequency while the rotor-side converter can be operated at different frequencies, depending on the speed of the blades.

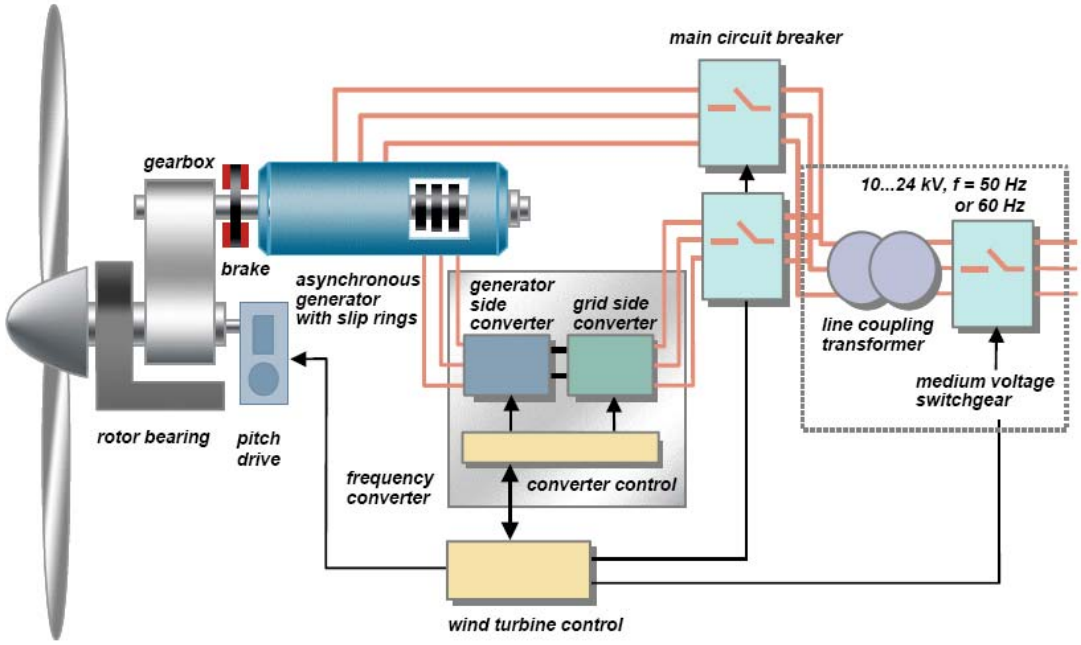

Figure 4 : Doubly fed induction generator (DFIG)

The output power of the machine is a combination of powers circulating from the rotor and the stator into the grid. In steady-state conditions the power portions in stator and rotor circuits depend on the slip value *s*. The slip can be positive or negative. At sub-synchronous speed the slip is positive. The power is circulating from the converter into the rotor. At super-synchronous speed the slip *s* is negative and the power is circulating from the rotor into the converter and into the grid. The super-synchronous speed is achieved by applying a negative sequence voltage in the rotor. This demonstrates that the back-to-back converter is capable of operating with power circulating in both directions. At synchronous speed there is no power exchange through the converter.

The basic power equilibrium equations with losses neglected are given by:

$$P_{er} = s\,P_r \tag{1.3}$$

$$P_m = (1-s)\,P_r \tag{1.4}$$

where P_{er} is the power circulating in the rotor (its direction depends on the slip sign) and P_m is the power from the wind (turbine). The power circulating through the air-gap is given by P_r. This power is added to the power circulating from the converter for negative slip and is reduced by the power entering into the converter for positive slip.

Both rotor-side and grid-side converters have the capability of generating or absorbing reactive power and can be used to control the reactive power or the voltage at the grid terminals. Most designs tend to supply reactive power to the system through the machine stator by effectively changing the d-axis excitation on the rotor.

A vector control strategy is used, where the rotor current is split into d-axis (flux producing) and q-axis (torque producing) components. Each component is then controlled separately. The d-axis component is controlled in order to regulate the machine power factor (effectively controlling the reactive power output of the machine). The q-axis component is controlled in order to keep the electrical torque of the machine constant.

1.7.2.1 Low Voltage Ride Through (LVRT)

Generally speaking, 'fault ride through' (FRT) or 'low voltage ride through' (LVRT) are generic terms pertaining to the various different technologies and methods used by manufacturers to ensure continued operation or longest connectivity of WECs during low voltage periods in the terminal voltage. Such low voltages are mostly due to fault conditions.

Most wind turbine manufacturers now offer a low voltage ride through system. This is achieved by a combination of modified blade pitch control algorithms that help to remove the mechanical power after a fault. An uninterruptible (UPS) power supply is used at the turbine to keep the control systems running during the fault. In addition, reactive dynamic power sources may be required to provide voltage support upon fault clearing to ensure proper voltage recovery.

The following common techniques are applied to ensure FRT/LVRT:

- Switching to modified control algorithms (power to speed control, APC)

- Immediate blade pitching (e.g. stall control)
- Use of converters to provide reactive power support (power-factor, voltage control)
- Coordination with crowbar protection
- Sacrificing real power in favour of reactive power to support the network

1.7.2.2 Crowbar protection

During a heavy fault, the DFIG current contribution will have to origin from the stator, directly to the grid, and from the rotor, through the converter. As a consequence of low voltages at machine terminals during a fault condition, the stator-side converter is limited in its ability to pass power to the grid. Then, the excess energy goes into the charging of the DC bus capacitor and thus the DC bus voltage rises rapidly. The crowbar protection is designed for this phenomenon. When the DC bus voltage exceeds a prescribed limit, the protection trips to short-circuit the capacitor and protect the converter power electronics components. The unit becomes disconnected from the system.

1.7.3 Full converter generator (FCG)

The concept in this case is to generate power using a conventional generator with DC field winding as shown in Figure 5. This approach has two basic advantages.

It allows for a gearless design. This avoids the mechanical complexity of gear and hydraulics. The generator can be directly coupled with the turbine and may spin at whatever rotational velocity as required. The frequency of the electrical output of the generator is then converted by a back-to-back frequency converter to the grid frequency (50 or 60 Hz). However, the gearless design typically means that the generator has a significantly larger diameter to accommodate a large number of pole pairs (84 poles, for example) and thus requires a more spacious nacelle (cover housing).

Through the use of a frequency converter the full electric output of the generator can be converted from a wide range of frequencies to the grid frequency. This means

that the wind turbine generator may operate at a wide range of speeds, thus once again providing the benefits of a variable speed drive unit. In addition, with the use of a voltage-source converter the grid side converter can independently control real and reactive powers. In this way the electrical grid and the generator are decoupled.

In this type of WEC there is greater flexibility for LVRT control, voltage regulation and reactive power control.

To achieve LVRT, the line side converter (or inverter) can stop gating the IGBTs if the voltage falls to excessively low levels and be essentially on stand-by to re-start once the fault clears. In addition, since the generator does not directly see the low network voltage during such an event, there are no important transients in rotor or stator currents produced in the machine. Voltage regulation is easily achieved with a voltage source converter through the control of the relative phase and magnitude of the voltage phasor produced by the voltage source converter as compared to the grid voltage phasor. This concept is not different from the one in a STATCOM and voltage source HVDC system.

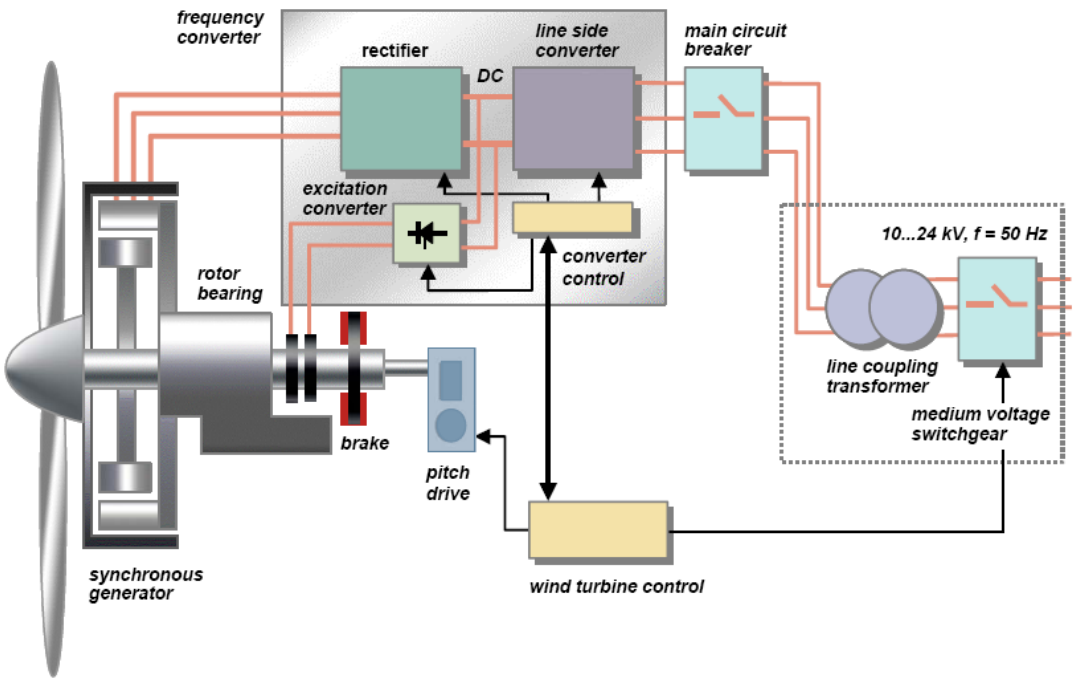

Figure 5: Full converter with conventional generator

1.7.4 Comparisons of WEC designs

The following criteria are applied to compare WEC designs and performance:

- Harmonic pollution
- Flicker level
- Gearbox stress
- LVRT controls
- Reactive power capacity

Considering that harmonic pollution is an important factor in power quality, it is observed that the conventional induction generator is the best for this criterion. It does not use power electronics and thus does not create harmonic pollution. As for the DFIG, its converter is only 1/3 of the rated power and its harmonic pollution is limited. The full converter uses a converter dimensioned to the rated power and consequently generates the highest harmonic pollution level.

For the flicker criterion, the conventional induction generator has the worst performance due to the fact that it has a system of fixed speed and each change in the wind speed will translate into a change in the turbine torque and the generator output. In the case of the DFIG, it is capable of applying current control to maintain a constant electrical torque. Rapid fluctuations in mechanical power can be temporarily 'stored' as kinetic energy. In the full converter generator, there is a decoupling condition between the converter line side and generator side resulting into a neglected flicker level.

The gearbox stress criterion disadvantages the conventional induction generator. Due to the fixed speed, each change in the wind speed will translate into a change in the turbine torque. Sudden changes in torque require a more robust drive train. The DFIG is capable of reduced mechanical stress due to its pitch control. The full converter is gearless.

When considering the LVRT criterion, the conventional induction generator is the worst in this field due to the fact that it basically trips after a fault because of reduced electrical power. This results in the turbine speeding up. Thus if the turbine is not disconnected after a certain time it may exceed its pullout torque and become unstable.

Therefore a under voltage protection is installed to disconnected the unit from the system during low voltage conditions.

The DFIG uses a combination of modified blade pitch control algorithms and is capable to remove the mechanical power after a fault. It also uses an uninterruptible (UPS) power supply at the turbine to keep the control systems running during the fault. In the FCG, the strategy used to achieve LVRT is by controlling the line side converter. This converter can stop gating the IGBTs if the voltage falls to excessively low levels. This is a standby and restart approach once the fault clears. In addition, since the generator does not directly see the low network voltage, there are no large transient rotor or stator currents produced in the machine.

In the reactive power capacity criterion the conventional induction generator has the worst performance since it can only consume reactive power. The DFIG with its converter size being 1/3rd of the rated power can only achieve a fraction of the total rating of the machine in reactive power output. The full converter with a converter at rated power allows a complete control of the terminal voltage. It can also perform in the condition without wind, with zero active power.

Although the DFIG design is now widely used, it can be predicted that the full converter (FCG) approach may eventually become more popular since it is more attractive from the network point of view. The decoupling between machine and grid dynamics, and the elimination of the gearbox (when using machines of sufficient number of poles to be directly coupled to the turbine) make the argument for full converter topologies quite convincing. Particularly when one considers the maintenance and unavailability costs associated with gearbox repairs in the DFIG design.

1.8 Wind turbine generator modelling challenges

This section presents an overview on the most important WEC components to help to better understand the modelling challenges and the contributions in this thesis.

The WEC model can be considered as a set of blocks (components), each block contributes to the static and dynamic behaviour of the WEC connected to the grid. The

principal (high-level) blocks are presented in Figure 6. There are two distinct categories; the mechanical blocks and the electrical blocks.

The mechanical components include the wind speed model, turbine aerodynamics, turbine mechanical protection, turbine mechanical controls (pitch control) and shaft dynamic model. This is related to "Wind", "Aerodynamic Torque" and "Mechanical Control" blocks shown in Figure 6.

The group of electrical components (blocks) include the generator, the interface with the grid, the converter controls, protection devices, relays of under/over voltage, relays for under/over frequency and crowbar protection. In this presentation the power electronics based converter is included in the "Electrical Generator" block. The other functions are placed in "Grid Interface"

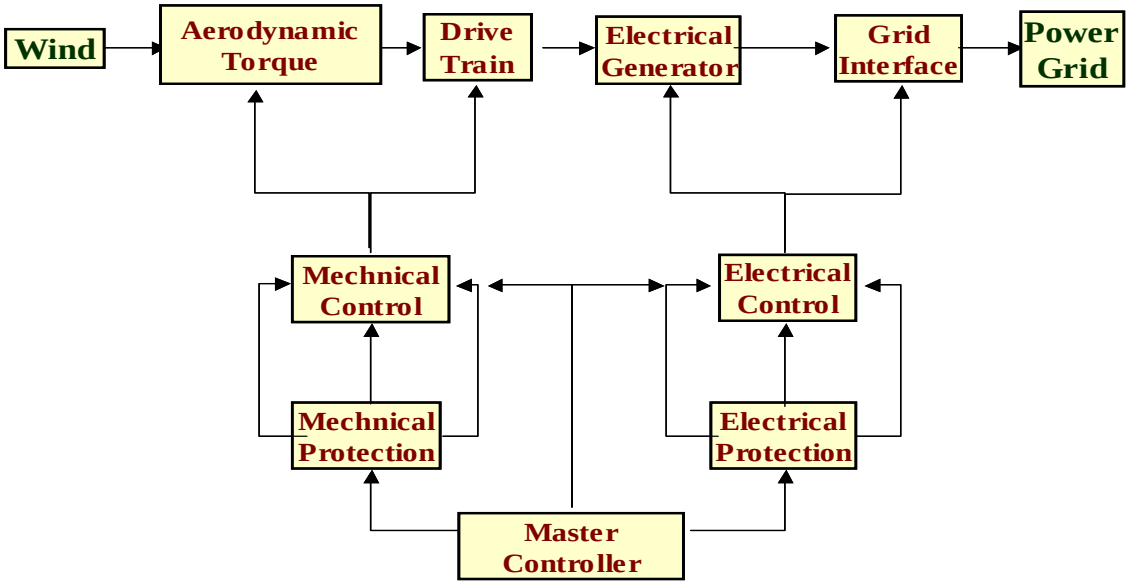

Figure 6 : Main blocks of the WEC model

The research presented in this thesis is related to component modeling, new modeling methods and the comparison between different modeling approaches and for different precision needs. Two types of WECs are considered: DFIG and FCG.

In the component modeling aspects, the works are in the initialization approaches and specific devices, such as the phase locked loop (PLL). In fact each component creates specific modeling problems especially when approximate (stability-type)

solution methods and models are used. Incorrect modeling of the PLL in PSS/E, for example, can cause phase measuring errors and cause significant errors (20%) in the active power computation.

In the field of the new modeling methods, this thesis proposes a mean-value type model based in an EMTP-type application, namely EMTP-RV. The advantages of such a model are in the capability to provide acceptable computational performance for longer simulation periods while maintaining acceptable precision. The more significant contribution is the capability to combine such models with detailed models for wind park performance studies.

An important part of the simulation of a WEC is the initialization process. In stability-type packages the time-domain simulation starts from a load-flow solution. The load-flow solution provides the initialization data for the dynamic model. As discussed earlier in this chapter, the complete simulated system initialization is of crucial importance. If the initialization process is not done correctly, state variables do not start from steady-state conditions. In such a case it is needed to simulate until all startup transients have decayed to zero and an equilibrium point is reached. This imposes wasted computing time and in some cases numerical instability conditions may occur or unacceptable operating conditions may be reached. The load-flow conditions constitute the basic operational requirements of the system in acceptable steady-state.

As explained earlier, in EMTP-type simulations the level of precision and details is much higher than in stability-type or simplified models. One of the most complicated problems is the initialization of power electronics devices. This is the case for the converter used in both DFIG and FCG designs. Although some techniques [6] have been published in the literature, such techniques remain theoretical and have not been generalized for arbitrary settings and topological conditions. Moreover, some techniques may require extensive computing times which make them unpractical. The method used in this thesis is based on a programmed-customized initialization of control systems for minimizing the effect of switching devices in the delaying of the steady-state. It also used load-flow transposition into steady-state solution.

In addition to problems related to the initialization of power electronics based devices, WEC studies require the proper initialization of power from given wind conditions. This allows the computation of the torque applied on the electrical generator. The Aerodynamic Torque bloc of Figure 6 needs the evaluation of the C_p matrix presented in a previous section of this Chapter. This poses some computational difficulties and precision issues.

The sophistication of modern networks and the need for optimization of installations and optimization of usage in energy resources, require more and more sophisticated studies. Sophistication implies precision. In this aspect the traditional usage of stability-type tools imposes many limitations. The EMTP-type simulation methods allow representing the actual electrical circuit of the WEC. In addition it is feasible to include mechanical representation: wind power development and control, wind effect representation and multimass representation of rotating parts.

The main drawback with EMTP-type solutions is the computational speed. The simulation time with large networks and numerous generators becomes unaffordable, 2 to 3 hours in some cases with typical time-steps below $20\,\mu s$. When the simulation interval is extended above 5 s, then the computing time increases further and in some situations it is necessary to wait 6 to 10 hours. This also depends on the size of the network and the number of WECs.

Wind parks can be simulated using aggregation techniques, but there are limits to the number of WECs in an aggregation. This is mainly due to problems in the scaling of the converter circuits. Also aggregation is less precise since several individual components, such as cables are not represented. There are also issues related to separate dispatching with connection point controls and more sophistication when studying wind impact.

Another issue with detailed simulations is related to the availability of data. Sophistication requires more information on the actual WEC design and controls. Such details are not necessarily available. Less data is needed in stability-type modeling.

The solution proposed in this thesis for solving the above problems is the development of a mean-value modeling approach in EMTP-type simulation methods, more specifically in the EMTP-RV environment. Mean value type models are tagged as MEVA (Mean Value) models. It will be demonstrated that MEVA models can be combined with detailed EMTP models in the same simulation. As detailed EMTP models, the MEVA modeling approach is also based on three-phase representation, but fast dynamics are neglected. There are similarities between MEVA modeling and stability-type models, but the MEVA model is more precise and has the significant advantage it its capability to be integrated into a detailed EMTP-type solution.

In a wide scale representation of a wind farm it may be necessary to model some parts with detailed EMTP models, while the WECs that are electrically far from the fault or perturbation location can be modeled using the MEVA approach. The combined simulation offers several advantages in computer timings and in modeling functions.

Hereinafter and for simplification purposes, the detailed EMTP models that are used for the ultimate precision will be tagged as DEMTP-type models.

In addition to the MEVA methodology proposed in this thesis, this thesis also presents another approach which is denoted hereinafter by Mean Value EMTP (MVEMTP). In this approach the commutation process of converters is replaced by controlled sources for representing an equivalent effect. This approach **[7][9]** is not completely new, but this thesis contributes new comparisons of results with the detailed DEMTP approach for practical wind generator models using identical control systems. A close match is achieved.

1.9 Methodology and deliverables

As a first step in this thesis it is required to develop functional WEC models. It is actually one of the contributions of this thesis. Such models were not readily available at the startup of this thesis. In fact WEC model development remains an ongoing research topic and encounters many complex challenges. Many contributions are required. The developed models in this thesis are based on generic technological information and data.

The models are capable of reproducing the typical behaviour of WECs under various simulation scenarios. Both individual models and wind parks models are considered. It is possible to apply aggregation techniques for the simulation of wind parks.

Two WEC technologies are considered: DFIG and FCG. Using two types of models, allows concluding on the generalization aspects of the proposed methods and models.

The PSS/E and EMTP-RV software packages are available at École Polytechnique. The development of models allows discovering the various limitations and performing comparisons. In addition, during this project, several research projects with wind generator manufacturers allowed gathering practical experience and learning the study requirements. It is however emphasized, that the presented models are generic and do not disclose any protected information and technology.

1.9.1 PSS/E models (stability-type)

The model developments are started with the stability-type approach using the PSS/E software package. This step allows establishing a basis for validating mean-value type models and also demonstrating the encountered difficulties. PSS/E is widely used in the industry for large scale power systems studies. Many utilities require the PSS/E model development for WECs connected to the grid. The network database is also often based on stability-type data or PSS/E data files. The data requirements for PSS/E studies are much less stringent than for EMTP-RV studies. In many cases it is not possible to obtain specific manufacturer details required in DEMTP-type models, whereas the number of specific information requirements is much less important in stability-type studies.

The PSS/E simulation results are used for both load-flow and dynamic studies (time-domain). The load-flow results are shown as phasors. It is needed to develop and implement specific functions for the initialization of dynamic studies. The time-domain results are provided in rms quantities with separate information on phasor angles.

It must be emphasized that the model design and implementation efforts in PSS/E are significantly different from EMTP-RV. In EMTP-RV the studied systems are mainly designed using readily available devices in a graphical user interface (GUI). Control system simulations are based on block diagrams also assembled using an interconnection of GUI blocks. It is also possible to enter user-defined models by typing equations or using primitive building functions available in libraries. In PSS/E the basic approach is the derivation and implementation of models. The simulation of control systems requires programming and compiler steps. Some pre-built components, such as rotating machine and exciter models, are available.

1.9.2 Mean value (MEVA) models

The next logical step towards an increased modeling precision is the development of mean value models (MEVA) for DFIG and FCG technologies. The innovation is in this new modeling approach and implementation in an EMTP-type solver. Although the MEVA modeling approach is inspired from the stability-type modeling, it is more precise due to its 3-phase representation and interaction with 3-phase circuits. It is also based on detailed waveform computations in time-domain. Moreover, it allows multi-time-frame (combined) simulations with DEMTP-type models.

MEVA models are compared to stability-type models and validated by DEMTP-type models. The contribution of MEVA models contributes an important milestone in this thesis.

1.9.3 Detailed EMTP-type models (DEMTP-type)

The detailed circuit-based approach uses the representation of converter circuits including IGBTs (insulated-gate bipolar transistor). It is based in the EMTP-RV software with a detailed 3-phase modeling of the surrounding grid network. Such modeling also allows including nonlinearities. Basically, all available details on the WEC circuits and controls are implementation. This is includes also specific details in protection systems. The rotating machine model (synchronous or asynchronous) is taken

directly from an EMTP-RV library of machine models. It includes fast and slow transients and highest precision in time-domain computations.

The DEMTP-type approach is used to validate the MEVA approach. Due to the level of sophistication in WEC models the establishment of such comparisons is very complex.

Model testing is based on various network study problems, such as faults, overvoltages, frequency control problems and islanding.

1.9.4 Contributions list

- DFIG models
  - PSS/E
  - MEVA: mean-value in EMTP
  - DEMTP: detailed EMTP
  - MVEMTP: mean-value detailed in EMTP
- FC models
  - MEVA
  - DEMTP
  - MVEMTP
- Comparative modeling
- Components, improvements
  - Models (Cp matrix, PLL, generator), initialization, setup
- Benchmarks
  - Slow and fast transients
  - Islanding
  - Power quality
  - Aggregation
- Establishment of basis for further research on wind generation at École Polytechnique de Montréal

CHAPTER 2. WIND GENERATOR COMPONENTS

2.1 Power computation

The power computed from the mechanical equations of the turbine is converted into mechanical input torque using the rotor speed variable. This is done in both time-domain and steady-state computations. The steady-state solution is performed for initialization of the WEC.

2.1.1 Power extraction from the air stream

Within its effective region, the rotor of a wind turbine absorbs energy from the air stream, and can therefore influence its velocity [10].

Figure 7 represents the flow that develops around a converter in an unrestricted air stream in response to prevailing transmission conditions, whereby the air stream is decelerated axially and deviated tangentially in the opposite direction to the rotation of the rotor.

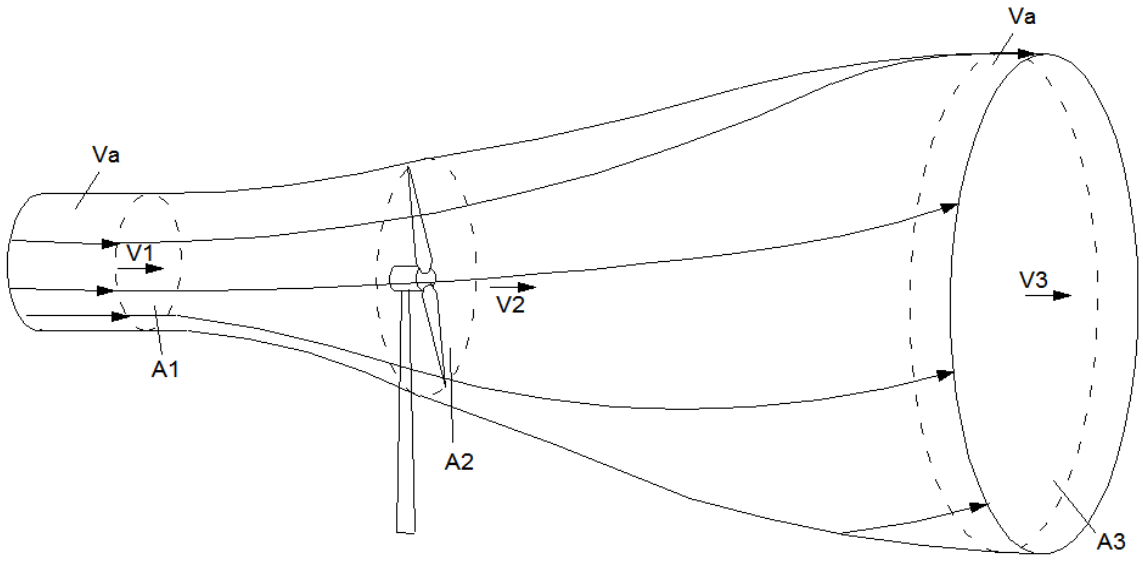

Figure 7: Air stream

The energy absorbed from a volume V_a of cross-section A1 and free speed of flow v_1 far upstream of the turbine, which results in a downstream reduction of flow speed to v_3, with a corresponding broadening of the cross-sectional area to A3, can be expressed as:

$$W_w = V_a \frac{\rho}{2}(v_1^2 - v_3^2) \tag{2.1}$$

where ρ is the air density as in equation (1.1). The wind turbine power may therefore be expressed as:

$$P_w = \frac{dW_w}{dt} \tag{2.2}$$

For an air volume flow in the rotor area $A2 = A_r$:

$$\frac{dV_a}{dt} = A_r v_2 \tag{2.3}$$

which results into the quasi steady-state equation for power:

$$P_w = A_r \frac{\rho}{2}(v_1^2 - v_3^2) v_2 \tag{2.4}$$

The power absorption and power condition of a turbine are therefore determined by the effective area A_r, by the wind speed, and by the changes occurring to theses quantities in the field of flow of the rotor.

According to Betz [10], the maximum wind turbine power output is given by:

$$P_{w_{max}} = \frac{16}{27} A_r \frac{\rho}{2} v_1^3 \tag{2.5}$$

It is achieved when:

$$v_2 = \frac{2}{3} v_1 \tag{2.6}$$

$$v_3 = \frac{1}{3} v_1 \tag{2.7}$$

Under normal operating conditions the nominal output is:

$$P_o = A_r \frac{\rho}{2} v_1^3 \tag{2.8}$$

The performance coefficient is defined under smooth flow conditions at the turbine:

$$C_p = \frac{P_w}{P_o} \tag{2.9}$$

The above expression is based upon the assumption that tubular axial air mass transport only occurs from the leading side of the entry area A1, to the exit area A3. A more detailed examination of the turbine and rotor blades can be carried out using the modified blade element theory, by introducing a radial wind speed gradient and by taking into account angular movement of the air stream.

The C_p coefficient can be plotted as a function of tip speed ratio and blade pitch angle β. The tip speed ratio is defined as:

$$\lambda = \frac{v_u}{v_1} \tag{2.10}$$

where v_u is the peripheral speed and v_1 is the wind speed.

For studies centered on transient mechanical or electrical effects in wind energy machines, the frequency ranges of the components to be examined take on special significance. For simulations that target power fluctuations in wind energy units and transient effects in wind farms, the time constants between the pitch setting range and the rotor range are decisive. The resulting frequencies vary from 0.01 Hz to 10 Hz. Equation (1.1) is the basic equation for determination of rotor performance.

2.1.2 Performance coefficient representation

The manufacturers usually provide turbine data in the form of C_p curves obtained through measurements or design tools. These nonlinear curves must be used in the modeling process for the determination of torque.

There are several methods that can be used to represent the performance coefficient. The programming of this coefficient impacts the modeling precision and

performance. It is also a requirement for the initialization process. The methods that have been tested in this thesis are:

- Transcendental function
- Polynomial function, obtained through a fitting process
- Exact matrix representation

These methods are explained below.

2.1.2.1 Classic transcendental function

This is the classic model used in the literature [11]:

$$C_p = c_1\left(\frac{c_2}{\lambda_i} - c_3\,\beta - c_4\,\beta^{c5} - c_6\right)e^{\left(\frac{-c_7}{\lambda_i}\right)} \tag{2.11}$$

$$\frac{1}{\lambda_i} = \frac{1}{\lambda + c_8\,\beta} - \frac{c_9}{\beta^3 + 1} \tag{2.12}$$

The parameters c_1 to c_9 are set according to wind speed variation. The parameters shown in Table 1 and illustrated in Figure 8 provide a better behavior when the variable wind speed operation is considered.

Table 1: Variable speed parameters

c_1	c_2	c_3	c_4	c_5
0.5	116.0	0.4	0.0	0.0
c_6	c_7	c_8	c_9	
5.0	21.0	0.08	0.035	

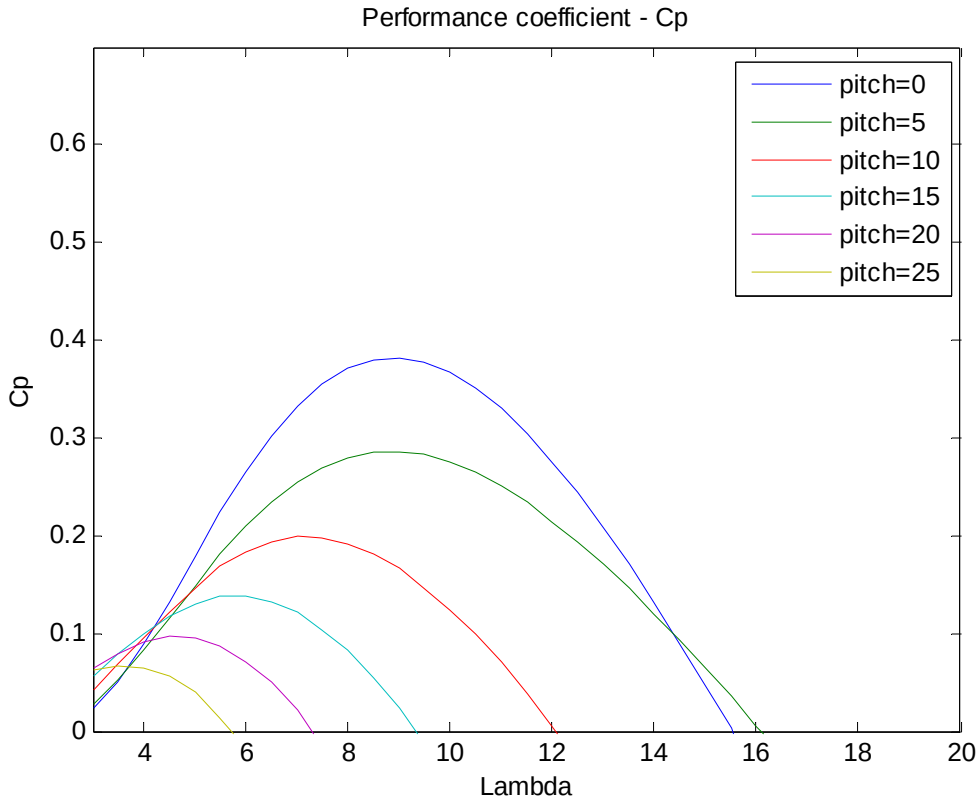

Figure 8: C_p transcendental equation, variable speed

2.1.2.2 Polynomial function

This approach is contributed in this thesis. The C_p function is two-dimensional, and not monotonous for both coordinates. It is difficult to interpolate. Using a matrix approach is inefficient since it must be processed at each simulation time-point and, in addition, creates initialization difficulties.

The approach proposed in this section is to use a fitting procedure for obtaining a polynomial representation. The fitting has been programmed in MATLAB [12]. The resulting generic formulation is given by:

$$C_p = \sum_{i=0}^{4} \sum_{j=0}^{4} a_{ij}\, \beta^i\, \lambda^j \tag{2.13}$$

where β is the pitch angle, λ is the tip speed ratio and a_{ij} is the polynomial coefficient.

2.1.2.3 Exact matrix representation

In this approach the C_p coefficient is stored as a large matrix.

In a generic case the matrix size is 200x25 elements. This matrix allows pitch variation from -2 degrees to 30 degrees and tip speed ratio variation from 0 to 20 pu. In this way all the operation condition are considered.

2.1.3 Initialization procedure

The C_p performance coefficient must be computed for initializing the WEC according to the scheduled output power.

In addition to the C_p matrix, the manufacturer usually provides a table function of active power as a function of rotor speed. In addition it is possible to obtain an active power table function as a function of wind speed. The wind speed can be also entered manually. From the input condition of power it is thus possible to determine the tip-speed ratio using equation (1.2). The next step is to determine the performance coefficient and the pitch angle. This is done through an iterative process where the pitch angle is calculated to verify the scheduled power within a given tolerance.

The pitch angle steps can be determined as follows:

$$\Delta\beta = \frac{\beta_{max} - \beta_{min}}{N_{step}} \tag{2.14}$$

where $\Delta\beta$ is the pitch variation step and N_{step} is the number of steps (iterations). The overall procedure is given by the following steps:

1. Input scheduled power and set the iteration counter to 0.
2. Set the pitch angle to β_{min}.
3. Advance iteration count.
4. Exit if the number of iterations is greater than N_{step}.
5. Calculate C_p using one of the procedures described above. Interpolation is used in the matrix representation.

6. Calculate the extracted power using equation (1.1).
7. Exit if the calculated power is close to the scheduled power within a specified tolerance.
8. Advance the pitch angle to the next value.
9. Go to step 3.

2.2 Wind model

The wind speed as a function of time can be considered [13] as the sum of three components: a constant, a ramp and a gust evolution. The typical function presented in Figure 9 can be described by

$$V(t) = V_{average} + V_{ramp}(t) + V_{gust}(t) \tag{2.15}$$

Such an equation allows testing the WEC performance due to wind perturbations.

Typical wind data can be found from regional information on the location of the wind park.

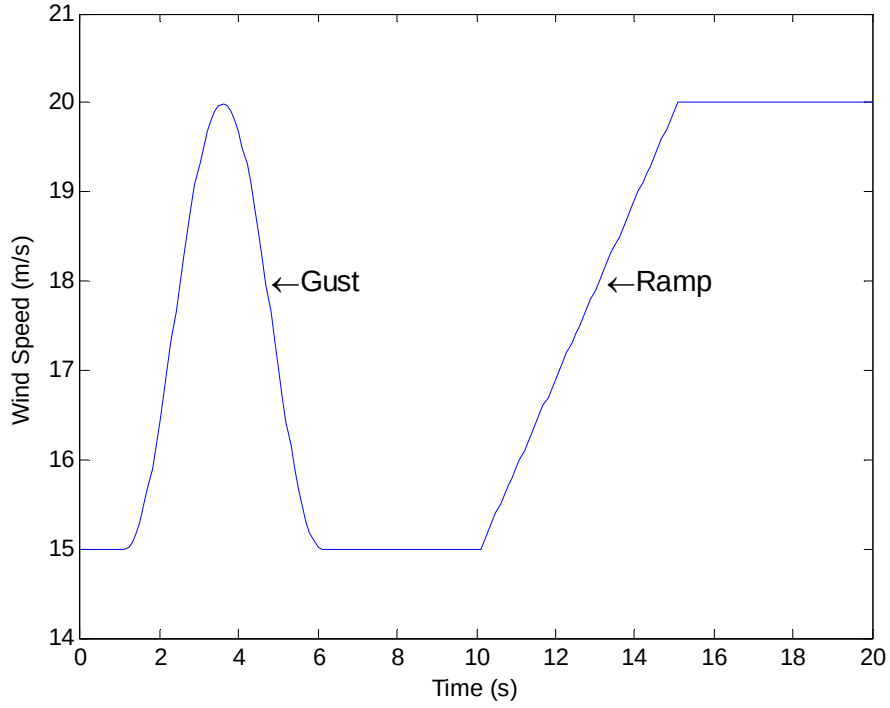

Figure 9: Wind speed function

2.3 Pitch control

2.3.1 Wind turbine control philosophies

Wind turbines are generally designed to deliver maximum output at wind speeds around 15 m/s. In case of stronger winds it is necessary to waste part of the excess energy of the wind in order to avoid damaging the wind turbine. According to equation (1.1), for a given wind speed, the only parameter that allows to control extracted power is the C_p parameter. This parameter depends on the type of turbine and on the type of design from the manufacturer. It is also a function of the pitch control.

2.3.2 Stall for fixed wind turbines, no pitch control

The blades are aerodynamically designed so that as the wind speed increases beyond a certain point the blade shape gradually begins to produce turbulence in the wind and thus eventually results in the blades stalling, much like an airplane that tries to climb to quickly at too sharp an angle of attack and thus stalls.

An advantage of this control system is that it avoids mechanically moving parts and some of the control associated to the pitch control.

Among the disadvantages is the fact that each change in the wind speed will translate into a change in the turbine torque and the generator output. This results into a more significant voltage flicker if the power system is weak. Additionally, due to the sudden changes of torque, it becomes necessary to build a more robust drive train for converting the torque into grid power.

2.3.3 Pitch controlled turbines

On a pitch controlled wind turbine the turbine's electronic controller checks the power output of the turbine several times per second. When the power output becomes too high, it sends an order to the blade pitch mechanism which immediately pitches (turns) the rotor blades slightly out of the wind. Conversely, the blades are turned back

into the wind whenever the wind drops again. The rotor blades thus have to be able to turn around their longitudinal axis.

According to equation (1.1), one way to capture the maximum amount of wind energy is by keeping C_p as high as possible during the operation of the wind turbine. During normal operation, the power may be controlled in the range from start-up wind speed to shutdown wind speed of a single speed generator turbine. When the wind speed is between start-up wind speed and nominal wind speed, the pitch angle is adjusted to optimize C_p. This can be achieved by programming the turbine output as a function of turbine speed based on a power-speed curve that leads to maintaining a fixed tip-speed ratio.

Wind turbines with no pitch control, when the wind speed is above nominal wind speed power output is limited to nominal power by utilizing the stall effect, and in the range of high wind speeds, the stall effect leads to a drop below nominal power.

In change wind turbines with pitch control, to get a flat power curve, constant nominal power in the range between nominal wind speed and shut-down wind speed, the pitch angle has to be adjusted accordingly.

Figure 10 compares the stall (no pitch control) and pitch operation of a wind turbine.

2.3.4 Pitch control model

The pitch control system is the method of feedback control that uses the PID controller as the main tool. The basic structure of a conventional feedback control system is shown in the Figure 11.

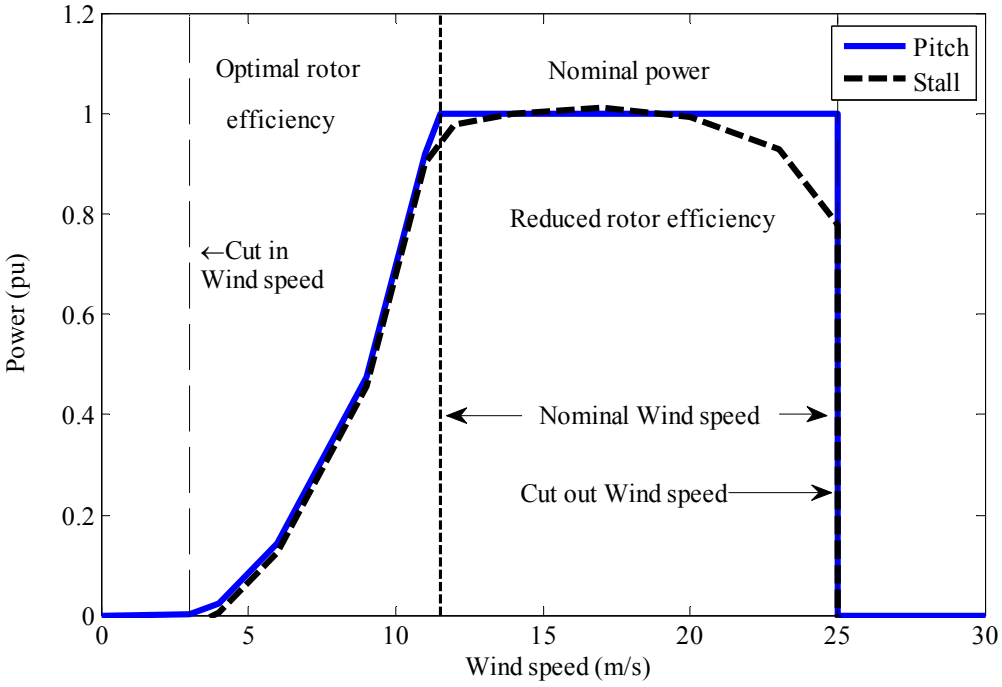

Figure 10: Stall and pitch operation of a wind turbine

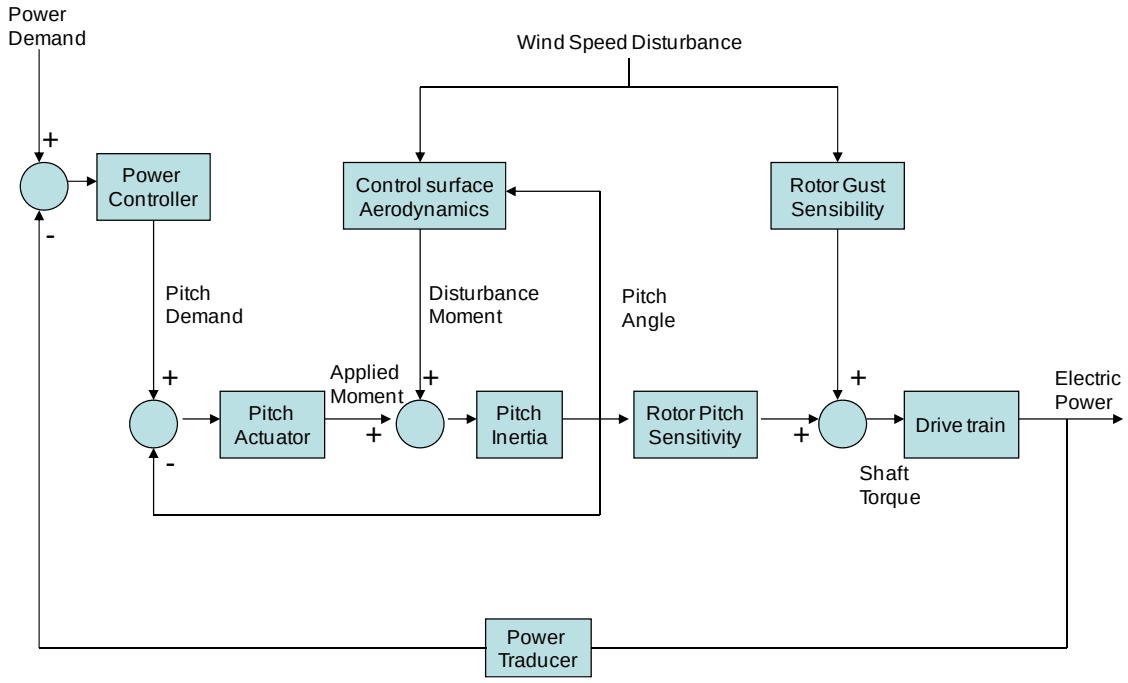

Figure 11: Pitch control model

The purpose of the control is to make the electrical power follow the set-point value of the power demand. To achieve this purpose, the pitch angle is changed at the command of the controller.

The disturbance is the wind speed. It can produce two disturbance effects. The first is on the blade surface which is traduced by a disturbance effect that must be compensated by the pitch actuator torque during the operation of angle modification. The second is due to fast speed (turbulence) variation that should produce fast electric power change which must be filtered to avoid unnecessary pitch movement. The first disturbance effect is neglected considering a perfect compensation of the pitch actuator. In change the second effect was modeled using the turbulence model.

The pitch inertia acts an output delays in front of an instantaneous input change condition. The error is the difference between the power demand and the electrical power output. The power controller determines first a pitch demand and then the pitch actuator is used to calculate the pitch angle. The variable electrical power is measured by the power transducer and used as input in this process.

The actual implementation of the pitch control for MEVA, PSS/E and DEMTP models is shown in Figure 12.

The pitch angle control model is a simplified version of a more complex electromechanical system. The pitch control function is to prevent mechanical and electrical damage. As consequence of high rotor speed the pitch is increased to reduce the generated power, by changing the operational C_p curve.

To prevent interaction with other control the pitch controller is active only the wind speed is higher than the wind speed threshold.

A simplified block diagram may be integrated by three main blocks; the pitch actuator, the pitch control and the pitch compensator. The pitch actuator represents the delay associated to communication and mechanical command to change the blade angle and the constraints inherent to blade angle modification, such as physical limits and rate variation limits (± 30 to ±90 degree and ±10 degree/s).

The pitch actuator can be represented by a low pass filter with a variable gain schedule G_s. The gain is linearly interpolated on pitch angle between β_{min} and β_{max}. Where β_{min} and β_{max} are pitch angle limits; T_p is the time constant in low pas filter of pitch actuator; $\frac{d\beta}{dt_{max}}$ is the maximum pitch angle rate limit; $\frac{d\beta}{dt_{min}}$ is the minimum pitch angle rate limit.

$$\varpi = \frac{\beta - \beta_{min}}{\beta_{max} - \beta_{min}} \tag{2.16}$$

$$G_s = \frac{1}{(1-\varpi)\beta_{min} + \varpi\,\beta_{max}} \tag{2.17}$$

The pitch control increases the pitch angle using a classic PI controller with anti-windup on the pitch limits to avoid the unlimited growth of the pitch angle where K_{pp} is the proportional gain in pitch regulator, K_{ip} is the integrator gain in pitch regulator. The difference between the rotor speed ω_r and the reference rotor speed ω_{ref} is used as input.

The pitch compensator limits to the rated value the output power during high wind condition, it uses a classic PI controller with anti-windup on the pitch limits to avoid the unlimited growth of the pitch angle; where K_{ic} is the integrator gain in pitch compensator, K_{pc} is the proportional gain in pitch compensator; the power error is used as input. The difference between the power order P_{inp} and the power reference P_{ref} is used as the power error of the torque control.

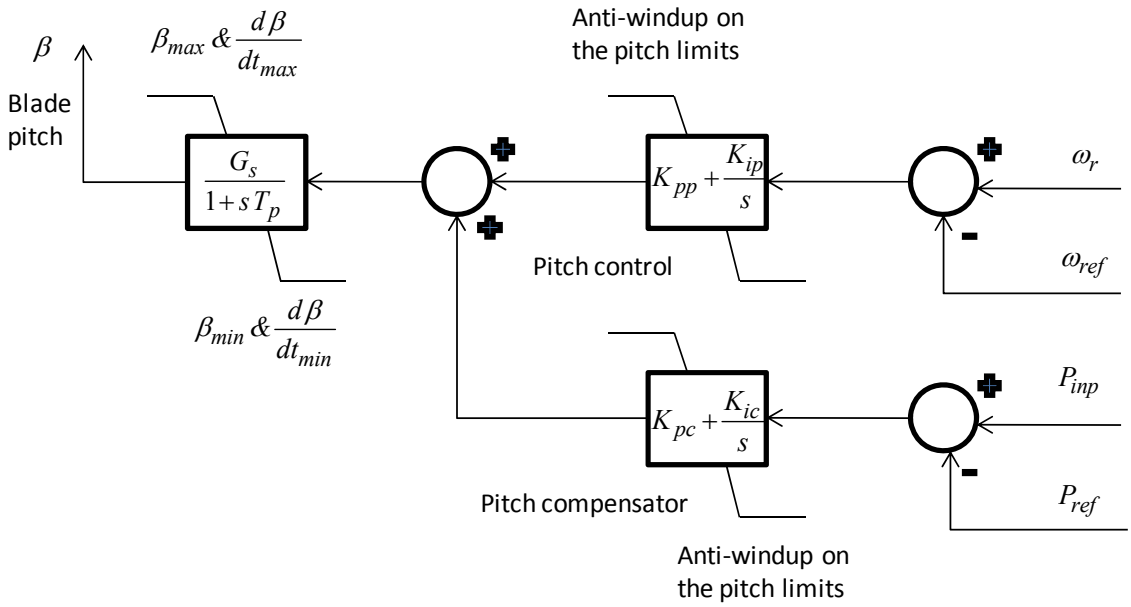

Figure 12 Pitch control model implementation, pu quantities

2.4 Asynchronous machine equations for MEVA and PSS/E models

The objective of this section is the presentation of the asynchronous machine model equations for dynamic simulations with PSS/E and EMTP-RV for the MEVA model. Contrary to built-in detailed machine models [4] in EMTP-RV, the mean value models presented here are not readily available and must be programmed [14] [15].

The simplified equivalent circuit used for the squirrel cage induction generator is the same as the one for the squirrel cage induction motor shown in Figure 13, with the only difference being the direction of currents.

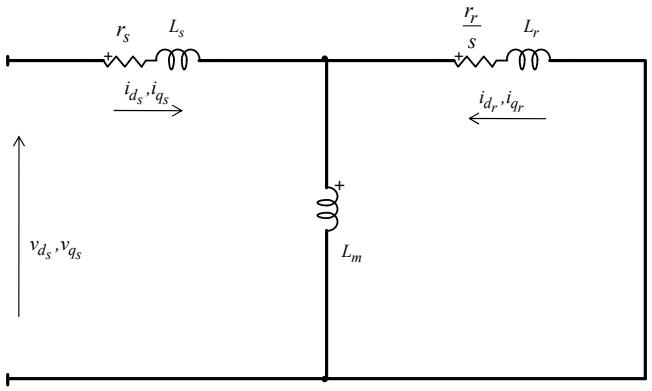

Figure 13: Equivalent circuit of an induction machine in steady-state

The equations are formulated in pu in terms of the real (d) and imaginary (q) axis, with respect to the network reference angle. In a synchronously rotating reference frame, the relations between the stator voltage V and d and q axis voltages are given by

$$v_{d_s} = V\,sin\left(-\theta_r\right) \tag{2.18}$$

$$v_{q_s} = V\,cos\left(\theta_r\right) \tag{2.19}$$

where θ_r is the electrical phase angle between the terminal voltage and the q axis. The subscript s stands for stator and r designates the rotor.

The stator and rotor voltages are given by

$$v_{d_s} = \frac{d\varphi_{d_s}}{dt} + r_s\, i_{d_s} - \omega_s\, \varphi_{q_s} \tag{2.20}$$

$$v_{q_s} = \frac{d\varphi_{q_s}}{dt} + r_s\, i_{q_s} + \omega_s\, \varphi_{d_s} \tag{2.21}$$

$$0 = \frac{d\varphi_{d_r}}{dt} + r_r\, i_{d_r} + p\,\theta_r\, \varphi_{q_r} \tag{2.22}$$

$$0 = \frac{d\varphi_{q_r}}{dt} + r_r\, i_{q_r} - p\,\theta_r\, \varphi_{d_r} \tag{2.23}$$

where φ denotes flux, r_s is the stator winding resistance, p is $\frac{d}{dt}$ operator, ω_s is the electrical frequency of the stator in rad/s and r_r is the rotor side resistance. The relation with the rotor angle and slip s is given by

$$p\,\theta_r = -s = \frac{\omega_r - \omega_s}{\omega_s} \tag{2.24}$$

For motor action $s > 0$ and for generator action $s < 0$.

To link the stator and rotor fluxes it is needed to write

$$\varphi_{d_s} = \left(L_s + L_m\right) i_{d_s} + L_m\, i_{d_r} \tag{2.25}$$

$$\varphi_{q_s} = \left(L_s + L_m\right) i_{q_s} + L_m\, i_{q_r} \tag{2.26}$$

$$\varphi_{d_r} = \left(L_s + L_m\right) i_{d_r} + L_m\, i_{d_s} \tag{2.27}$$

$$\varphi_{q_r} = \left(L_s + L_m\right) i_{q_r} + L_m\, i_{q_s} \tag{2.28}$$

where L_s is the stator winding inductance and L_m is the mutual inductance (see Figure 13).

Under steady-state conditions both $\frac{d\varphi_{d_s}}{dt}$ and $\frac{d\varphi_{q_s}}{dt}$ are zero. The elimination of rotor currents gives

$$v_{d_s} = r_s\, i_{d_s} - \omega_s\, L'\, i_{q_s} - \omega_s\, L_k\, \varphi_{q_r} \tag{2.29}$$

$$v_{q_s} = r_s\, i_{q_s} + \omega_s\, L'\, i_{d_s} + \omega_s\, L_k\, \varphi_{d_r} \tag{2.30}$$

$$\frac{d\varphi_{d_r}}{dt} = -\frac{r_r}{L_r + L_m}\varphi_{d_r} + \frac{r_r\, L_m}{L_r + L_m} i_{d_s} - p\,\theta\,\varphi_{q_r} \tag{2.31}$$

$$\frac{d\varphi_{q_r}}{dt} = -\frac{r_r}{L_r + L_m}\varphi_{q_r} + \frac{r_r\, L_m}{L_r + L_m} i_{q_s} + p\,\theta\,\varphi_{d_r} \tag{2.32}$$

$$i_{d_s} = \frac{v_{q_s} - \omega_s\, L_k\, \varphi_{d_r}}{\omega_s\, L'} - \frac{r_s}{\omega_s\, L'} i_{q_s} \tag{2.33}$$

$$i_{q_s} = -\frac{v_{d_s} - \omega_s L_k \varphi_{q_r}}{\omega_s L'} + \frac{r_s}{\omega_s L'} i_{d_s} \tag{2.34}$$

where

$$L' = L_s + L_m - \frac{L_m^2}{L_r + L_m} \tag{2.35}$$

$$L_k = \frac{L_m}{L_r + L_m} \tag{2.36}$$

The following change of variable can be applied for flux:

$$\varphi'_{d_r} = \frac{L_m}{L_r + L_m} \varphi_{d_r} \tag{2.37}$$

$$\varphi'_{q_r} = \frac{L_m}{L_r + L_m} \varphi_{q_r} \tag{2.38}$$

Equations (2.31) and (2.32) are now written as

$$\frac{d\varphi'_{d_r}}{dt} = -\frac{r_r}{L_r + L_m} \varphi'_{d_r} + r_r \left(\frac{L_m}{L_r + L_m} \right)^2 i_{d_s} - p\,\theta_r\,\varphi'_{q_r} \tag{2.39}$$

$$\frac{d\varphi'_{q_r}}{dt} = -\frac{r_r}{L_r + L_m} \varphi'_{q_r} + r_r \left(\frac{L_m}{L_r + L_m} \right)^2 i_{q_s} + p\,\theta_r\,\varphi'_{d_r} \tag{2.40}$$

Equations (2.33) and (2.34) are also converted into

$$i_{d_s} = \frac{v_{q_s} - \omega_s \varphi'_{d_r}}{\omega_s L'} - \frac{r_s}{\omega_s L'} i_{q_s} \tag{2.41}$$

$$i_{q_s} = -\frac{v_{d_s} + \omega_s \varphi'_{q_r}}{\omega_s L'} + \frac{r_s}{\omega_s L'} i_{d_s} \tag{2.42}$$

The following set of complex variables is defined using the complex operator j:

$$\varphi'_r = \varphi'_{d_r} + j\,\varphi'_{q_r} \tag{2.43}$$

$$i_s = i_{d_s} + j\,i_{q_s} \tag{2.44}$$

$$e_s = v_{d_s} + j\,v_{q_s} \tag{2.45}$$

$$e'_r = j\,\omega_s\,\varphi'_r \tag{2.46}$$

To obtain

$$\frac{d\varphi'_r}{dt} = -\frac{r_r}{L_r + L_m}\varphi'_r + r_r\left(\frac{L_m}{L_r + L_m}\right)^2 i_s - j\, p\, \theta_r\, \varphi'_r \tag{2.47}$$

The combination of equations (2.46) and (2.47) results into:

$$\frac{de'_r}{dt} = -\frac{r_r}{L_r + L_m}e'_r + j\,\omega_s\, r_r\left(\frac{L_m}{L_r + L_m}\right)^2 i_s - j\, p\, \theta_r\, e'_r \tag{2.48}$$

The combination of equations (2.41), (2.42) and (2.44) results into:

$$i_s = \frac{-\left(\omega_s\, \varphi'_r + j e_s\right)}{\omega_s L'} - j\frac{r_s}{\omega_s L'} i_s = \frac{e_s - e'_r}{j\omega_s L' + r_s} \tag{2.49}$$

and

$$\left(j\omega_s L' + r_s\right) i_s = e_s - e'_r \tag{2.50}$$

The open circuit time-constant T_o is defined as:

$$\frac{1}{T_o} = \frac{r_r}{L_r + L_m} \tag{2.51}$$

which is combined with equation (2.35) to give

$$r_r\left(\frac{L_m}{L_r + L_m}\right)^2 = \frac{1}{T_o}\left(L_s + L_m - L'\right) \tag{2.52}$$

Finally, equation (2.52) is replaced into equation (2.48) to give:

$$\frac{de'_r}{dt} = -\frac{1}{T_o}\left[e'_r - j\,\omega_s\left(L_s + L_m - L'\right) i_s\right] - j\, p\, \theta_r\, e'_r \tag{2.53}$$

The complex power entering the machine is given by

$$S_e = j\omega_s\left(\varphi'_{d_r} + j\,\varphi'_{q_r}\right) conj\left(i_{d_s} + j\, i_{q_s}\right) \tag{2.54}$$

From which it is possible to write the electrical torque equation:

$$T_e = \frac{\Re\left(S_e\right)}{\omega_s} = \frac{\Re\left[e'_r\, conj\left(i_s\right)\right]}{\omega_s} \tag{2.55}$$

This equation can be further simplified by neglecting resistances and noticing that the equivalent circuit of the machine gives

$$0 = \omega_s L_m \left(i_{d_s} + j\, i_{q_s} \right) + \omega_s \left(L_r + L_m \right) \left(i_{d_r} + j\, i_{q_r} \right) \tag{2.56}$$

and using equations (2.37) and (2.38) we obtain

$$S_e = -j\omega_s \left(\varphi_{d_r} + j\, \varphi_{q_r} \right) \left(i_{d_r} - j\, i_{q_r} \right) = \omega_s \left(-j\, \varphi_{d_r}\, i_{d_r} - \varphi_{d_r}\, i_{q_r} + \varphi_{q_r}\, i_{d_r} - j\, \varphi_{q_r}\, i_{q_r} \right) \tag{2.57}$$

$$T_e = \frac{\Re\left(S_e \right)}{\omega_s} = \varphi_{q_r} i_{d_r} - \varphi_{d_r} i_{q_r} \tag{2.58}$$

2.5 Generator/converter model for MEVA and PSS/E models

2.5.1 Doubly fed induction generator

In this (DFIG) model it is assumed that steady-state equations are acceptable, since the stator and rotor flux dynamics are fast in comparison with grid dynamics and the converter controls basically decouple the generator from the grid.

The stator and rotor voltages are given by

$$v_{d_s} = \frac{d\varphi_{d_s}}{dt} - r_s\, i_{d_s} - \omega_s\, \varphi_{q_s} \tag{2.59}$$

$$v_{q_s} = \frac{d\varphi_{q_s}}{dt} - r_s\, i_{q_s} + \omega_s\, \varphi_{d_s} \tag{2.60}$$

$$v_{d_r} = \frac{d\varphi_{d_r}}{dt} - r_r\, i_{d_r} - p\,\theta_r\, \varphi_{q_r} \tag{2.61}$$

$$v_{q_r} = \frac{d\varphi_{q_r}}{dt} - r_r\, i_{q_r} + p\,\theta_r\, \varphi_{d_r} \tag{2.62}$$

From equation (2.24)

$$p\,\theta_r = s = \frac{\omega_s - \omega_r}{\omega_s} = 1 - \omega_{r_{pu}} \tag{2.63}$$

The pu subscript will be dropped in the following equations to simplify presentation. In equations (2.59) to (2.63), the flux variations are set to zero. The flux equations are similar to equations (2.25)-(2.28), but with a negative sign on the right hand side due to generator notation.

From the above assumptions (using fundamental frequency reactances instead of inductances) it can be written in generator notation and in pu [15].

$$v_{d_s} = -r_s\, i_{d_s} + \left[\left(X_s + X_m \right) i_{q_s} + X_m\, i_{q_r} \right] \tag{2.64}$$

$$v_{q_s} = -r_s\, i_{q_s} - \left[\left(X_s + X_m \right) i_{d_s} + X_m\, i_{d_r} \right] \tag{2.65}$$

$$v_{d_r} = -r_r\, i_{d_r} + \left(1 - \omega_r\right) \left[\left(X_s + X_m \right) i_{q_r} + X_m i_{q_s} \right] \tag{2.66}$$

$$v_{q_r} = -r_r\, i_{q_r} - \left(1 - \omega_r\right) \left[\left(X_r + X_m \right) i_{d_r} + X_m i_{d_s} \right] \tag{2.67}$$

Equations (2.18) and (2.19) remain applicable in this context.

The active and reactive powers, that are shown in the Figure 14, depend on the stator and converter currents as follows

$$P = v_{d_s}\, i_{d_s} + v_{q_s}\, i_{q_s} + v_{d_c}\, i_{d_c} + v_{q_c}\, i_{q_c} \tag{2.68}$$

$$Q = v_{q_s}\, i_{d_s} - v_{d_s}\, i_{q_s} + v_{q_c}\, i_{d_c} - v_{d_c}\, i_{q_c} \tag{2.69}$$

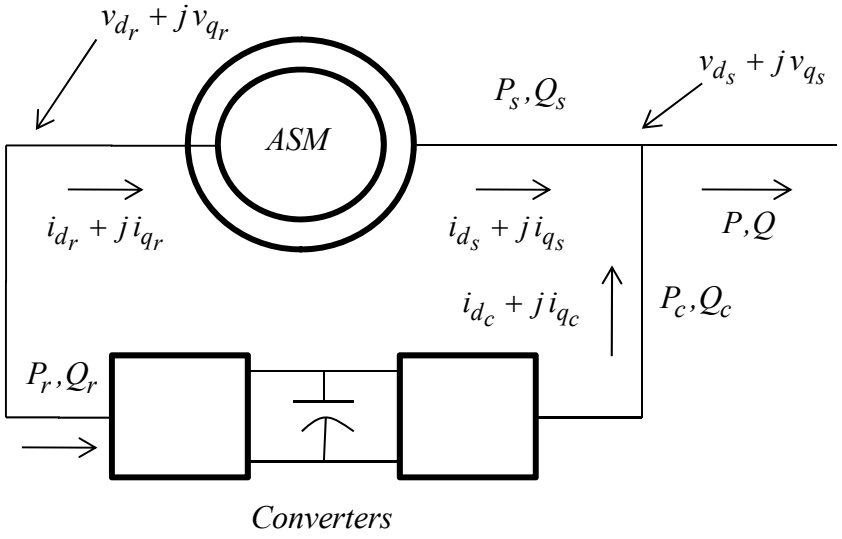

Figure 14: DFIG design

where

P is the net active power generated by the DFIG,

Q is the net reactive power generated or absorbed by the DFIG,

P_s is the active power generated by the stator of the asynchronous machine,

Q_s is the reactive power generated or absorbed by the stator of the asynchronous machine,

P_c is the active power output by the grid side converter,

Q_c is the active power output by the grid side converter,

v_{d_s} is the d component of the stator voltage

v_{q_s} is the q component of the stator voltage

v_{d_c} is the d component of the terminal voltage of grid side converter, it is equal to v_{d_s}

v_{q_c} is the q component of the terminal voltage of grid side converter, it is equal to v_{q_s}

The converter powers, integrated in the equations (2.68) and (2.69), on the grid side are explicitly written as

$$P_c = v_{d_c}\, i_{d_c} + v_{q_c}\, i_{q_c} \tag{2.70}$$

$$Q_c = v_{q_c}\, i_{d_c} - v_{d_c}\, i_{q_c} \tag{2.71}$$

whereas on the rotor side they become

$$P_r = v_{d_r}\, i_{d_r} + v_{q_r}\, i_{q_r} \tag{2.72}$$

$$Q_r = v_{q_r}\, i_{d_r} - v_{d_r}\, i_{q_r} \tag{2.73}$$

v_{d_r} is the d component of the rotor voltage

v_{q_r} is the q component of the rotor voltage

i_{d_r} is the d component of the rotor current

i_{q_r} is the q component of the rotor current

Assuming a lossless converter model, the active power of the converter becomes equal to the rotor active power and the grid converter is set such as reactive power on the grid is equal to zero.

$$P_c = P_r \tag{2.74}$$

$$Q_c = 0 \tag{2.75}$$

The active and reactive power injected into the grid can be approximated by neglecting stator resistance and assuming that the d-axis coincides with the maximum of stator flux.

$$P = P_s + P_r \tag{2.76}$$

$$Q = Q_s \tag{2.77}$$

The contribution of the active power from the rotor P_r, through the dc link is added on the grid side. It can be replaced by the increment of the current proportional to active power, the dc link may be neglected without changes in the dynamic performance of that depends the fast response of power electronics based converter.

The maximum voltage is 90 degrees ahead and aligned on the q-axis. In this condition

$$v_{d_s} + j\, v_{q_s} = 0 + j\, v_{q_s} \tag{2.78}$$

$$v_{d_s} + j\, v_{q_s} = 0 + j\, V \tag{2.79}$$

$$\varphi_{d_s} + j\, \varphi_{q_s} = \varphi + j\, 0 \tag{2.80}$$

$$I_s = i_{d_s} + j\, i_{q_s} \tag{2.81}$$

Consequently

$$P + jQ = j\, v_{q_s} \left(i_{d_s} - j\, i_{q_s} \right) = V\, i_{q_s} + j\, V\, i_{d_s} \tag{2.82}$$

With this definition, the current i_{q_s} controls the active power output, while the current i_{d_s} controls the reactive power output.

Following equations (2.25), (2.26) and (2.80), and using generator notation

$$\omega_s\, \varphi_{d_s} = V = -\left(X_s + X_m \right) i_{d_s} - X_m\, i_{d_r} \tag{2.83}$$

$$\omega_s\, \varphi_{q_s} = 0 = \left(L_s + L_m \right) i_{q_s} + L_m\, i_{q_r} \tag{2.84}$$

it becomes possible to write

$$i_{d_s} = \frac{-V - X_m\, i_{d_r}}{X_s + X_m} \tag{2.85}$$

$$i_{q_s} = \frac{-X_m\, i_{q_r}}{X_s + X_m} \tag{2.86}$$

Equation (2.85) can be combined with equation (2.82) to give

$$Q = -\frac{X_m\, V\, i_{d_r}}{X_s + X_m} - \frac{V^2}{X_s + X_m} \tag{2.87}$$

The current i_{d_r} can be considered as the sum of two parts, generation and magnetization. It is shown in the Figure 15.

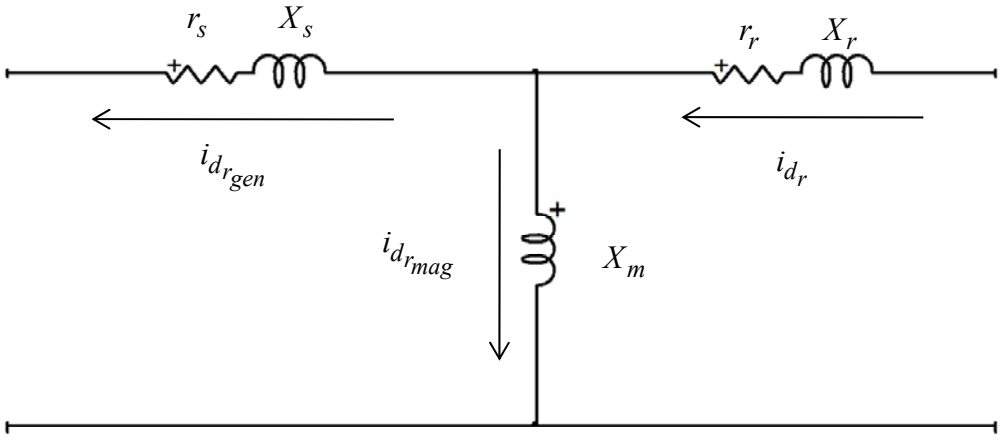

Figure 15: Component of generation and magnetization of current i_{d_r}

$$i_{d_r} = i_{d_{r_{gen}}} + i_{d_{r_{mag}}} \tag{2.88}$$

To operate with unity power factor it is necessary to put

$$i_{d_{r_{mag}}} = \frac{-V}{X_m} \tag{2.89}$$

in equation (2.87). Considering that the reactive power exchange with the grid can be also written as

$$Q = Q_{gen} + Q_{mag} \tag{2.90}$$

the net reactive power exchange between the stator and the grid is equal to

$$Q_{gen} = -\frac{X_m\, V\, i_{d_{r_{gen}}}}{X_s + X_m} \tag{2.91}$$

The basic mechanical equation for the 1-mass model is given by

$$2H\frac{d\omega_r}{dt} = T_m - T_e \tag{2.92}$$

Where H is the inertia constant in seconds and the torque T_m is the applied mechanical torque in pu. The electromagnetic torque equation can be written using equations (2.82) and (2.86)

$$T_e = \frac{P}{\omega_s} = \frac{V\, i_{q_s}}{\omega_s} = -\frac{V\, X_m\, i_{q_r}}{\omega_s\left(X_s + X_m\right)} \tag{2.93}$$

In the generic case, it is possible to use a multimass model given by

$$p\boldsymbol{\theta}_\mathbf{m} = \boldsymbol{\omega}_\mathbf{m} \tag{2.94}$$

$$\mathbf{J_m}\, p\boldsymbol{\omega}_\mathbf{m} + \mathbf{D_m}\, p\boldsymbol{\theta}_\mathbf{m} + \mathbf{K_m}\, \boldsymbol{\theta}_\mathbf{m} = \mathbf{T_a} \tag{2.95}$$

where the subscript m designates mechanical quantities, $\mathbf{J_m}$ is the diagonal matrix of moments of inertia, $\boldsymbol{\omega}_\mathbf{m}$ is the vector of speeds, $\boldsymbol{\theta}_\mathbf{m}$ is the vector of angular positions, $\mathbf{D_m}$ and $\mathbf{K_m}$ are the tridiagonal matrices of damping and stiffness coefficients respectively and the vector of torques is given by

$$\mathbf{T_a} = \begin{bmatrix} T_{m1} & \cdots & T_{mi} & -T_{gen} \end{bmatrix}^T \tag{2.96}$$

where T_{mi} is the mechanical torque of ith turbine section and T_{gen} is the electromagnetic (see [16]) generator torque. It is also needed to account for the gearbox ratio as follows.

$$\omega_{m2} = \frac{\omega_{m1}}{GBR} \tag{2.97}$$

The wind turbine mechanical system consists of a light generator with moment of inertia J_{m1} and its gearbox connected by a shaft of finite stiffness to a heavy turbine with moment of J_{m2}.

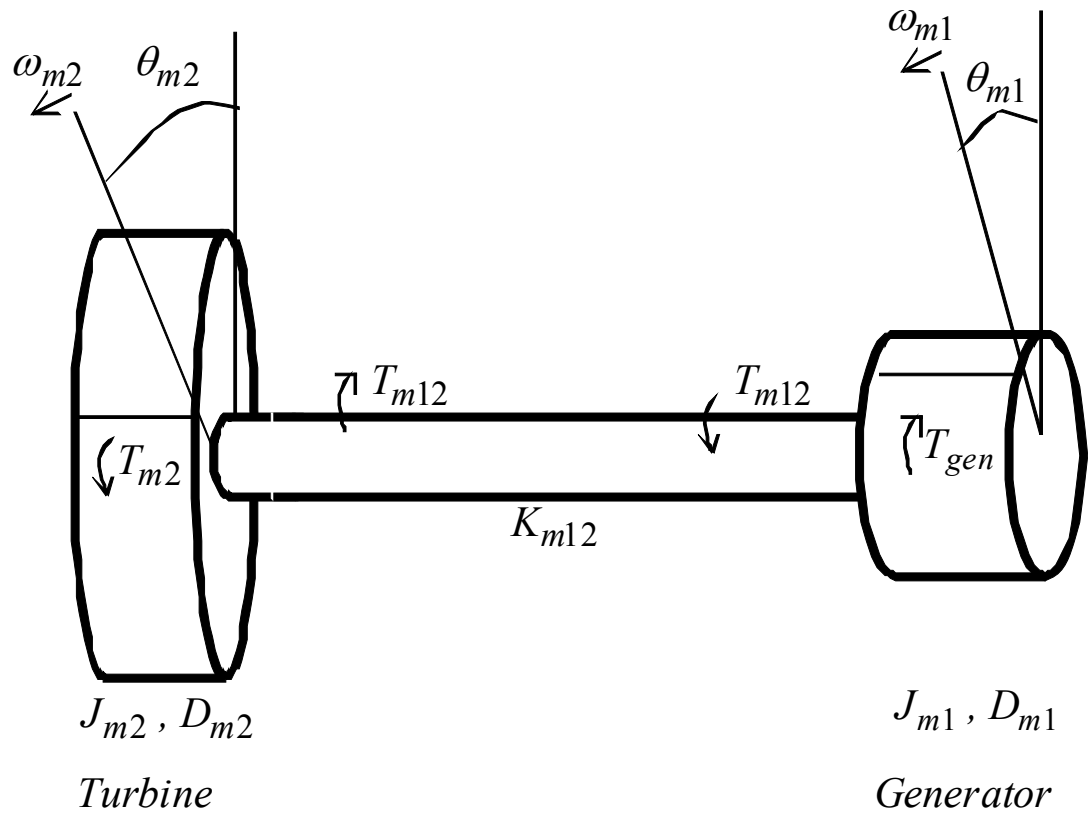

Figure 16: Drive train

The tortional stiffness K_{m12} defines the relationship between the torque transmitted T_{m12} and the angular twist, $\theta_{m2} - \theta_{m1}$, between the two ends of the shaft:

$$T_{m12} = K_{m12}\,(\theta_{m2} - \theta_{m1}) \tag{2.98}$$

Converter dynamics are simplified assuming that they are much faster than electromechanical transients. Thus the converter is modeled as an ideal current source, where i_{q_r} and i_{d_r} are used to control the rotor speed and voltage respectively.

The converter can be modeled as a low-pass filter with the time constants $T_{d_{conv}}$ and $T_{q_{conv}}$. The differentials of converter currents become

$$\frac{di_{q_r}}{dt} = \left(i_{q_{r0}} - i_{q_r}\right)\frac{1}{T_{q_{conv}}} \tag{2.99}$$

$$\frac{di_{d_r}}{dt} = \left(i_{d_{r0}} - i_{d_r}\right)\frac{1}{T_{d_{conv}}} \tag{2.100}$$

where

$$i_{q_{r0}} = -\frac{\left(X_s + X_m\right)P}{X_m V} \tag{2.101}$$

Using equations (2.88), (2.89) and (2.91) $i_{d_{r0}}$ can be written

$$i_{d_{r0}} = -\frac{Q_{gen}\left(X_s + X_m\right)}{X_m\ V} - \frac{V}{X_m} \tag{2.102}$$

The last equation considers with net reactive power exchange Q_{gen} between the stator and the grid.

2.5.2 Full converter generator

In this case the generator is a permanent magnet synchronous generator whose block diagram in dq coordinates is shown in Figure 17. All equations are written in pu and in generator notation.

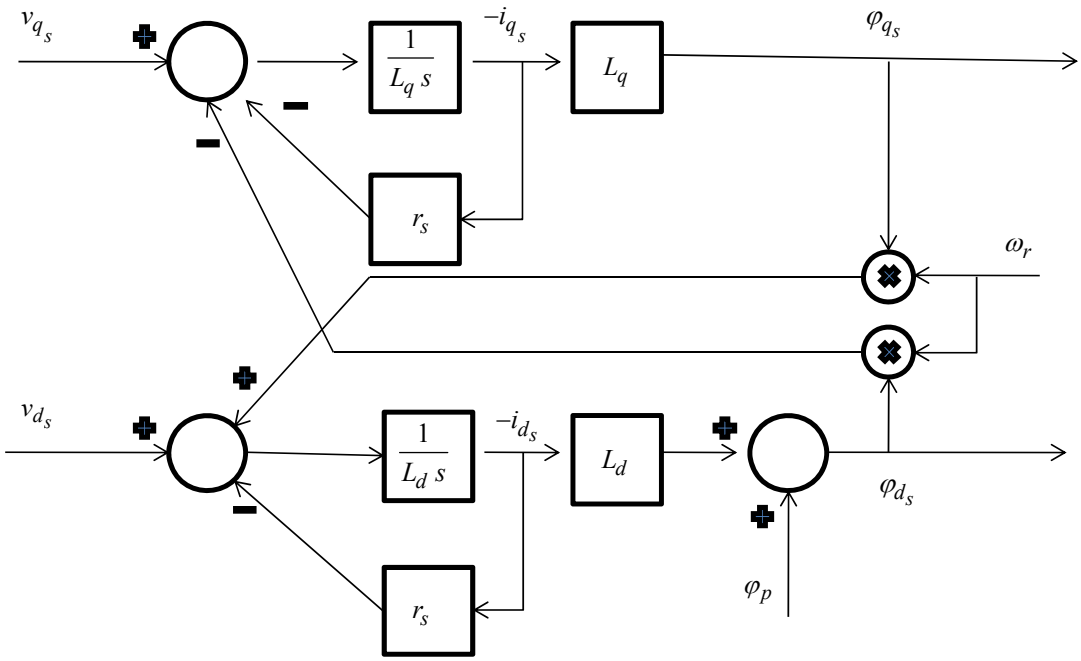

Figure 17: Permanent magnet generator diagram

The steady-state model of the full converter generator, also assumes that the stator and rotor flux dynamics are fast when compared to grid dynamics. The converter controls are assumed to decouple the generator from the grid and the flux variations $\frac{d\varphi_{q_s}}{dt}$ and $\frac{d\varphi_{d_s}}{dt}$ are ignored.

The equations (2.59) and (2.60) remain applicable. The relations between stator fluxes and generator currents are given by

$$\varphi_{q_s} = -L_q\, i_{q_s} \tag{2.103}$$

$$\varphi_{d_s} = -L_d\, i_{d_s} + \varphi_p \tag{2.104}$$

where L_q and L_d are the q-axis and d-axis inductances, see Figure 17, and φ_p is the permanent flux. The differentials of the above fluxes are set to zero. From equations (2.59) and (2.60).

$$v_{d_s} = -r_s\, i_{d_s} + \omega_r\, L_q\, i_{q_s} \tag{2.105}$$

$$v_{q_s} = -r_s\, i_{q_s} - \omega_r \left(L_d\, i_{d_s} - \varphi_p \right) \tag{2.106}$$

The active and reactive powers of the generator shown in Figure 18, are found from

$$P = v_{d_s}\, i_{d_s} + v_{q_s}\, i_{q_s} \tag{2.107}$$

$$Q = v_{q_s}\, i_{d_s} - v_{d_s}\, i_{q_s} \tag{2.108}$$

The active and reactive powers injected into the grid depend only on the grid side currents of the converter and are given by equations (2.70) and (2.71). Here the converter d and q-axis voltage equations are taken from equations (2.18) and (2.19)

$$v_{d_c} = V\, sin(-\theta) \tag{2.109}$$

$$v_{q_c} = V\, cos(\theta) \tag{2.110}$$

where θ is the grid voltage phase.

If the converter is lossless and the power factor is unitary, then the output powers of the generator become

$$P = P_c \tag{2.111}$$

$$Q = 0 \tag{2.112}$$

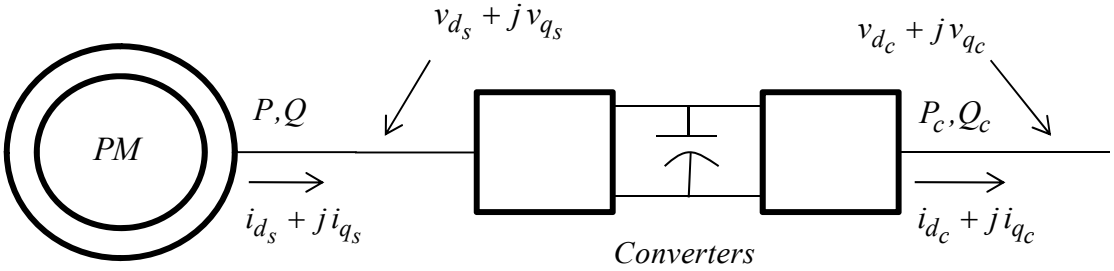

Figure 18: Full converter design

The reactive power injected into the grid is controlled by the converter current i_{d_c}, like in the equation (2.82).

$$P_c + j\, Q_c = V\left[sin(-\theta) + j\, cos(\theta)\right]\left(i_{d_c} - j\, i_{q_c}\right) \tag{2.113}$$

and results into

$$i_{d_c} - j\, i_{q_c} = \frac{P_c\, sin(-\theta) + Q_c\, cos(\theta)}{V} + j\,\frac{Q_c\, sin(-\theta) - P_c\, cos(\theta)}{V} \tag{2.114}$$

From equation (2.111) and the real part of equation (2.114), it is found that the converter reactive power is controlled by the current i_{d_c}

$$Q_c = \frac{1}{cos(\theta)} V\, i_{d_c} + tan(\theta) P \tag{2.115}$$

The 1-mass representation is given by equation (2.92). The electromagnetic torque equation is given by

$$T_e = \varphi_{d_s} i_{q_s} - \varphi_{q_s} i_{d_s} \tag{2.116}$$

Converter dynamics are simplified since they are assumed to be much faster than the electromechanical transients. The converter is modeled as an ideal current source, where i_{q_s}, i_{d_s} and i_{d_c} are used for rotor speed control and generator reactive power control, and the reactive power grid converter control respectively. Considering that the power electronic delay may be modeled by a low pass filter with time constant, T_{ep} is, T_{eq} is and T_{dc} to the currents i_{q_s}, i_{d_s} and i_{d_c} respectively. The following differential equations are written for these currents

$$\frac{di_{q_s}}{dt} = \frac{i_{q_{s_0}} - i_{q_s}}{T_{ep}} \tag{2.117}$$

$$\frac{di_{d_s}}{dt} = \frac{i_{d_{s_0}} - i_{d_s}}{T_{eq}} \tag{2.118}$$

$$\frac{di_{d_c}}{dt} = \frac{i_{d_{c_0}} - i_{d_c}}{T_{dc}} \tag{2.119}$$

where $i_{q_{s_0}}$ is the initialization value of the q component of the stator current,

$i_{d_{s_0}}$ is the initialization value of the d component of the stator current,

$i_{d_{c_0}}$ is the initialization value of the d component of the converter current on the grid side.

If on the generator side, the maximum of the stator flux coincides with the d-axis, the maximum of the voltage is 90 degrees ahead and coincides with the q-axis. The equations (2.78) to (2.81) remain valid for voltage and current of generator. Then, if the stator resistances are neglected, the initialization value of the active power P may be calculated with equation (2.107), the reactive power Q of the generator with equation (2.108) and the reactive power on the grid converter side Q_c with equation (2.115).

$$Q = v_{q_s} i_{d_s} = \omega_r \left(\varphi_p - L_d \, i_{d_s} \right) i_{d_s} \tag{2.120}$$

From (2.120) a quadratic equation may be obtained whose solution is a function of the reactive power of the generator

$$i_{ds}{}^2 - \frac{\varphi_p}{L_p} i_{ds} + \frac{Q}{\omega_r \, L_d} = 0 \tag{2.121}$$

$$i_{d_{s0}} = \frac{\varphi_p}{2L_d} - \sqrt{\frac{\varphi_p^2}{\left(2\,L_d\right)^2} - \frac{Q}{\omega_r \, L_d}} \tag{2.122}$$

$$P = v_{q_s} i_{q_s} = \omega_r \left(\varphi_p - L_d \, i_{d_s} \right) i_{q_s} \tag{2.123}$$

$$i_{q_{s0}} = \frac{P}{\omega_r \left(\varphi_p - L_d \, i_{d_{s0}} \right)} \tag{2.124}$$

$$i_{d_{c0}} = \frac{P \sin\left(-\theta\right) + Q_c \cos\left(\theta\right)}{V} \tag{2.125}$$

2.5.3 Generator/converter model

The doubly fed asynchronous generator model and the full converter synchronous generator model, allow to simulate the generator by representing the slow mechanical dynamics, but neglecting the fast dynamics of the stator and rotor flux linkages [19][17][18].

According to the DFIG equations (2.68) and (2.69) and the full converter equation (2.113), a generator/converter model may be represented using the block diagram of Figure 19.

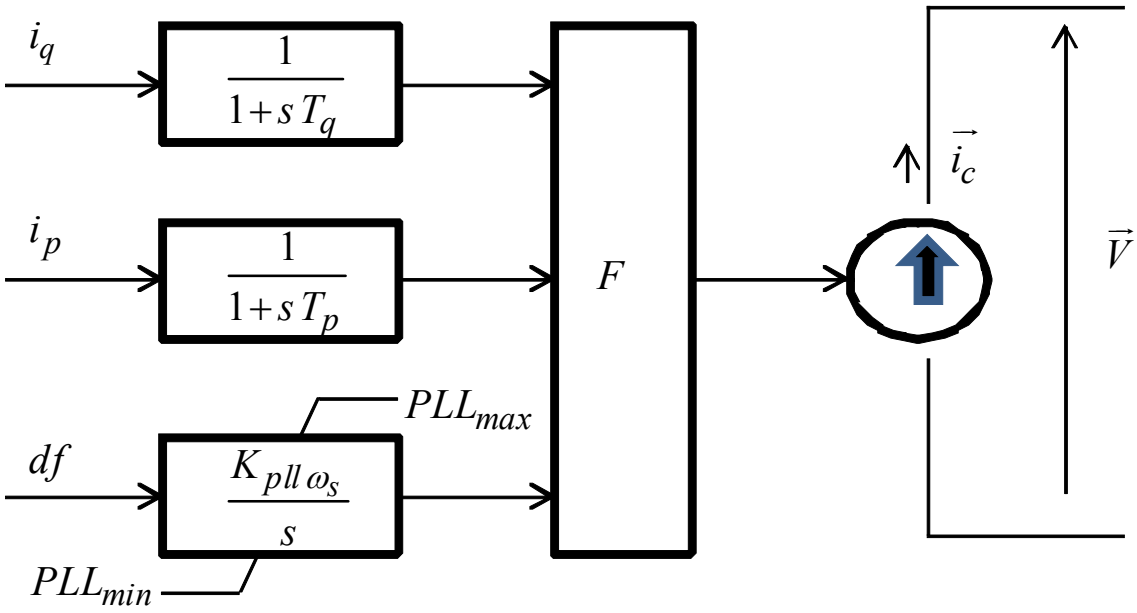

Figure 19: Generator/Converter model for MEVA and PSS/E models

The above generator/converter model neglects the dynamic variation of fluxes in the conventional generator and transforms its algebraic equations to reflect the fast control action [18].

The current source injects to the grid a current with two components. The component i_p is proportional to the active power and the component i_q is proportional to the reactive power. Two low pass filters are used in Figure 19 (time constants T_q and T_p) to simulate the electronic delay. In this way the converter is represented by two time constants.

The following equations are valid taking the terminal voltage, the converter voltage to the FC or stator voltage in the DFIG.

The converter d and q voltages are given by:

$$v_{d_c} = V\,sin(-\theta) \tag{2.126}$$

$$v_{q_c} = V\,cos(\theta) \tag{2.127}$$

where θ is the grid voltage phase. The converter current and voltage are given by

$$v_c = V\,e^{-j\theta} \tag{2.128}$$

$$i_c = (i_p - j\,i_q)\,e^{-j\theta} \tag{2.129}$$

where v_c is wind generator terminal voltage, it is the same that $\vec{V}$, and i_c is the total current injected to the grid, Figure 19. The generator/converter powers on the grid side are explicitly written as

$$S_c = (V\,e^{-j\theta})\,conj((i_p - j\,i_q)\,e^{-j\theta}) \tag{2.130}$$

$$S_c = V\,(i_p + j\,i_q) = P_c + j\,Q_c \tag{2.131}$$

Where P_c and Q_c are initially found from the load-flow solution. In consequence the initialisation values are

$$i_{p_0} = \frac{P_c}{V} \tag{2.132}$$

$$i_{q_0} = \frac{Q_c}{V} \tag{2.133}$$

where

i_c is the current injected into the grid by the current source of Figure 19,

i_q is the current proportional to the reactive power,

i_p is the current proportional to the active power,

df is the grid frequency deviation,

X' is the transient equivalent reactance,

θ is the terminal voltage phase angle,

T_q is the reactive current converter time constant,

T_p is the active current converter time constant,

K_{pll} is the PLL gain,

PLL_{min} is the PLL minimum limit,

PLL_{max} is the PLL maximum limit,

F is the built current function i_c from the components.

The frequency deviation of the grid is reflected through the modification of the phase angle θ.

With the conditions given for the DFIG in the section 2.5.1, the maximum voltage is 90 degrees ahead and aligned on the q-axis. Equation (2.82) is used to write

$$i_q = i_{d_s} \tag{2.134}$$

$$i_p = i_{q_s} \tag{2.135}$$

The same equivalence is found for the full converter (section 2.5.2) model.

The value of the transient equivalent reactance X' is different from the one found using equation (2.35) for the asynchronous machine. Experiments recommend a value of 0.8 pu for best simulation results.

2.6 Torque control and active power order for PSS/E, MEVA and DEMTP

To control the rotor speed it is necessary to control the equilibrium between mechanical and electrical powers. One possible alternative is to regulate the rotor speed by acting on the pitch angle and the produced power by acting on the electromagnetic torque. In consequence, two control loops are used, one for the produced power and another one for the rotor speed.

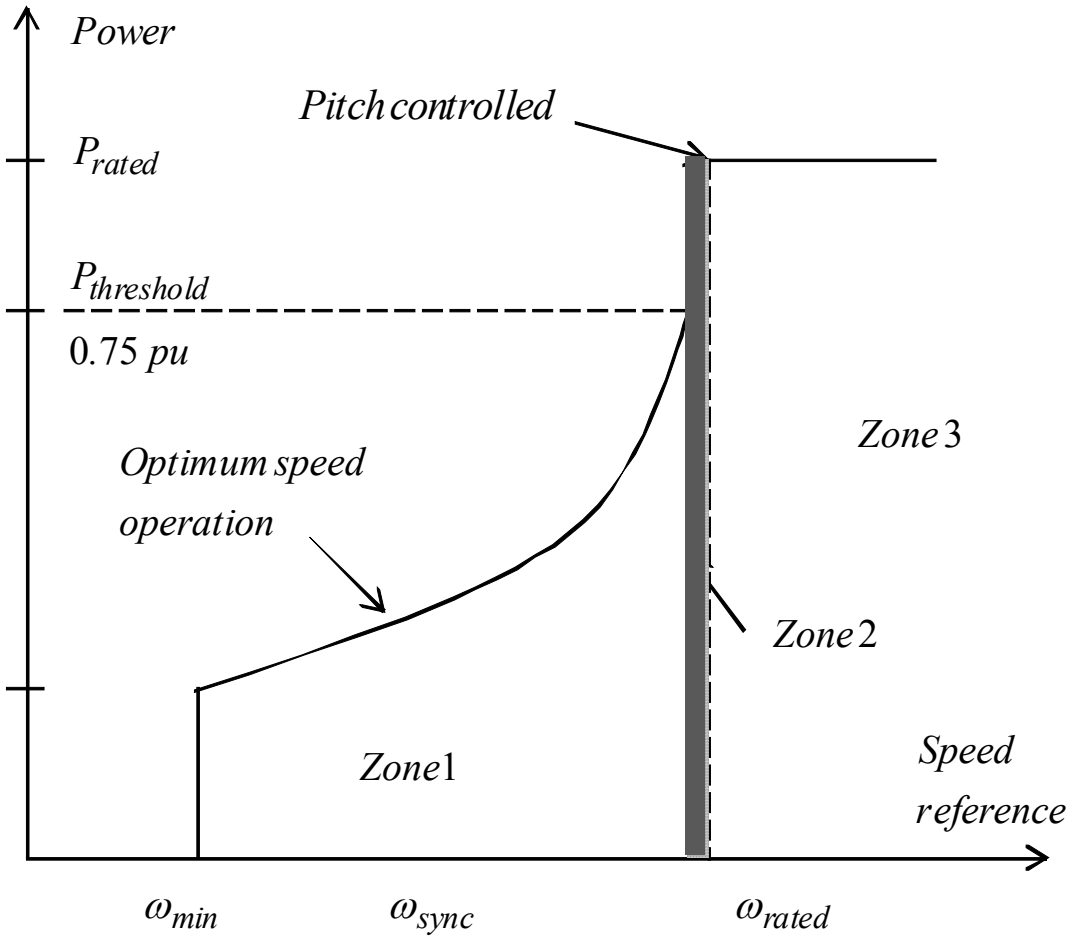

Figure 20: Power vs Speed reference curve.

The controller is operated across three different zones: low, intermediate and high wind speed zones (see Figure 20). In zone 1, with low wind speed, the system is operated at optimal rotor speed according to rotor aerodynamics in order to extract the maximum energy from the wind. In zone 2, with intermediate wind speed (below the nominal wind speed) the rotor speed is limited by a high slope ramp, to prevent a sudden discontinuity in the power set point between the zones 1 and 3. In zone 3, the wind speed is now high enough to allow nominal power production. In this zone we want to maintain the rotor speed and the produced power at their nominal values.

In zone 2 to prevent adverse interactions between the power control and speed control the following control strategy is used. An available mechanical power threshold

of 0.75 pu, determined by the limit of optimal energy extraction, switches from the optimal energy extraction mode to the high wind speed mode with little variation in the rotor speed. The reference speed is kept constant for operation at nominal slip and for power level above power threshold. In this condition the pitch control limits the output power to the rated power.

The reference speed is reduced for power levels below power threshold; it tracks the power changes to produce optimal energy extraction. In this condition the speed control is realized by means of the torque control and the output power order is sent to the converter control. When the available mechanical power is less than the rated power, the wind is below nominal wind, the pitch angle adopts the minimum value to optimize the mechanical power.

The torque PI controller has upper and lower torque limits to give constant power operation above rated power, and to track the optimum C_p curve when operating between the upper and lower speed limits.

The controller design is shown in Figure 21 for MEVA, PSS/E and DEMTP models. The torque control uses the speed error as input to a PI controller with anti-windup on the power limits. The torque limitations are according to the power limitations.

The active power order is the result of the torque control output by the rotor speed. This power is filtered by a low pass filter and limited by its rated value and the power rate limits, both operations are done by the washout filter. These limitations are according the physical limits of the generator.

This active power with rate limit is named P_{inp}. It is an input of the pitch compensator and participates in the input of the washout filter. These washout filters serve to attenuate the low frequencies of the input signal that cause the output signal to reach its limits, while keeping the high frequency of the input signal unchanged.

The overshoot is used as input signal to the washout. It is obtained by the difference between P_{inp} and P_{inp} limited in magnitude. When the input signal has only

low frequency components, like in steady state conditions, the washout output will be null and P_{ord} will be equal to P_{inp} limited in its magnitude. During a transient, the input signal will have a high frequency component; this high frequency will be kept unchanged by the washout filter which results in an acceleration of the response without limit violation.

The high frequency governs the response during a transient, but individual components of high frequency are of short duration; thus avoiding reaching the limits.

The power order P_{ord} is the combination of the output from the washout filter with P_{inp} limited in its magnitude.

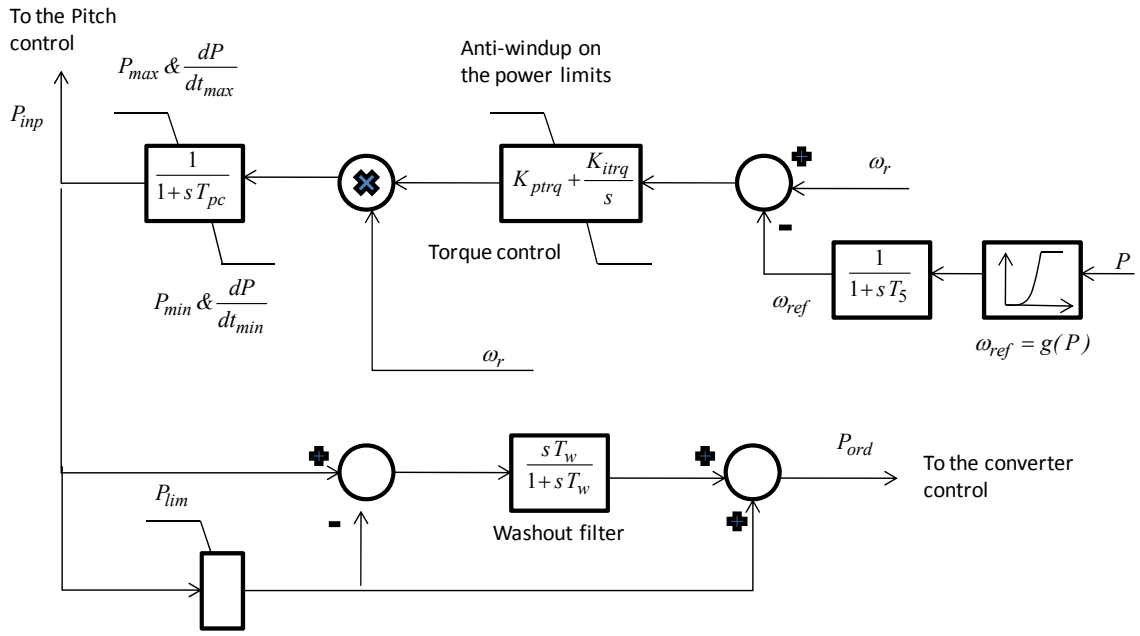

Figure 21: Torque Control/Power order for MEVA, PSS/E and DEMTP

In the Figure 21, T_{pc} is the time constant of the low pas filter of the power regulator; K_{ptrq} is the proportional gain in the torque control; K_{itrq} is the integral gain in the torque control; P_{max} is the maximum limit of the power regulator; P_{min} is the

minimum limit of the power regulator; $\frac{dP}{dt_{max}}$ is the maximum power rate limit; $\frac{dP}{dt_{min}}$ is the minimum power rate limit; T_w is the washout filter time constant; T_5 is the low pass filter time constant used by the ω_{ref} when tracking the power changes in the mode of optimal energy extraction; the table function (curve) $\omega_{ref} = g(P)$ tracks the P variation to update the reference rotor speed, P is the output active power. The curve is obtained from the manufacturer test of the turbine running at slow speed.

The input current i_p in Figure 19 is obtained by dividing the power P_{ord} by the terminal voltage magnitude. The current is limited by a maximum value.

2.7 Reactive power control for PSS/E, MEVA and DEMTP

The DFIG may exchange reactive power with the grid as shown in equation (2.87). The limit in the reactive power exchange is imposed by the converter capability. Based on the converter current limit, the unitary power factor operation of the DFIG is a way to reduce the converter current to only the active component. In some other designs the reactive power contribution to the grid is a constant quantity. The reactive power value is fixed manually in the field by the manufacturer to reach the terminal voltage level without overloading the converter. Additional shunt compensation may be necessary in some cases.

The grid access code elaborated by utilities, does not distinguish the requirement levels between conventional thermal generation and wind generation. Both voltage control and power factor control are required at the interconnection point. If a wind park is not able to perform according to utility requirements, the solution is the application of FACTs devices at the interconnection point. Some manufacturers have a DFIG design with voltage control that permits to control the power factor as in a conventional generator.

The full converter design has more capabilities for exchanging reactive power with the grid. The size of the converter is bigger than in the DFIG case. It is designed to

handle the full generator power through the converter. The full converter, contrary to DFIG, permits zero power operation controlling the voltage at the interconnection point. Its elaborate current limiter limits the active current component permitting the reactive current component to rise to a desired power factor value at the interconnection point.

The reactive power controller of Figure 22, has two inputs: terminal voltage and generated reactive power. The controller output is the voltage E_q'' which is proportional to the reactive power generation. Finally the input current i_q in the Figure 19, is obtained by dividing E_q'' by the transient reactance of the machine.

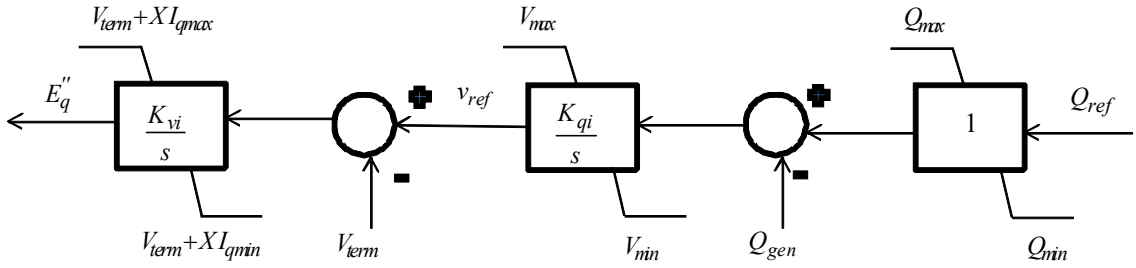

Figure 22: Reactive Control model

The value of Q_{ref} in Figure 22 is calculated from the load-flow condition, it remains constant during time-domain simulations. The reactive power limits are set according the converter limits. The error of reactive power, difference between Q_{ref} and the instantaneous value of the reactive power Q_{gen}, is integrated to update the voltage reference. The error on voltage, difference between the v_{ref} and V_{term}, is integrated to result into the output voltage E_q''. The voltage limits are set according to the grid interconnection code. The limiter operation presents different limits during the fault and steady-state condition. This effect is equivalent to having two different voltage gains K_{vi}, a high limit during faults and zero for steady-state conditions.

When a high value of K_{vi} is kept during all operating conditions, it may result into an oscillatory recovery voltage after a fault condition. When a low value of K_{vi} is kept during all operating conditions, it results into a slow and low recovery voltage after a fault. Voltage collapse may occur if the voltage level is too low.

In the Figure 22, Q_{max} is maximum reactive power limit in the controller, Q_{min} is minimum reactive power limit in the controller, V_{max} is maximum voltage limit in the controller, V_{min} is minimum voltage limit in the controller, K_{vi} is voltage integrator gain, K_{qi} is the reactive power integrator gain, $X I_{q\,max}$ is the maximum limit with zero terminal voltage, $X I_{q\,min}$ is the minimum limit with zero terminal voltage and v_{term} is the terminal voltage.

2.8 Protection system for PSS/E, MEVA and DEMTP

Three relays are used to protect the wind turbine generator, under/over frequency protection, under/over voltage protection and crowbar protection. The crowbar protection will be described only in the DEMTP modeling approach since it can be directly represented only in such a model.

The under/over frequency and under/over voltage relays are protection models, that are located at the generator bus. In this way the WTG frequency and voltage are continuously monitored to send the trip signal to the breaker during an under- or over-frequency/voltage condition.

These relays disconnect individual WTGs and each WTG has its own protection system.

Both frequency and voltage relays are threshold relays. This is explained in Figure 23. The operation is based on the monitoring of an electrical variable which is compared with a threshold. When the excursion of the electrical variable remains under the threshold for a duration greater than the pickup time, then after a step time delay, a trip signal will be sent to the breaker that will trip the generator. The breaker acting delay is

also included. If the excursion of an electrical variable remains below the pickup time no trip signal is sent to the breaker.

Four relay models are included as delivered in this work:

- the under voltage relay named LOVOLT;
- the overvoltage relay named HIVOLT;
- the under frequency relay named LOFREQl;
- the over frequency relay named HIFREQ.

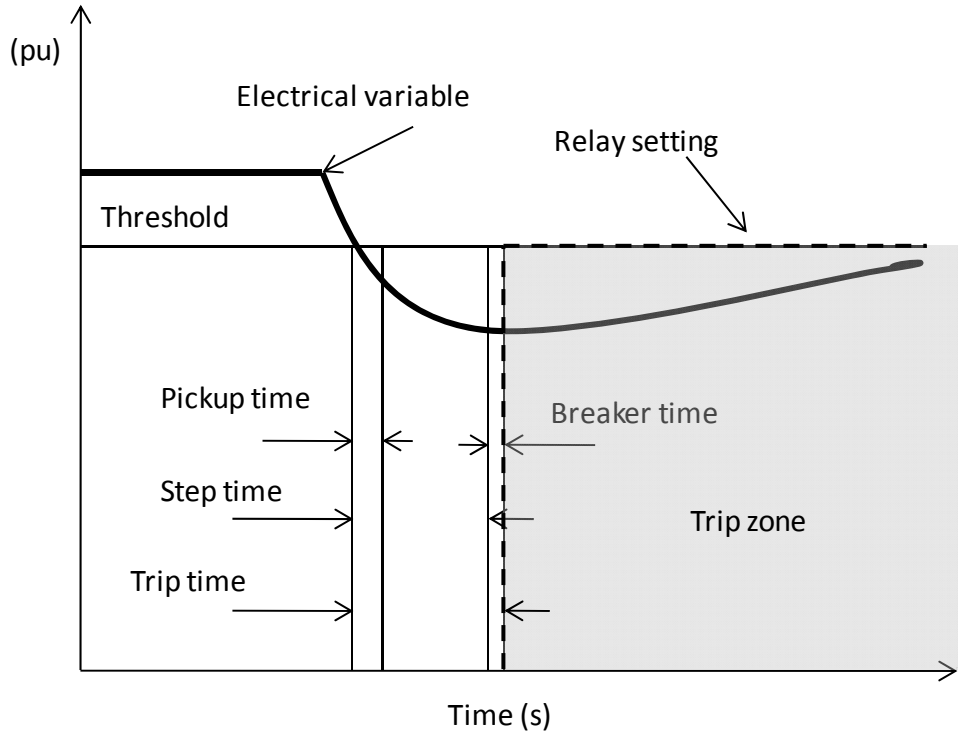

Figure 23: Threshold relay

The settings of relays used in this document are taken from **[20]** and shown in Figure 24 and Figure 25. Both figures include a ride through zone and a trip zone. In the ride through zone the wind turbine generator must have the ability to remain connected to the grid during a transient condition that placed the electrical variable inside the ride through zone. Outside the ride through zone the wind generator has the right to be disconnected from the grid.

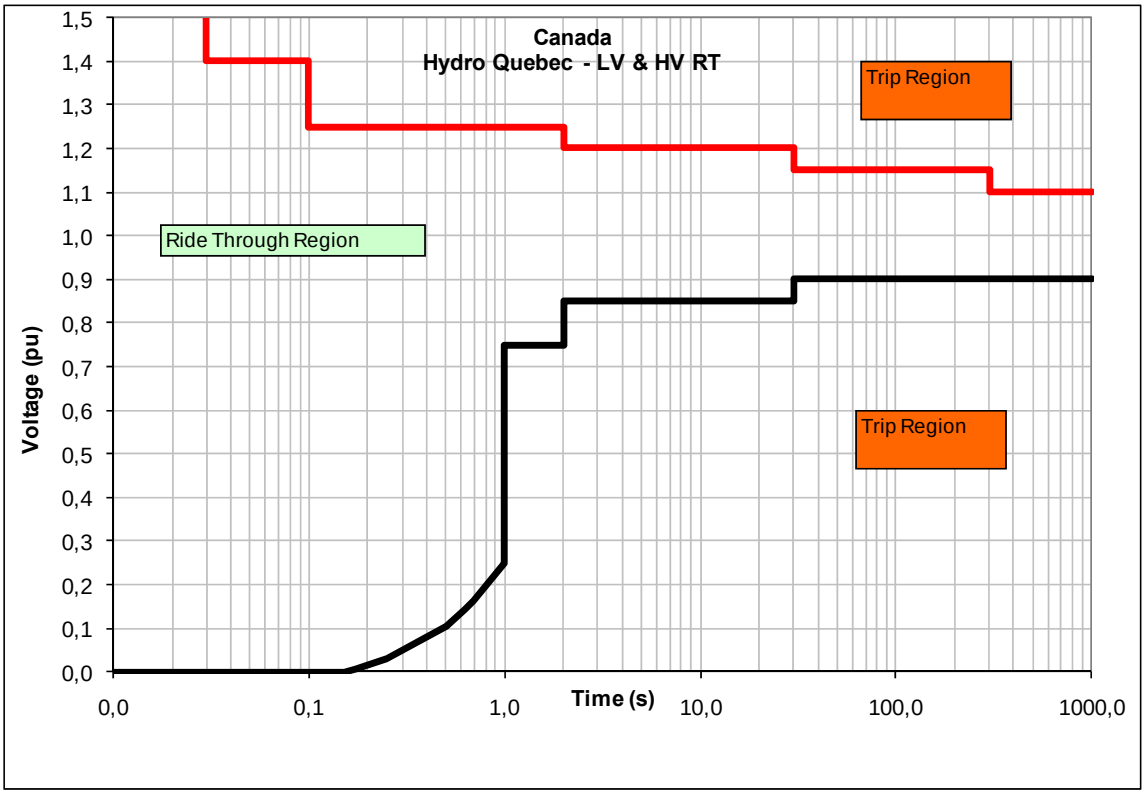

Figure 24: Under/Over Voltage protection

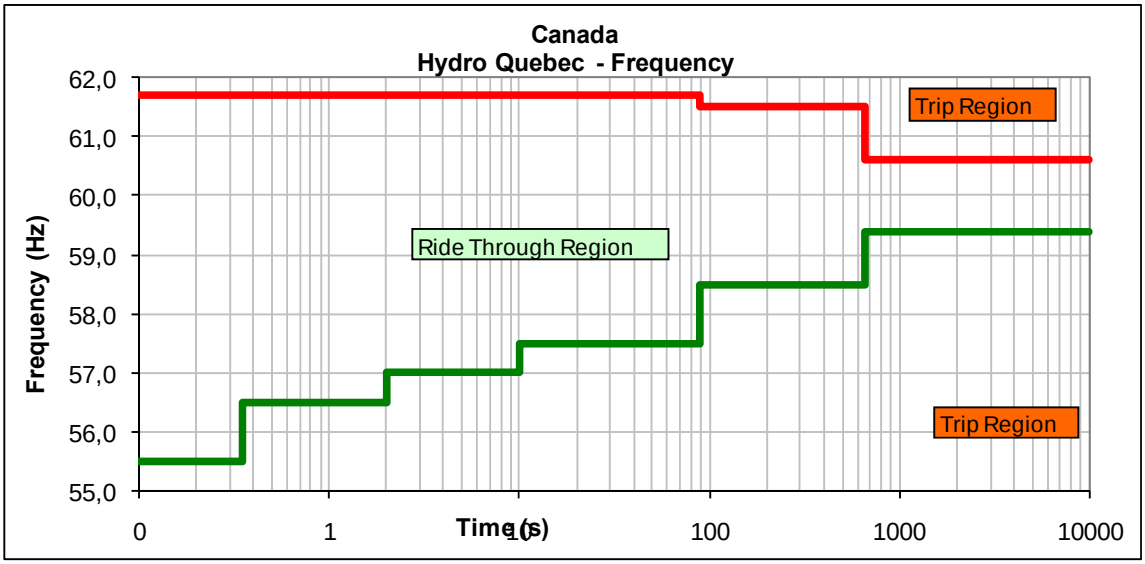

Figure 25: Under/Over Frequency protection

2.9 Initialization step for PSS/E and MEVA models

An important step in all WTG simulations is the initialization step. In both PSS/E and MEVA models the related packages provide load-flow solution capability which must be used to initialize the time-domain simulation. If the initialization process is not done correctly, the computational time may increase dramatically before the steady-state is reached. Moreover, in some cases, the time-domain solution may lead into erroneous on undesirable steady-state conditions.

The electrical initialization of the converter/generator block was presented for PSS/E and MEVA models in the section 2.5.3.

For DEMTP modelling, initialization procedures will be presented in CHAPTER 5.

This section presents initialization for mechanical variables for DFIG and FC models.

From the wind speed, it is necessary to calculate the initial state of the control blocks related to the pitch angle and the angular twist of the shaft model (see Figure 16 and equations (2.94)-(2.98)).

There are two options. In the first option, power allocation is determined directly by the load-flow solution. In the second option the initial input data is wind speed. Both options use the power output vs wind speed typical curve provided by the manufacturer.

During the initialization stage and the first simulation second the wind speed is considered as constant.

The initial wind speed has to verify the mechanical power produced by the turbine P_w (1.1) which is equal to the active power found in the load-flow solution P.

$$P_w = P \tag{2.136}$$

The more direct way to determine the initial wind speed is by means of the power vs wind speed curve as in Figure 26. Such curves are normally provided by the manufacturer.

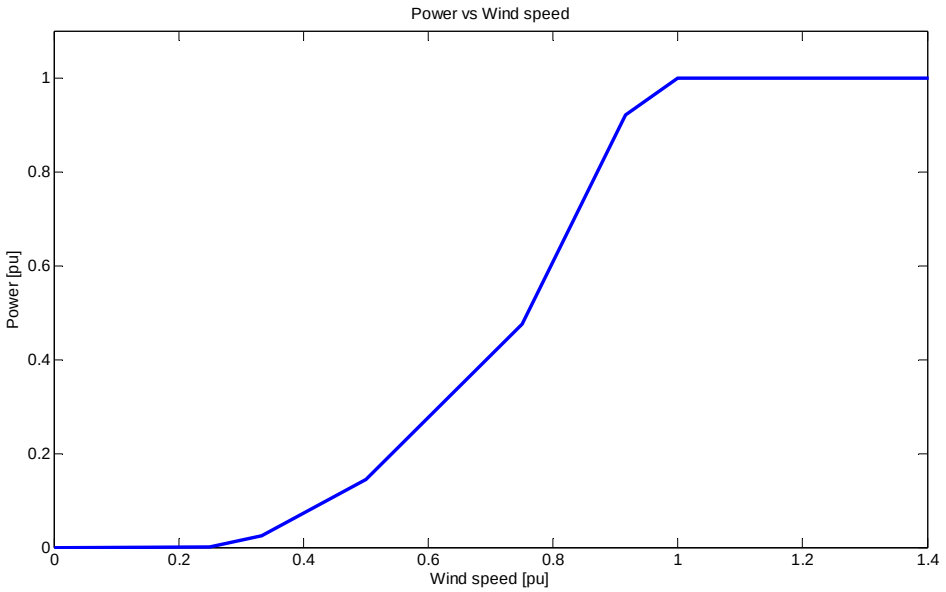

Figure 26: Power vs wind speed (typical manufacturer data)

If P is known from the load-flow solution then the curve of Figure 26 gives the initial wind speed. The following component to be initialized is the shaft model.

In steady-state conditions it is possible to write (see equations (2.94)-(2.98))

$$T_{m2} = T_{gen} = T_{m12} = K_{m12}(\theta_{m2} - \theta_{m1}) \tag{2.137}$$

Where T_{m2} is the mechanical torque of turbine, T_{m12} is the transmitted mechanical torque and T_{gen} is the electromagnetic, $(\theta_{m2} - \theta_{m1})$ is the difference of the angular positions between the two mass, K_{m12} is the stiffness coefficient.

To determine the initial torque and the initial twist angle we need to first solve for the rotor speed and the synchronous speed using the curve output power vs rotor speed shown in Figure 27.

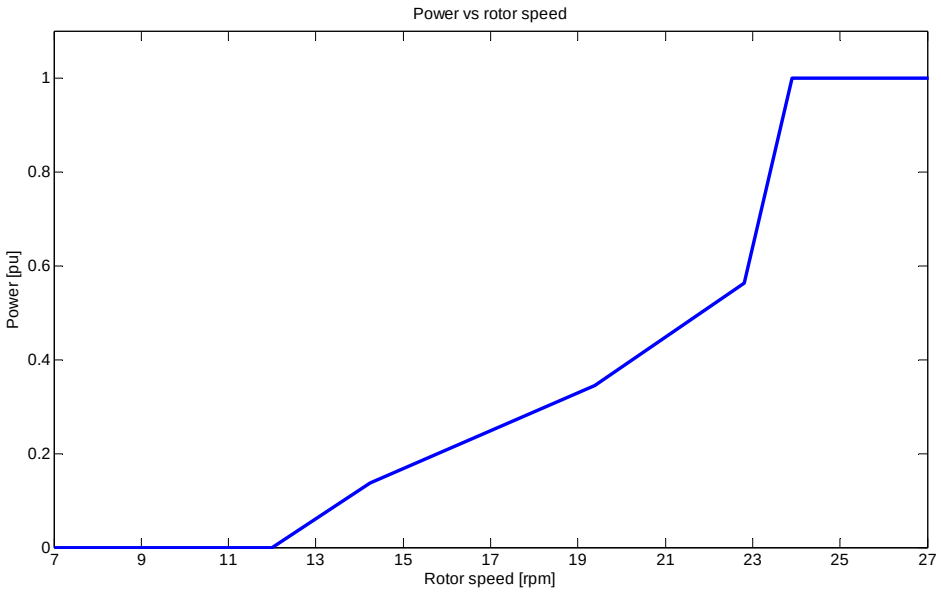

Figure 27: Power vs rotor speed (rpm), (typical manufacturer data)

From the RPM (rotations per minute) speed

$$\omega_{m2} = \frac{\omega_{m2_{rpm}} 2\pi}{60} \tag{2.138}$$

$$\omega_s = \frac{60\, f}{P_p\, GBR} \tag{2.139}$$

$$s = \frac{\omega_s - \omega_{m2}}{\omega_s} \tag{2.140}$$

$$T_{gen} = \frac{P}{1-s} \tag{2.141}$$

$$\theta_{m2} - \theta_{m1} = \frac{T_{gen}}{K_{m12}} \tag{2.142}$$

where P_p is the number of pole pairs, GBR is the gear box ratio, ω_{m2} mechanical speed, ω_s synchronous speed, s is initial slip, $(\theta_{m2} - \theta_{m1})$ is initial twist angle.

The pitch angle is found using the iterative process described in section 2.1.3.

CHAPTER 3. PSS/E model, DFIG

This chapter describes the simulation model of a DFIG of 1.5 MW. It is a generic model used in the evaluation of wind power impact on power systems, see also [21].

The implementation of this model in the PSS/E software is related to the available numerical methods, options and limitations. It is a complex task. The simulation is performed in two steps: first the load-flow, then the dynamic simulations.

This model is for positive sequence studies of electromechanical transients. It is not suitable for fast transients. As previously explained, fast dynamics have been simplified or eliminated from model equations. To include this model into the PSS/E environment, it is necessary to develop two programs written in languages supported in PSS/E. These languages (program modules) are FLEX and IPLAN. Differential equations are written using FLEX (it resembles FORTRAN) and IPLAN is used for various preparation procedures and automations in studies. It includes all input and output management functions.

In addition to the solution of differential equations, the FLEX program calculates all variables and prepares the necessary updates during the time domain simulations.

The FLEX module includes a function that generates the wind input perturbations as shown in Figure 9. The model of the turbine is represented by the equation (1.1) with a C_p function of the turbine rotor speed, the pitch angle and its geometry that verifies the information of the manufacturer (see section 2.1.2.2. and Figure 2).

The representation of pitch control is shown in Figure 12, torque control is conformal to Figure 21, the reactive power control is from Figure 22 and the protection functions are presented in Figure 24 and Figure 25. The converter generator model is shown in the Figure 19 and the PLL model will be described below in the following section 3.1.2.

The complete model block diagrams are shown in Figure 28 part 1 and Figure 29 part 2.

The drive train model described by equations (2.95)-(2.98) includes the option of single and double mass modeling.

The model setup through IPLAN offers to allocate power using wind speed or load flow solution. The allocation may be based on an unlimited number of generators, as in a full scale wind park.

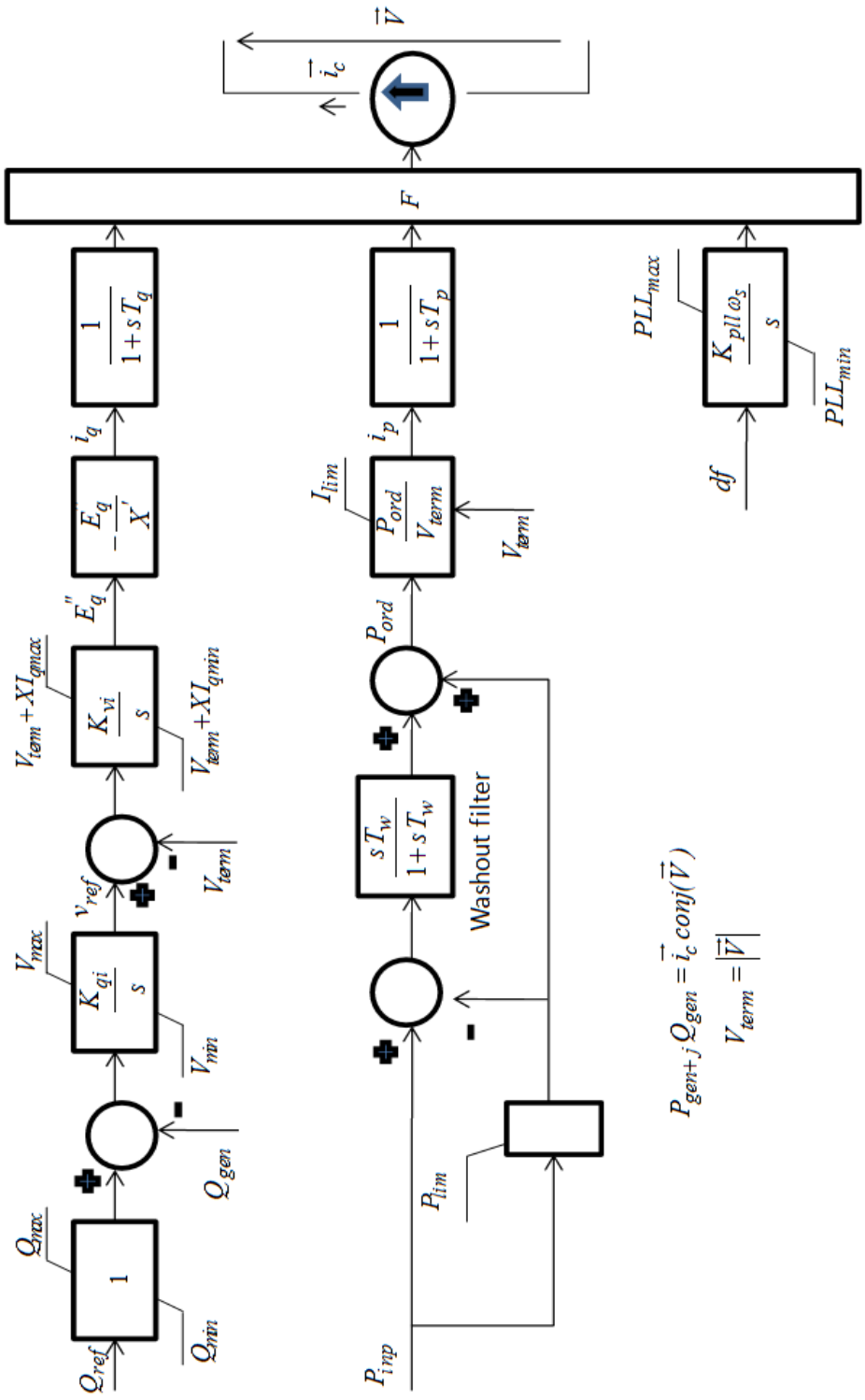

Figure 28: PSS/E DFIG block diagram (Part 1)

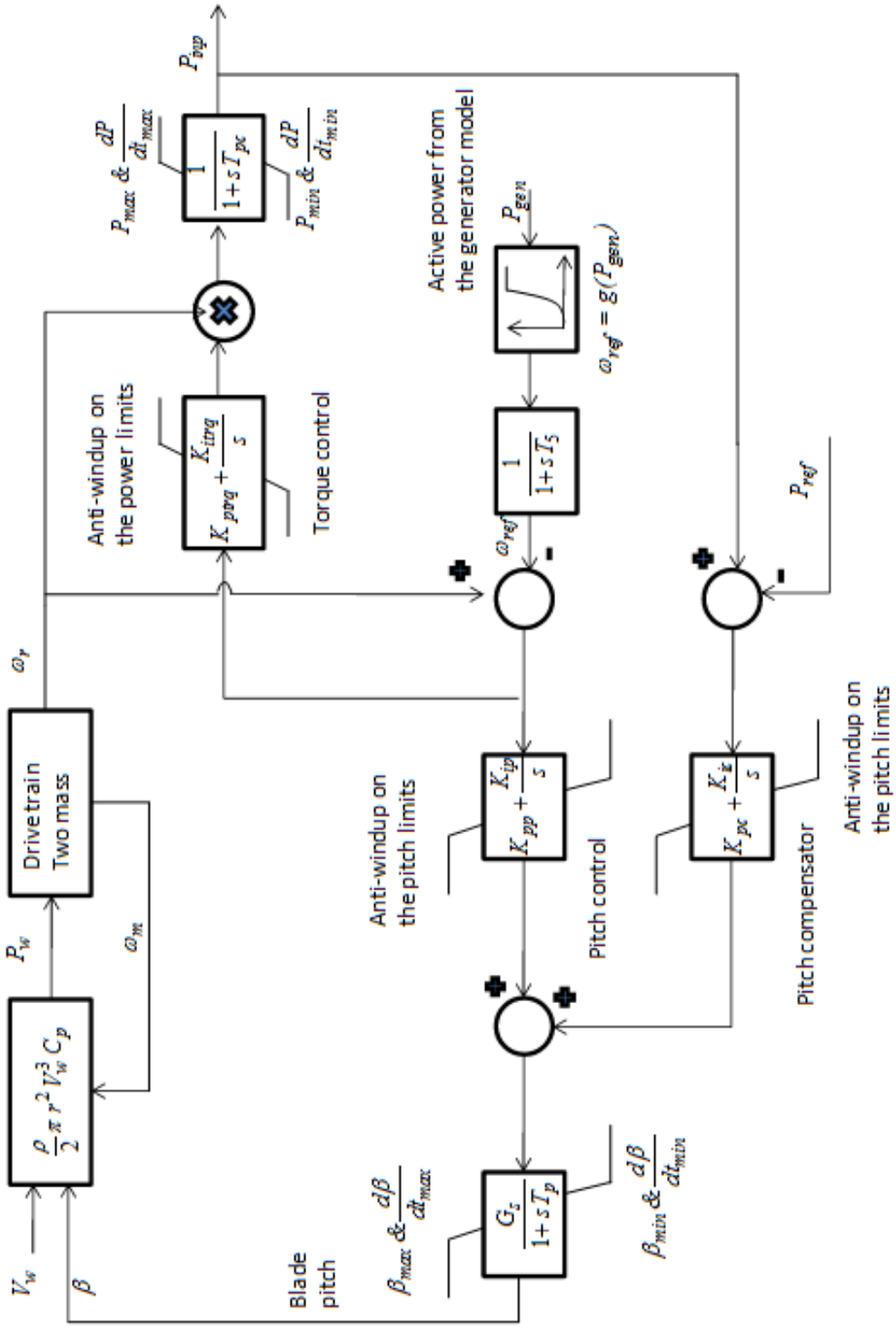

Figure 29: PSS/E DFIG block diagram (Part 2)

3.1 Phase-locked loop (PLL) for PSS/E, MEVA and DEMTP

The DFIG (and FC) models have converter controls based on a phase-locked loop. The phase-locked loop in the DFIG synchronizes the generator rotor with the stator and in the full converter case, the inverter with the grid.

The converter PLL has the effect of establishing a reference frame for the WTG voltages and currents, shown as the D and Q axis in the phasor diagram of Figure 30.

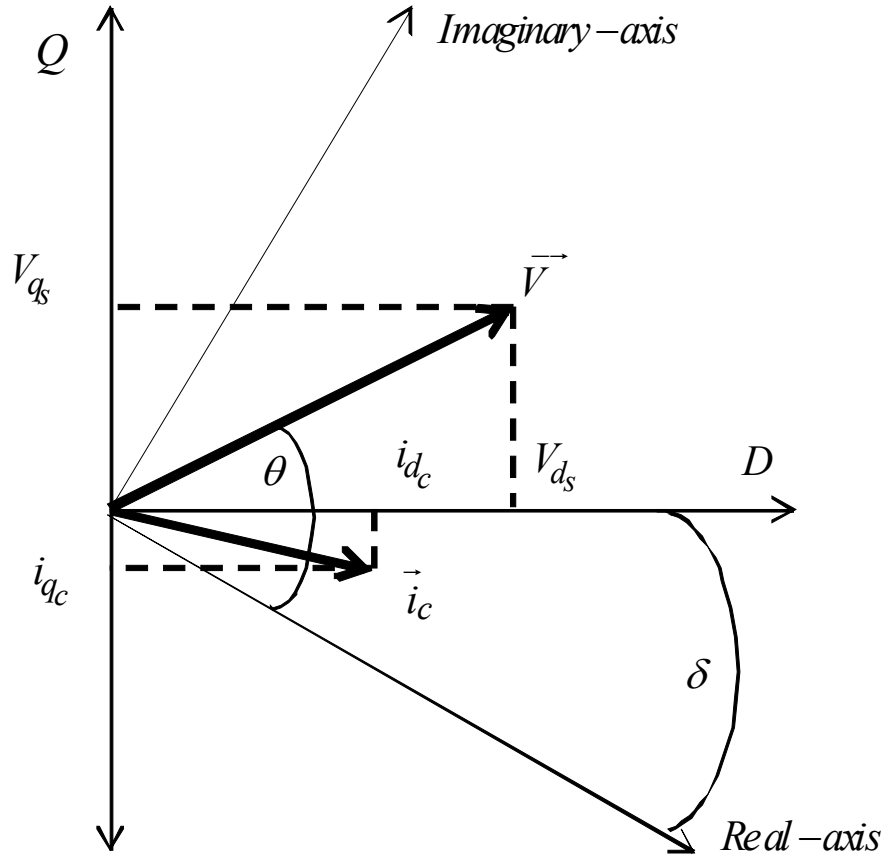

Figure 30: Reference frame

In steady-state conditions, the D-axis is aligned with $\vec{V}$ (see Figure 19), in consequence the phase angles θ and δ are equal. During transients the angle θ can change instantaneously (system disturbances), but the rate of change of δ is limited by the PLL logic.

The maximum voltage is at zero degree and aligned on the d-axis. In this condition

$$\vec{V} = v_{d_s} + j\, v_{q_s} = V + j\, 0 \tag{3.1}$$

$$\vec{i}_c = i_{d_c} - j\, i_{q_c} \tag{3.2}$$

Consequently (see also equation (2.82), (2.113) and (2.131)).

$$P + jQ = v_{d_s}\left(i_{d_s} + j\, i_{q_s}\right) = V\, i_{d_s} + j V\, i_{q_s} \tag{3.3}$$

With this definition, the current $i_p = i_{ds}$ controls the active power output, while the current $i_q = i_{q_s}$ controls the reactive power output.

3.1.1 PLL implementation in PSS/E

The phase variation in synchronous machine is obtained using the integral of the machine speed deviation, so it is related to the mechanical equations of the machine, (2.94) and (2.95).

In grids with only conventional generators with prime mover controlling their speeds, the phase angle deviation may be calculated from the speed variation (2.94) and the machine pair of poles. In this case the dynamic responses of the speed deviation and the phase angle deviation are influenced by the inertia of the machine and the speed response of the prime mover found on the mechanical power.

Many assumptions commonly used in stability type programs, such as PSS/E, are becoming less valid with the presence of power electronics in power systems. The more relevant assumptions in relation with wind generation are: the stator flux distribution is considered always sinusoidal, the iron losses and part of the copper losses are neglected, stator voltage and current are sinusoidal at the fundamental frequency, and the magnetic saturations of transformer and asynchronous machine are neglected. When the wind generation includes a power electronic converter it is considered as a linear device, such as its behavior at rated condition is extended to the fault condition. The only frequency present in the rotor current of the asynchronous machine is given the product of the slip

by the nominal frequency and the variation of machine flux is neglected due to the fast control action of the electronic switching devices.

In the case of wind generation the way to remain in synchronism with the grid is by means of a PLL. The PLL is an electronic device available to calculate the terminal voltage phase angle. As a first approach to the PLL model in PSS/E, the frequency deviation of the grid is calculated using an internal PSS/E function named BSFREQ. The BSFREQ function calculates the frequency deviation at each bus of the network. Thus the frequency deviation df of the grid is translated into a phase angle modification in the current source (see Figure 19). The last step is using an integrator circuit combined with a limiter to avoid the jumps. The block diagram of the generator-converter model of Figure 19 includes this first PLL model.

A second approach, shown in Figure 31 is inspired from the detailed PLL model used in EMTP-RV. It presents a PLL based on the DQ frame theory. The instantaneous to polar transformation uses as input the RMS value of the terminal voltage. The polar output is rotated and the imaginary component of the phasor (equivalent to the Q component) is calculated to become the input of the PI controller. The PI controller output is proportional to the frequency deviation, which is integrated and scaled to give the phase angle δ of Figure 30.

The variables used in Figure 31 are defined as follows:

δ_t is the PLL phase angle at the instant t,

δ_{t-1} is the PLL phase angle at the instant t-1,

θ is instantaneous phase angle of the terminal voltage,

K_{pll} is the integral gain of the PLL in pu,

PLL_{max} is the maximum limit of the PLL in pu,

PLL_{min} is the minimum limit of the PLL in pu,

ω_s is the electrical frequency in rad/s.

The phase angle δ defines the stationary position of D axis relative to the real axis. Both angles θ and δ are equal in steady-state conditions, but during transients the angle θ can change instantaneously. After the transient the PLL must align the terminal voltage phasor with the D-axis to verify equation (3.1) and supply the active and reactive powers given by equation (3.3). The way to reach this objective is by nullifying the Q component of the terminal voltage (3.1).

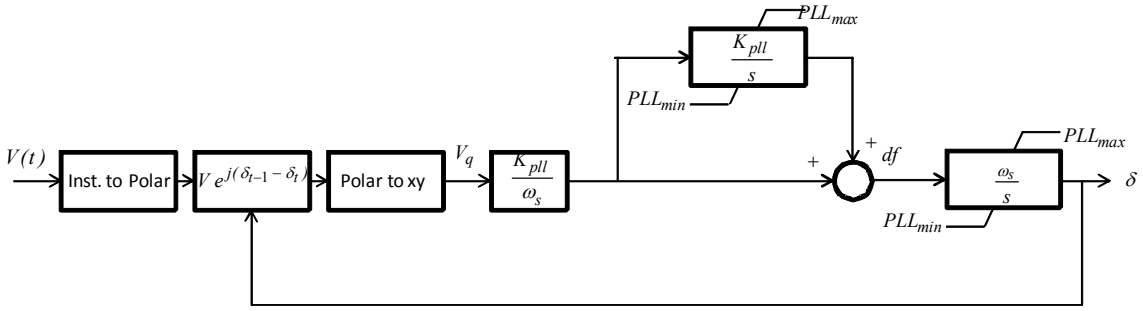

Figure 31: PLL dq0 in PSS/E

3.1.2 PLL problems and solutions in PSS/E

In both of the above PLL models implemented in PSS/E, the problem is the lack of ability to track the correct phase angle during transient events present in large transmission systems, such as loss of dynamic stability or tripping of high voltage lines.

To understand the wrong PLL behaviour, let us consider a large transmission system after a fault. It is known that when the power system stability is reached without load shedding or machine tripping, the active power output of each machine of the system should remain at the dispatch value as a consequence of the combined actions of the prime mover and excitation systems.

In the wind generation case, the synchronization with the grid is produced by PLL action. With a wrong phase voltage angle, still with the correct value of the current control, the active power output will be wrong. In consequence when the large transmission scenario includes wind power and the PLL of the WTG has a wrong operation, two problems occur, in the first one the WTG increases or decreases the active power output without modification in the mechanical power input and in the

second one the active power mismatch produced by the WTG is absorbed by the conventional system machines.

To evaluate the impact of a transient event on the PLL behavior lest us define an active power difference ΔP as the mismatch between the initial steady state and the final state. The Figure 32 and Figure 33 show important mismatches with ΔP of 20 and 29% respectively. These mismatches were caused by a jump of phase angle. The first jump of phase was caused by a far three-phase-fault followed by a trip of line. The second jump is caused by a swing of the equivalent generator after a 6 cycle three-phase-fault near a far hydro plant.

The phase mismatch results from the combination of two factors, the usage of a simplified version of the PLL and the typically large integration time-step used in PSS/E, typically half cycle of the fundamental system period.

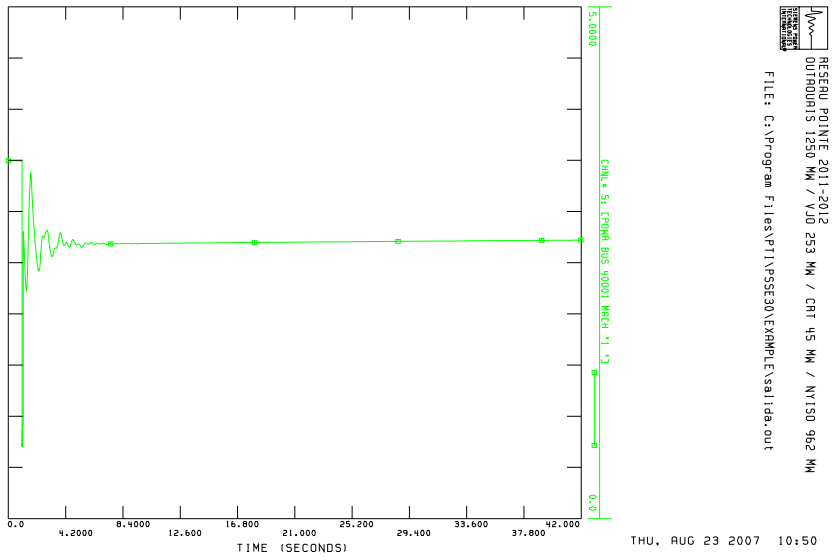

Figure 32: 3-phase fault and line trip case, active power output of WTG, ΔP =20%

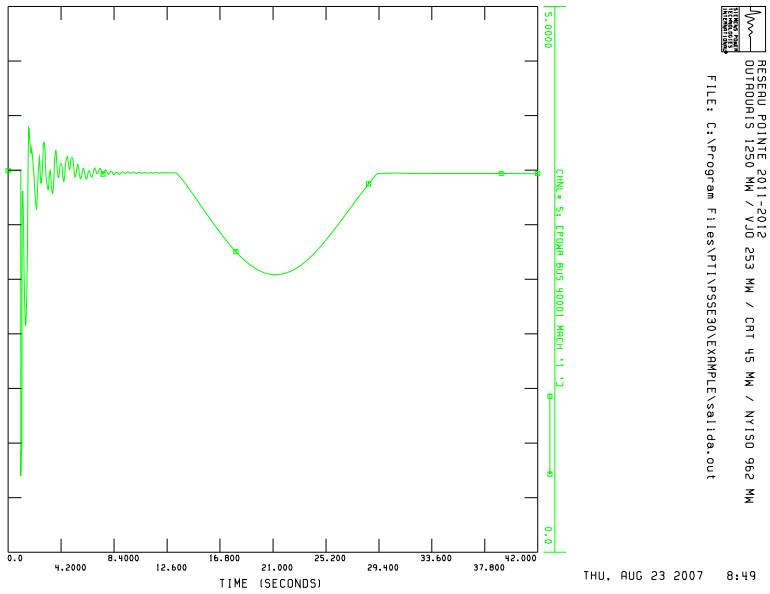

Figure 33: Active power output of WTG, with jump of phase, ΔP =29%

The solution proposed in this work is a PLL based in the correction of the phase angle using an instantaneous logic dependent on the active power. This strategy is based on the concept used in the representation of power electronics, where the fast dynamics may be represented as algebraic equations or on/off logic and that the slow dynamics may be represented by the motion equation. Thus the solution of the problem is a PLL model that combines both concepts.

The primitive PLL representation in PSS/E was based on the principle of integration of the bus frequency deviation (df) obtained from the internal PSS/E function BSFREQ. That is done by means of the knowledge of the index associated to the bus number. The instantaneous variation is obtained after a low pass filter with a time constant defined in the PSS/E parameters.

Based on the testing of various cases, two different behaviors were found to limit the application of the internal function BSFREQ. When wind gust speed variation is simulated, the frequency deviation remains limited, below 0.1 Hz, and no phase error was produced. On the other hand, the three phase-fault case followed by the trip of a line

produces instability of the terminal voltage and phase angle, with large phase error and terminal voltage oscillations in the WTG. Using a logic to detect these two situations, it is possible to decide when the phase angle correction is necessary.

The logic will be enabled as a combination of voltage level and $\left|\frac{df}{dt}\right|$ used to distinguish the far fault condition. The enabling condition can be set to generator voltage over 0.7 pu and a $\left|\frac{df}{dt}\right|$ greater than 0.1 pu and stops when any one of these two conditions are not reached. The process lasts 300 ms (empirical value used for most cases) or stops if the output power reaches the minimum error condition, with a tolerance of 1%.

Considering the power transmission through a reactance X, the phase angle must increase or decrease according to the target variation of the output active power as follows

$$V_s = E_s \angle \theta_s \tag{3.4}$$

$$V_r = E_r \angle \theta_r \tag{3.5}$$

$$P_s = Real\left(\frac{E_s^{\,2} - E_s\, E_r \angle \theta_s - \theta_r}{-jX}\right) \tag{3.6}$$

$$P_s = \frac{E_s . E_r}{X} cos\left(\theta_s - \theta_r + \frac{\pi}{2}\right) \tag{3.7}$$

$$P_s = \frac{E_s . E_r}{X} sin(\theta_s - \theta_r) \tag{3.8}$$

Let us define $P_{old} = P_s$, initial steady state value of active power and the tolerance ε ,

$$P_{max} = (1+\varepsilon) P_{old} \tag{3.9}$$

$$P_{min} = (1-\varepsilon) P_{old} \tag{3.10}$$

After a perturbation the instantaneous active power output is P and considering a $\Delta\theta_s > 0$, if $P_{min} \le P \le P_{max}$ no additional phase compensation is needed. If $P \le P_{min}$

$$P_{new} = \frac{E_s . E_r}{X} sin(\theta_s + \Delta\theta_s - \theta_r) \rightarrow P \leq P_{new} \quad (3.11)$$

If $P \geq P_{max}$:

$$P_{new} = \frac{E_s . E_r}{X} sin(\theta_s - \Delta\theta_s - \theta_r) \rightarrow P \leq P_{new} \quad (3.12)$$

If the active power is lower than the accepted minimum value then the phase angle must be increased using a ramp function. If the active power is greater than the maximum value then the phase angle must be decreased by a ramp function.

The process is detailed below:

1) calculate the phase variation using only the BSFREQ function;

2) compare the output active power with the tolerance range

3) phase compensation:

if the output active power is in the range no correction is necessary,

if the output active power is lower than the minimum value then the phase variation is increased by a constant value,

if the output active power is greater than the maximum value then the phase variation is decreased by a constant value.

4) the phase variation is limited between PLL_{min} and PLL_{max} ;

5) the phase variation is integrated to obtain the phase angle.

This process is repeated at each simulation time-point to compensate the phase angle according to the output active power.

The new PLL was used to repeat the simulation shown in the Figure 32. The result is shown in Figure 34.

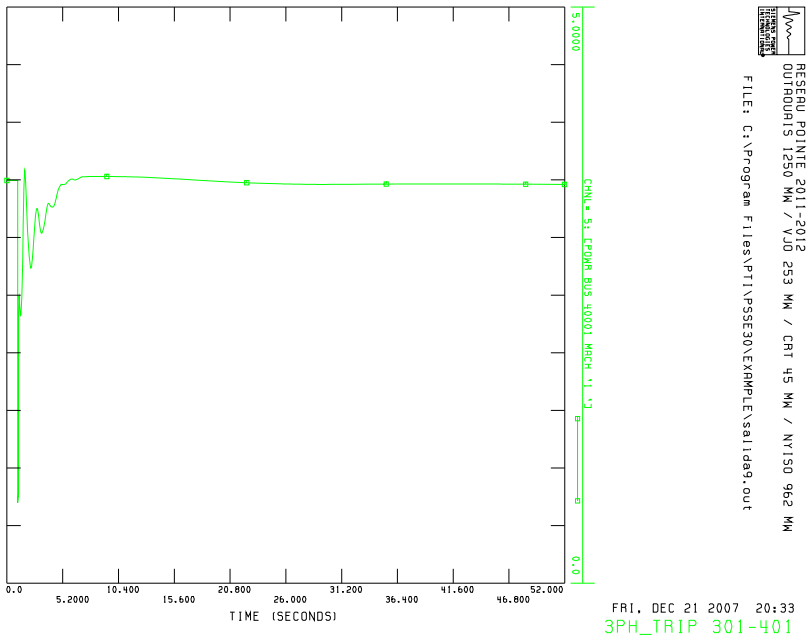

Figure 34: Active power WTG with improved PLL model

3.2 PSS/E DFIG model benchmark

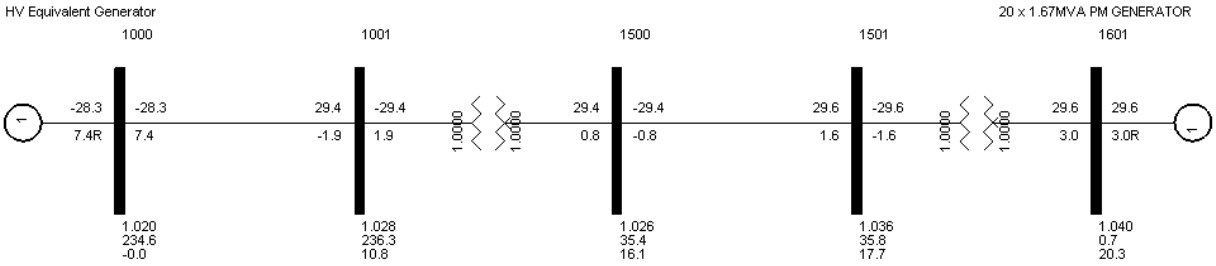

Figure 35: First benchmark, PSS/E DFIG model test

Two benchmarks are used to test the PSS/E DFIG model, the first one is shown in Figure 35 and the second one in Figure 36. The benchmark data files to run load flow and dynamics are in Appendix A. The load flow solutions shown in both figures are used as initial conditions to the time domain simulation.

The first benchmark represents a distribution system of a wind farm section which is connected to the grid equivalent with a short circuit power equal to ten times the wind farm generation. Typical short circuit impedance values are 5.5% for the wind generator transformer, 10% for the step up transformer (high voltage) and 10% for the cable feeder.

The first benchmark was designed to test the control response to a near fault and other local perturbations, such as voltage steps and wind profiles. This benchmark avoids problems present in large transmission systems, such as oscillation modes, loss of dynamic stability or the trip of high voltage lines that may stress the PLL calculation problems outlined in section 3.1.2.

Several types of different perturbations, such as fault, step of reference and wind profiles, were applied on the first benchmark to test the model response using single mass and double mass models for the generator shaft. The Tests 1 to 5 are performed using a single mass for the WTG and the Tests 6 and 7 use a double mass model for the WTG.

The second benchmark shown in Figure 36 (see Appendix A for complete PSS/E data) was used to test the aggregation degree which is described below in Test 8. The aggregation test considers two cases with 500 MW of power generation, the first one with a single machine and the second one with 15 machines.

The following tests are used to validate the performance of the model developed for this thesis. The performance verifies normal behaviour based on experiments on such models and comparisons with detailed models based in EMTP-RV.

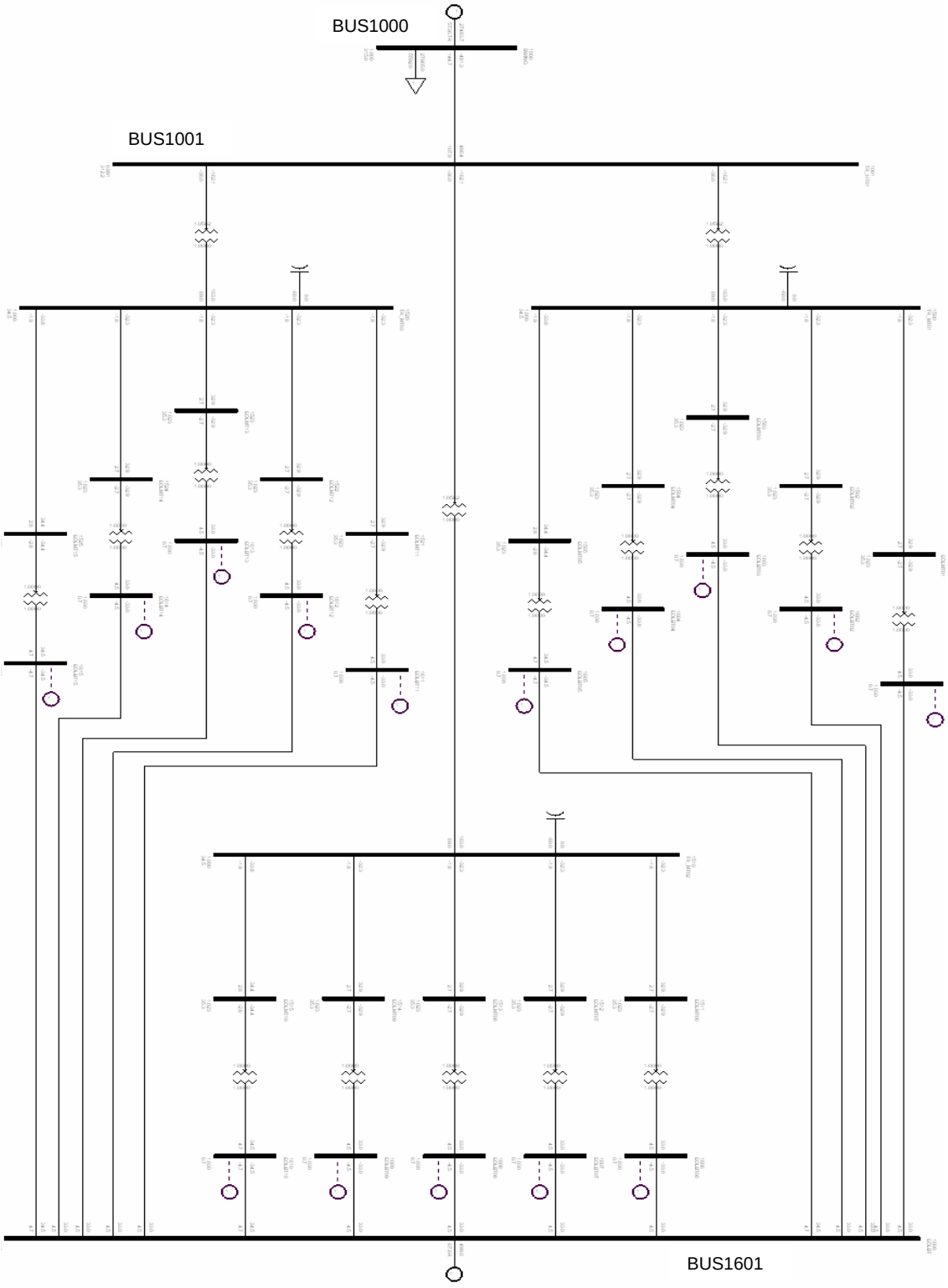

Figure 36: PSS/E DFIG model, aggregation test benchmark

3.2.1.1 Test 1, Small perturbation

The Test 1 consists in the application of a small perturbation. The perturbation is a step change of ±5% on the terminal voltage of the equivalent with the objective of obtaining a linear response of the controls.

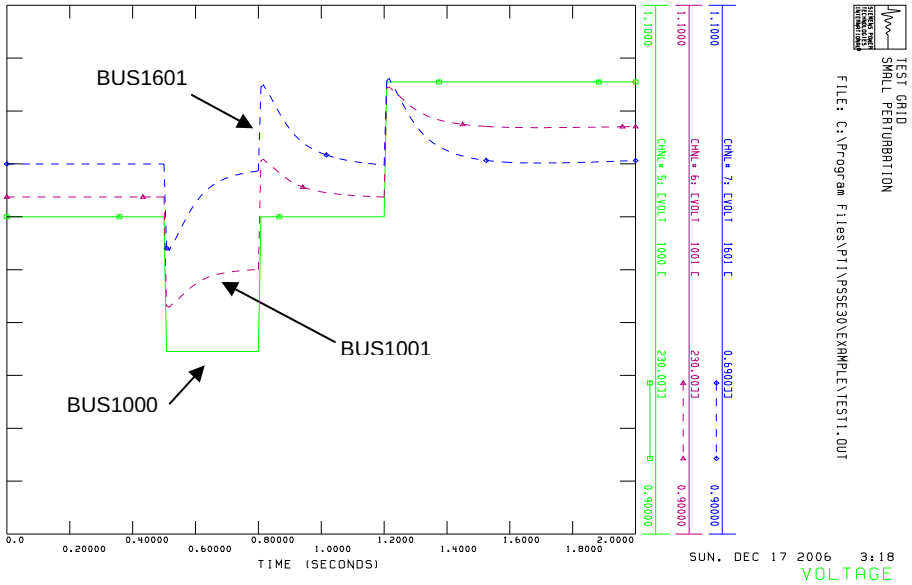

Figure 37: Test 1; Voltage, BUS1000, BUS1001 and BUS1601.

The voltage step was applied to the Grid voltage on BUS1000. At the beginning the WTG terminal voltage (BUS1601) tracks the grid voltage but finally the WTG terminal voltage is controlled at its reference value. The Figure 37 also shows the voltage at the intermediate BUS1001.

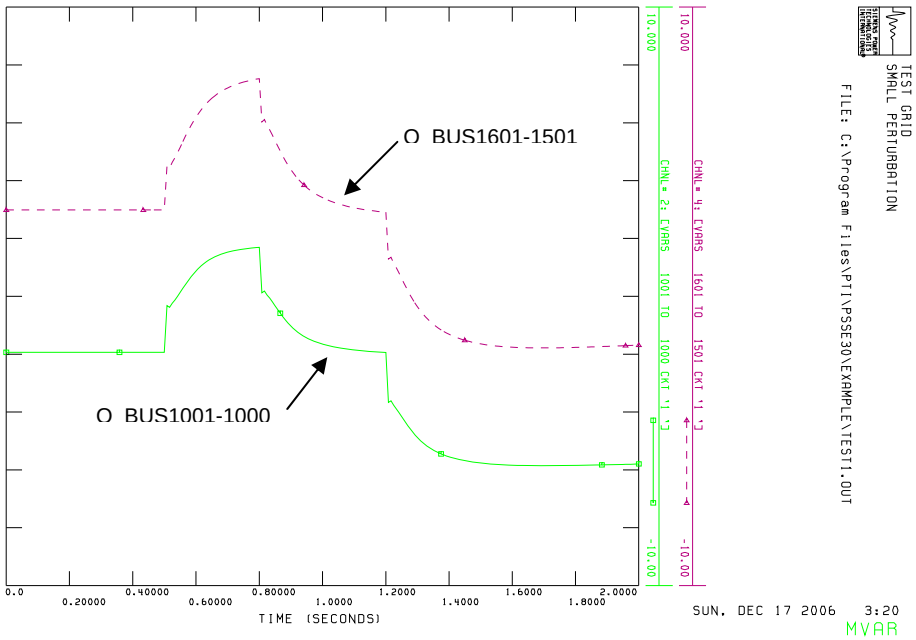

Figure 38: Test 1; Reactive power, BUS1601-BUS1501 and BUS1001-BUS1000.

The Figure 38 shows a voltage step applied to the Grid voltage on BUS1000. The reactive power of the WTG on BUS1601 rises when the voltage step lowers and drops when the voltage step rises, but it does not reach neither the maximum limit nor the minimum limit of the reactive power.

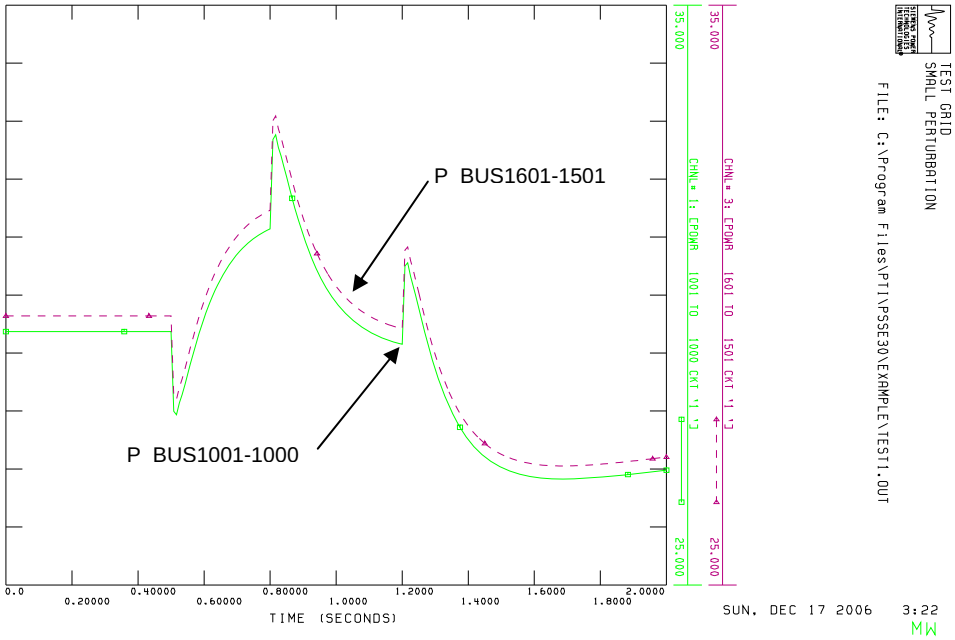

Figure 39: Test 1; Active power, BUS1601-BUS1501 and BUS1001-BUS1000.

The mechanical power remains constant since the wind is constant. In consequence the active power injected by the WTG on the BUS1601 will remain constant in the final steady-state after perturbation. This trend is shown in the Figure 39.

The transient peaks of the active power shown in the Figure 39 are related to the delay introduced by the low pass filter on the controlled current (see Figure 28). The pitch angle remains constant with the step voltage change.

3.2.1.2 Test 2, Large perturbation

The Test 2 is an application of a large perturbation of ±30% on the terminal voltage on BUS1000. The objective is to reach a limit condition on the control. The voltages are shown in Figure 40.

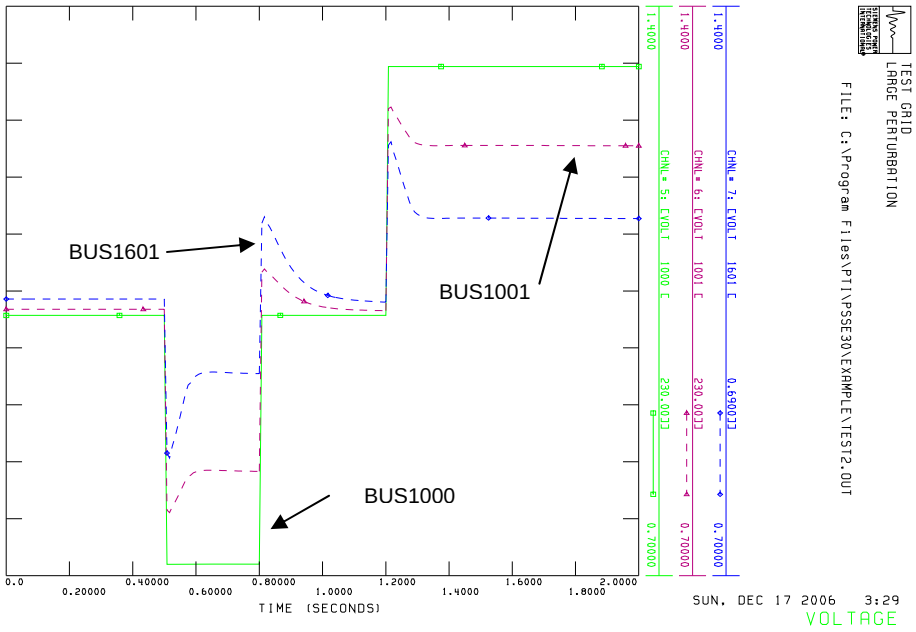

Figure 40: Test 2; Voltage, BUS1601, BUS1000 and BUS1001.

The voltage step was applied to the Grid voltage BUS1000. At the beginning the WTG terminal voltage on BUS1601 tracks the grid voltage but finally the WTG terminal voltage is not controlled and remains far from its reference value, that is the consequence of the saturation of the reactive power limits of the WTG.

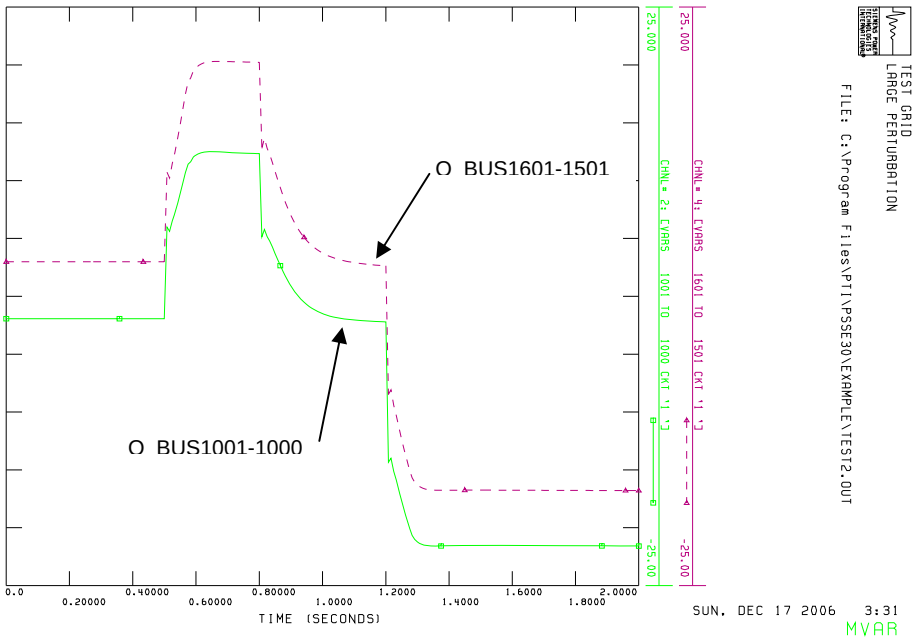

Figure 41: Test 2; Reactive power, BUS 1601-1501 and BUS 1001-1000.

The voltage step was applied to the Grid voltage at BUS1000, the reactive power of the WTG in the direction BUS1601-1501, rises when the voltage step lowers and drops when the voltage step rises.

The maximum and minimum limits of the reactive power are reached. In consequence the terminal voltage will not be controlled in its reference value.

The mechanical power is constant since the wind is constant, but the active current limit I_{lim} was reached (see Figure 28). After the perturbation the active power returns into its linear zone and becomes constant as shown in Figure 42.

The transient peaks of the active power shown in Figure 42 are related to the delay introduced by the low pass filter of the controlled current shown in Figure 28.

The pitch remains constant with the step voltage change.

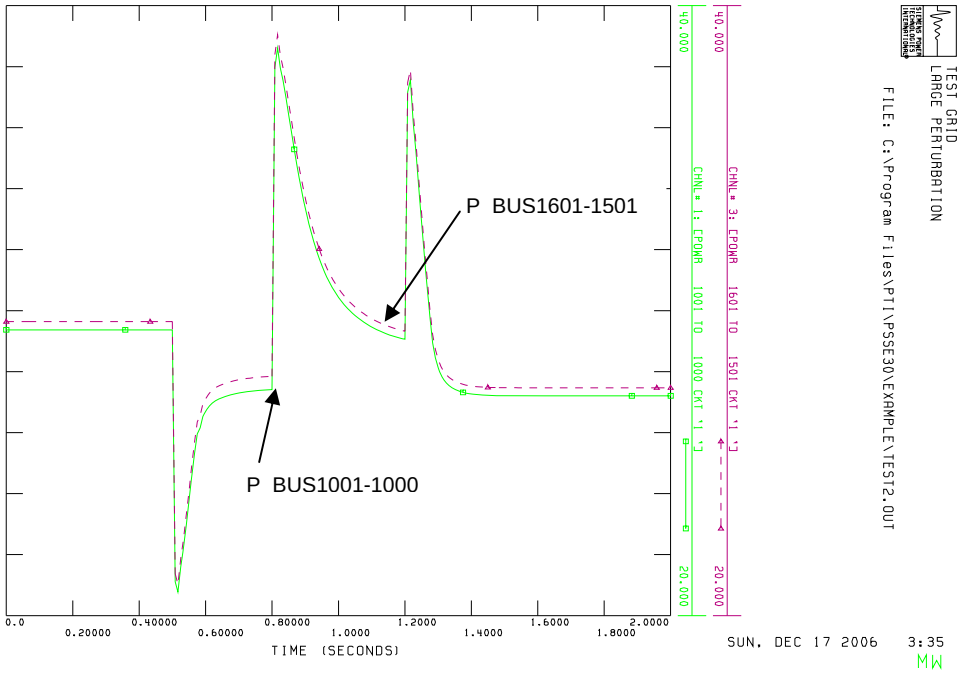

Figure 42: Test 2; Active power, BUS1601-BUS1501 and BUS1001-BUS1000.

3.2.1.3 Test 3, Three phase fault

The Test 3 consists of a three phase fault applied at the interconnection point BUS1001, through a fault resistance of 150 Ohms during 100 ms.

In Figure 43 the voltage drops near 0.15 pu during the time of fault at the interconnection BUS1001. This voltage does not reach zero due to the fault resistance of 150 ohms. After the fault is cleared a small voltage overshoot happens as a result of the fast voltage control.

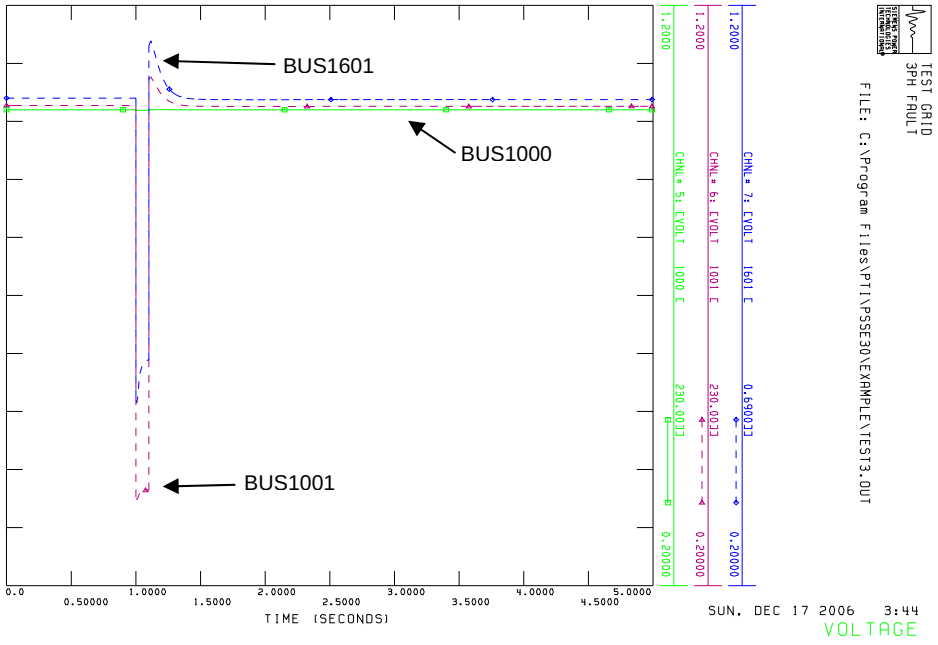

Figure 43: Test 3; Voltage, BUS1601, BUS1000 and BUS1001.

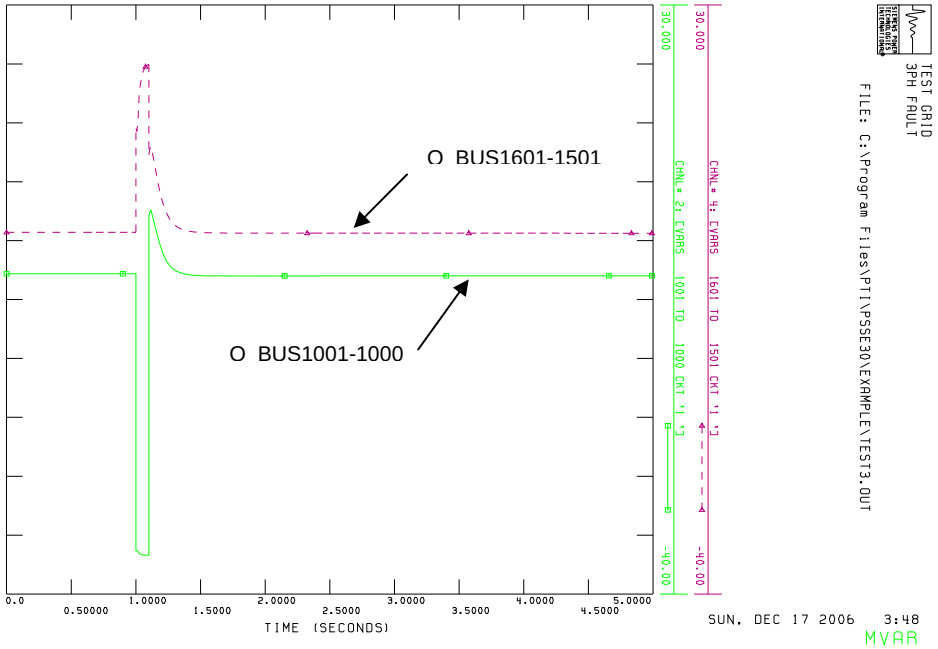

Figure 44: Test 3; Reactive powers, BUS1601-BUS1501 and BUS1001-BUS1000.

According to Figure 44, both generators on BUS1601 and BUS1000, contribute with reactive power to the fault.

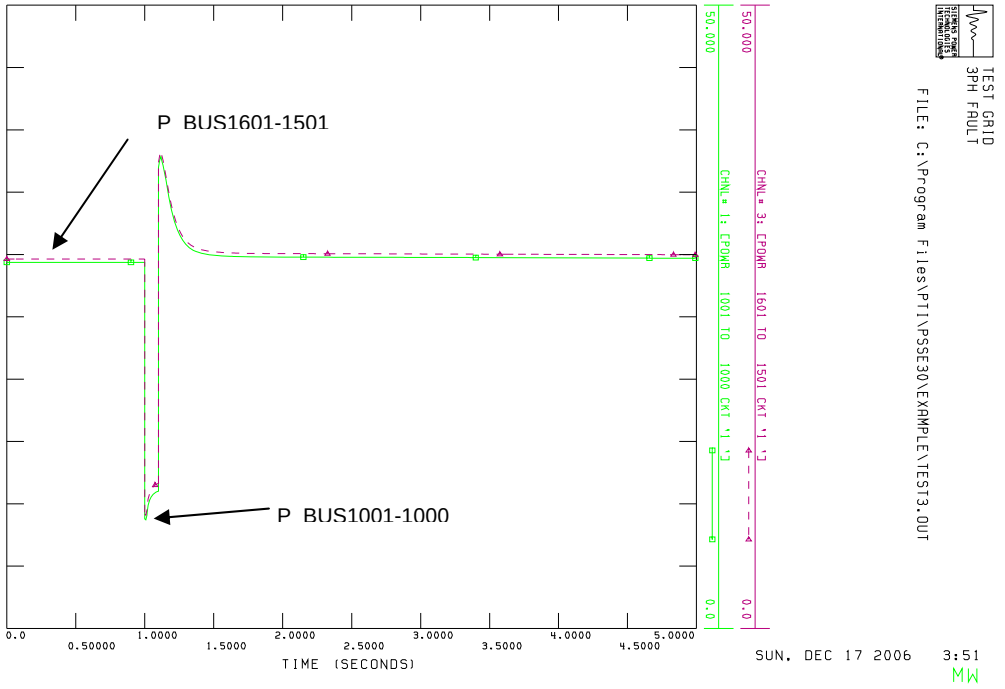

Figure 45: Test 3; Active power, BUS1601-1501 and BUS1001-1000.

The active powers are shown in Figure 45. The active power of the WTG, on BUS1601-BUS1501, tracks the voltage waveform. Due to the reduced voltage, the control current is raised and reaches the current upper limit, see I_{lim} in Figure 28.

The pitch angle changes to control the over-speed and overload during the fault duration (see Figure 46).

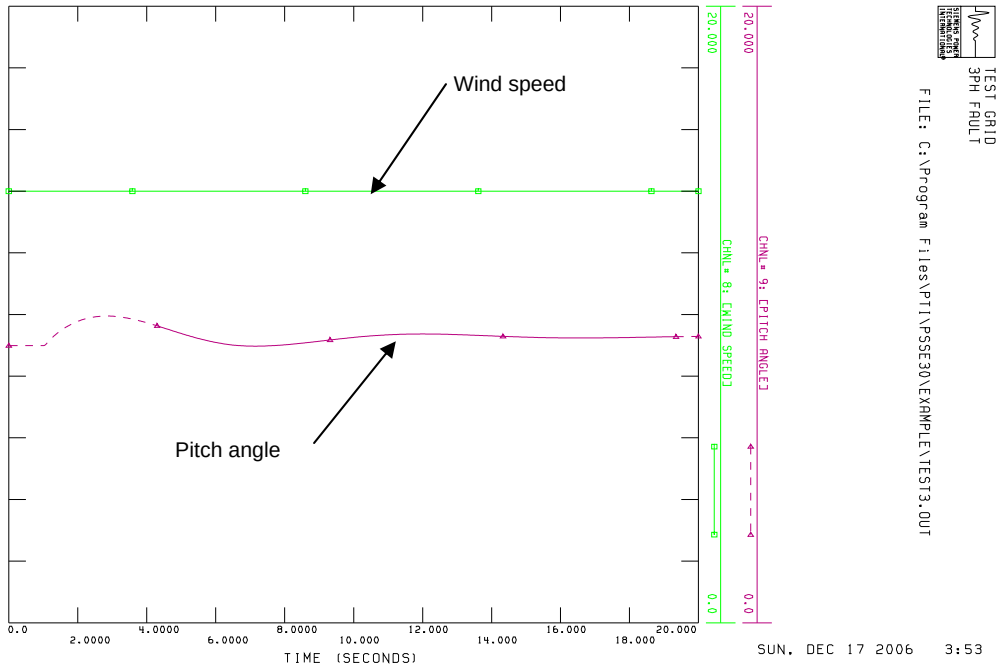

Figure 46: Test 3; Pitch and wind speed, BUS1601.

3.2.1.4 Test 4, Wind gust simulation

The Test 4 consists in the application of two wind perturbations. The first one is a wind gust. The second perturbation is a wind gust followed by a wind ramp. Results of the first perturbation are shown in Figure 47 to Figure 50. Results of the second perturbation are shown in Figure 51 to Figure 54.

The wind perturbation affects the generated active power. Due to the active power variation the voltage may change and affect the reactive power. The pitch angle controls the power variation accurately, in consequence the voltage doesn't change significantly and that is shown in Figure 47. The reactive power variation is light due to the light voltage variation shown in Figure 48. The pitch action controls accurately the over speed and only a small change of the active power occurs (see Figure 49). The wind gust is tracked by the pitch angle control to avoid the over speed and the possible overload (see Figure 50).

The pitch angle controls the power variation accurately, in consequence the voltage does not modify significantly from the initial values as shown Figure 51.

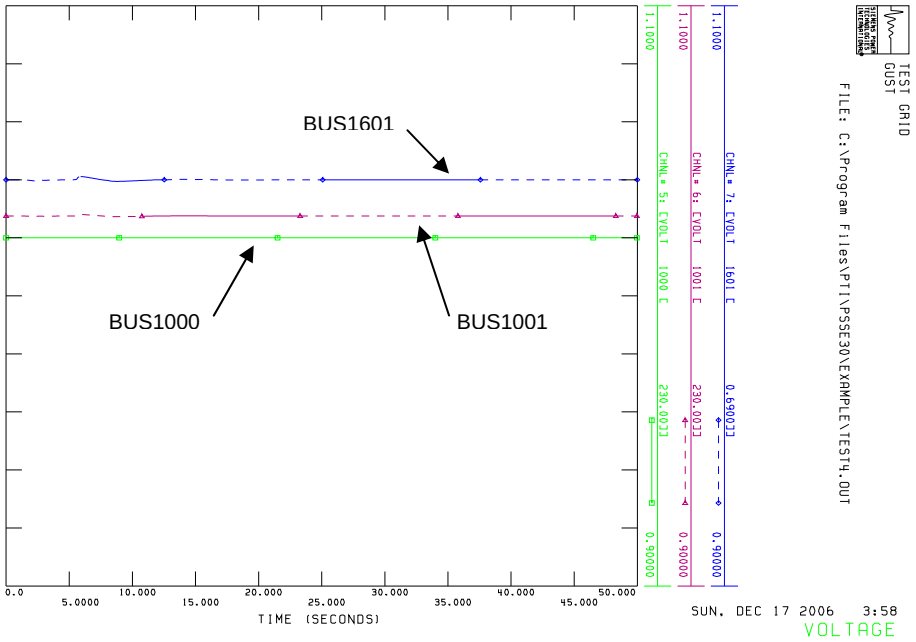

Figure 47: Test 4; Voltage with gust, BUS1601, BUS1000 and BUS1001.

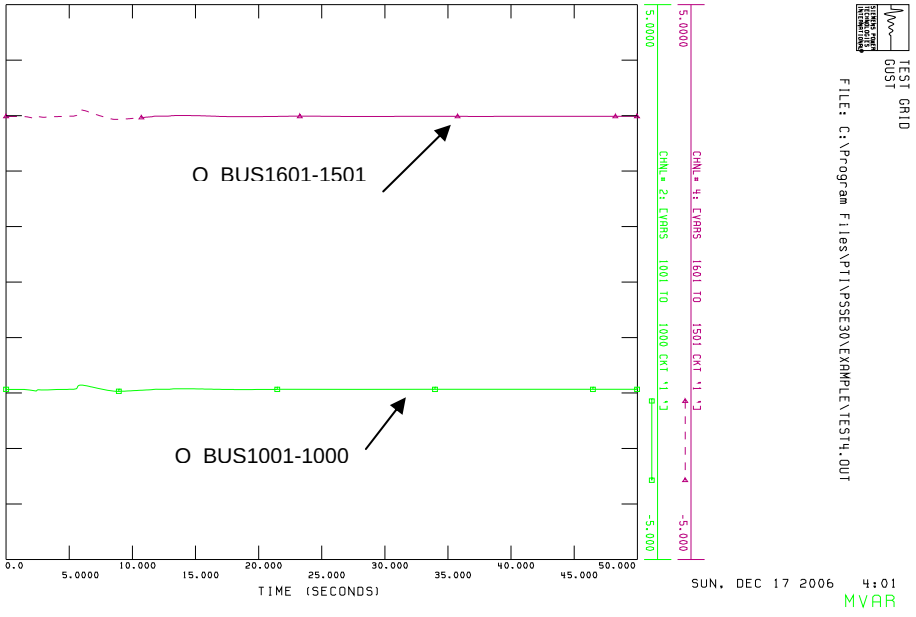

Figure 48: Test 4; Reactive power with gust, BUS1601-1501 and BUS1001-1000.

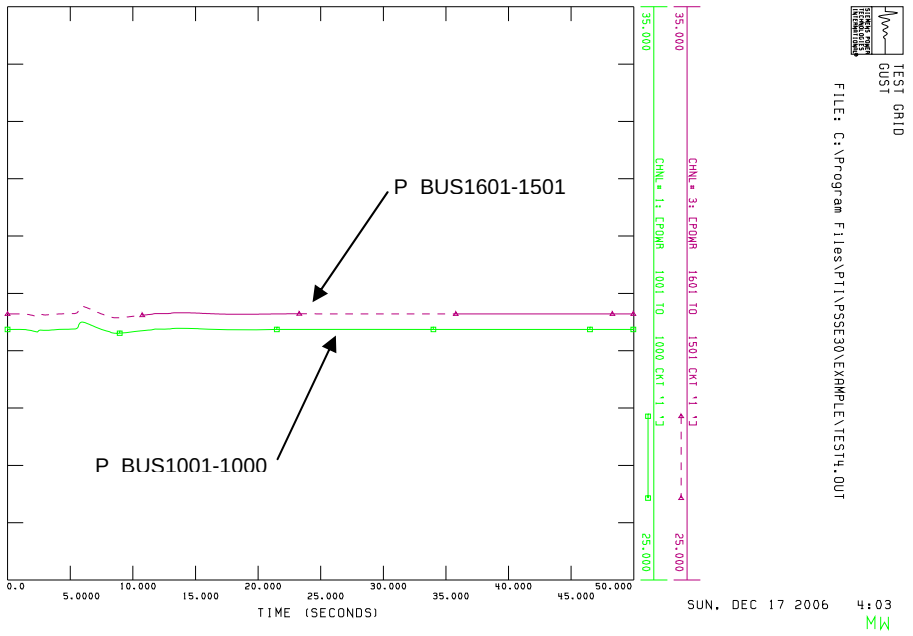

Figure 49: Test 4; Active power with gust, BUS1601-1501 and BUS1001-1000.

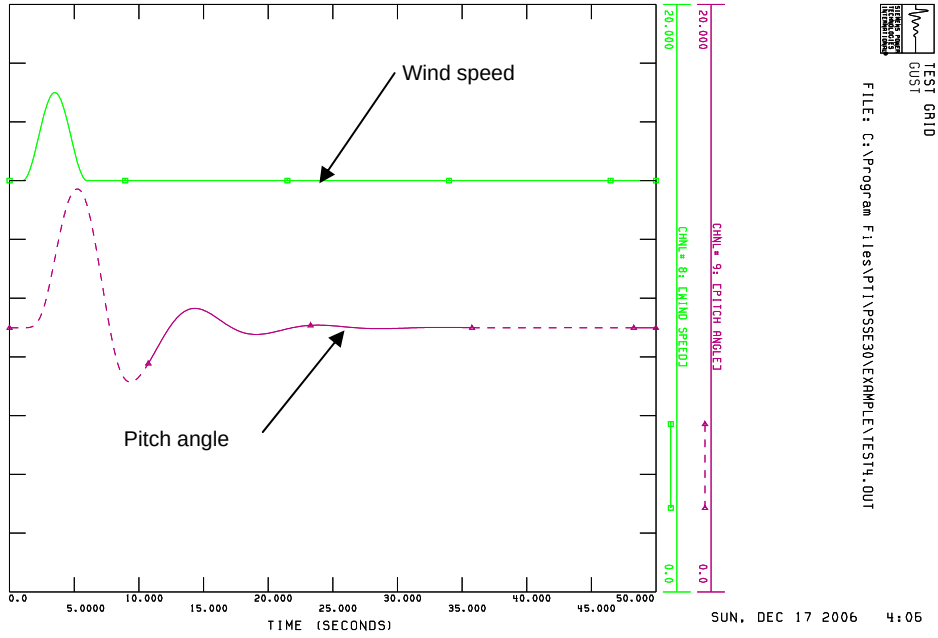

Figure 50: Test 4; Pitch and wind speed with gust, BUS1601 and BUS1001.

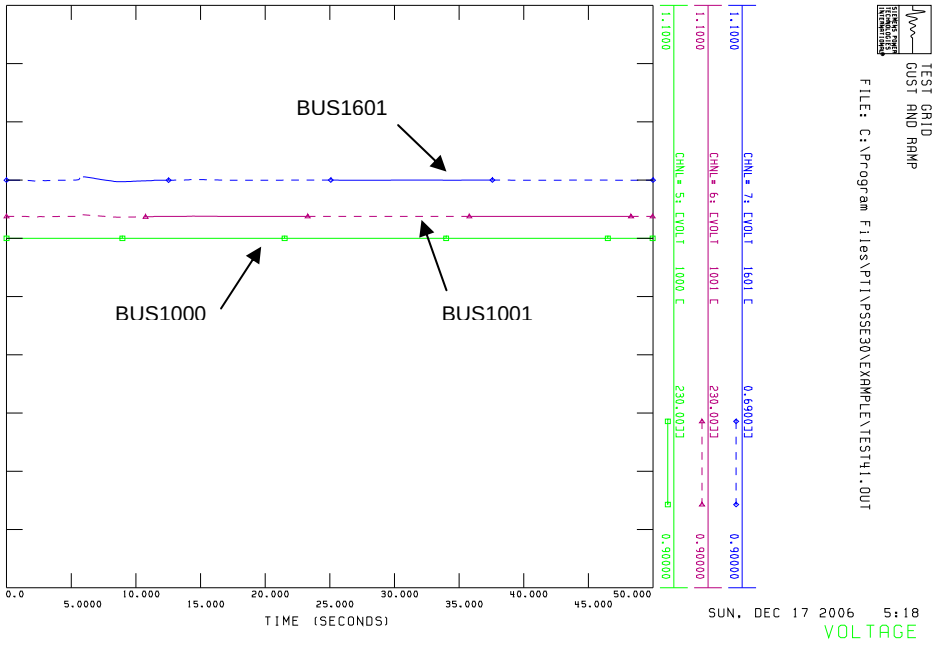

Figure 51: Test 4; Voltage with gust and ramp, BUS1601, BUS1000 and BUS1001.

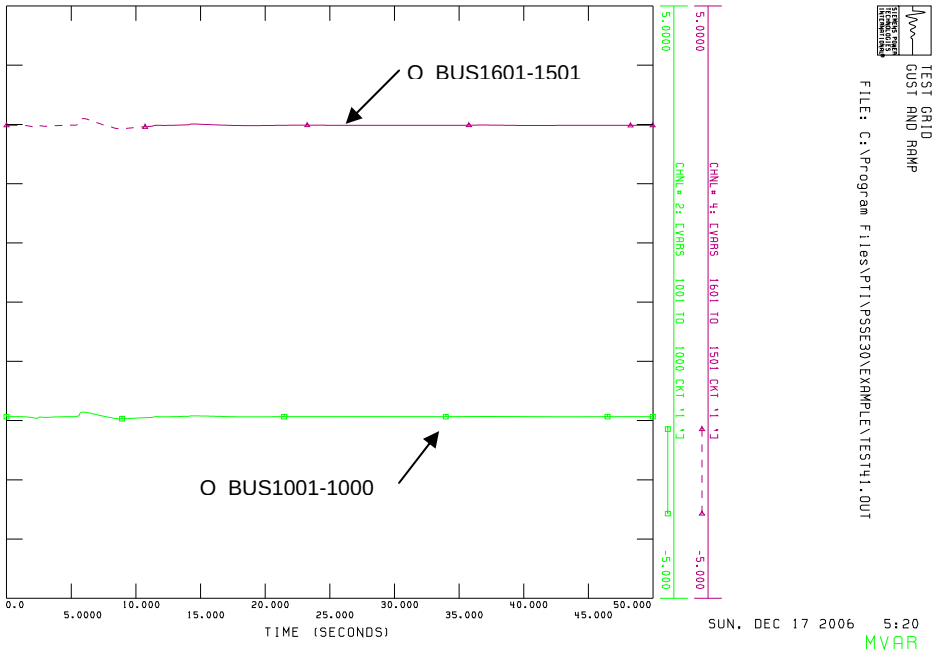

Figure 52: Test 4; Reactive power with gust and ramp, BUS1601-1501 and BUS1001-1000.

The reactive power variation is light due to the light voltage variation (see Figure 52). The pitch angle action controls accurately the over speed and over load. Only a little change of the active power occurs as seen in Figure 53.

The wind gust and ramp are tracked by the pitch angle control to avoid the over speed and possible overload (see Figure 54).

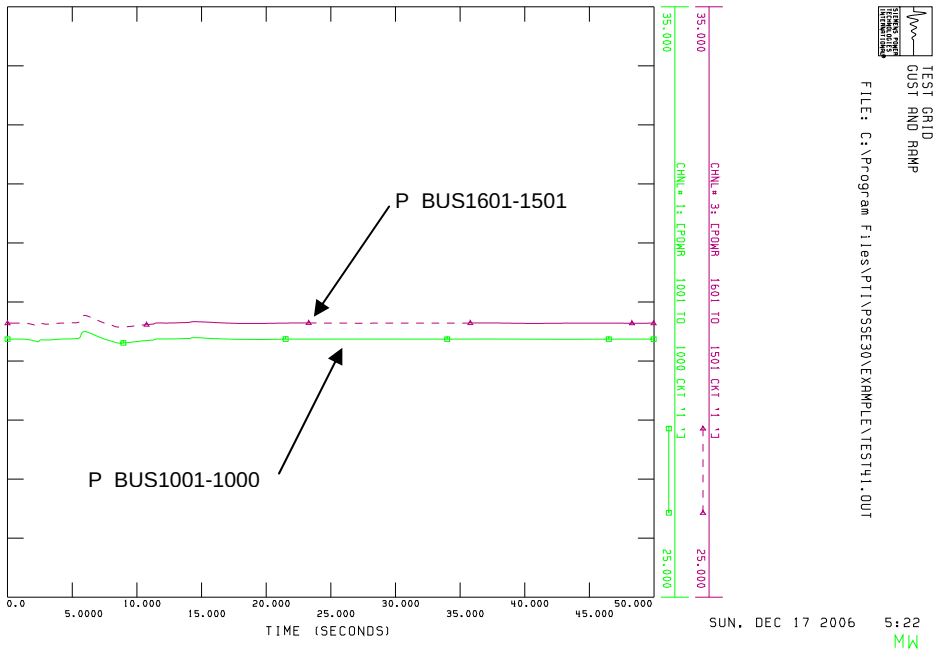

Figure 53: Test 4; Active power with gust and ramp, BUS1601-1501 and BUS1001-1000.

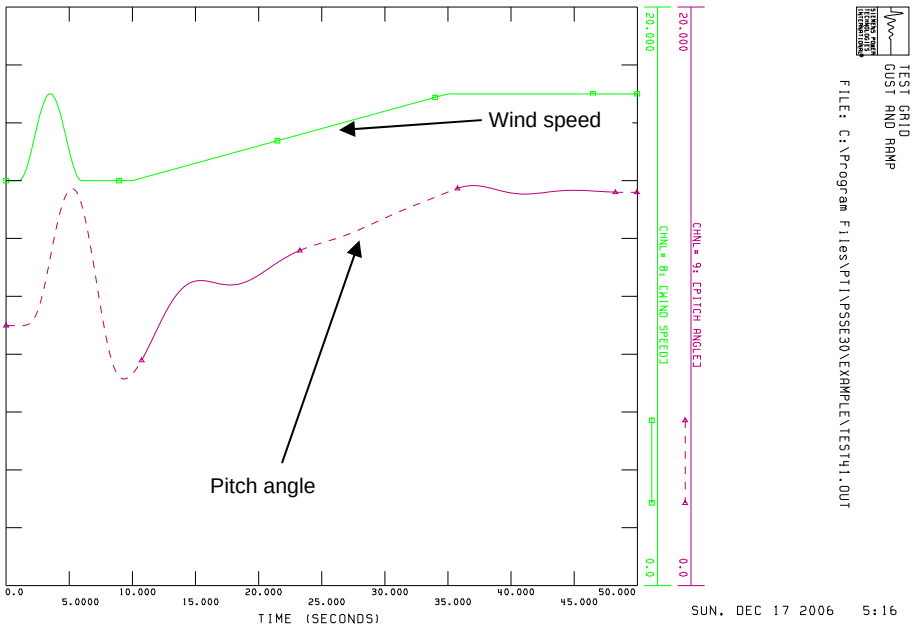

Figure 54: Test 4; Pitch and wind speed with gust and ramp, BUS1601 and BUS1001.

3.2.1.5 Test 5, Single phase fault

The Test 5 simulates the application of single phase fault during 100 ms at the interconnection point, BUS1001, with a fault resistance of zero ohm.

Figure 55 shows the voltage drop during the duration of fault, but the voltage does not reach zero due to the single phase fault. After the fault is cleared a little overshoot occurs as a result of the fast voltage control.

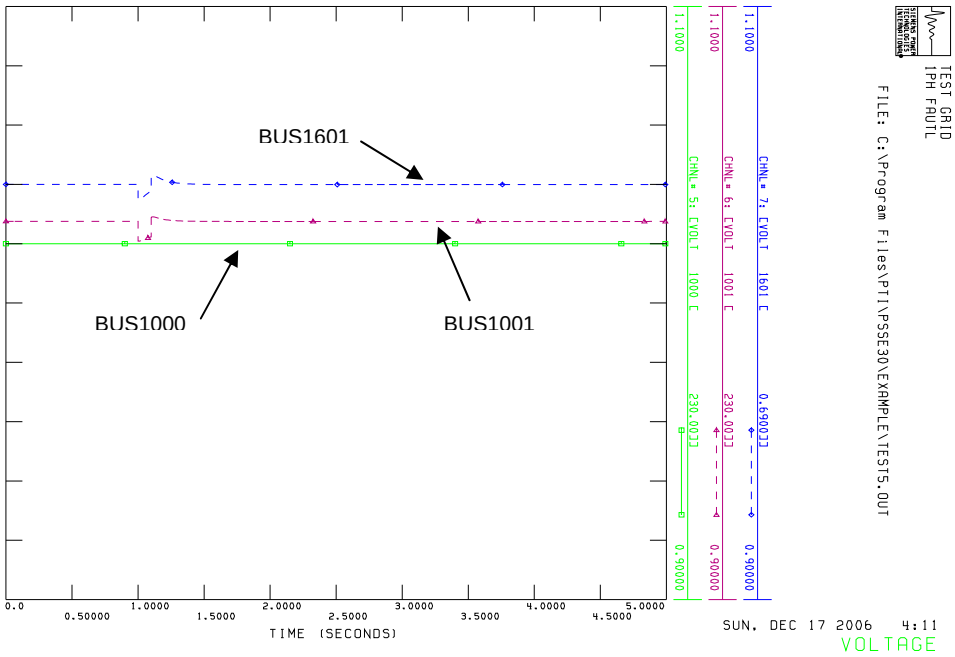

Figure 55: Test 5; Voltage, BUS1601, BUS1000 and BUS1001.

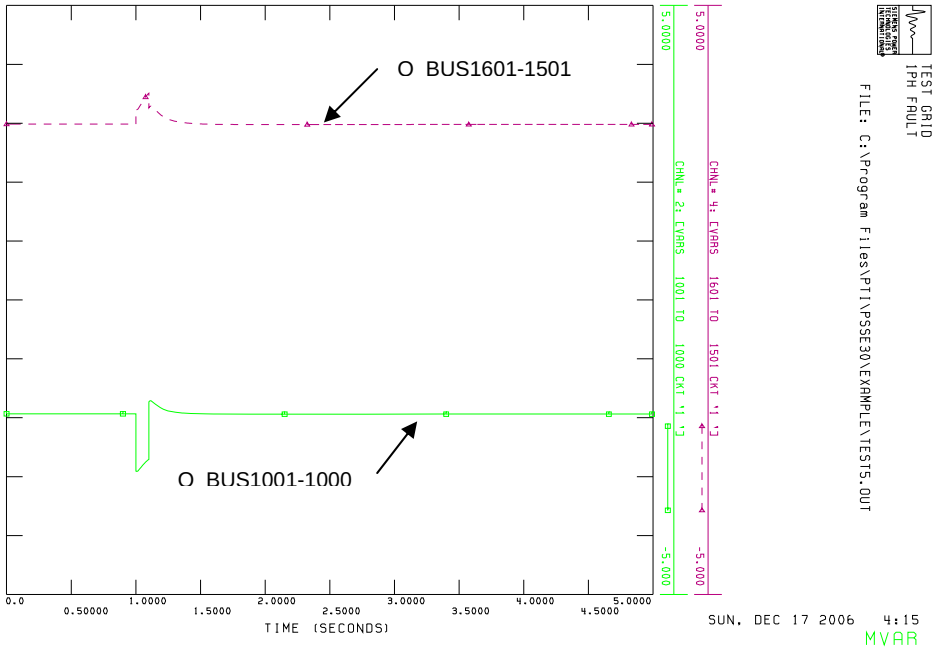

Figure 56: Test 5; Reactive power, BUS1601-1501 and BUS1001-1000.

Both generators on (BUS1000 and BUS1601) are shown in Figure 56 to contribute with reactive power to the fault.

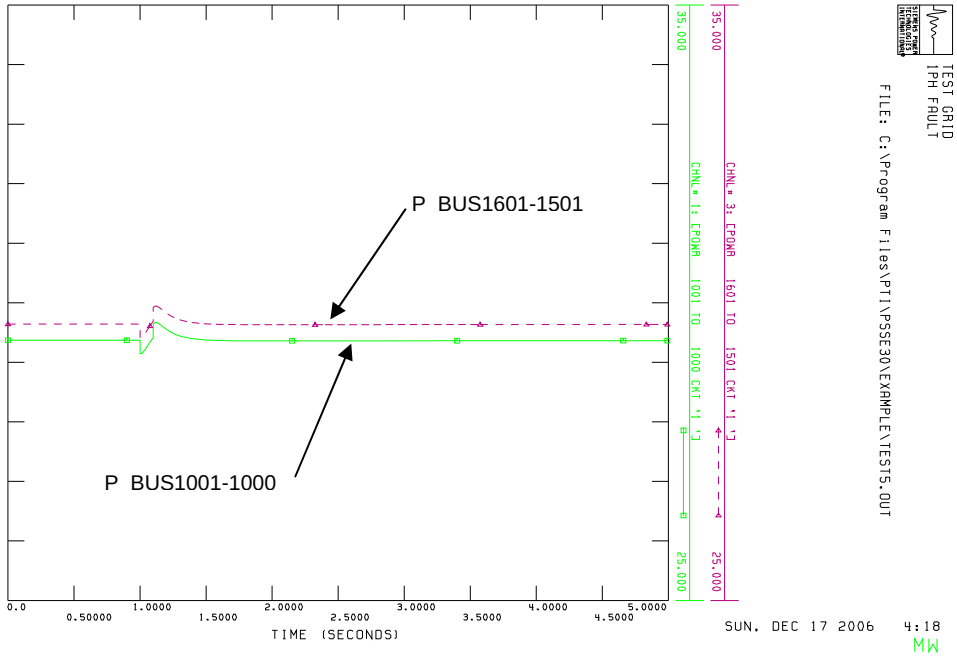

Figure 57: Test 5; Active power, BUS1601-1501 and BUS1001-1000.

The Figure 57 shows that the active power tracks the voltage waveform in the same way as the three phase fault test.

No pitch action was necessary to control the overspeed nor the overload of active power.

3.2.1.6 Test 6, Three phase fault with double mass model

The Test 6 compares the single and double mass models of the drive train for a three phase fault with 100 ms of duration applied at the interconnection point BUS1001 with fault resistance of 150 Ohms.

The same electrical and mechanical variables are presented to compare both models. The electrical variables that present the oscillatory effect correspond to the

double mass model. This is due to the fact that the first torsional mode of the shaft was excited by the three phase fault.

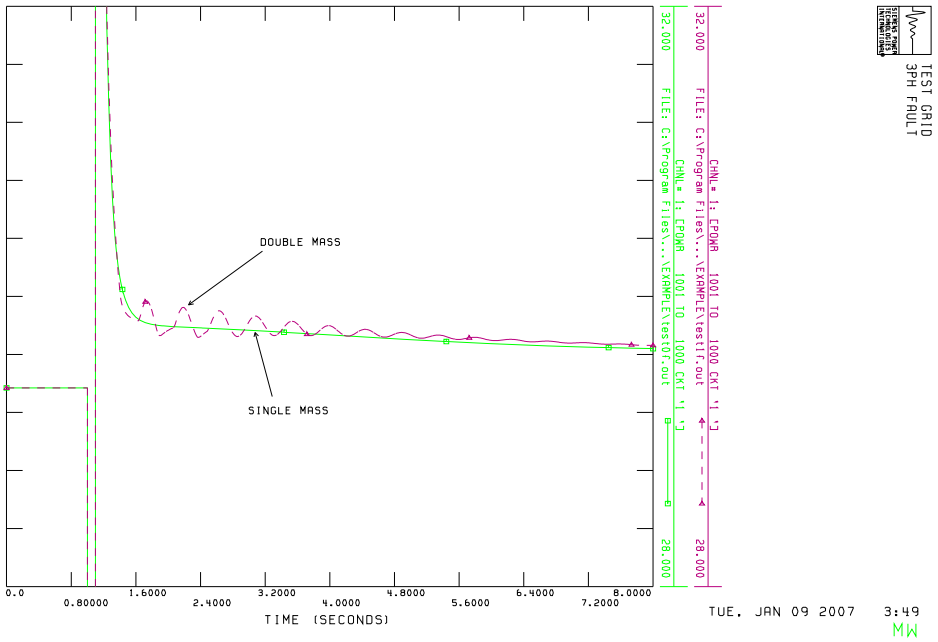

Figure 58: Test 6; Active power, Single vs double mass, BUS1001-1000

Figure 58 shows the comparison of the active power generated by WTG. The double mass model presents an oscillation due to the fact that the first torsional mode of the shaft was excited by the three phase fault. The oscillation mode may be seen in the pitch angle of the double mass model, shown in Figure 59.

The light generator (WG) mass has a larger speed oscillation amplitude than the heavy turbine (WT). This difference on speed oscillation amplitudes is shown in Figure 60.

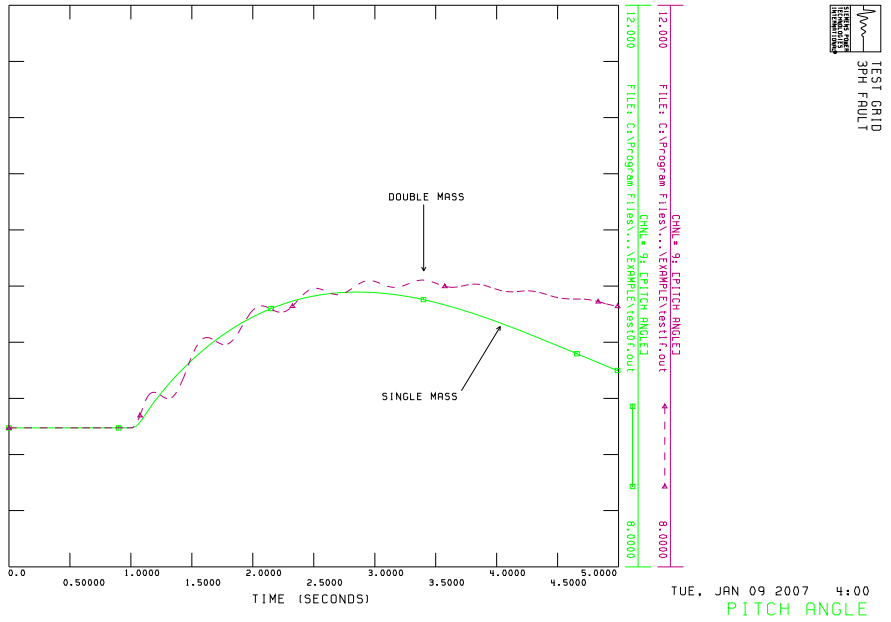

Figure 59: Test 6; Pitch angle, Single vs double mass, BUS1601

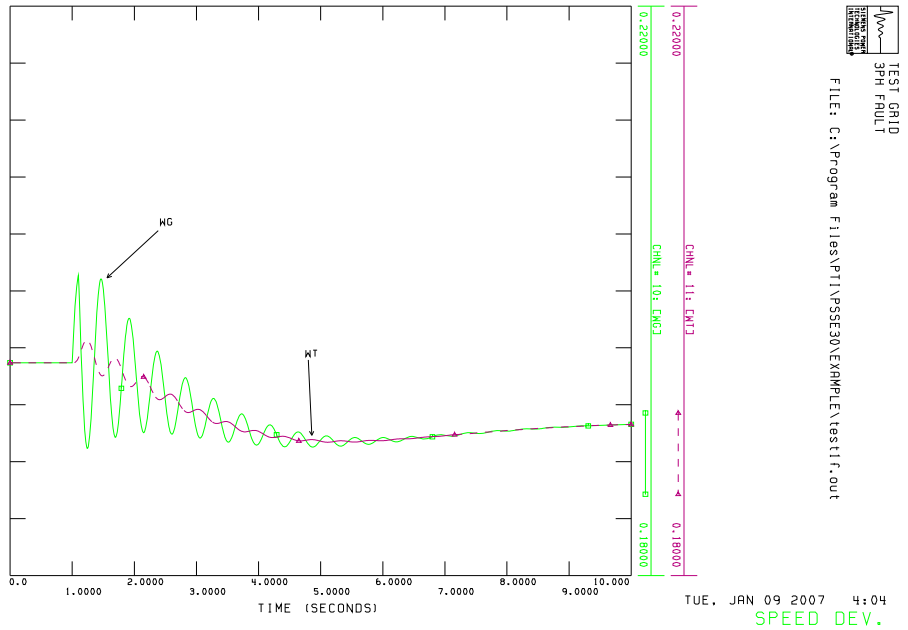

Figure 60: Test 6; Speed deviation two mass model, BUS1601

3.2.1.7 Test 7, Wind gust with double mass model

The Test 7 compares the simulations with wind gust of Figure 63 for single and double mass models of the shaft. Figure 61 presents the differences of amplitude of the pitch angle oscillation introduced for the mutual damping of the double mass model. The mutual damping is null in the single mass model.

Figure 62 presents the difference of amplitude of the speed deviation introduced for the mutual damping of the double mass model. The mutual damping is null in single mass model.

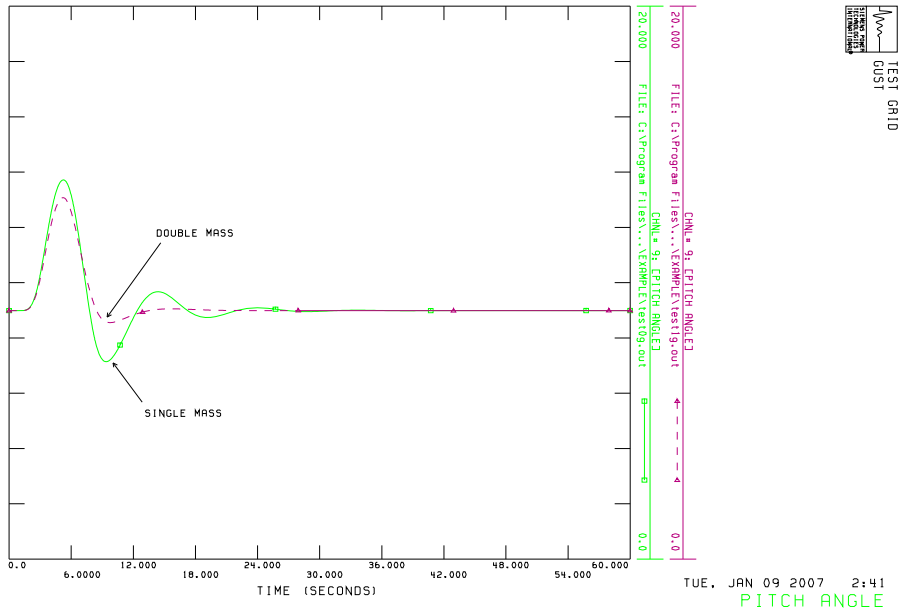

Figure 61: Test 7; Pitch angle, Single vs double mass, BUS 1601

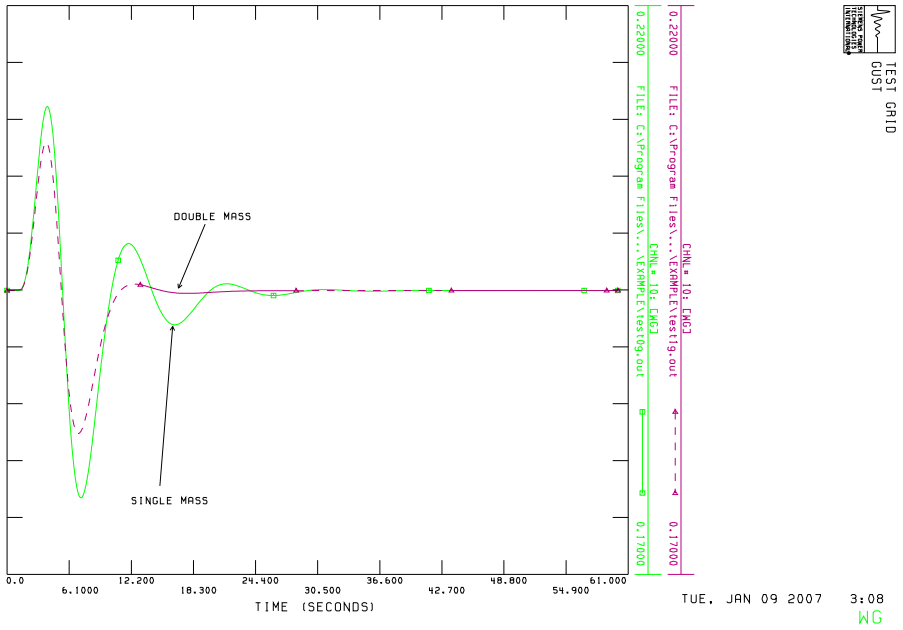

Figure 62: Test 7; Speed deviation, Single vs double mass, BUS 1601

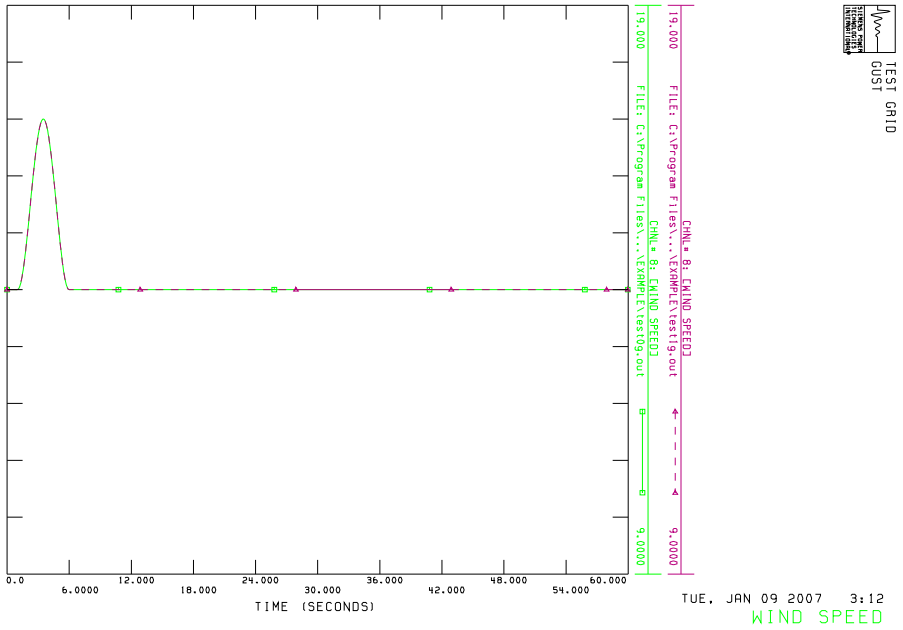

Figure 63: Test 7; Wind speed to single and double mass, BUS 1601

3.2.1.8 Test 8, Three phase fault to aggregation degree test.

The Test 8 considers a three phase fault simulation to perform aggregation degree test. The fault was applied during 100 ms at the interconnection point (BUS1001), with a fault resistance of zero ohm. The same simulation fault is repeated two times. The first one with 15 machines of 33 MW to complete a total of 500 MW is shown in Figure 64 and the second one with only one machine equivalent of 500 MW is shown in Figure 65.

The Figure 64 and Figure 65 show a perfect match of the active power of the generator of BUS1000. Also Figure 64 includes the generation of BUS1601 of 33 MW and Figure 65 includes the generation of BUS1600 of 500 MW. In this case, except for a scale factor of 15 the power variation is the same.

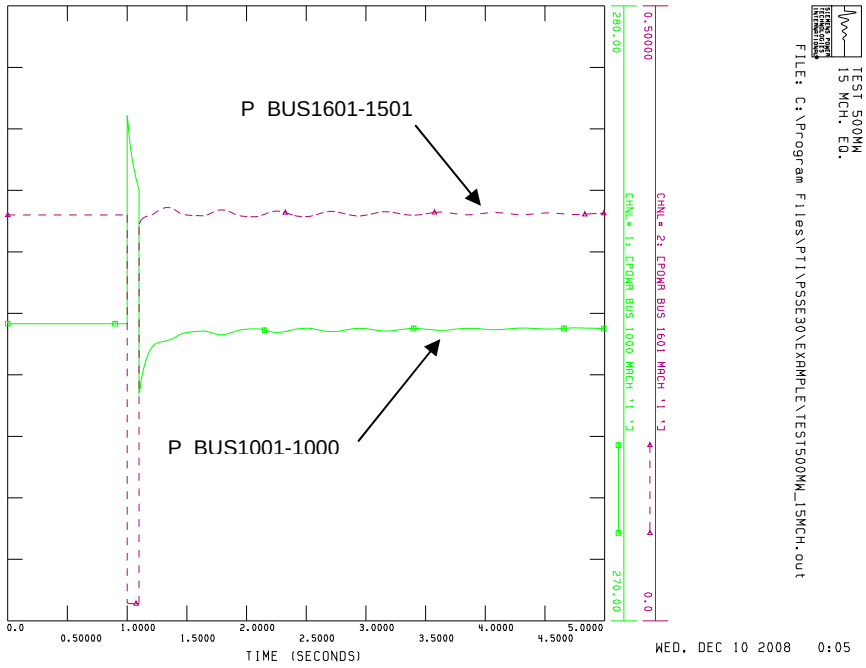

Figure 64: Test 8; Active Power at 1000 and 1600 (15x33MW)

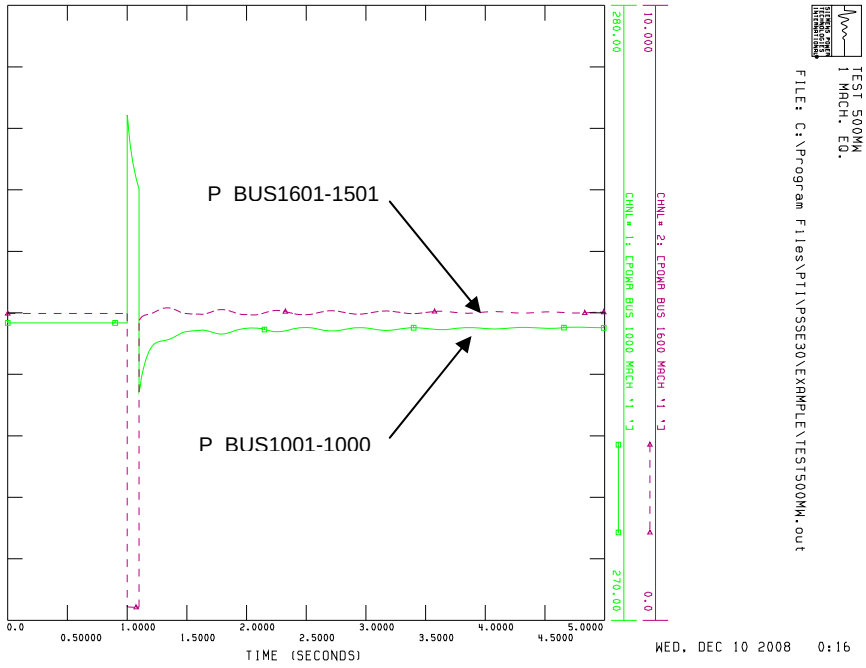

Figure 65: Test 8; Active Power at 1000 and 1601 (1x500MW)

3.3 PSS/E DFIG model validation for torque computations

The purpose of this section is to compare simulation results from the Wind Turbine Generator (WTG) model in the PSS/E software to an equivalent case setup in the GH Bladed [22]. The presented WTG is again of 1.5 MW (DFIG). The objective is the validation of the mechanical behaviour of the PSS/E model using the Bladed program. It also inherently validates the computation of torque for the other models in this thesis.

GH Bladed is used by wind turbine and component manufacturers, certification agencies, design consultants and research organizations across the world. A number of modules are available, covering steady state analysis, dynamic load simulations, analysis of loads and energy capture, batch processing and automated report generation, interaction with the electrical network and model linearization for control design.

Bladed is a program used by wind generator designers and includes a detailed wind generator model that makes possible the accurate representation of the real unit with its mechanical and electrical control devices. Random wind component, wind turbulence and shadow effects are taken into account in this program.

The simulation results with Bladed presented in this document were performed by a wind generator manufacturer.

3.3.1.1 Test case setup

The PSS/E benchmark is setup to reproduce the same study conditions as in Bladed. It is based on a 2 bus grid that represents a single generator machine of 1.5 MW at 0.69 kV of terminal voltage with its unit transformer and an equivalent generator on the 34.5 kV side. The benchmark diagram is shown in Figure 66.

The DFIG operates in the vicinity of rated power at 2096 RPM, at 116% speed or -16% slip. The generator speed range is between 1200 and 2400 rpm, and the synchronous speed is 1800 rpm, that means the rotor speed can be controlled over a range of ±33%.

From 20 RPM at the turbine, the generator runs with constant torque. This results in a constant load of the complete systems. The acceleration of the turbine beyond a certain limit is avoided by sufficient pitching. At maximum power, 1150 kW of active power comes from the stator and 350 kW from the rotor. For this reason the DFIG produces fewer harmonics compared to a variable speed machine with an asynchronous motor where the power is all fed though the converter.

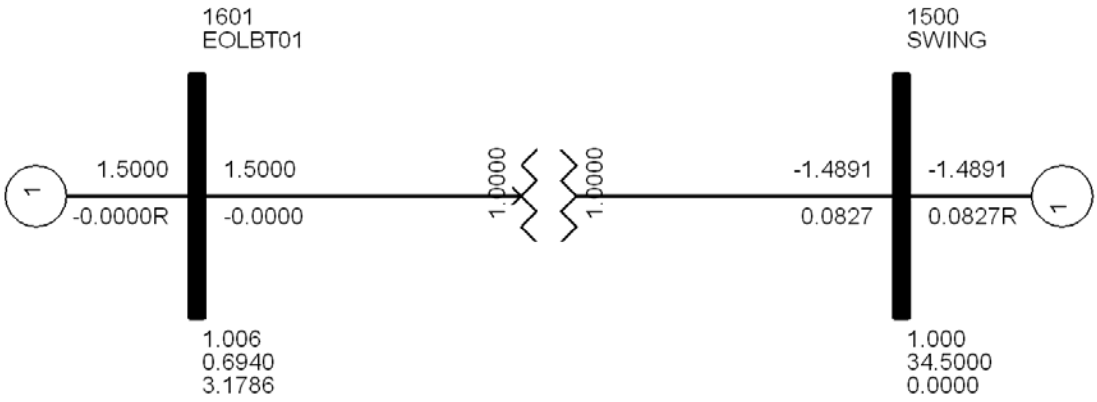

Figure 66: Validation Benchmark

The validation of the mechanical behaviour of the PSS/E model using the Bladed program is based here on the simulation of 2 wind speed perturbations: gust and gust-ramp. Amplitude and duration are shown in Figure 67 and Figure 71 respectively.

Validation results are shown in the following figures.

Figure 67 shows the average wind gust applied to the WTG. The Bladed simulator has an additional random wind component to represent turbulence.

Figure 68 shows the pitch angle response to the wind gust application. The curve offset is due to the differences in the CP matrix, resulting in a different initial pitch angle. This little difference in the initial pitch angle does not modify the dynamic behaviour of the average value.

Figure 69 shows that the average wind gust applied to the PSS/E model and the average wind gust augmented with a random wind component applied in Bladed, will both produce similar mechanical turbine torques. The same conclusion is valid for the rotor speed shown in Figure 70.

The assumptions made here for the PSS/E model mechanics are thus verified with more advanced representation for mechanical perturbation details. This is also providing us validation for Torque equations used in all models in this thesis.

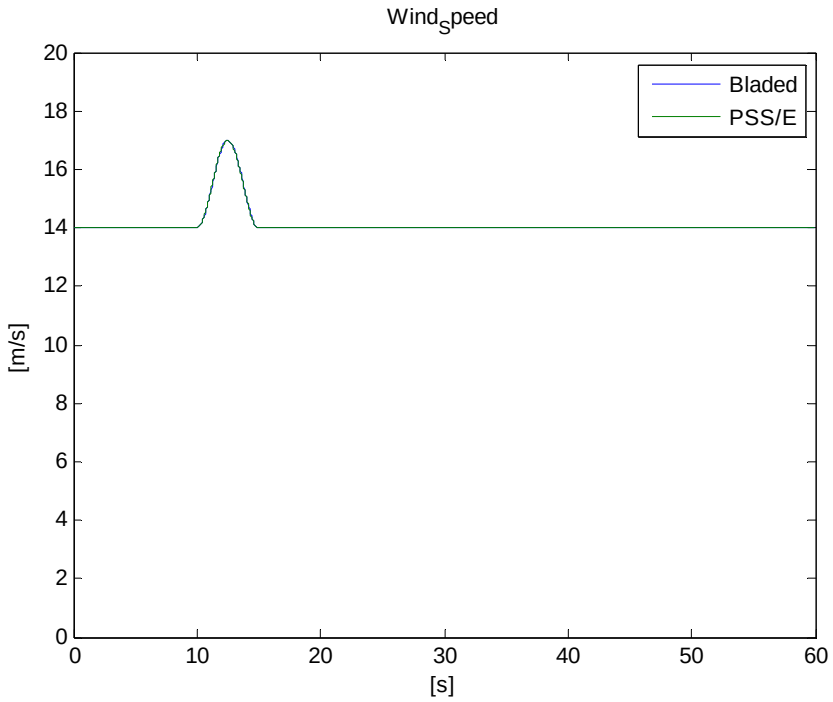

Figure 67: Wind speed (m/s), validation with Bladed, Wind Gust test

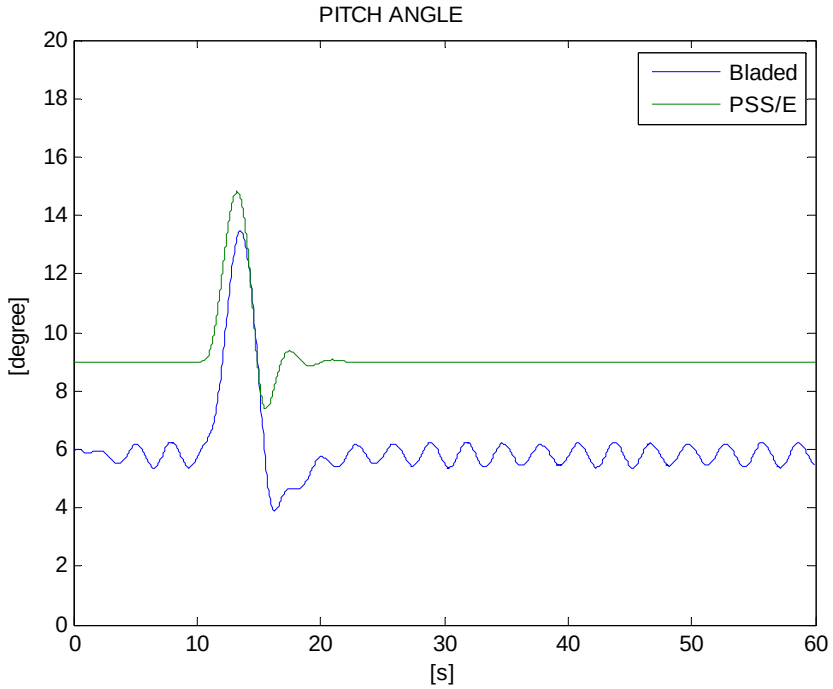

Figure 68: Pitch angle in degrees, validation with Bladed, Wind Gust test

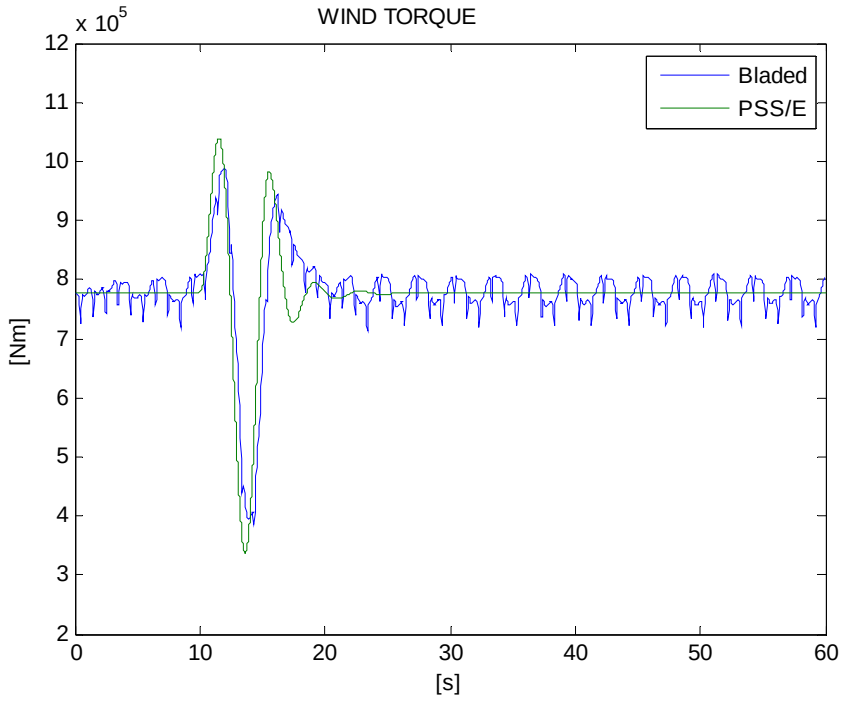

Figure 69: Wind torque (Nm), validation with Bladed, Wind Gust test

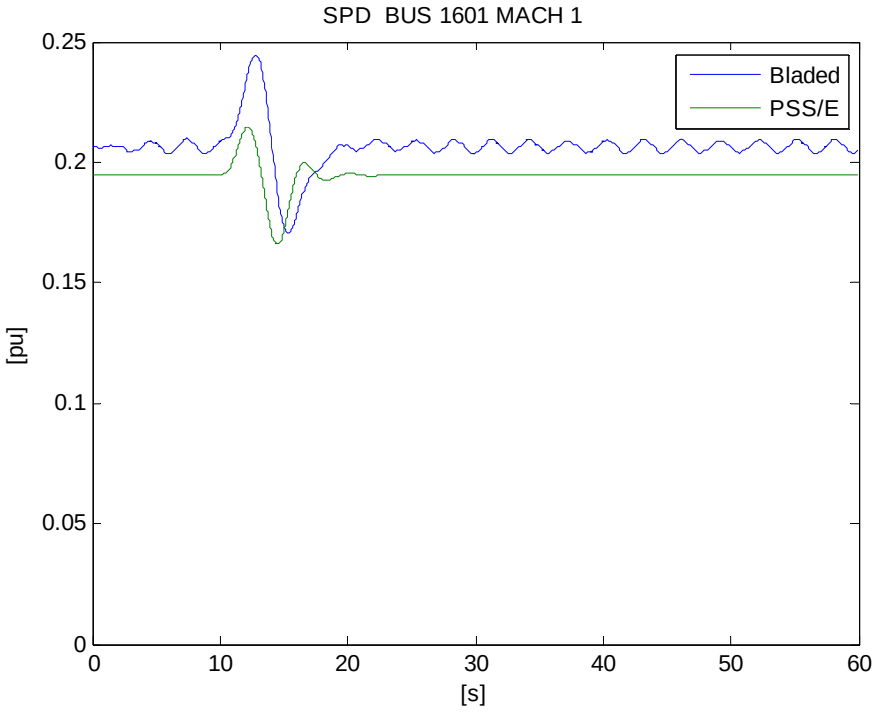

Figure 70: Speed deviation in pu, validation with Bladed, Wind Gust test

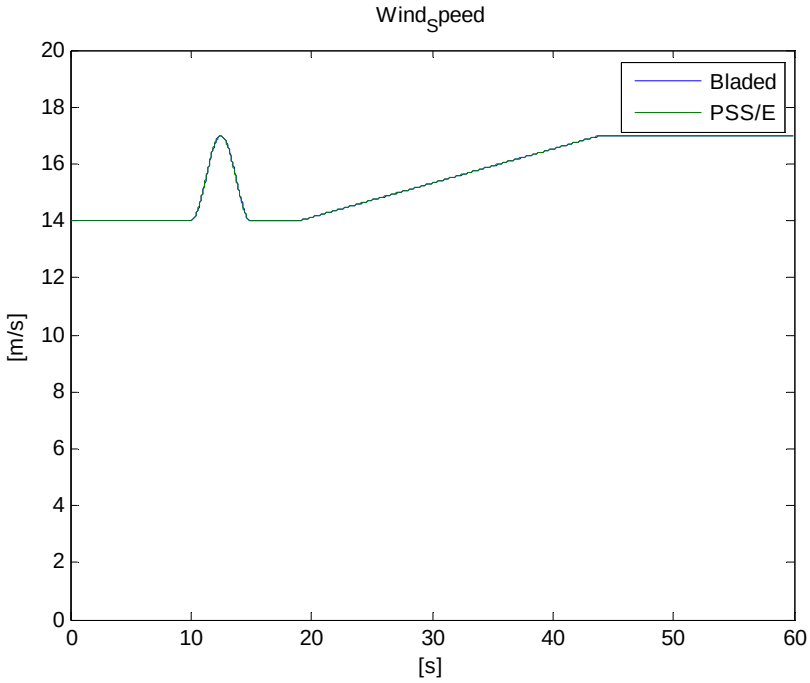

Figure 71: Wind speed (m/s), validation with Bladed, Wind Gust and Ramp test

Figure 71 shows the average wind gust followed by a ramp applied to the WTG. The Bladed simulator includes also a random wind component to represent turbulence.

Figure 72 shows that the model of the pitch angle in PSS/E tracks the response to the wind gust and ramp applications using Bladed with only an offset of 2 or 3 degrees.

The Figure 73 shows a mechanical turbine torque which validates again the PSS/E model. The ramp presence is remarked by the oscillation of the mechanical torque of the PSS/E model near 45 seconds.

The Figure 74 shows the rotor speed deviation validation. The ramp presence is remarked by the oscillation of the mechanical rotor speed deviation of the PSS/E model near 45 seconds.

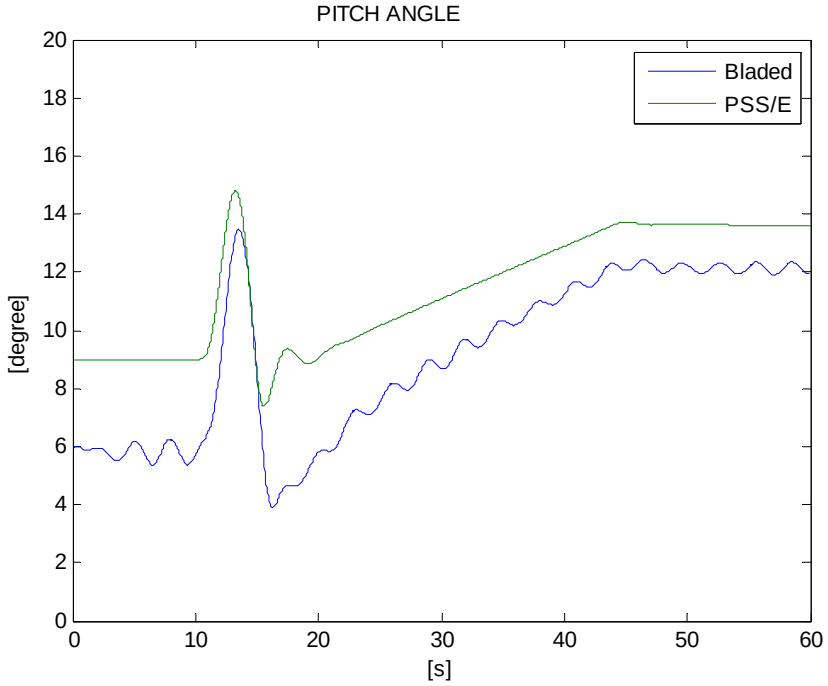

Figure 72: Pitch angle in degrees, validation with Bladed, Wind Gust and Ramp test

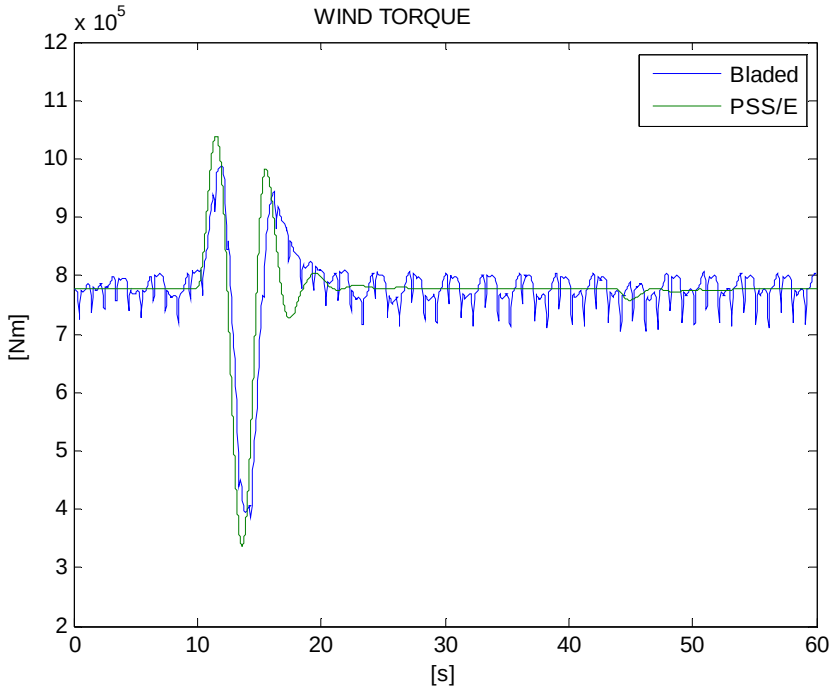

Figure 73: Wind torque (Nm), validation with Bladed, Wind Gust and Ramp test

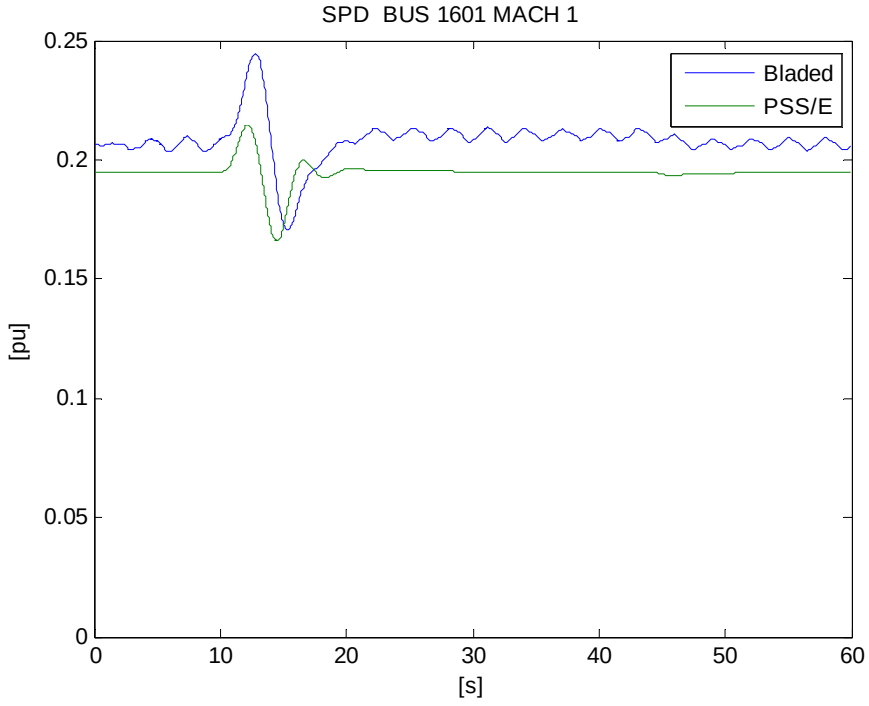

Figure 74: Speed deviation in pu, validation with Bladed, Wind Gust and Ramp test

CHAPTER 4. MEVA model, DFIG and FC

4.1 DFIG MEVA MODEL

The top level view of the DFIG MEVA model in EMTP-RV with its initialization devices is shown in the Figure 75. The DFIG_WTG, mean value model, device is a subnetwork with several subnetworks for its various modeling function and control systems.

Almost all parameters of the device can be modified through its mask. There are two external interfacings points (pins). The right pin is a 3-phase pin allowing to connect the DFIG_WTG device to the 3-phase network. The left pin is used for providing the random variation of the wind speed. The mean wind speed is found inside the top level mask as parameter.

Each DFIG_WTG device can represent one or more generators, or include an entire park.

Since the model must be initialized it is need to perform a Load flow solution followed by a steady-state solution. In EMTP-RV this is achieved using separate layers of components for the different solution modules. As show in Figure 75, each DFIG_WTG device is paired with a Load-Flow constraint device (LF device) and a ideal voltage source. The LF device is used in the Load-Flow solution layer. It provides the PQ constraints of the DFIG_WTG. The LF device is used in the load flow solution and together with other LF devices, it allows calculation the Load-Flow solution phasor for the complete network.

The steady-state and the following time-domain solution can be started from the Load-Flow solution.

This is a two step process: the first step is the Load-Flow solution and the second steps is the steady-state solution automatically followed by the time domain solution.

In the steady-state solution the ideal voltage source is used to provide the phasors found in the Load-Flow solution. The voltage source is disconnected before the first

time point computation in the time domain solution, but allows to initialize the state variables of the simulated network. At the same time the DFIG_WTG is turned on and starts controlling its internal source for the rest of simulation. It is also noticed that the DFIG_WTG must provide the same PQ constraints and must be given Load-Flow solution voltage and phase angle at its terminal. To reproduce this same behaviour with the DFIG_WTG model, the values of Pschedule, Qschedule and Vschedule must be included in the main mask of the DFIG_WTG device. In this way and according to the method described in the section 4.1.1, the initialization of the MEVA model is fast and accurate.

4.1.1 Model mask

When the DFIG_WTG device is double clicked it opens a subcircuit mask with a collection of parameters. Each device can be given a separate set of parameters for the same subnetwork contents. Most parameters are physical parameters for the representation of the machine model. Only a few parameters must be adjusted to represent various operation conditions and match available simulation results.

Basically the parameters that must be adjusted are in the Generator Data and Scheduled Data of the main mask model.

Generator Data:

Nmachines = Number of machines

S_rated = Aparent rated power in (VA) per machine

V_rated = RMSLL Terminal voltage in (V)

f_rated = Rated frequency in (Hz)

Scheduled Data:

Vschedule = Terminal voltage in pu, value from the load flow solution

Pschedule = Active power in pu, value from the load flow solution

Qschedule = Reactive power in pu, value from the load flow solution

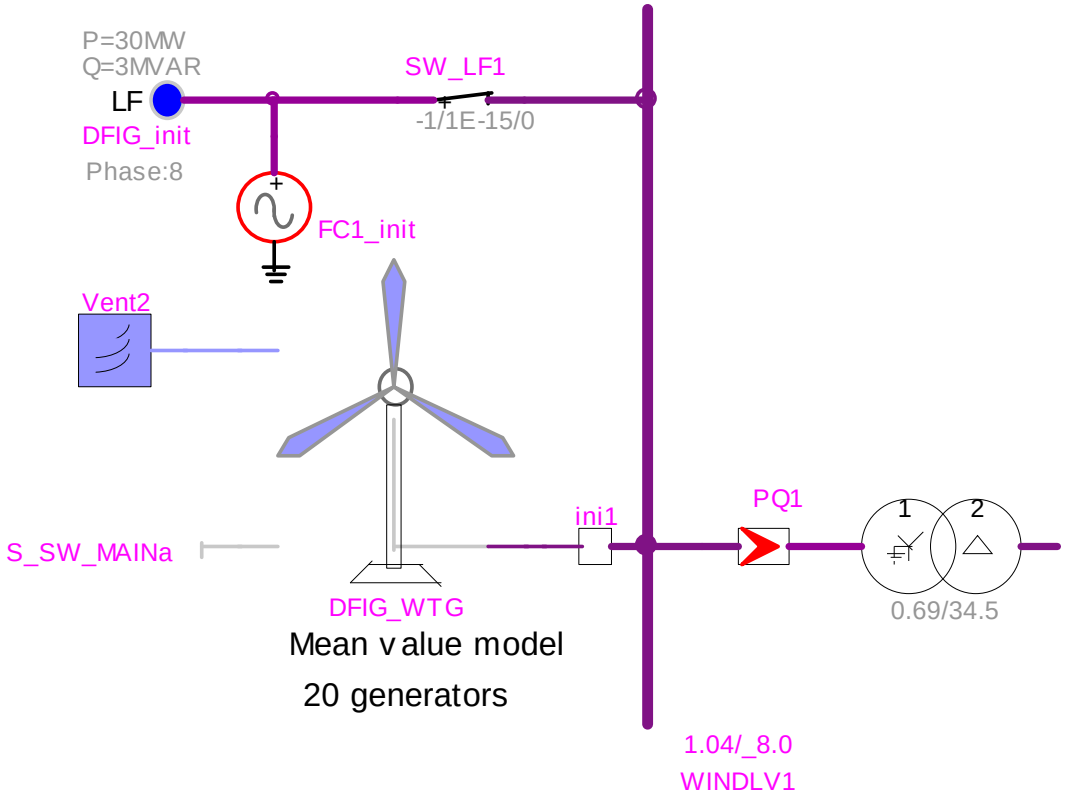

Figure 75: Top level device view of the DFIG_WTG

The initialization of the mechanical variables (wind speed, pitch angle and slip) is obtained using the method described in section 2.1.3 and by running a MATLAB script.

The Mask window with all initialization procedures is shown in Figure 76. Additional values which are found in the initial condition values window.

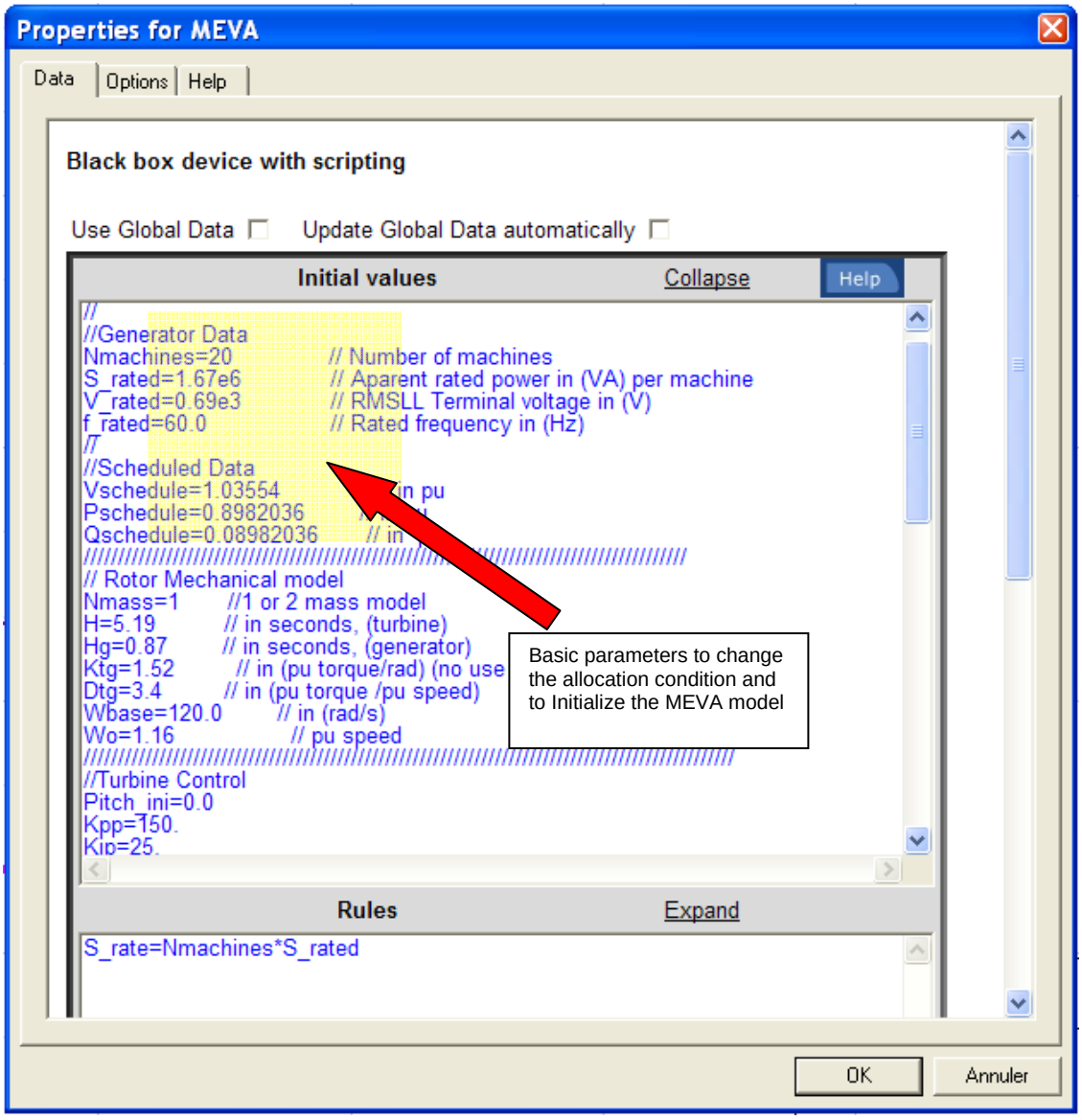

Figure 76: Initial value window

4.1.2 DFIG block components.

The subnetwork found under the symbol of DFIG_WTG shown in the Figure 75 is shown in the Figure 77. The MEVA modelling approach shares the same PSS/E model blocks defined in CHAPTER 2, in consequence the blocks contents in Figure 77 are directly related.

- For the wind block Vent2 in Figure 75, see the section 2.2.

- For the mechanical turbine model, Wind power in Figure 77, see the section 2.1.2.3.
- For the pitch control, Turbine control in Figure 77, see the section 2.3.4.
- For the rotor model, Rotor in Figure 77, see the section 2.5.1.
- For the reactive control, Q control in Figure 77, see the section 2.7.
- For the torque and power control, Turbine control and converter current limiter in the Figure 77, see the section 2.6.
- For the protection block model, Protections in Figure 77, see the section 2.8.

A new trend from power utilities is to demand the WTG contribution to frequency regulation. The MEVA model includes an additional component as compared the PSS/E model, for the active power control implemented into the converter current limiter block. Additionally, a new PLL without time step limitation problems (described in the section 3.1.2) is included into the converter generator model.

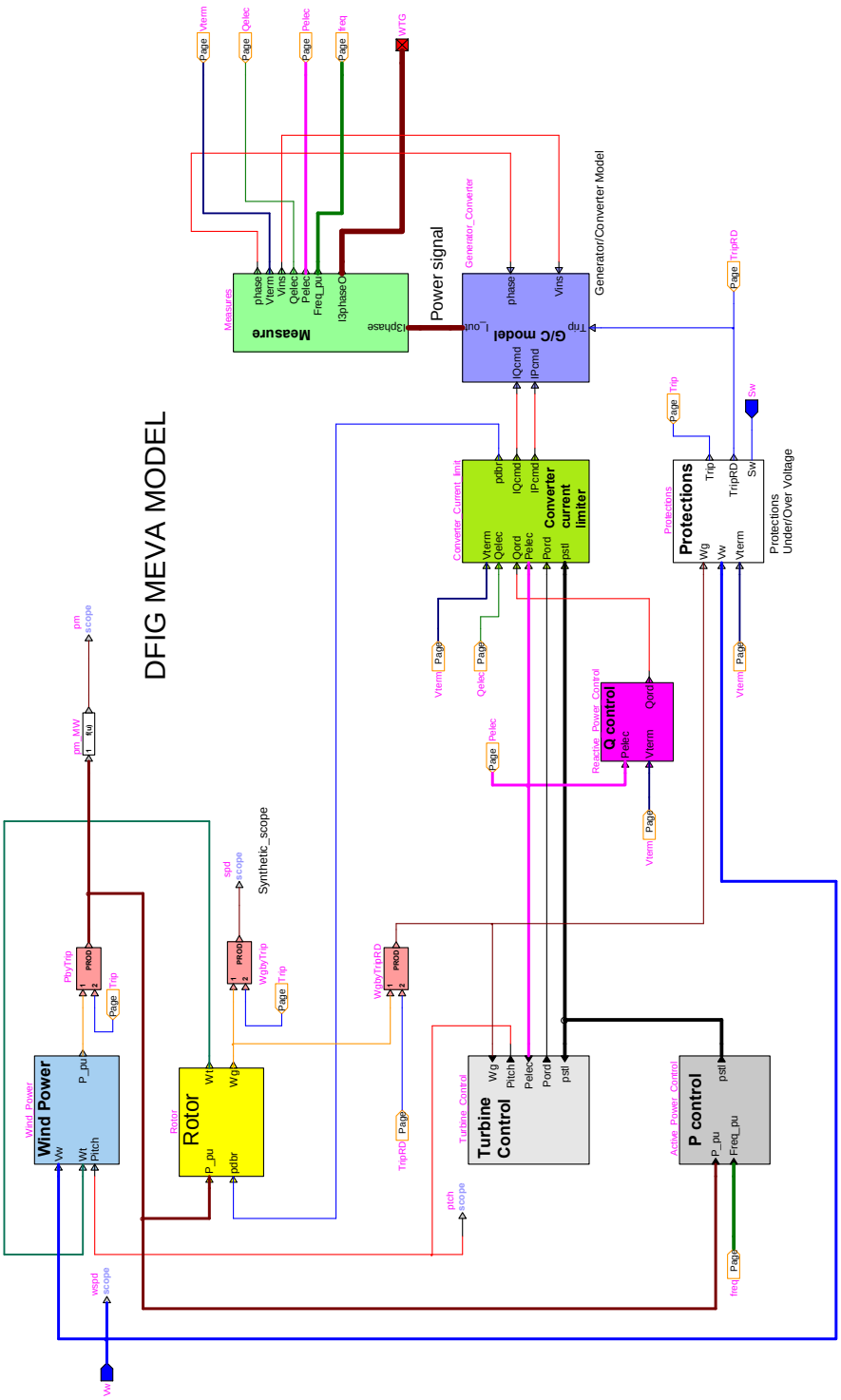

Figure 77: Model block components

4.1.2.1 Active power control

The grid access code, elaborated by power utilities, does not distinguish the requirement levels between conventional thermal generation and wind generation. In this context when the utility requirements surpass the wind generator performance, the wind generator manufacturer solution is often the addition of an active power control (APC) system with the following objectives:

- enforce a maximum wind farm power output;
- provide a specified power margin by generating less power than available;
- enforce a farm power ramp rate limit;
- respond to the system frequency excursions.

In normal conditions with near nominal system frequency, the control is either enforcing a maximum wind farm output or providing a specific margin by generating less power than is available from the wind, e.g. 95% of the available power. This is illustrated in the Figure 78.

In response to frequency excursions, the control switches into another mode and calculates a farm power order as a function of the system frequency. This path requires a higher than usual power order for the low frequency events and lower than usual power order for the high frequency events. Thus the wind farm will generate additional power in response to the loss of other generating facilities or less power in response of the loss of load by load shedding relays. Each WTG should have an active power control with the power order signal provided by the wind farm control.

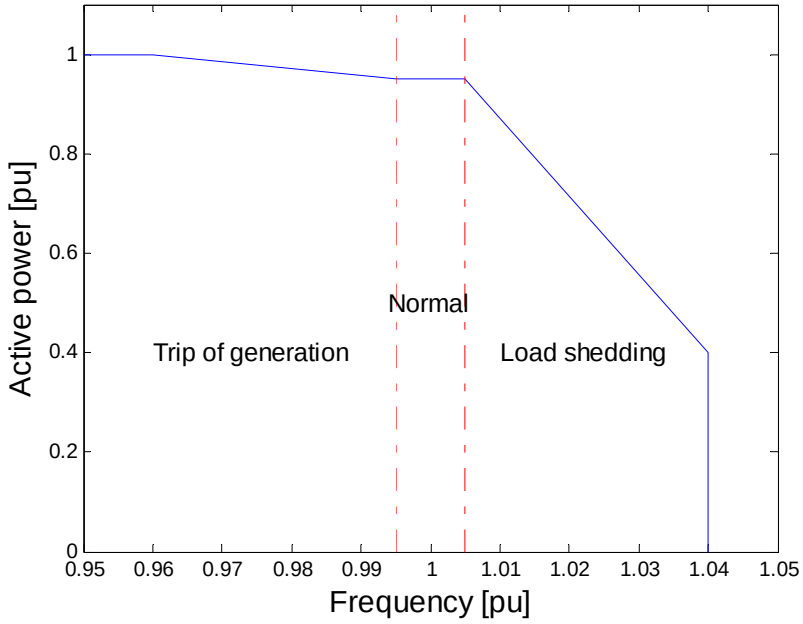

Figure 78: Active power control.

4.1.2.2 Generator/converter control model

This model is the equivalent between the generator and the field converter and provides the interface between the WTG and the network. Its mechanical states are represented in the turbine model blocks.

Unlike a conventional generator model, all of the flux dynamics have been eliminated to reflect the rapid response to the high level commands from the electric control through the converter. The net result is a controlled three phase current source that computes the required injected currents into the network in response to the flux and the active current command from the electrical control model. These controlled sources also incorporate the fast acting converter control to mitigate the overvoltage by reducing current output. It is shown in the Figure 79.

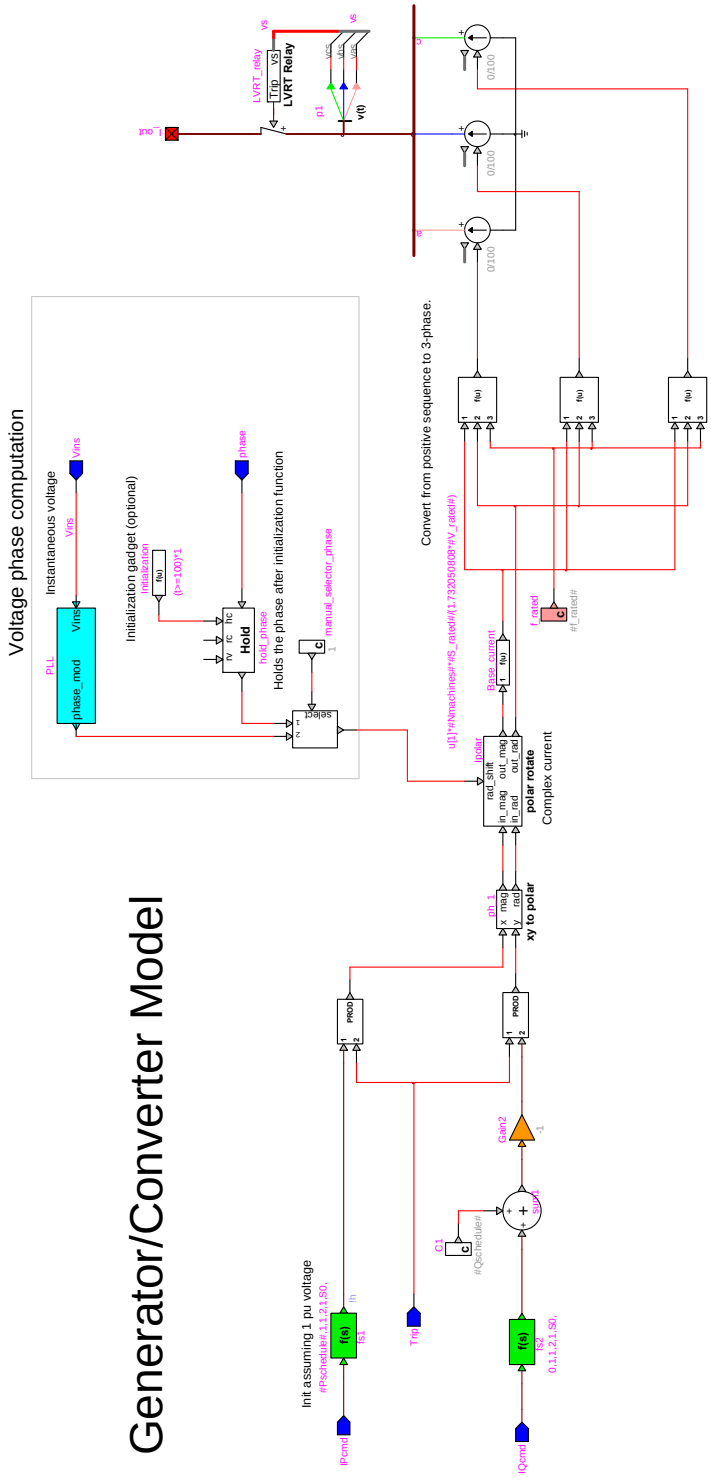

Figure 79: Generator/converter MEVA model

The two low-pass filters are simple approximations to the complex fast electronic control system. The converter control includes a PLL to syncrhonize the generator rotor currents with the stator. The PLL has the effect of establishing a reference frame to the WTG voltage and current. As shown in section 3.1 a new PLL model is used in the MEVA approach.

4.1.2.3 The PLL for the MEVA model

The MEVA approach consists in the development of a reduced order three phase DFIG model using the EMTP-RV program, without the network simplifications used in the stability type programs, such as PSS/E. The generator/converter model has a three phase current source where the phase angle is determined by a PLL based on the transformation from time domain to phasor domain. The phase angle of the terminal voltage, calculated from the transformation considers a fixed period associated to the fundamental frequency.

The PLL model presented here is based on the initial idea presented in [23]. It is integrated to the MEVA model. The proposed method is described in the context of modulation theory. It is restated and rearranged here in the context of the model proposed in this thesis.

Let x be continuous, real valued, not necessary periodic function. Assume further that a finite $T>0$ is given. For every $s \in R$ define an associated time limited function. One may view x_w^s as a windowed version of the original function x. The window being of length T and centered about s.

$$x_w^s : [s-\frac{T}{2}, s+\frac{T}{2}] \rightarrow R \tag{4.1}$$

$$x_w^s(t) \begin{cases} x(t);\ t \in [s-\frac{T}{2}, s+\frac{T}{2}] \\ 0\ otherwise \end{cases} \tag{4.2}$$

With $x_w^s(t)$ it is possible define a periodic function $x_p^s(t)$ by appropriately patching together the windowing function $x_w^s(t)$.

With each center point $s \in R$ we associate a periodic function $x_p^s(t)$. Another way should be, for a given value of the parameter T, every continuous real valued, induce a family of periodic function $x_p^s(t)$, indexed by the centered point s. The Fourier series that responds to the periodic function $x_p^s(t)$ is given by

$$x_p^s(t) = \sum_{k=-\infty}^{\infty} ck(s).exp(jkwt) \tag{4.3}$$

Thus the complex coefficient $ck(s)$ as instantaneous Fourier coefficient or instantaneous phasor associated with a given function x and a window length T.

$$ck(s)=\frac{1}{T}\int_{s-\frac{T}{2}}^{s+\frac{T}{2}} x(t).exp(-jkwt).dt \tag{4.4}$$

$$w=2\pi/T \tag{4.5}$$

Given that the Fourier coefficient are complex numbers, the phase angle is calculated as a function of the real and imaginary components of each coefficient.

$$\delta=arctan(y,x) \tag{4.6}$$

The phase angle obtained in this way and using a typical EMTP time step of 250 μs, has shown to eliminate problems found in the PLL representation in PSS/E.

4.1.3 Model Tests

The benchmark of Figure 80 is used to test the DFIG MEVA model representing a wind farm integrated by an equivalent generator type DFIG of 20 machines (33.4 MVA) dispatched with P=30 MW. All benchmark data is included in the Appendix B.

Several types of different perturbations, such as three phase bus fault, different wind profiles and change of voltage order, were applied on the first benchmark to test the model response using a single mass model for the shaft.

The numerical time-step is 250 μs

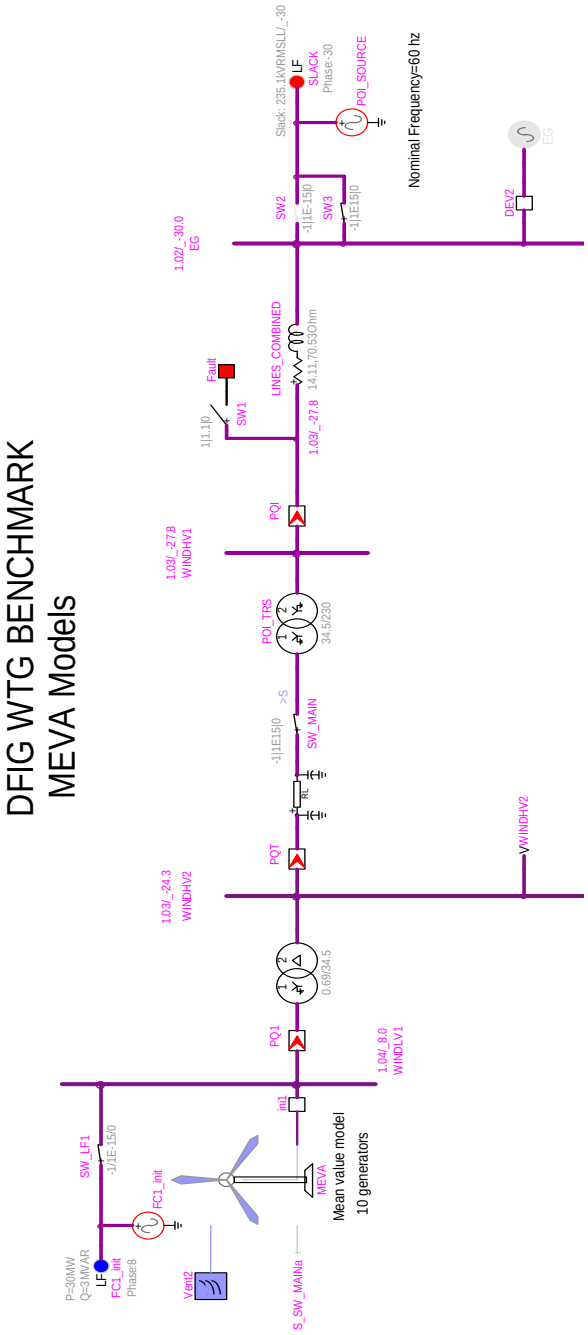

Figure 80: DFIG MEVA benchmark

The following perturbations are applied:

- Test 1, Small perturbation of ±5% on the terminal voltage of the equivalent was applied with the objective of obtain a linear response of the controls.
- Test 2, Three phase fault on the interconnection point through a fault resistance of 30 Ohms is applied during 100 ms.
- Test 3, Wind ramp simulation.

When Figure 80 the results are compared to the PSS/E results (see Figure 35) it is concluded that PSS/E is able to reproduce approximately MEVA modelling results. PSS/E is however less precise due to its large numerical integration time-step and approximation in the network model.

The higher accuracy of the MEVA model is confirmed by the detailed DEMTP reference.

4.1.3.1 Test 1, Voltage perturbation

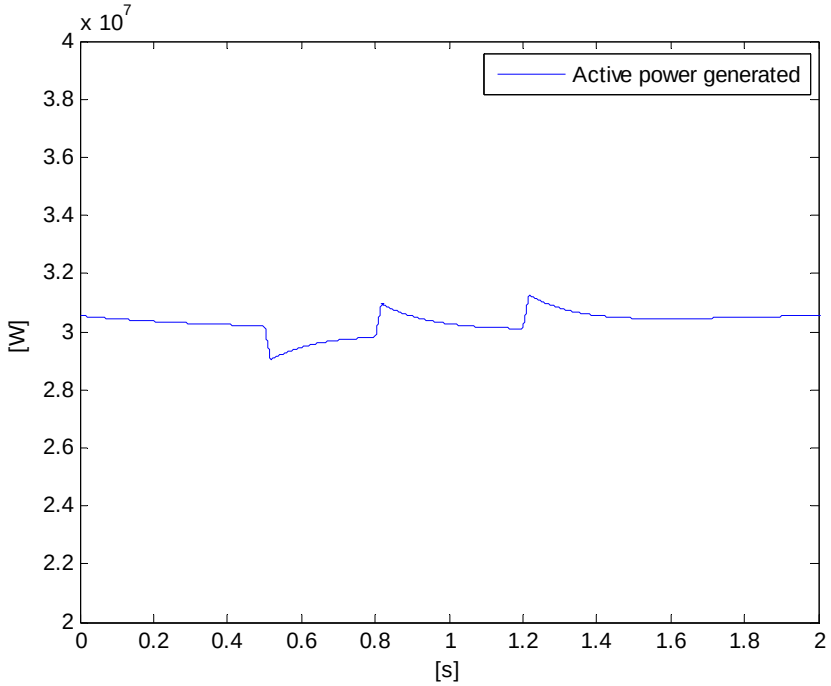

Figure 81: Active power injected from the wind farm.

The mechanical power remains constant since the wind is constant. In consequence the active power injected by the WTG at the bus WINDLV1, will remain constant in the final steady-state after perturbation. This trend is shown in Figure 81.

The wind speed is constant and equal to 11.5 m/s. The pitch angle is also constant and equal to zero. The Figure 82 show the reactive power of the WTG measured at PQ1. It rises when the voltage step lowers and drops when the voltage step increases but it does not reach the limits of reactive power.

The perturbation is a step change of ±5% on the Grid voltage on bus EG. The Figure 83 shows the terminal voltage of the WTG at the bus WINDLV1. This voltage tracks the grid voltage but finally the WTG Terminal voltage is controlled at its reference value.

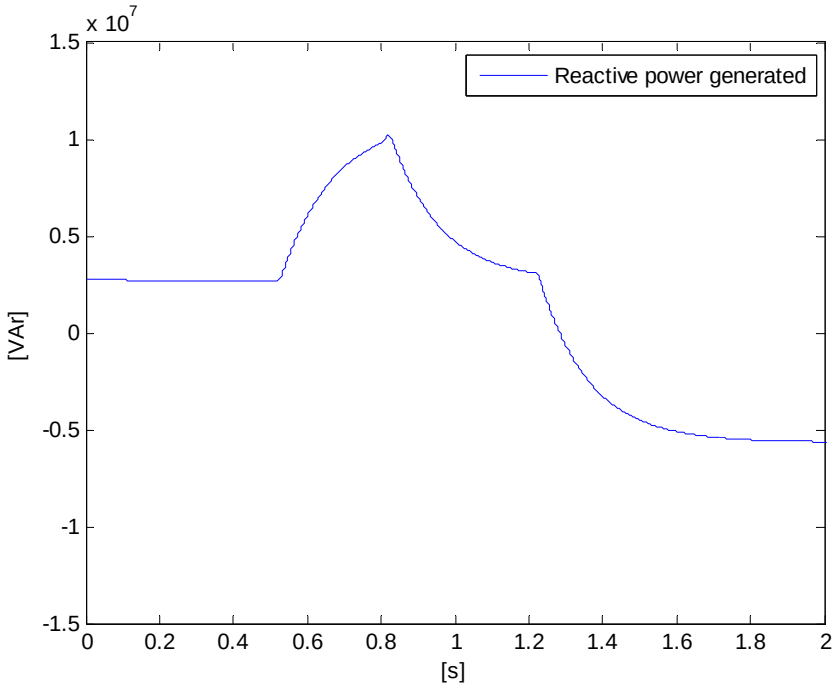

Figure 82: Reactive power injected from the wind farm.

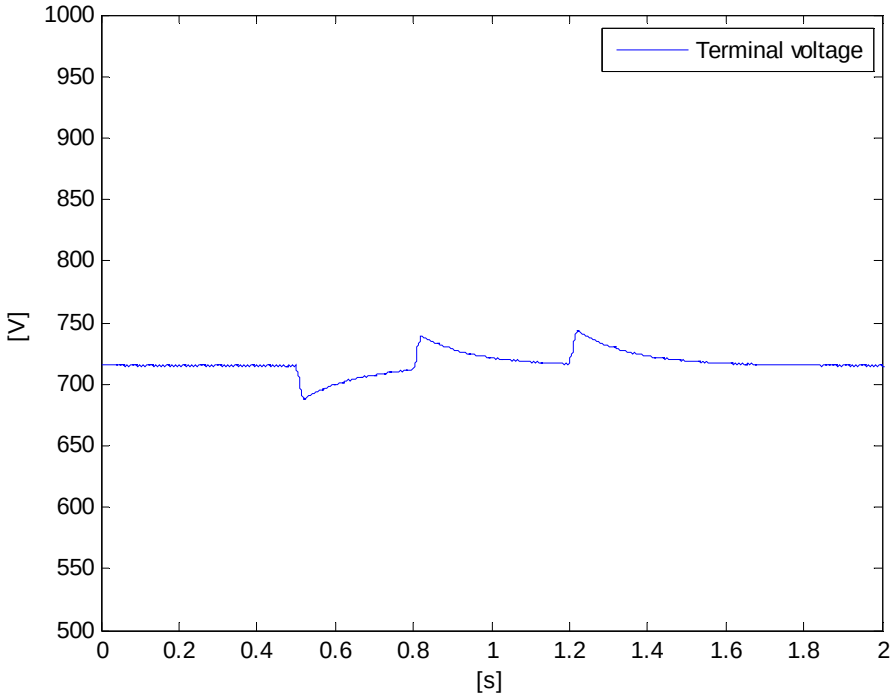

Figure 83: Voltage at terminal bus of wind generator.

4.1.3.2 Test 2, Three phase fault

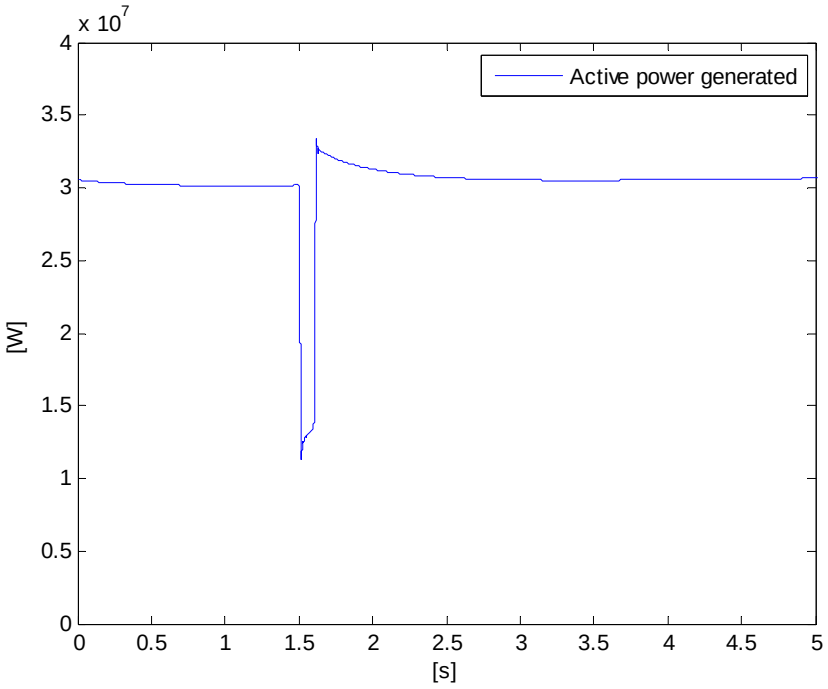

Figure 84: Active power injected from the wind farm

The active power of WTG is shown in Figure 84. The active power measured at PQ1 tracks the voltage waveform. Due to the reduced voltage, the control current is raised and reaches the current upper limit.

The Figure 85 shows as the reactive power injected by the WTG at the bus WINDLV1. It contributes with reactive power to the fault.

The Figure 86 shows the terminal voltage drops near 0.4 pu during the time of fault at the interconnection bus WINDHV1. This voltage does not reach zero due to the fault resistance of 150 Ohms. After the fault is cleared a small voltage overshoot is observed as result of the fast voltage control.

The pitch angle changes by only few degrees to control the over-speed and overload during the fault duration (see Figure 87). The wind speed is constant and equal to 11.5 m/s.

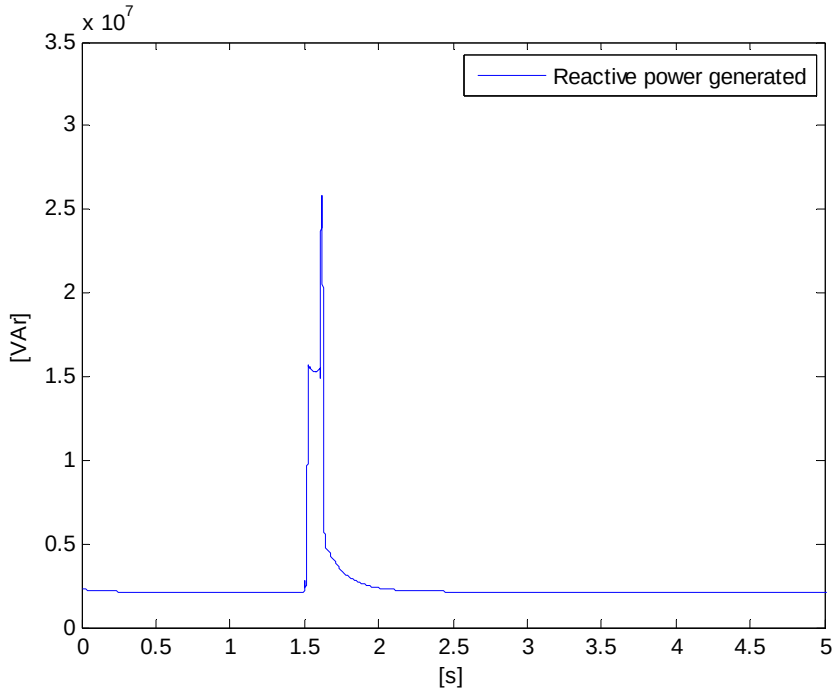

Figure 85: Reactive power injected from the wind generator

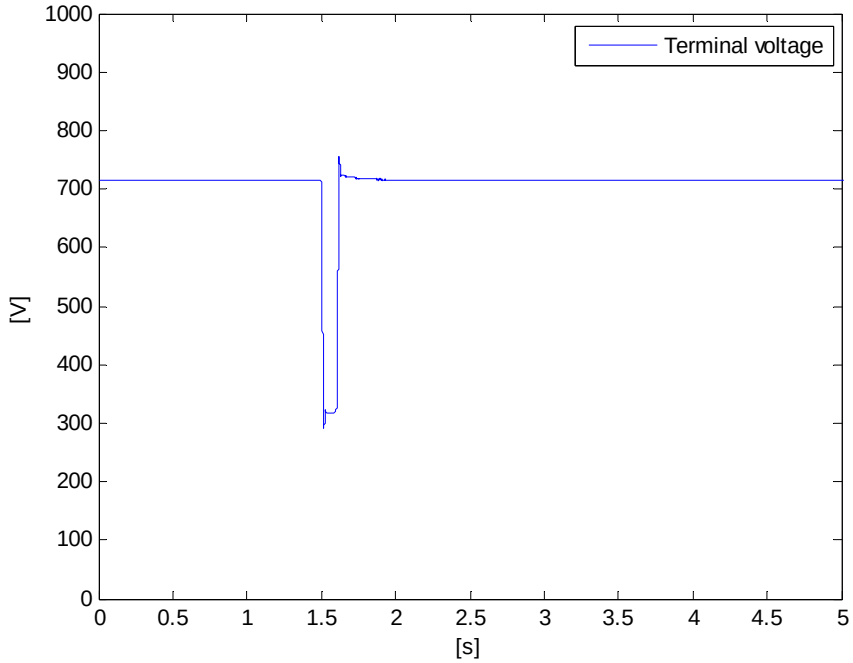

Figure 86: Voltage at terminal bus of wind generator.

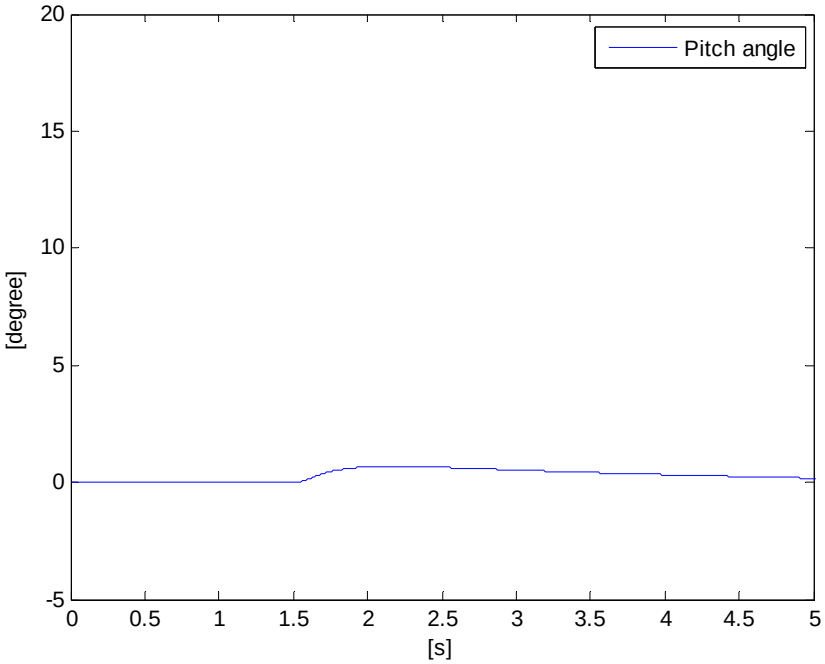

Figure 87: Pitch angle of wind generator.

4.1.3.3 Test 3, Wind Ramp

The Figure 88 shows the wind ramp applied to the WTG at the bus WINDLV1. The pitch action controlled accurately the over speed and only a small change of the active power of WTG occurs (see Figure 89).

The wind ramp is tracked by the pitch angle control to avoid the over speed and the possible overload (see Figure 90).

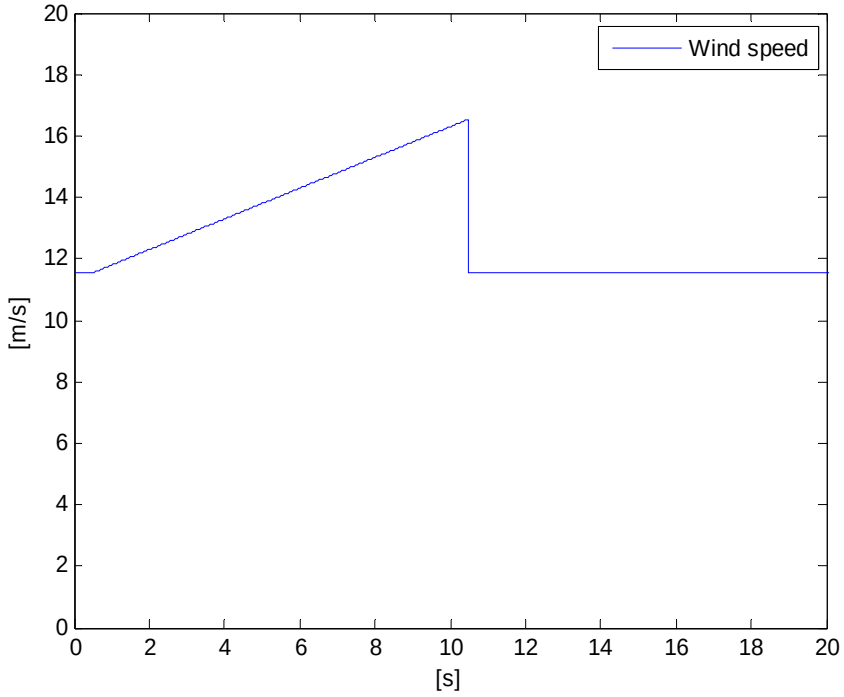

Figure 88: Wind speed.

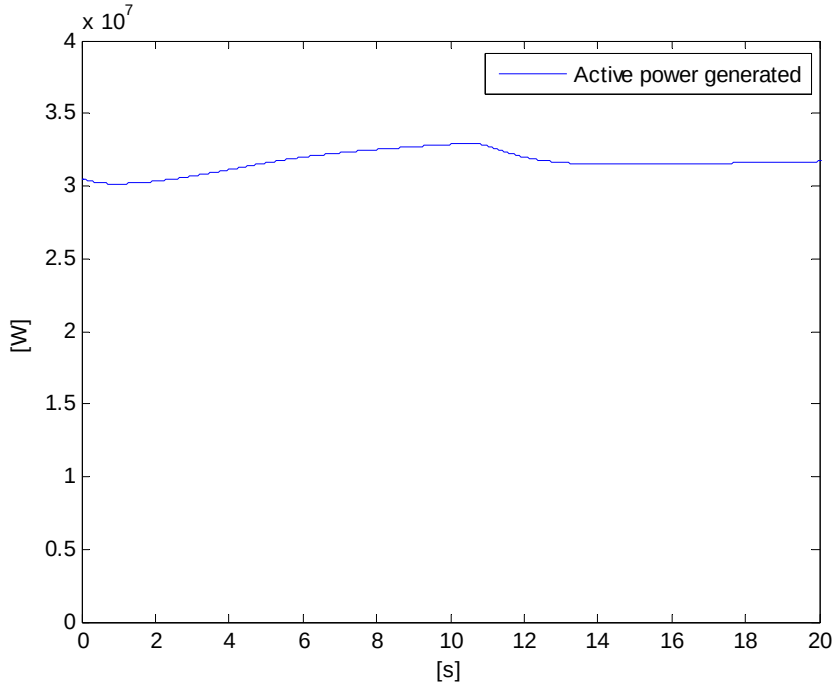

Figure 89: Active power injected from the wind farm.

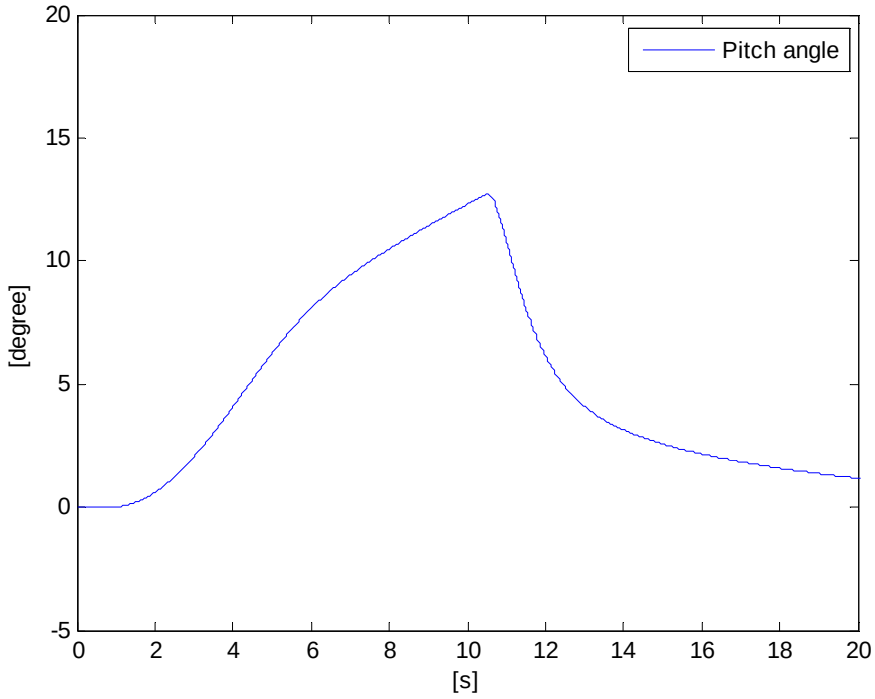

Figure 90: Pitch angle of the wind generator.

4.2 Full converter MEVA model

The top level view of the Full Converter (FC) MEVA model with its initialization devices is shown in Figure 91.

The FC MEVA has a bigger converter than the DFIG version and allows a better voltage control and reactive power control. Since the generator is completely decoupled from the grid, the active power control is more accurate.

The FC_WTG device shown in Figure 91 is a subnetwork with several subnetworks for its various modeling functions and control systems.

Almost all parameters of the device can be modified through its mask. There are two external interfacings points (pins). The right pin is a 3-phase pin allowing to connect the FC_WTG device to the 3-phase network. The left pin is used for providing the random variation of the wind speed. The mean wind speed is found inside the top level mask as parameter.

Each FC_WTG device can represent one or more generators and include a complete wind farm.

Since the model must be initialized it is need to perform a Load flow solution followed by a steady-state solution. The LF device provides the PQ constraints of the FC_WTG. The LF device is used in the load flow solution and together with other LF devices, it allows the calculation the Load-Flow solution phasor for the complete network. The steady-state and the following time-domain solutions can be started from the Load-Flow solution.

In the steady-state solution the ideal voltage source is used to provide the phasor found in the Load-Flow solution. The voltage source is disconnected before the first time point computation in the time domain solution, but allows to initialize the state variables of the simulated network. At the same time the FC_WTG is turned on and starts controlling its internal source for the rest of simulation. It is also noticed that the FC_WTG must provide the same PQ constraints and must be given Load-Flow solution voltage at its terminal. To reproduce this same behaviour with the FC_WTG model, the values of Pschedule, Qschedule and Vschedule must be included in the main mask of the FC_WTG device. In this way and according to the method described in the section 2.9, the initialization of the MEVA model is fast and accurate.

The contents of the breaker connecting the FC_WTG to its network are shown in Figure 91.

4.2.1 Model mask

When the FC_WTG device is double clicked it opens a subcircuit mask with a collection of parameters. Each device can be given a separate set of parameters for the same subnetwork contents. Most parameters are physical parameters for the representation of the machine model. Only a few parameters must be adjusted to represent various operation conditions and match available simulation results.

Basically the parameters that must be adjusted are found in the Generator Data and Schedule Data of the main mask model.

Generator Data:

Nmachines = Number of machines

S_rated = Aparent rated power in (VA) per machine

V_rated = RMSLL Terminal voltage in (V)

f_rated = Rated frequency in (Hz)

Scheduled Data:

Vschedule = Terminal voltage in pu, value from the load flow solution

Pschedule = Active power in pu, value from the load flow solution

Qschedule = Reactive power in pu, value from the load flow solution

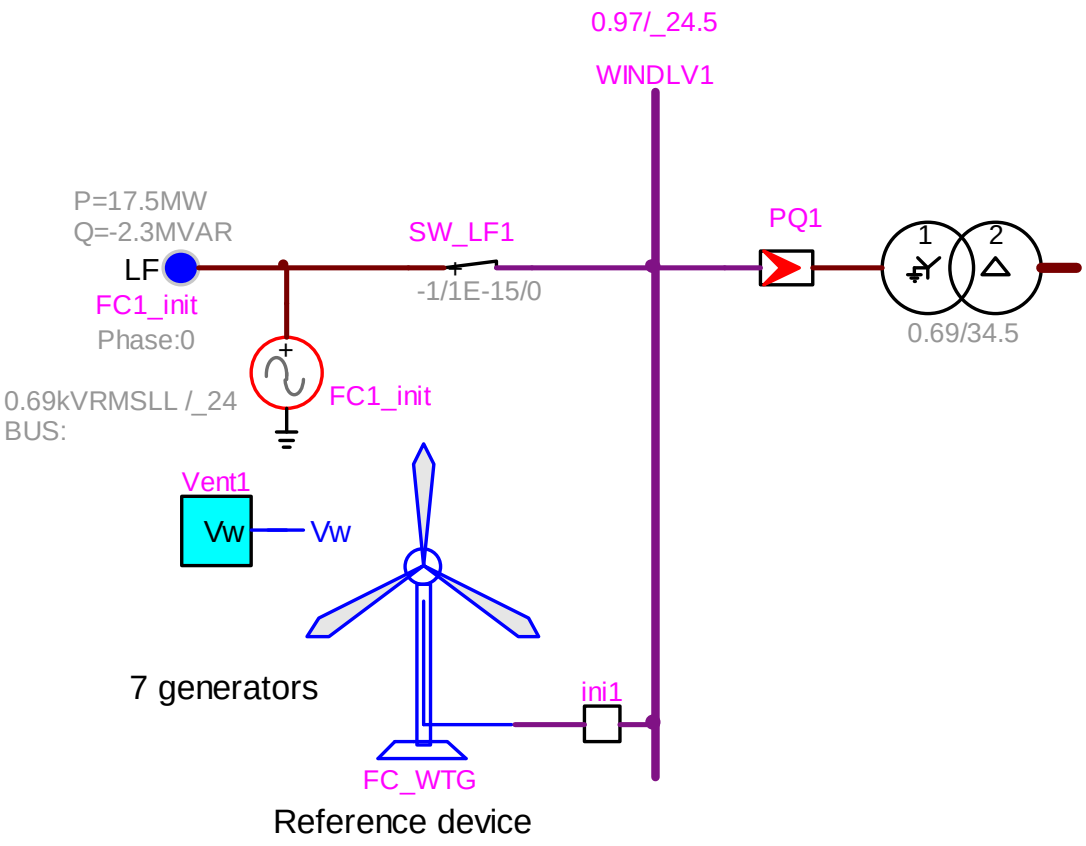

Figure 91: Top level device view of the FC_WTG and Initialization switches for connecting the FC WTG in the time-domain solution

Additional parameter values which are found in the initial condition values window, Figure 92, it divide in sections Rotor Mechanical model, Turbine Control, Active Power Control, Reactive Power Control, Dynamic Breaker Resistor, Low Voltage Power Logic, Converter Current Limit, Protection.

The Normal operation is defined by default parameters values. There are also some optional parameters, such as:

- Activation or desactivation of the active power control.
- To select the alternative of reactive power control and priority selection.

The initialization of the mechanical variables; wind speed, pitch angle and slip; are obtained using the method described in section 2.1.3 (through a MATLAB script). The wind speed is introduced into the wind block and the initial pitch angle into the main mask.

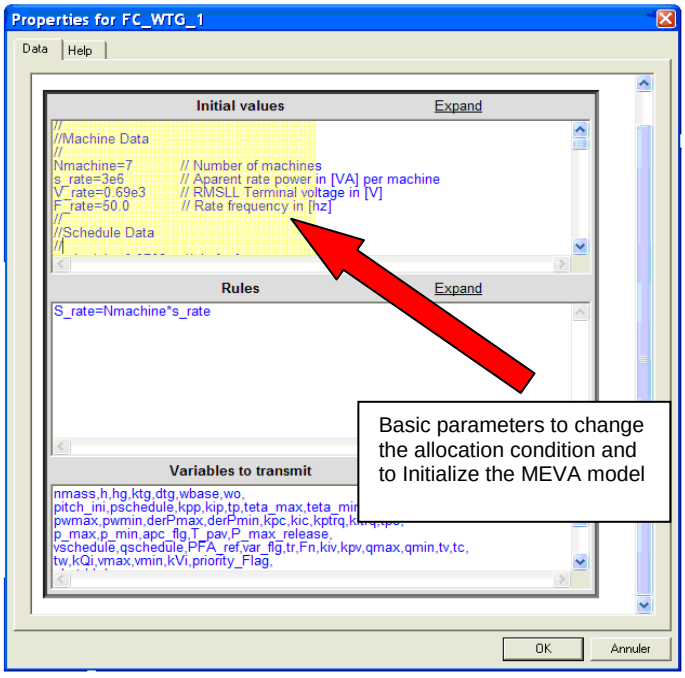

Figure 92: Initial value window for the MEVA model

4.2.2 Full converter block components.

The FC model components are found in Figure 93.

The MEVA modelling approach shares the same PSS/E model blocks defined in CHAPTER 2, in consequence the blocks presented in Figure 93 are directly related:

- For the wind block, vent1 of the in the Figure 91, see the section 2.2,
- For the mechanical turbine model, Wind power in the Figure 93, see the section 2.1.2.3,
- For the pitch control, Turbine control in Figure 93, see the section 2.3.4,
- For the rotor model, Rotor in the Figure 93, see the section 2.5.1,
- For the reactive control, Q control in Figure 93, see the section 2.7,
- For the torque and power control, Turbine control and converter current limiter in Figure 93, see the section 2.6,
- For the protection block model, Protections in Figure 93, see the section 2.8.

The MEVA model includes additional components in addition to the PSS/E model blocks, all included into the current converter limit block of Figure 93:

- Converter Current Limit (CCL),
- Dynamic Breaker Resistor (BR),
- Low Voltage Power Logic (LVPL),
- LVRT voltage support (VS)
- Priority selector of P or Q in the current limit (PS).

A complete description of each function is given in the subsections below.

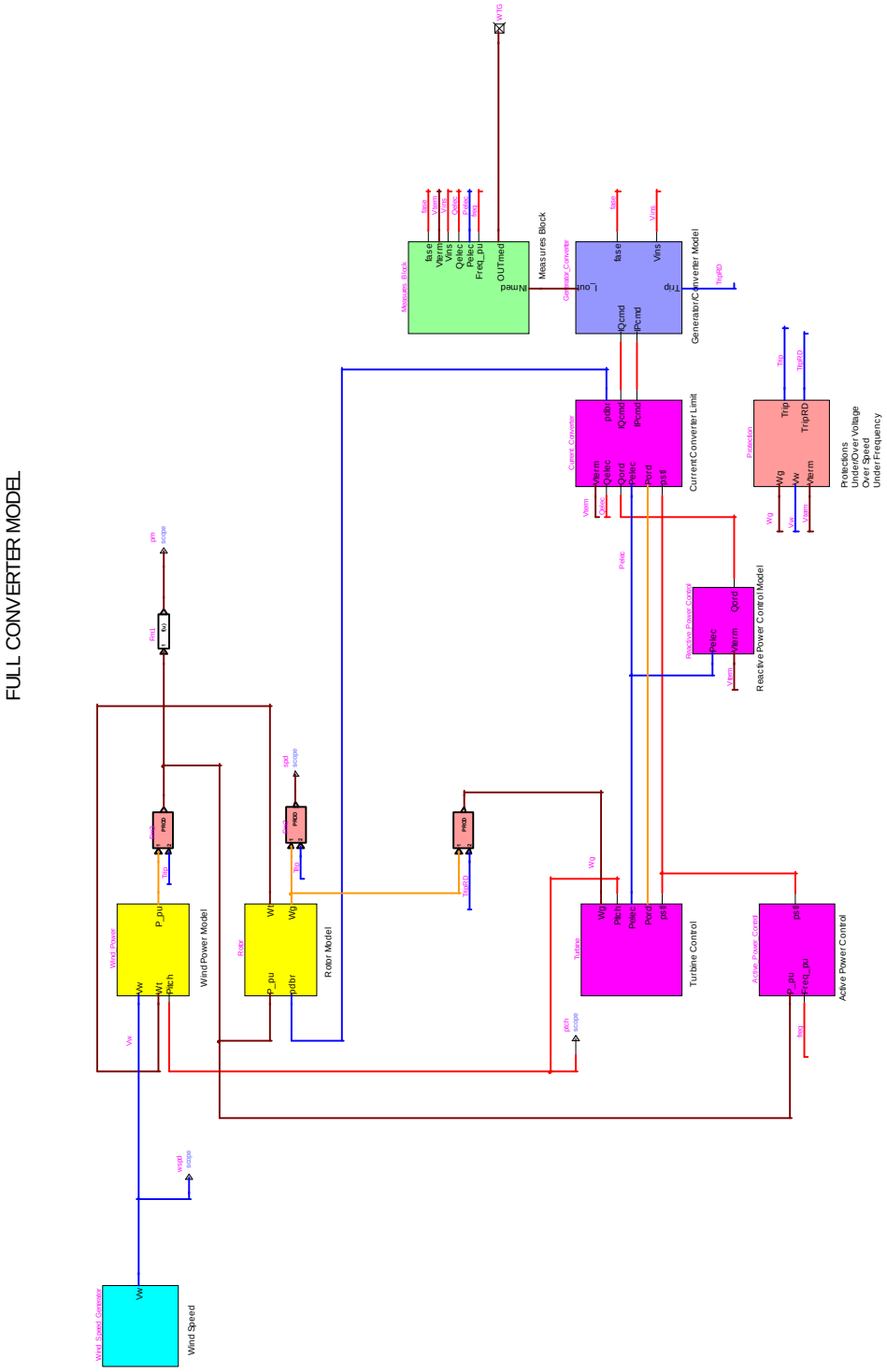

Figure 93: Model block components

4.2.2.1 Current converter limiter control block

This block is essentially the same as the current converter limiter shown in Figure 28, it additionally includes the new characteristic associated with FC CCL-BR-LVPL-Q Priority and LVRT support, which modify the original block connection. It is shown in Figure 94. This model calculates the active and reactive powers to be delivered to the system based over inputs from the turbine model, Pord from the power/torque control model shown in Figure 21, and the supervisory var controller, Qord. Qord can also be held constant or determined by a power factor regulator.

The electrical control is a simplified representation of the converter control system. This model monitors the generator reactive power and the terminal voltage to compute the command currents IQcmd and IPcmd shown in Figure 94 and equation (3.2). The voltage error is multiplied by a gain and integrated to compute the current command. The magnitude of the gain determines the effective time constant associated with the voltage control loop. The IQcmd is limited due to the hardware constraints.

The active current command is computed by dividing the active power order, from the wind turbine model, by the generator terminal voltage. The active current command is limited to the short term active current capability of the converter.

The primary structural change to the model was to generate the reactive current command rather than a flux command. Additional functions include a dynamic breaking resistor, low voltage power logic, converter current limit and LVRT voltage support will be developed in the follow section.

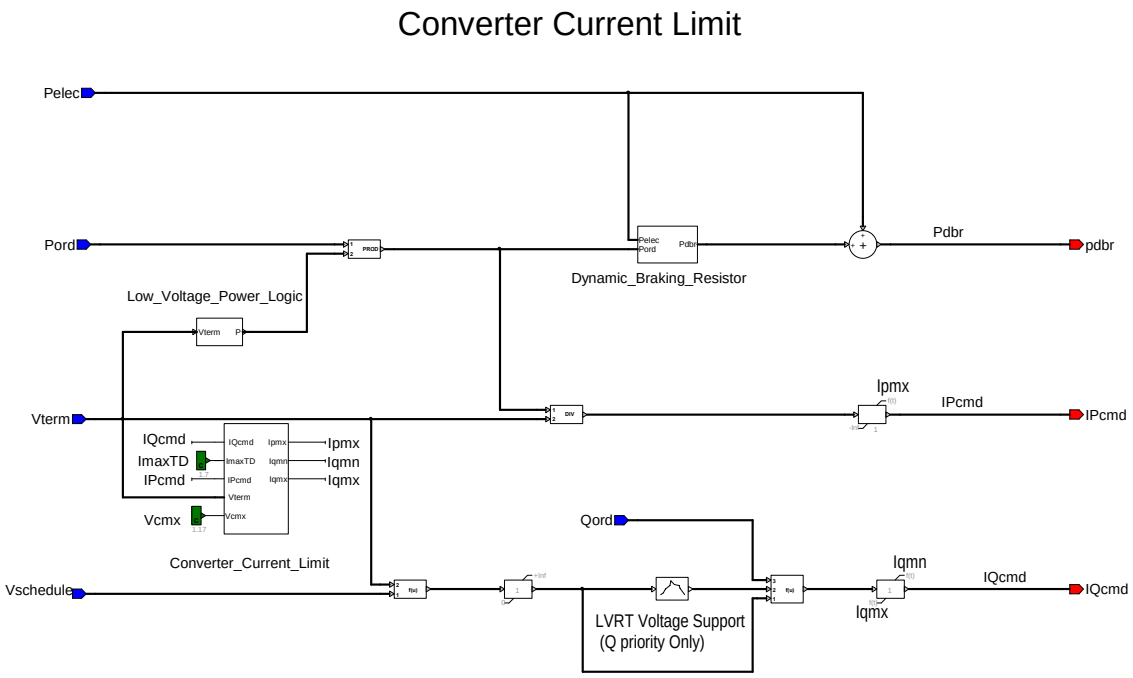

Figure 94: Current converter limiter

4.2.2.2 Dynamic breaking resistor

The objective of the dynamic breaking resistor is to minimize the WTG response to the large system disturbances, such as extended periods of low voltage. This is accomplishing by absorbing energy in the breaking resistor when the power order is significantly greater than the electric power delivered to the grid. In this model (Figure 95) the power order is compared with the actual electric power to determine the power absorbed by the breaker resistor, Pdbr. This is integrated to determine the resulting energy to the breaker resistor, E_dbr, shown in Figure 95. As long as the energy level is less than the threshold, Ebst of 0.2 pu, no other actions occurs. When the energy level exceeds the threshold the resulting error signal is greather than zero and the amount the power absorbed by the dynamic breaker resistor is reduced. This ensures that the energy capability of the resistor is respected.

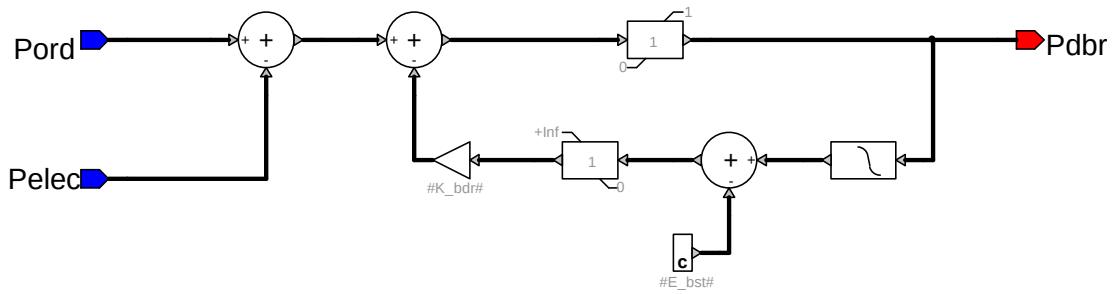

Figure 95: Dynamic breaker resistor

4.2.2.3 Low voltage power logic

The low voltage power logic reduces the system stress during the fault, due to ramping down effect, and immediately following faults, due to ramping up.

When the terminal voltage falls below a given threshold, Vdown in Figure 96, the power order ramps down and then when the terminal voltage recovers to a level above a different threshold, Vup in Figure 96, the power order ramps up. In general the ramp up will be at a slower rate than the ramp down. Again, this is intended to reduce system stress.

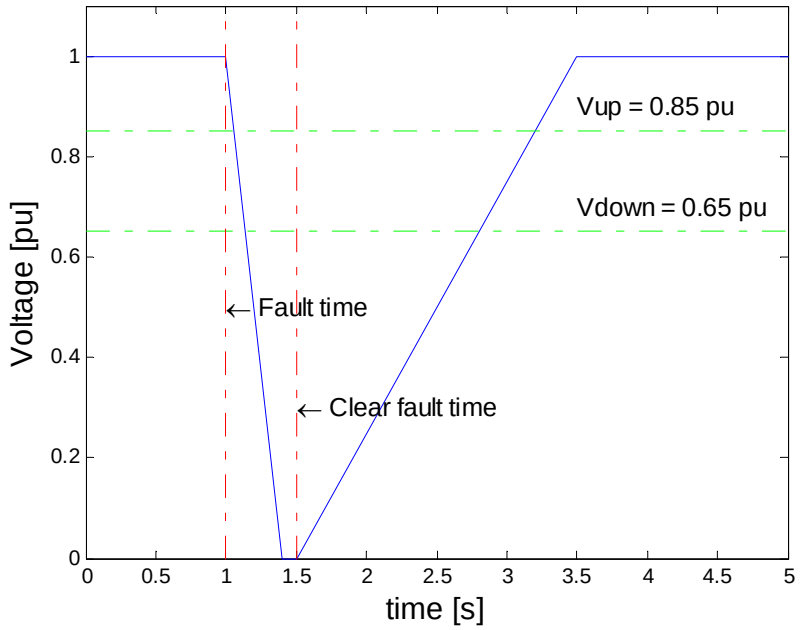

Figure 96: Low voltage power logic

4.2.2.4 LVRT voltage support

A LVRT voltage support function is available in the FC model. The voltage function show the reactive current output as a function of the terminal voltage reduction. The Figure 97 shows that for faults that results in more than 50% of reduction in the voltage, this function provides 100% of the reactive current output. For a fault that results in less than 10% of reduction in the voltage, no action beyond that of the other control is taken. For a fault that results between 10% and 50% of reduction in the voltage, the reactive current output varies as it is shown in the figure below.

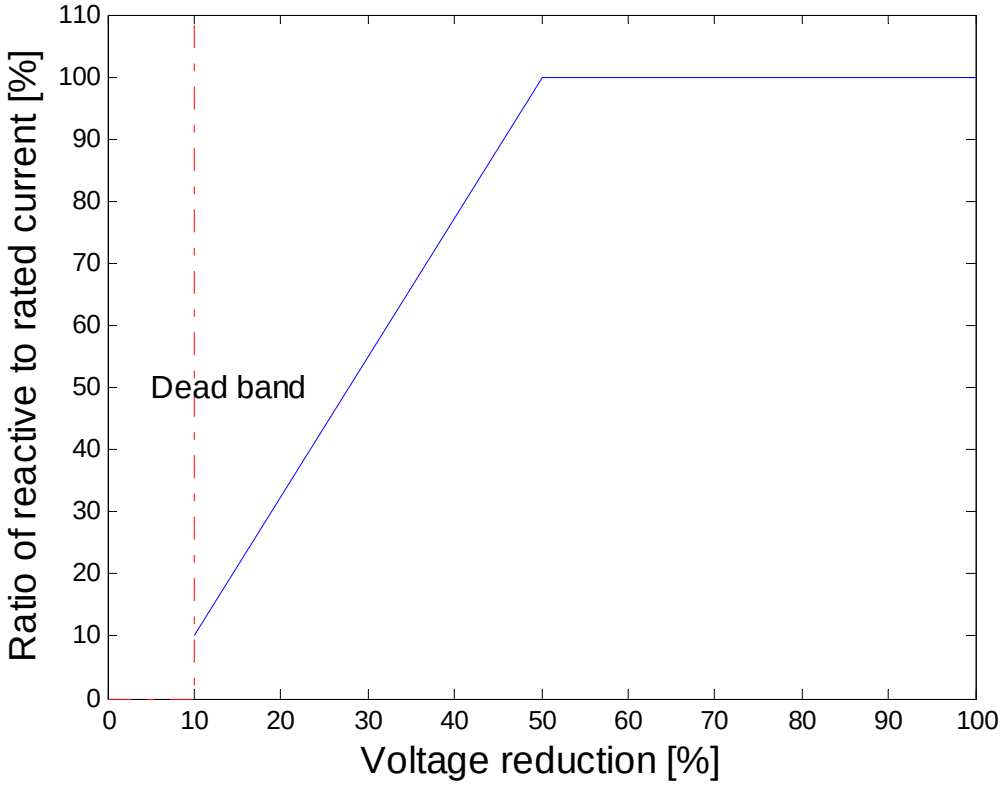

Figure 97: LVRT function

4.2.2.5 Priority of P or Q

The objective of this function is to prevent the combination of active and reactive currents to exceed converter capability. Flag selector determines the operation condition to the priority of P or Q.

4.2.3 Model tests

The benchmark of Figure 98 is used to test the FC MEVA model. The benchmark represents a wind farm with three equivalent generators of 21MVA, 9MVA and 27MVA. The scopes obtained during the simulation are always for FC_WTG_1. The benchmark data is given the Appendix C.

FULL CONVERTER WTG BENCHMARK

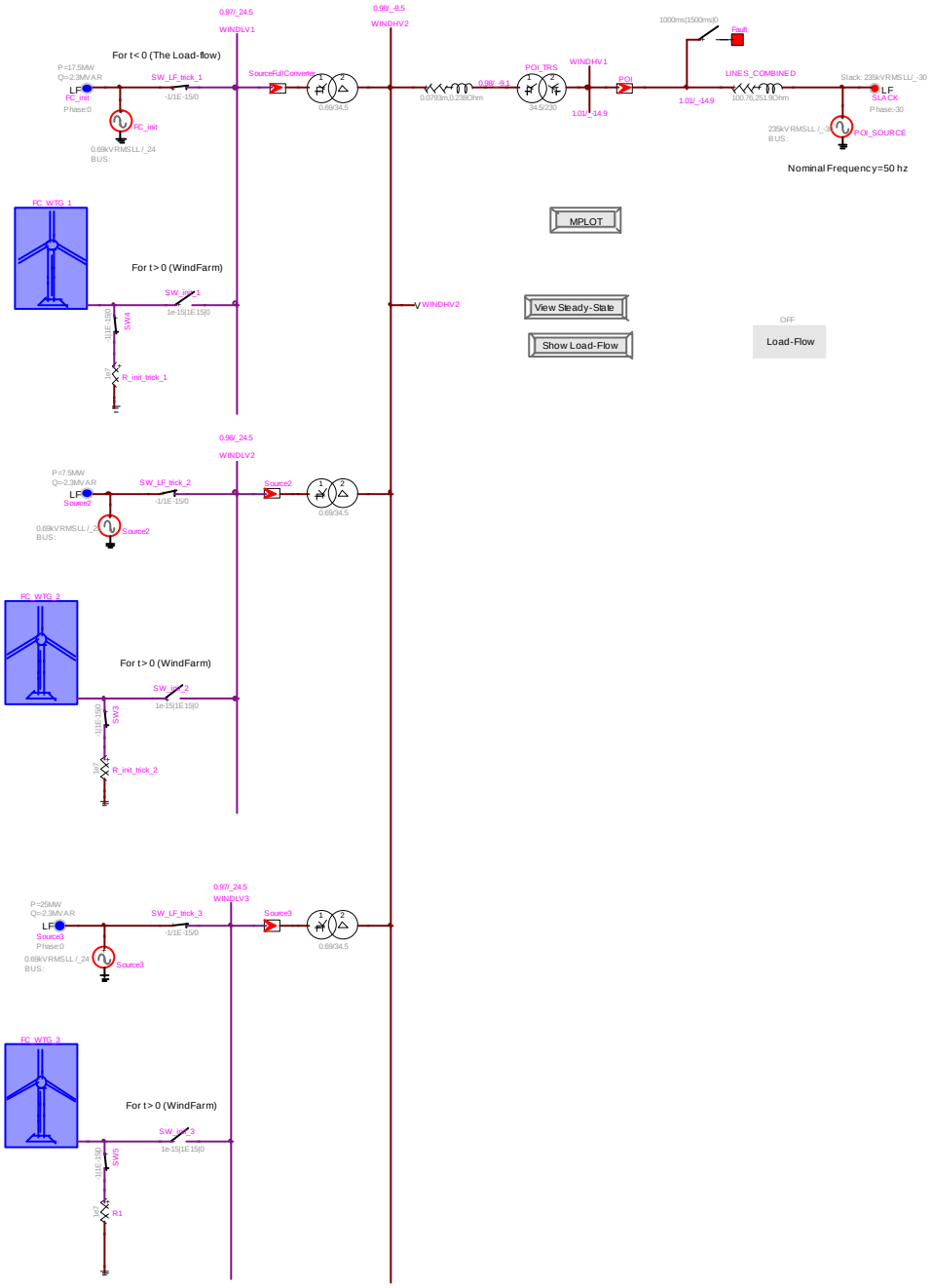

Figure 98: Full converter benchmark, MEVA FC model

The perturbation used in this test include the three phase Bus Fault limited by a resistance. The light fault resistance was of 215 Ohms and the heavy fault resistance was of 38 Ohms. Additionally different Wind Profiles, change of power order and change of frequency were applied. The following tests are performed:

- Test 1: simulation with decreasing wind speed ramp. Figure 99 to Figure 101 show the behaviour for decreasing wind speed ramp. The turbine decreases its speed in 11 s, the rotor speed, the electrical power and mechanical power are zero after 11 s.
- Test 2: simulation with increasing wind speed ramp. Figure 102 to Figure 104 show the behaviour for decreasing wind speed ramp. At 16 s the wind speed passes the wind speed limit of 25 m/s. At 19 s the turbine trips.
- Test 3: response with low voltage power logic to heavy fault at the interconnection point bus Windhv1 (Figure 105 to Figure 108). The fault has been applied at 1 s, the voltage at the bus Windhv1 drops to 0.15 pu during 0.5 s. The power logic was activated during the heavy fault event.
- Test 4: response for a fault at the bus Windhv1. These simulation results are shown in Figure 109 to Figure 111. The fault has been applied at 1 s, the voltage at the bus drops to 0.7 pu during 0.5 s. The power logic is not activated in light fault events.
- Test 5: converter current limit reduction with Q priority. This test shows the response to the test of converter current limit reduction, ImaxTD, with Q priority. The ImaxTD step down is generated by a signal generator (see Figure 112) and applied to the FC_WTG control. At 1 s the reduction has been applied, the current has been limited from 1.7 to 0.8 pu (see Figure 112 to Figure 116).
- Test 6: response of the active power control to the frequency rise starting at 1 s. The frequency ramp (see Figure 117) is generated by a signal generator and applied to the FC_WTG control. The frequency ramp increases from 1.0 pu to 1.02 pu. As result of the control function Active Power Control a power reduction occurs. Simulation results are shown in Figure 117 to Figure 119.

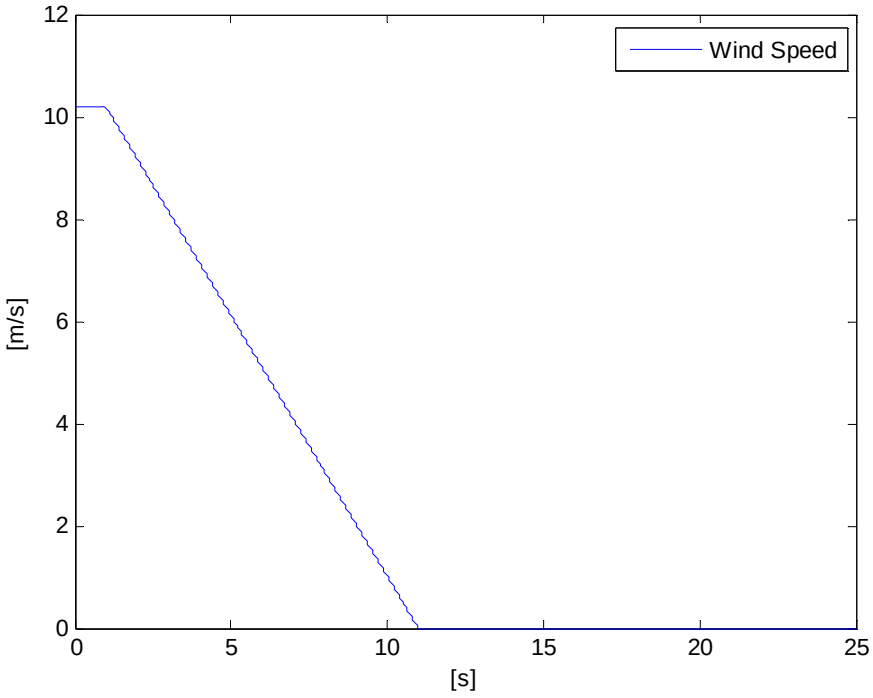

Figure 99: Wind speed applied to FC_WTGs, Test 1

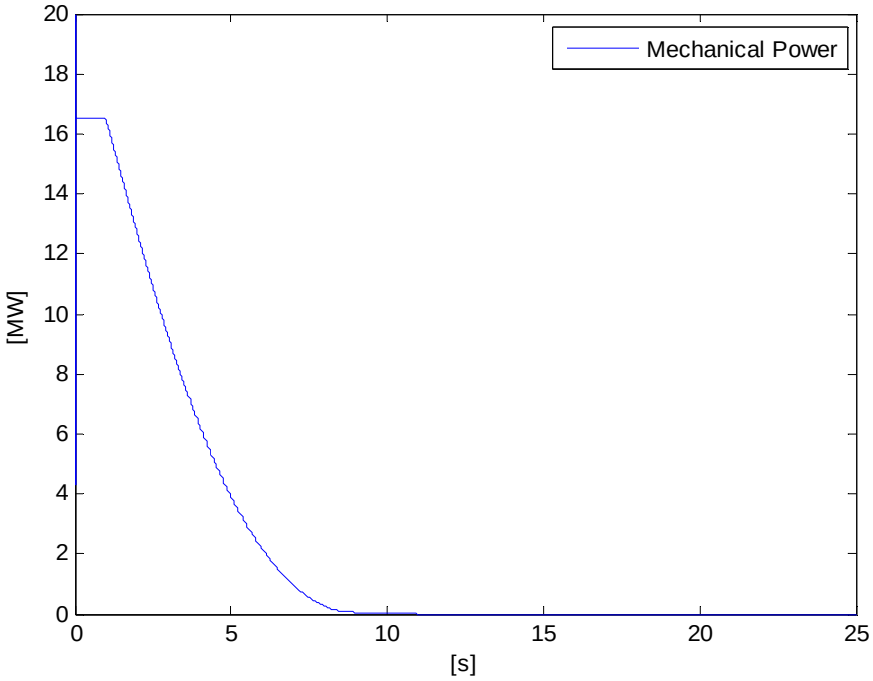

Figure 100: Mechanical power of the FC_WTG_1 turbine, Test 1

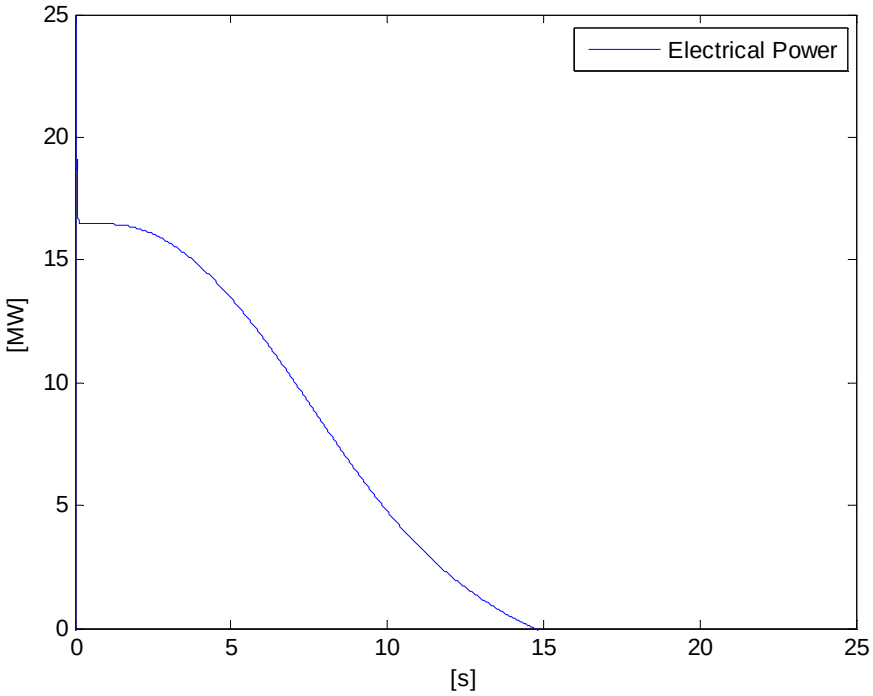

Figure 101: Electrical power output of the FC_WTG_1, Test 1

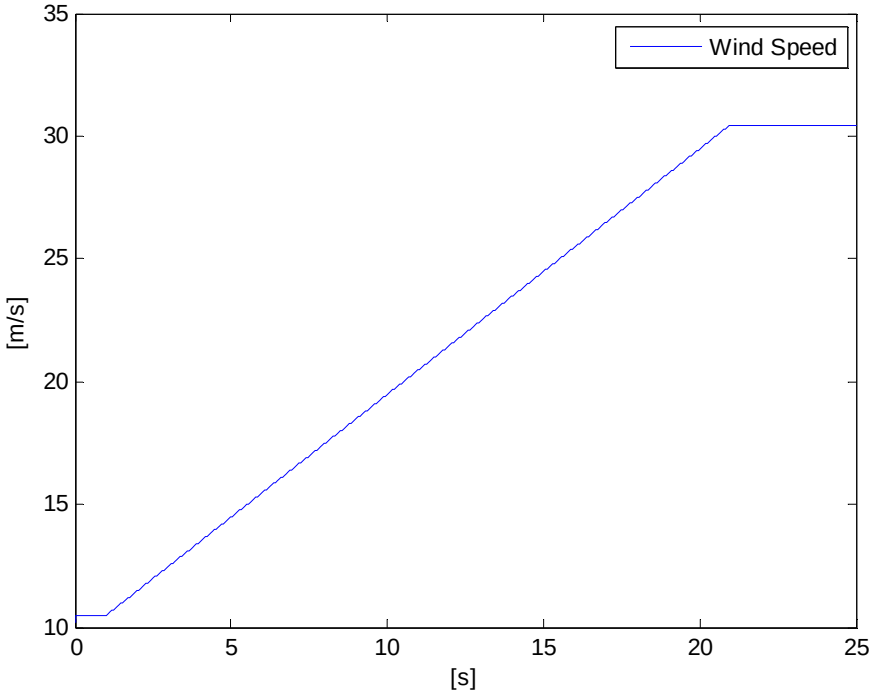

Figure 102: Wind speed applied to the FC_WTGs, Test 2

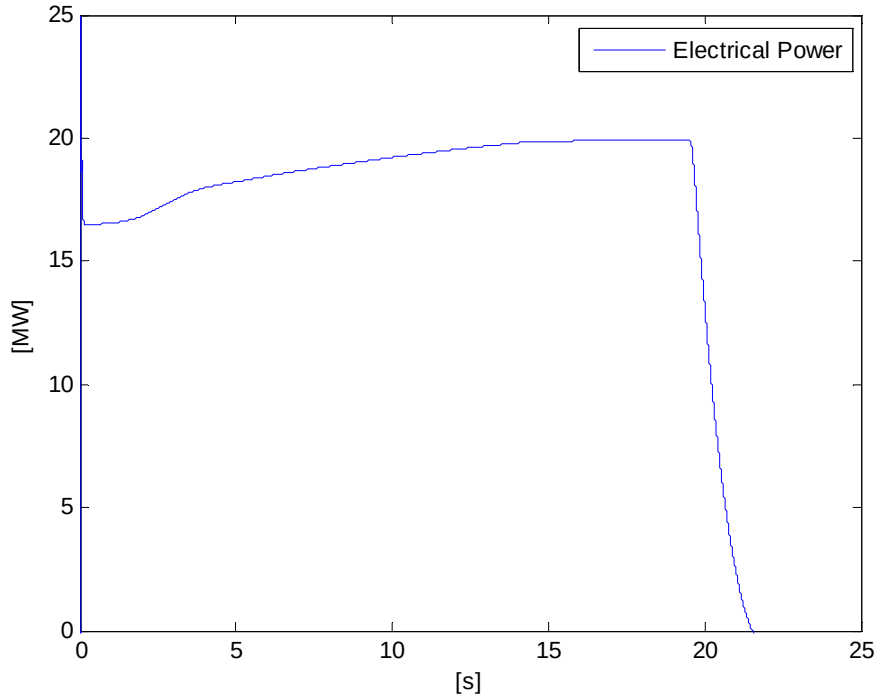

Figure 103: Electric power output of FC_WTG_1, Test 2

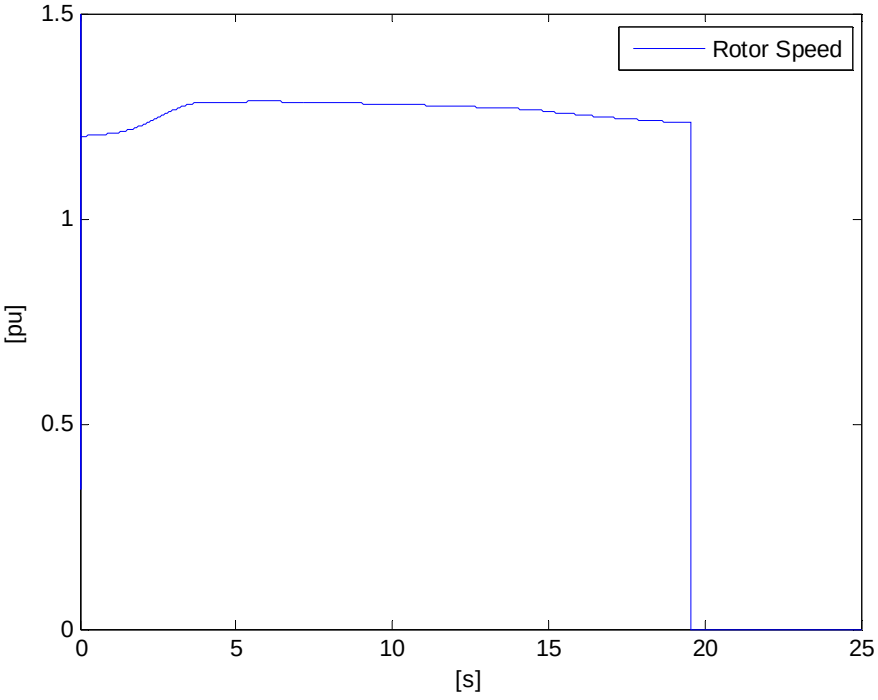

Figure 104: Turbine rotor speed in pu of FC_WTG_1, Test 2

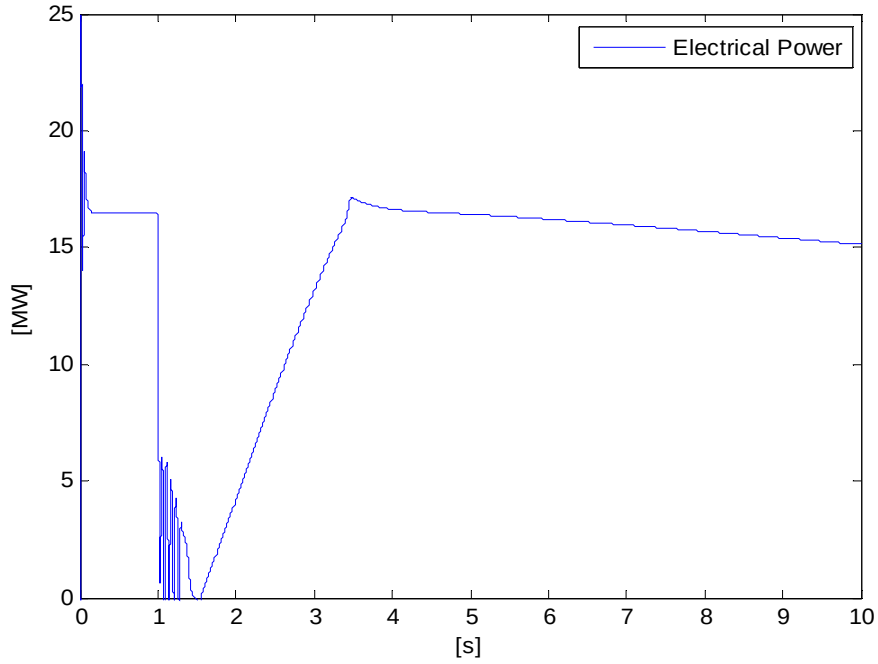

Figure 105: Electric power output of the FC_WTG_1, Test 3

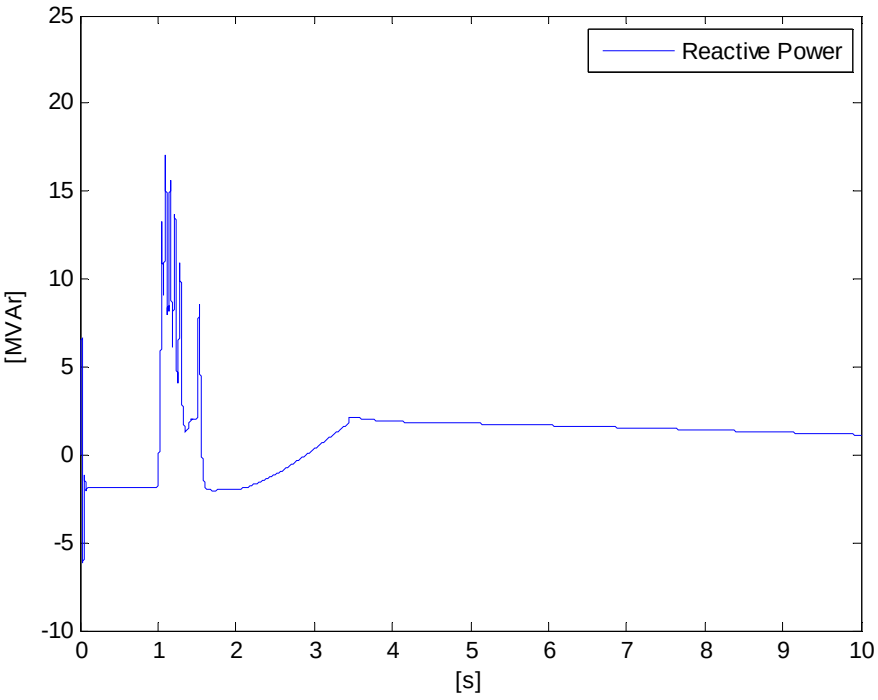

Figure 106: Reactive power output of the FC_WTG_1, Test 3

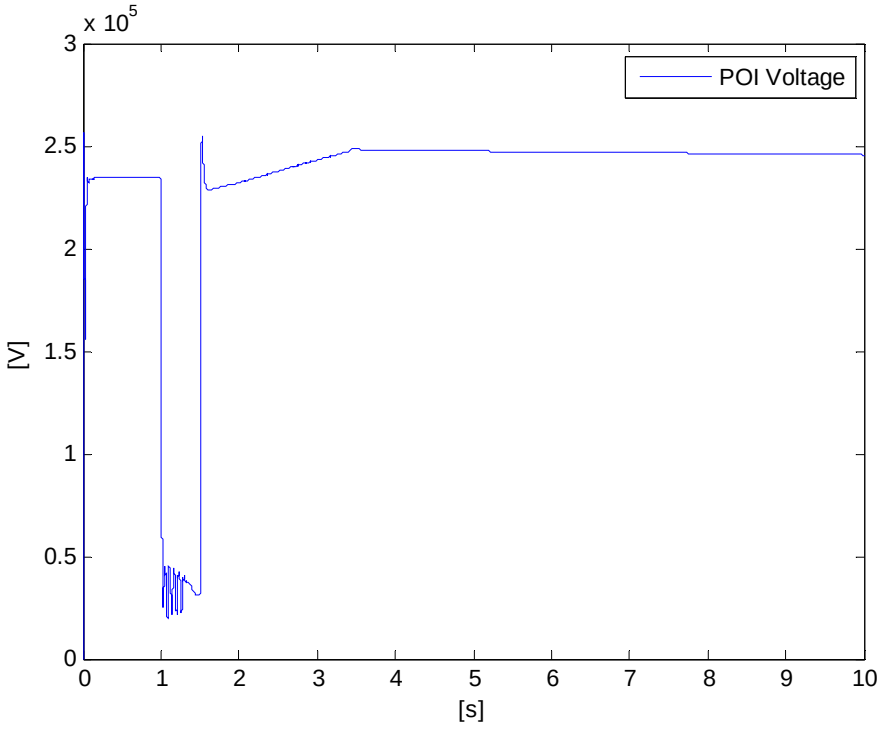

Figure 107: Voltage at bus WINDHV1, Test 3

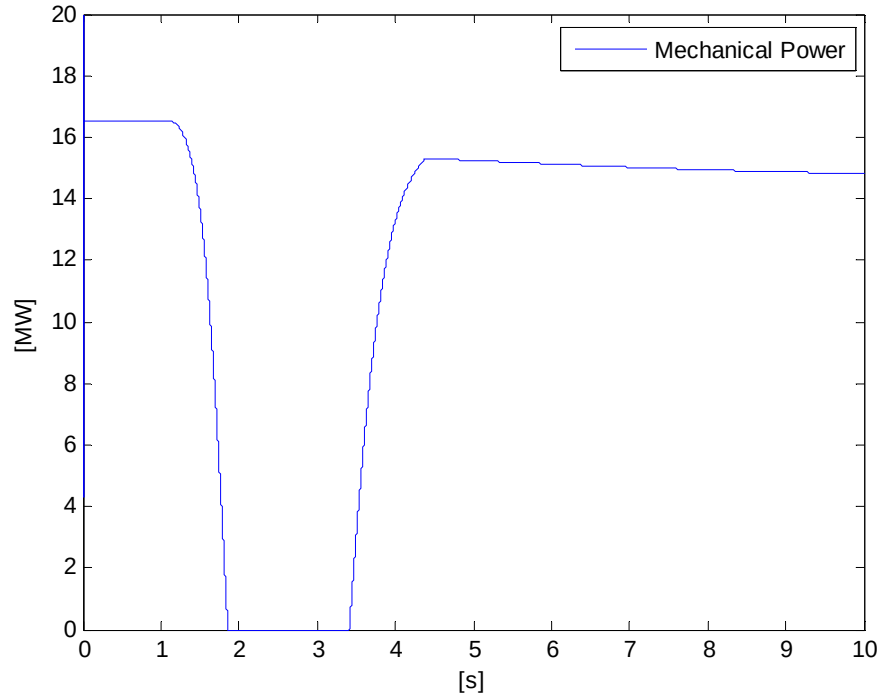

Figure 108: Mechanical power of the FC_WTG_1 turbine, Test 3

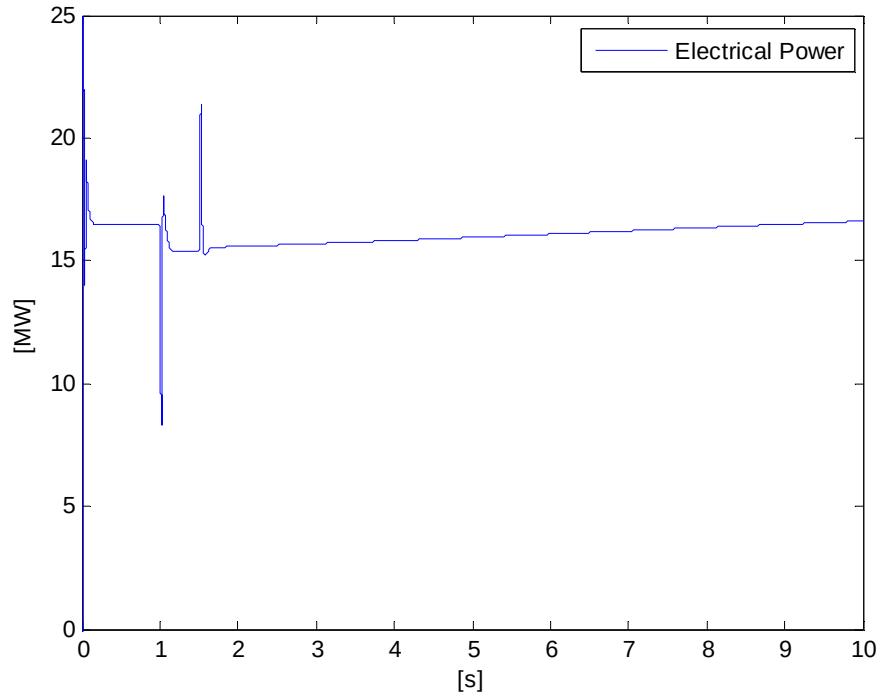

Figure 109: Electric power output of the FC_WTG_1, Test 4

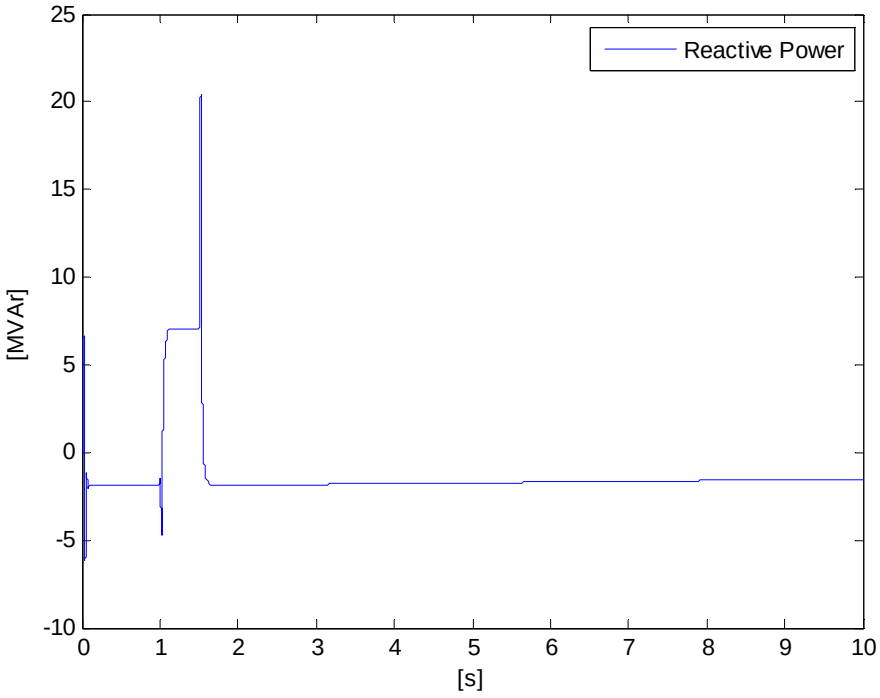

Figure 110: Reactive power output of the FC_WTG_1, Test 4

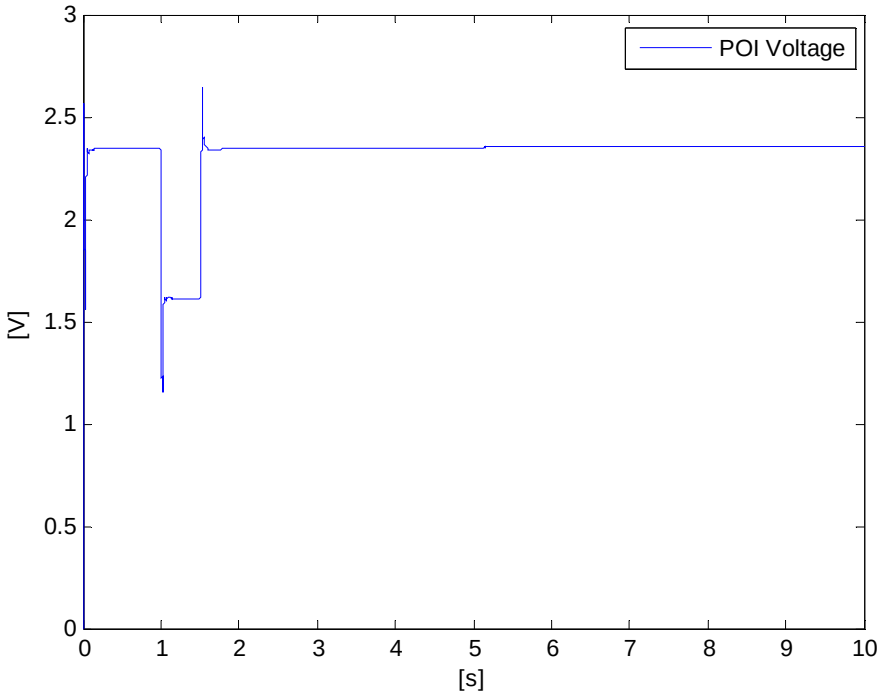

Figure 111: Voltage at bus WINDHV1, Test 4

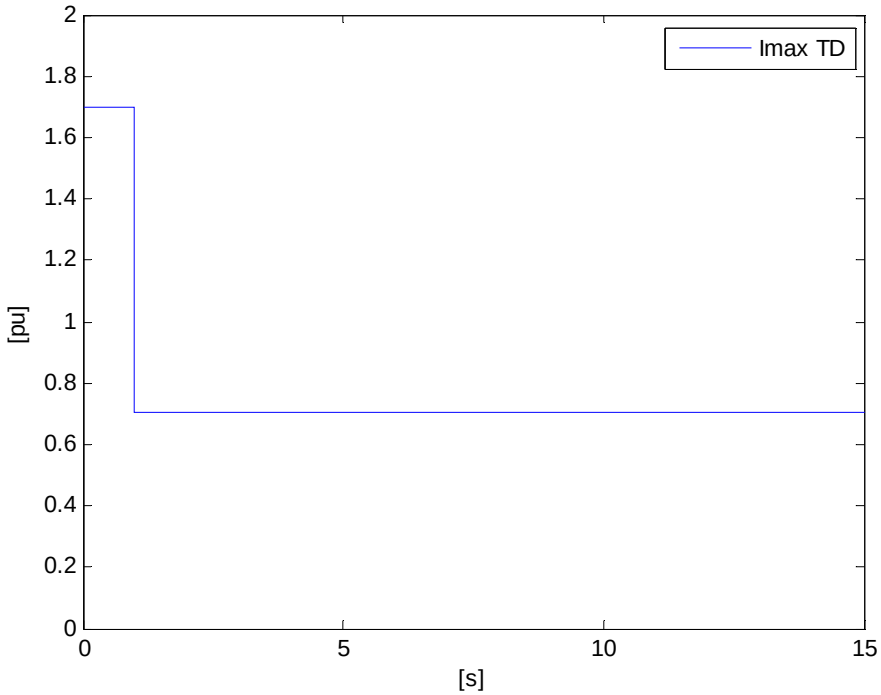

Figure 112: Current limit reduction ImaxTD applied to the current converter limiter block of the FC_WTG_1, Test 5.

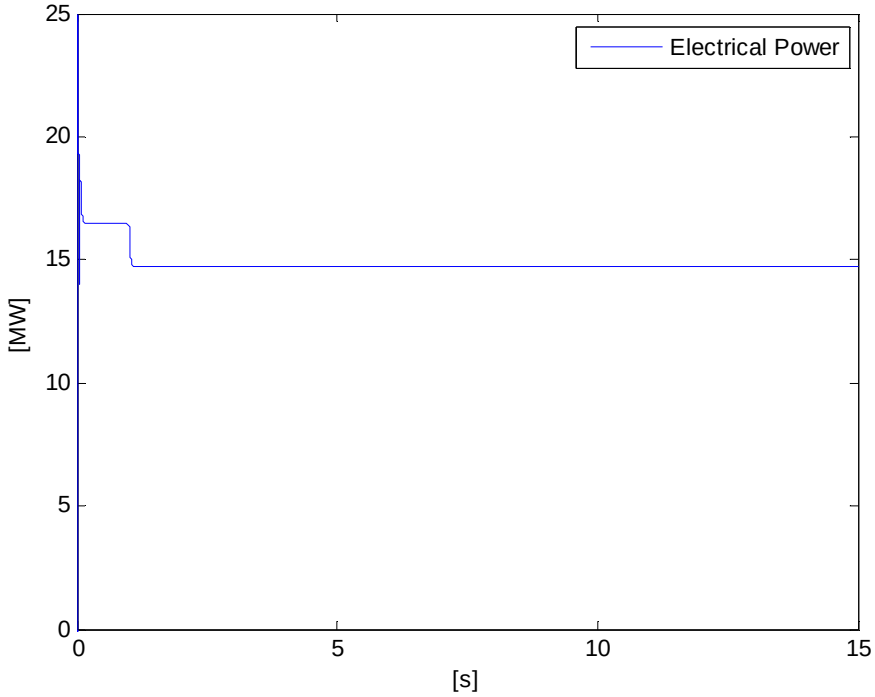

Figure 113: Electric power output of the FC_WTG_1, Test 5.

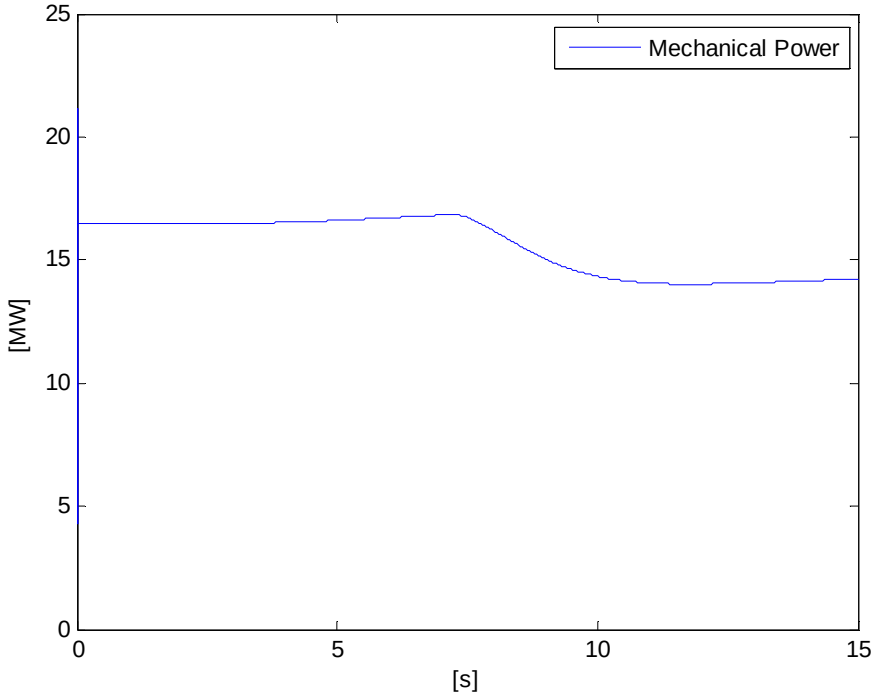

Figure 114: Mechanical power output of the FC_WTG_1, Test 5.

The following two figures show the breaker resistance operation, the energy and the power absorbed.

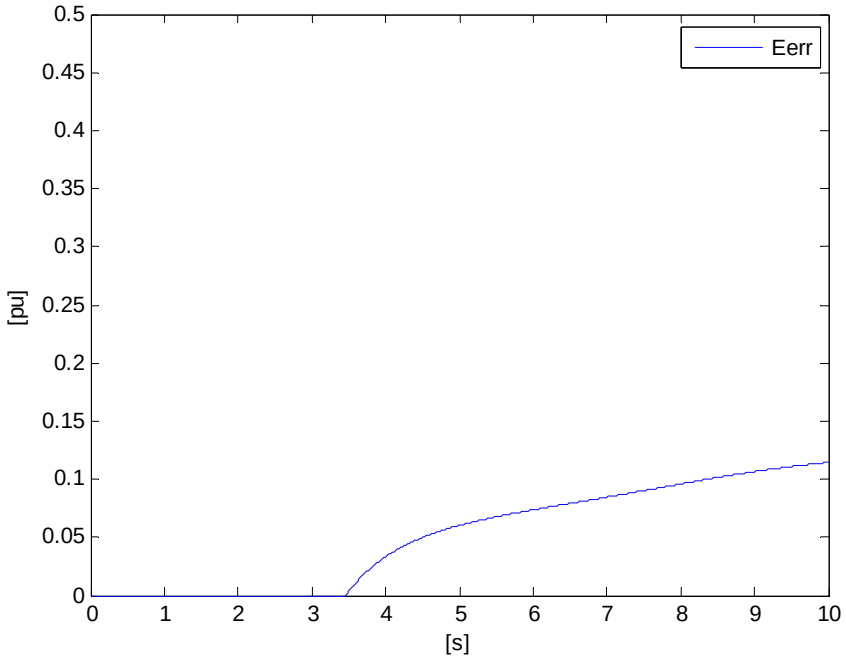

Figure 115: Dynamic resistor, absorbed energy (see Figure 95), Test 5

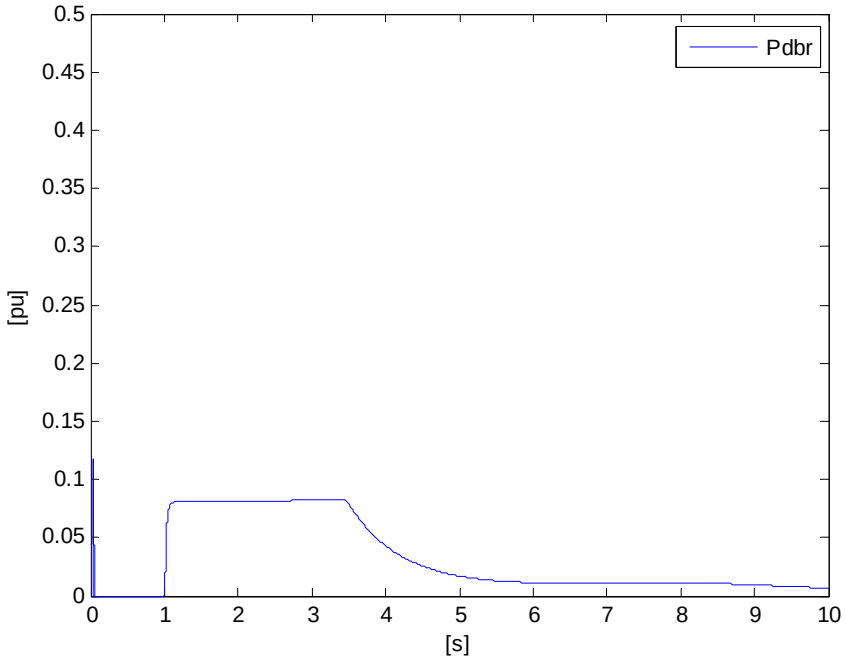

Figure 116: Dynamic resistor, absorbed power, Pdbr (see Figure 95), Test 5.

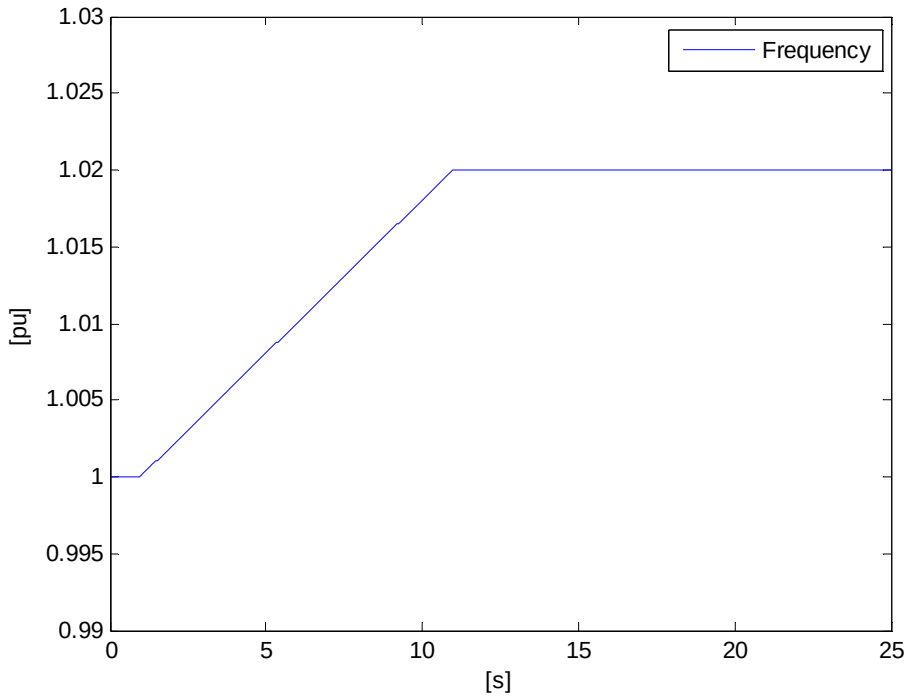

Figure 117: Frequency in pu at the terminal bus WINDLV1, Test 6

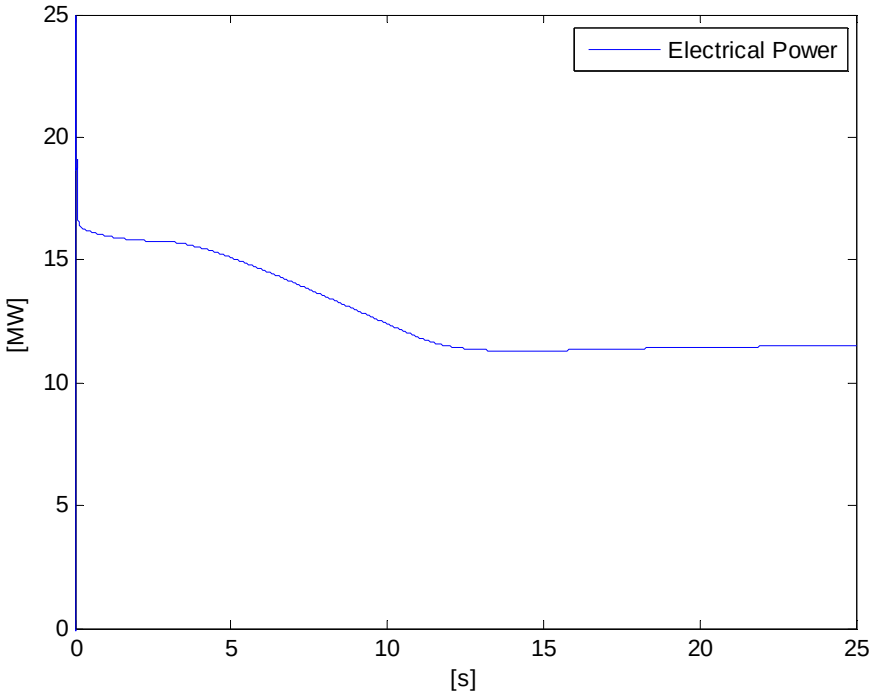

Figure 118: Electric power output of the FC_WTG_1, Test 6.

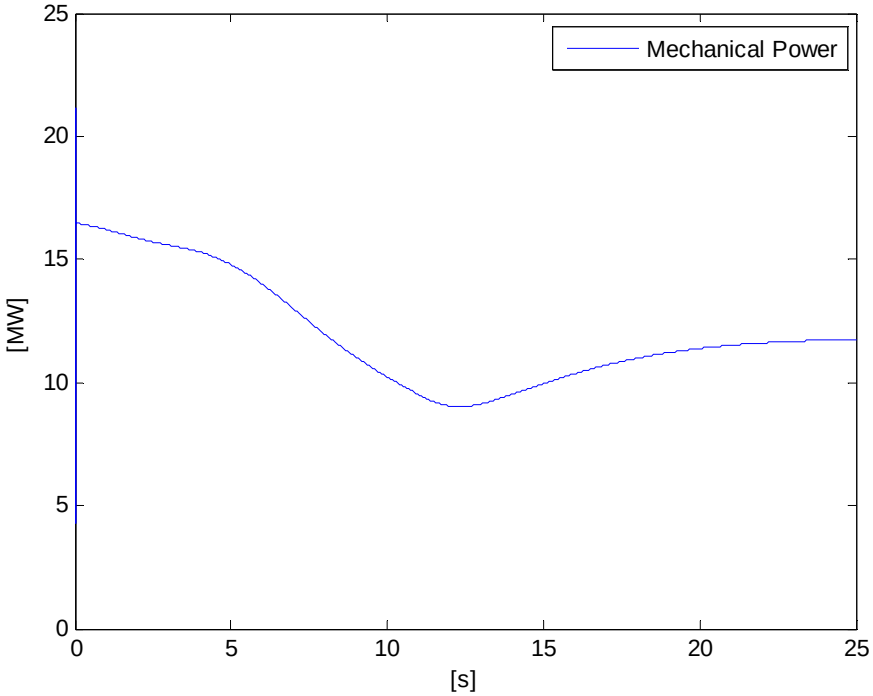

Figure 119: Mechanical power of the FC_WTG_1 turbine, Test 6.

CHAPTER 5. DEMTP Model, DFIG and FC

5.1 DFIG DEMTP model

The detailed EMTP (DEMTP) model presented in this section is an EMTP type model implemented in EMTP-RV. The model can be initialized and connected to any EMTP-RV network. It constitutes a detailed wound rotor asynchronous generator with a converter connected between the stator and rotor of the machine. This model is based on the vector control theory that allows the decoupled control of the active and reactive powers. The active power is determined from the controls associated to the mechanical equation of the WTG. The reactive component is associated to the voltage control at the WTG terminals or the reactive power constraints.

The top level view of the DFIG_WTG with its initialization devices is shown in Figure 120. The DFIG_WTG device is a subnetwork with several subnetworks for its various modeling functions and control systems.

Almost all parameters of the device can be modified through its mask. There are two external interfacings points (pins). The right pin is a 3-phase pin allowing to connect the DFIG_WTG device to the 3-phase network. The left pin is used for providing the random variation of the wind speed. The mean wind speed is given inside the top level mask as a parameter. Each DFIG_WTG device can represent one or more generators and include a wind farm.

Since the model must be initialized it is needed to perform a load flow solution followed by a steady-state solution. In EMTP-RV this is achieved using separate layers of components for the different solution modules. As shown in Figure 120 each DFIG_WTG device is paired with a load-flow constraint device (LF device) and an ideal voltage source. The LF device is used in the load-flow solution layer. It provides the PQ constraints of the DFIG_WTG. The LF device is used in the load-flow solution and together with other LF devices, it allows the calculation of the load-flow solution phasor for the complete network.

The steady-state and the following time-domain solutions can be started from the load-flow solution. This is a two step process: the first step is the load-flow solution and the second step is the steady-state solution automatically followed by the time domain solution. In the steady-state solution the ideal voltage source is used to provide the phasors found in the load-flow solution. The voltage source is disconnected before the first time point computation in the time domain solution, but allows to initialize the state variables of the simulated network. At the same time the DFIG_WTG is turned on and starts controlling its internal source for the rest of the simulation. It is also noticed that the DFIG_WTG must provide the same PQ constraints and must be given the load-flow solution voltage at its terminal. To reproduce this same behaviour with the DFIG_WTG model, a MATLAB script calculates from the results of the LF device the converter reference voltages and currents.

The contents of the breaker connecting the DFIG_WTG to its network are shown in Figure 121. An artificial device is set to avoid EMTP_RV warning messages on floating conditions in the steady-state solution and before its connection in the time-domain solution.

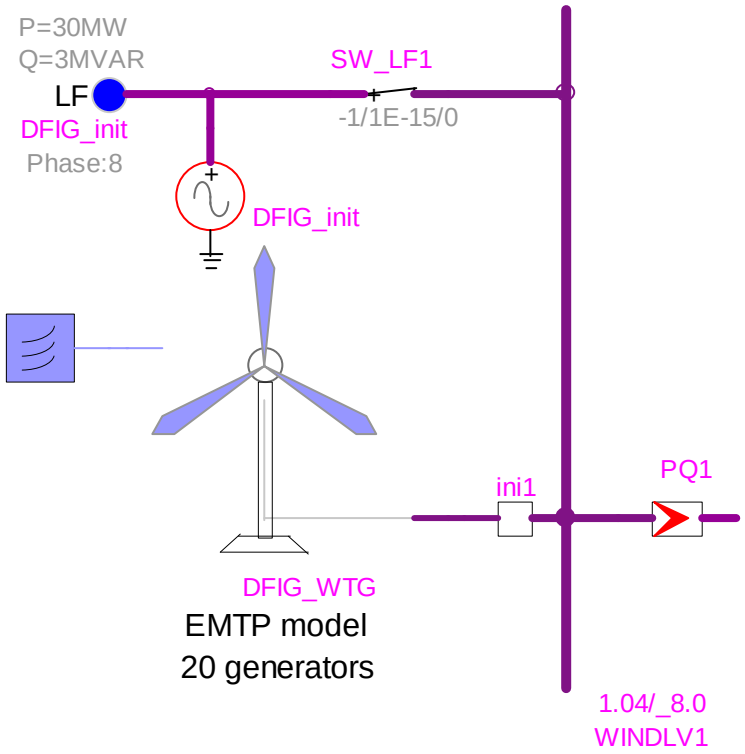

Figure 120: Top level device view of the DFIG_WTG

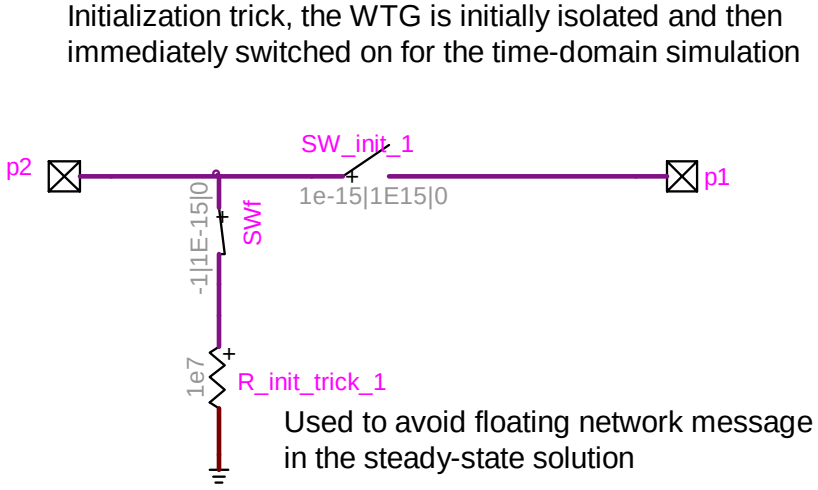

Figure 121: Initialization switches for connecting the WTG in the time-domain solution

5.1.1 Model initialization

The initialization script is presented in the section 5.1.8. The MATLAB script produces an output file named IC_DFIG.txt which is copied and pasted inside the main mask of the DFIG_WTG model in the section of initial values (Figure 122).

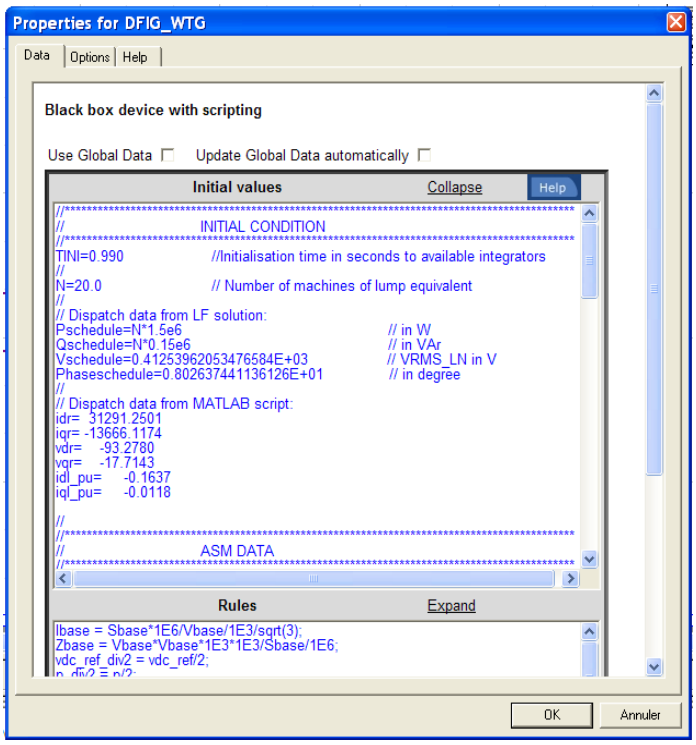

Figure 122: DFIG_WTG mask, DEMTP model.

5.1.2 Top level circuit

The top level circuit of the DFIG_WTG shown in Figure 123. I, is composed of functional blocks for various model sections.

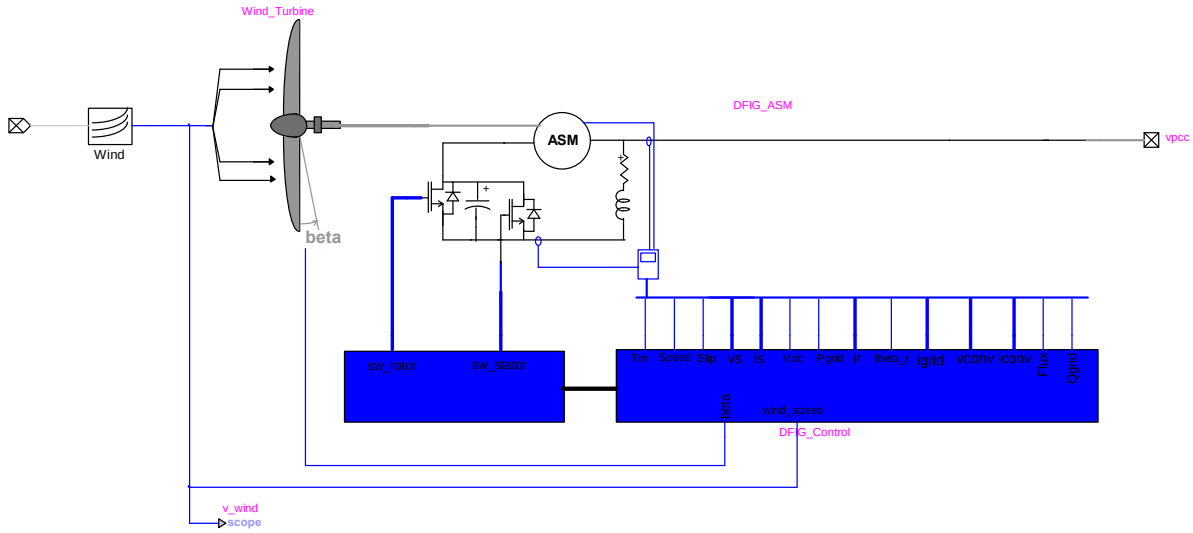

Figure 123: Top level circuit block of the DFIG_WTG.

The model is built using EMTP-RV control devices and implements the control functions according the manufacture information.

The various top level functions are also composed of one or more subcircuits. The subcircuits include comments and references about the operation or the simulation options. The following sections are used to provide a quick description of each top level function mainly for providing a simple reference. All parameters are defined inside the DFIG_WTG top level mask.

The DEMTP modelling approach shares the same PSS/E model blocks defined in the CHAPTER 2. The following references can be used:

- For the wind block, see the section 2.2,
- For the mechanical turbine model, see the section 2.1.2.3,
- For the pitch control, see the section 2.3.4,
- For the rotor model, see the section 2.5.1,
- For the reactive control, see the section 2.7,
- For the torque and power control, see the section 2.6,
- For the protection block model, see the section 2.8.

The DEMTP model includes additional components and new characteristics as compared to the PSS/E and MEVA model blocks. These are the current limiter and the firing control of converters. They are described below.

5.1.2.1 DFIG_ASM

The double feed asynchronous generator utilizes a wound-rotor induction generator with an ac-dc-ac converter, dc link, between the stator and the rotor terminals and two IGBT bridges. The wind generator arrangements are shown in Figure 124.

Additionally a input filter Lchoke, Rchoke and Cshunt on the line converter side, two measurement points, several points of input/output signals are used in different control blocks, LVRT protections and crowbar protection.

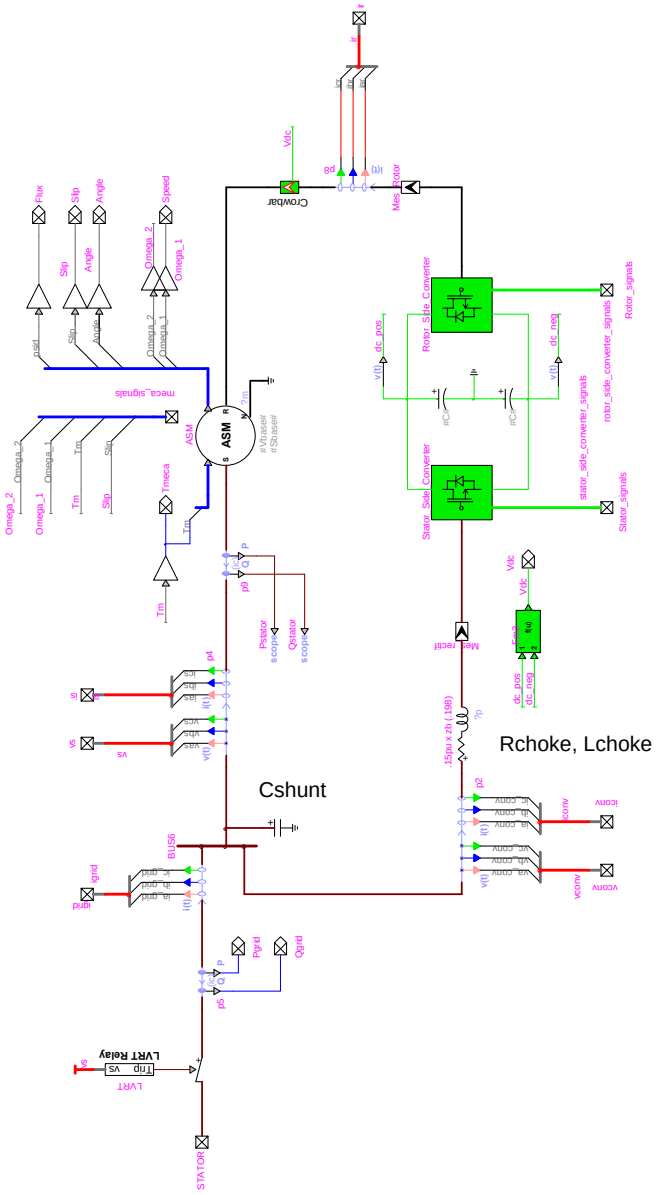

Figure 124: Top level circuit block

5.1.2.2 IGBT bridge

The IGBT bridge on the line converter side is one of the two bridges that operates with the PWM command signals (s1 to s6). There are inductances and resistances belonging to the bridge (Rpont and Lpont). It is shown in Figure 125.

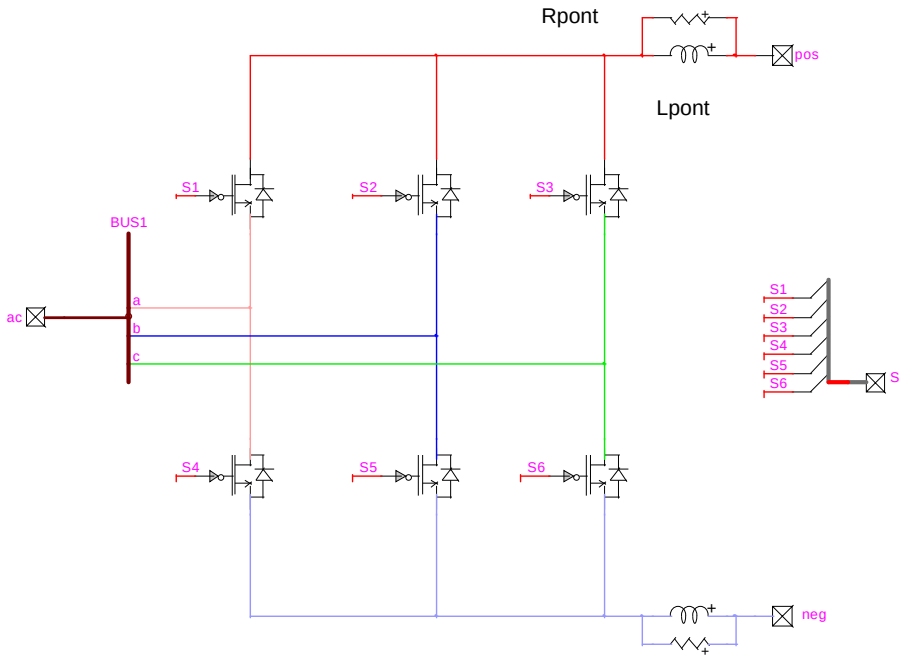

Figure 125: Switch bridge on the line converter side.

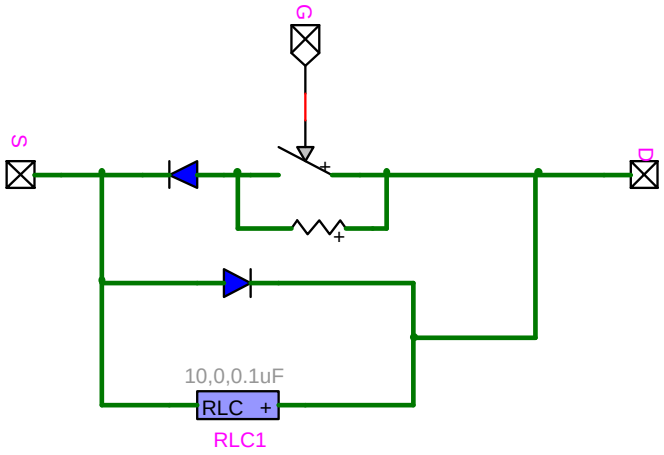

Figure 126: IGBT model

The IGBT is modeled according to the diagram of Figure 126. It is a combination of an ideal controlled switch, nonlinear resistance for the classical diode equation and a snubber (RLC branch).

5.1.2.3 Measurement system on the rotor side circuit

On the rotor circuit there is a measurement block (Mes_Rotor, Figure 124). The frequency on the rotor side is variable with the rotor speed. The nominal power is reached with a slip of -16%, in consequence taking the initial slip equal to -16%, the mean frequency must be near 9.6 Hz, since 60Hz times 0.16.

To perform a measurement without errors it is needed to extract the fundamental component of the rotor frequency. This is done using two filters centered at 9.6 Hz. These two filters are used to measure the phase current and line-to-line voltage to finally calculate the instant active power.

5.1.2.4 Crowbar protection

The crowbar protection model is located at the rotor side, this protection is continuously monitoring the dc bus voltage and triggering a short circuit switch on the rotor in the case of an abnormal operation condition. The abnormal conditions are defined as the under/over dc voltage outside the band of ±10% around the rated value. It is shown in Figure 127.

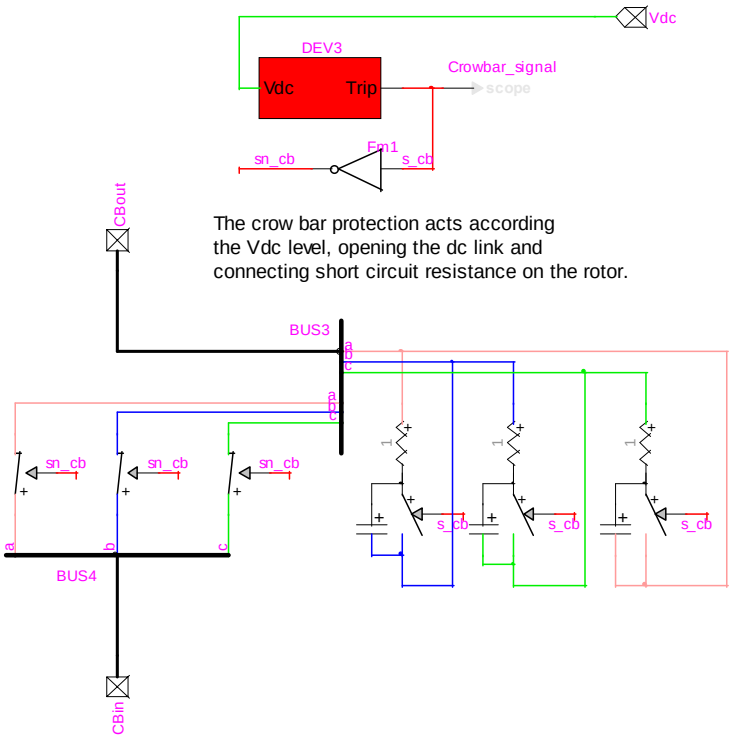

Figure 127: Crowbar Protection

5.1.3 DFIG Control

The top level circuit of the DFIG Control is composed of the common blocks described in the CHAPTER 2 and section 5.1.2 that defined the mechanical control and the slow electrical controls.

Figure 128 shows the complete set of the line side and the rotor side controls. The torque regulator and volt/var regulator belong to the category of slow control, developed in Figure 28, and the rest belongs to the category of fast control that will be developed in following section.

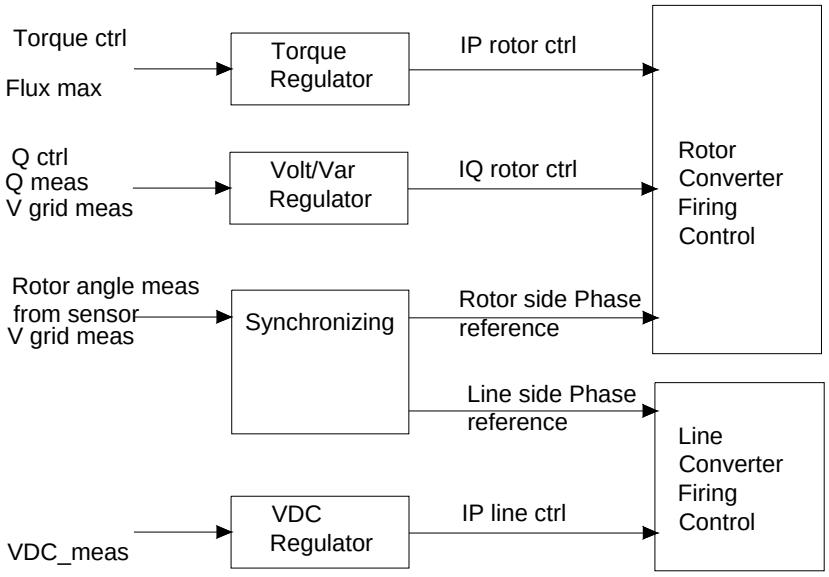

Figure 128: Line and rotor side control

5.1.3.1 Synchronizing function, PLL in DEMTP model

The synchronizing function is illustrated in Figure 129. This consists of a PLL based upon measured terminal voltage and the rotor angle from a position sensor on the shaft. The line side converter uses the PLL angle reference directly, while the rotor converter shifts the angle reference by the rotor position.

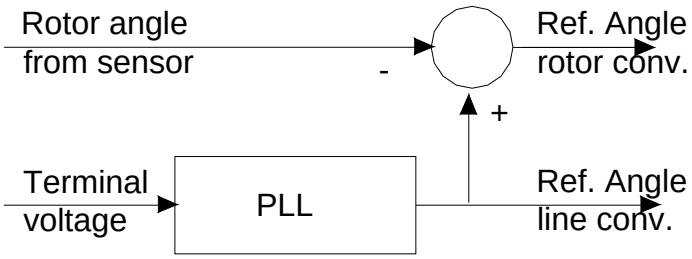

Figure 129: Synchronization function

Figure 130 shows the detailed version of the PLL model implemented in EMTP-RV. The PLL inputs are the three phase instantaneous voltages and the base voltage. The outputs are the phase angle, its sin and cos functions, and the instantaneous frequency.

The three instantaneous voltages are transformed in pu by dividing by Vbase. These three pu signals are projected according to the dqo frame reference. Given the Park transformation matrix

$$\theta = \omega t \tag{5.1}$$

$$P_{dqo} = \frac{2}{3}\begin{bmatrix} cos(\theta) & cos(\theta - \frac{2\pi}{3}) & cos(\theta + \frac{2\pi}{3}) \\ -sin(\theta) & -sin(\theta - \frac{2\pi}{3}) & -sin(\theta + \frac{2\pi}{3}) \\ \frac{1}{2} & \frac{1}{2} & \frac{1}{2} \end{bmatrix} \tag{5.2}$$

The transformation of the stator voltages gives

$$\begin{bmatrix} v_d \\ v_q \\ v_o \end{bmatrix} = P_{dqo}\begin{bmatrix} v_a \\ v_b \\ v_c \end{bmatrix} \tag{5.3}$$

Figure 130 shows that the q component of the terminal voltage is integrated during an average period, as result of this process, it obtains a null value during steady state condition.

The integration during an average period is calculated by means of two functions, the first function calculates the integral value over a sliding period and the second one calculates the average value over the sliding period.

In the transient condition the previous value is the input of the PI controller which has as output the instantaneous frequency variation in rad/s. Dividing by a scale factor of 2π, after a filter and limiter blocks the frequency in Hz is calculated.

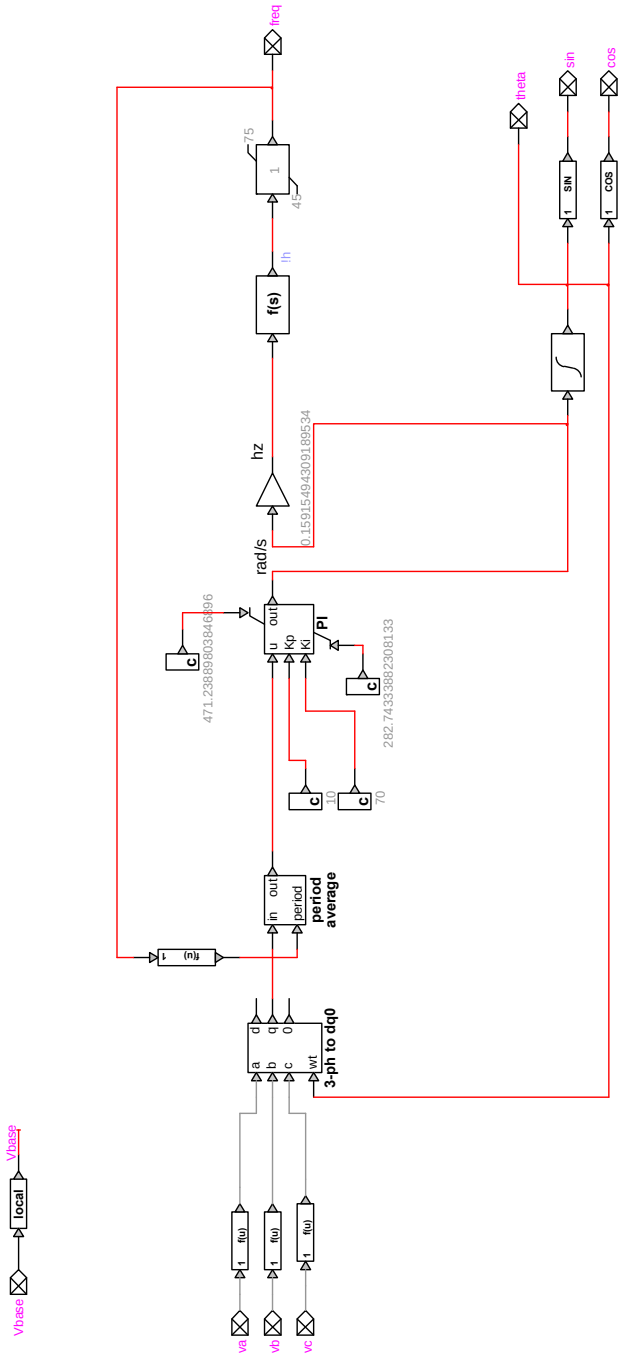

Figure 130: PLL implementation in EMTP-RV.

The instantaneous phase angle is obtained by the integration of the instantaneous frequency variation in rad/s. The variable $\omega.t$ is updated continually.

5.1.3.2 Line and rotor converter firing control

The PWM principle consists in controlling by means of a switching operation a given mean voltage value from a constant direct voltage. Then, the pulse-width modulation uses a square wave whose pulse width is modulated resulting in the variation of the average value of the waveform. An oscillator is used to generate a triangle or sawtooth waveform and a control set the level of the steady reference voltage, see Figure 131. A comparator compares the sawtooth voltage with the reference voltage. When the sawtooth voltage rises above the reference voltage, a power electronic switch is switched on. As it falls below the reference, it is switched off. This gives a square wave output.

If we consider a square waveform Y with a low value of zero, a high value Y_{max} and a duty cycle D, the average value of the waveform is given by:

$$\overline{Y}=D\ Y_{max} \tag{5.4}$$

From this, it is obvious that the average value of the signal is directly dependent on the duty cycle D.

For both converters the carrier waveform generated by the signal generator has a unitary amplitude at 3000 Hz and three reference waveforms are used for phases a, b and c. The phase and frequency are given by the PLL angle and the dq voltage fast controller on line and rotor side using the park transformation.

The three reference waveforms are scaled for V_{dc} (se equations (5.5) and (5.6)) and compared with the carrier resulting into the switch signals to the IGBT bridge. The Figure 132 shows six signals divided in three columns; s1-s4 , s2-s5 and s3-s6; to control the IGBT bridge. In each column a control signal is sent to the upper switch and the complementary signal to the lower switch.

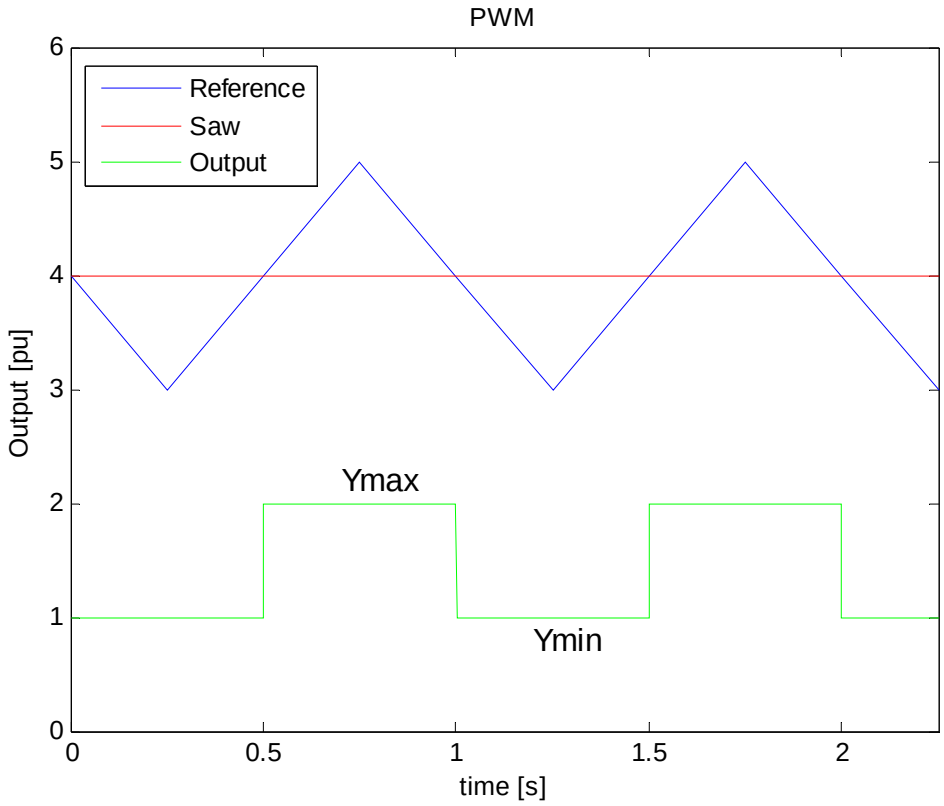

Figure 131: PWM principle

One common method of generating the PWM pulses uses comparison of the output voltage to synthesize (60 Hz in this case) with a triangular wave at the switching frequency (1080 Hz in this case). This is the method implemented in this work.

In the 3-Phase PWM, the line-to-line RMS output voltage is a function of the DC input voltage and of the modulation index m as given by the following equation [24]

$$V_{LL_{rms}} = \frac{m}{2}\sqrt{\frac{3}{2}}V_{dc} \tag{5.5}$$

In consequence, the required value for the modulation index to obtain 1 pu generated voltage by the converter is

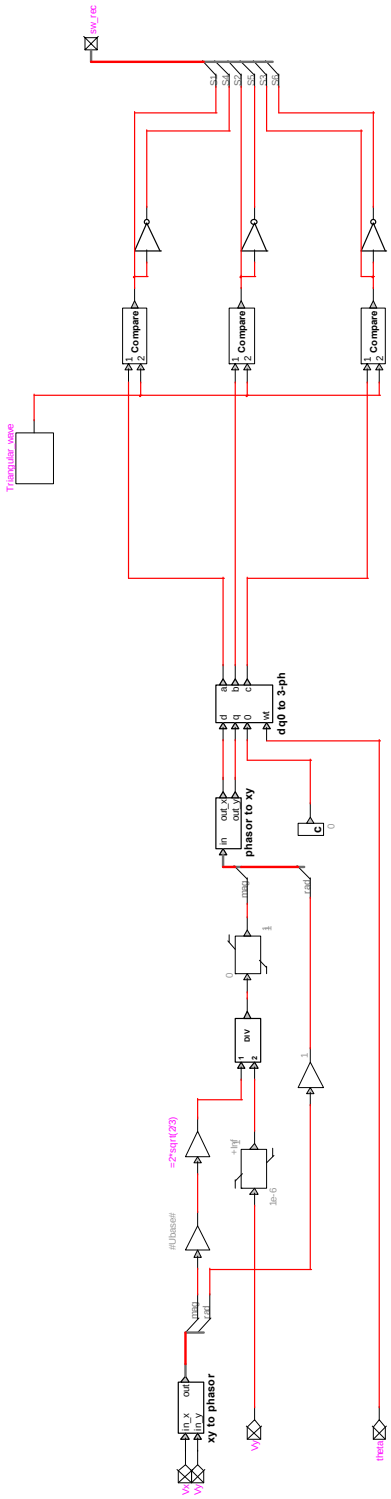

Figure 132: PWM implementation

$$m = \frac{V_{nom}\, 2\sqrt{2/3}}{V_{dc}} \tag{5.6}$$

where V_{nom} is the RMS line-to-line nominal voltage of the line side converter or the nominal voltage of the rotor in the rotor side converter. In Figure 132, it is shown that the nominal value V_{nom} is replaced by the load-flow voltage $V_{schedule}$ to match better during the initialization process.

5.1.4 Current limiter

Before reaching the PWM control, both currents used for the slow control (see d and q currents in Figure 28) are limited using the current maximum of the stator and rotor. The limiter works with active power preference in front to the reactive power, it calculate the active current limits and reactive currents limits. It is shown in Figure 133.

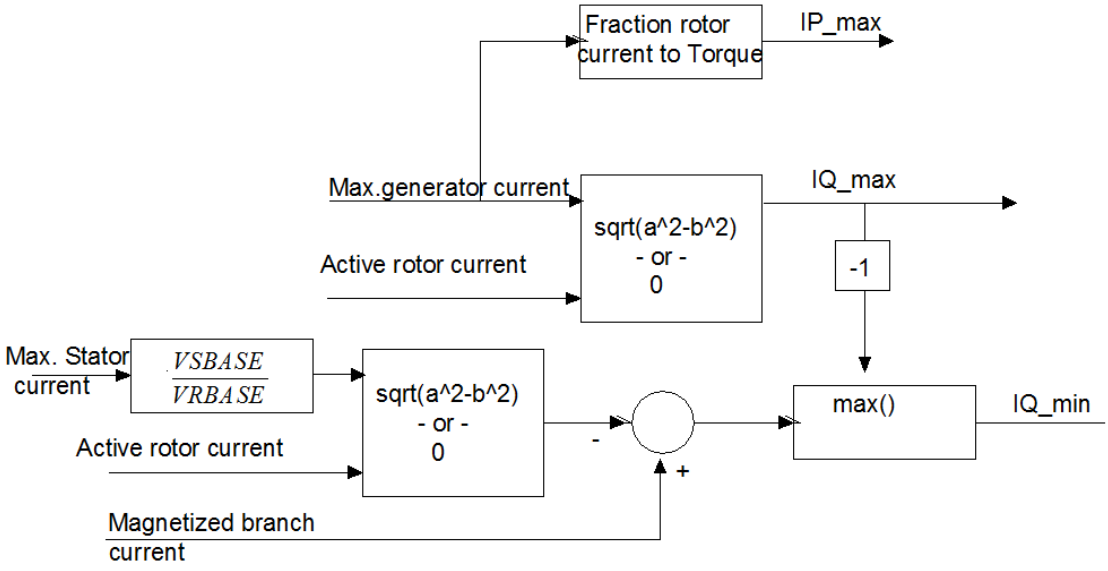

Figure 133: Current limiter

5.1.5 Rotor reference voltage for the PWM controller

The DFIG control includes two types of control processes; the slow control, similar to the control of the active and reactive power in the CHAPTER 3 of PSS/E and CHAPTER 4 of MEVA model, and fast control used to control the PWM switching strategy. Basically the rotor side control considers two PI controllers, one of them is proportional to the active power and the other is proportional to the reactive power.

The error signal in each controller is determined by the difference between the dq rotor currents measured and the dq currents reference. The dq current references are obtained by the sum of two components, the first component came from the initialization process, Id_ref and Iq_ref, and the other current components, IQ and IP, that result of the current output of the slow controllers, volt/var defined in the section 2.7 and torque controllers defined in the section 2.6 respectively. In the Figure 28 part 1 the control currents i_q and i_p are equivalents to the control currents IQ and IP shown in Figure 134.

Given that the reference current is calculated on the stator frame reference, the measured rotor current must be projected on the same reference frame. In this way, it is necessary first to calculate the dq0 rotor components and after that to rotate by an angle ψ (the slip angle from the rotor axis to the stator axis frame reference). This angle is the negative of the rotor angle due to the negative clockwise rotation reference.

This process is executed in two steps. First using the Park transformation matrix

$$\begin{bmatrix} i_{d_r} \\ i_{q_r} \\ i_{o_r} \end{bmatrix} = P_{dqo} \begin{bmatrix} i_{a_r} \\ i_{b_r} \\ i_{c_r} \end{bmatrix} \tag{5.7}$$

and the rotation matrix

$$R = \begin{bmatrix} cos(\psi) & -sin(\psi) & 0 \\ sin(\psi) & cos(\psi) & 0 \\ 0 & 0 & 1 \end{bmatrix} \tag{5.8}$$

we obtain

$$\begin{bmatrix} i_{\alpha_r} \\ i_{\beta_r} \\ i_{o_r} \end{bmatrix} = R \begin{bmatrix} i_{d_r} \\ i_{q_r} \\ i_{o_r} \end{bmatrix} \tag{5.9}$$

Now it is possible to compare both currents, the reference current and the measured rotor current, since they are expressed on the same reference frame, and obtaining the error signal.

The voltage output signal in the stator reference frame is the sum of the initialization rotor voltages (Vd_ref and Vq_ref) and the output from the PI controller, Vrd and Vrq, as shown in Figure 134.

Finally to get the three-phase sinusoidal reference signals for the converter firing control, the voltage signals must be rotated using the R^{-1} transformation, to pass from the stator to the rotor, and finally the ${P_{dq0}}^{-1}$ transformation to pass from dq0 to abc phase components:

$$R^{-1} = \begin{bmatrix} cos(\psi) & sin(\psi) & 0 \\ -sin(\psi) & cos(\psi) & 0 \\ 0 & 0 & 1 \end{bmatrix} \tag{5.10}$$

$$\begin{bmatrix} v_d \\ v_q \\ v_o \end{bmatrix} = R^{-1} \begin{bmatrix} v_\alpha \\ v_\beta \\ v_o \end{bmatrix} \tag{5.11}$$

$${P_{dq0}}^{-1} = \begin{bmatrix} cos(\theta) & -sin(\theta) & 1 \\ cos(\theta - \frac{2\pi}{3}) & -sin(\theta - \frac{2\pi}{3}) & 1 \\ cos(\theta + \frac{2\pi}{3}) & -sin(\theta + \frac{2\pi}{3}) & 1 \end{bmatrix} \tag{5.12}$$

$$\begin{bmatrix} v_a \\ v_b \\ v_c \end{bmatrix} = {P_{dq0}}^{-1} \begin{bmatrix} v_d \\ v_q \\ v_o \end{bmatrix} \tag{5.13}$$

where θ is the phase calculated from the frequency dictated by the PLL.

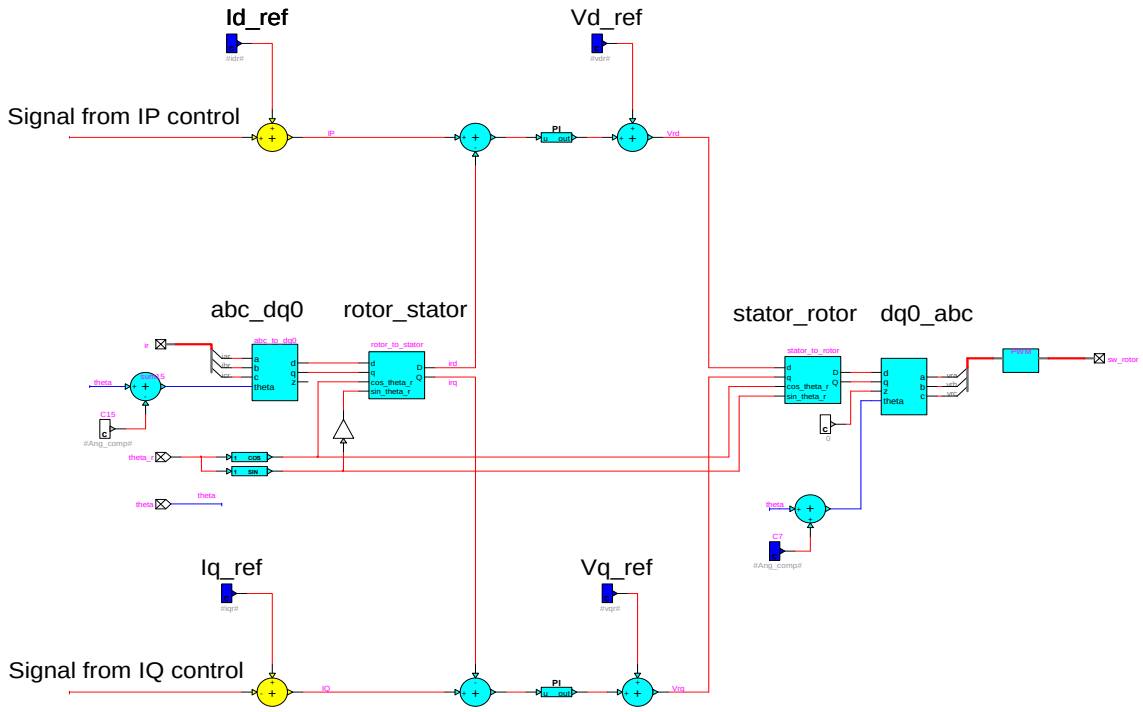

Figure 134: Rotor side PWM controller

5.1.6 Line reference voltage for PWM controller

By means of a current regulator shown in Figure 135 it is possible to obtain the dq voltage outputs in pu, which enter line side PWM block from two PI controllers that act separately on the dq current components. The line side PWM controller is shown in Figure 135. The measured current on the line side of the converter branch must be scaled for the current base to obtain a pu value and after using the Park transformation result the dq current components used as input of the current regulator.

The id_ref current reference is the output of the output of the dc voltage controller.

The iq_ref current reference is a constant calculated during the initialization process.

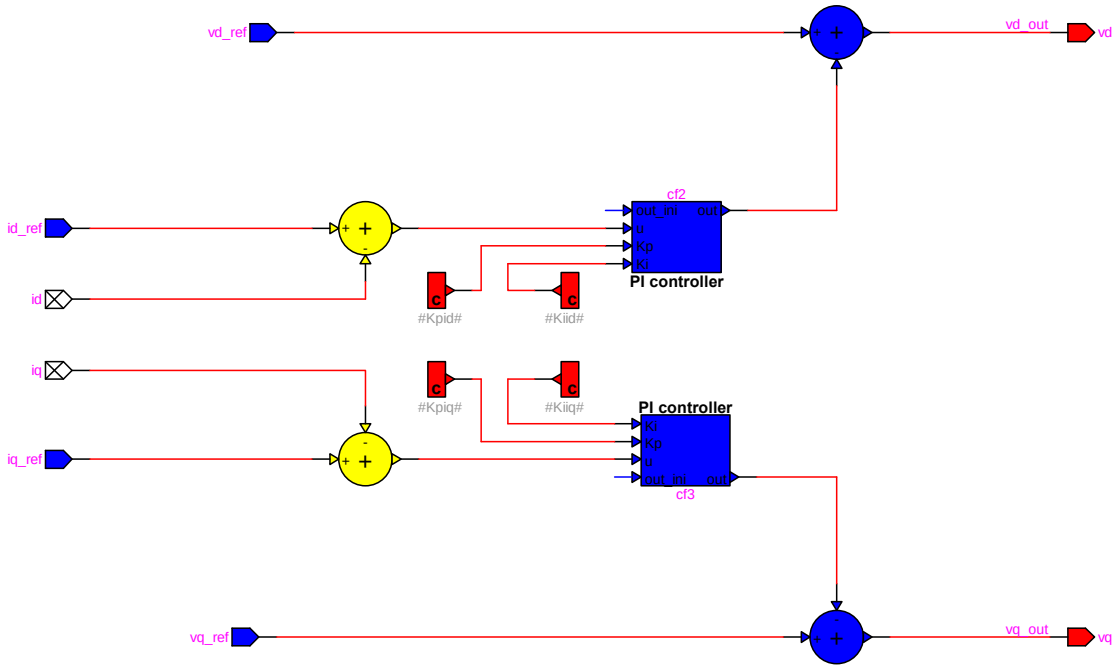

Figure 135: Line side controller

As it is shown in the top level circuit of Figure 135, to get the reference voltage according to the dq axis, it is need to consider the difference between the terminal voltage and the voltage on the converter filter impedance (Z_{choke}):

$$v_{d_{ref}} = -r_{choke}\, i_d + l_{choke}\, i_q + v_d \tag{5.14}$$

$$v_{q_{ref}} = -r_{choke}\, i_q - l_{choke}\, i_d + v_q \tag{5.15}$$

5.1.7 DEMTP mechanical initialization

Due to the fact that harmonics are present in the injected rotor current, a transient condition is created only fundamental frequency is used. The time constant of this phenomenon is limited to 0.5 s, the minimum time to reach the steady state condition. The strategy to accelerate the convergence of the electric variables to their values corresponding to the load-flow solution is reached when during this period the wind

speed is considered constant. After the period of 0.5 s is elapsed, the wind speed is a again considered as variable.

5.1.8 DEMTP electrical initialization

Without the initialization process presented in this thesis for calculating the rotor voltage and current references, the time to reach the steady state, represented by a load flow solution, should be in the order of 6 to 8 s of simulation time (see Figure 141). In addition the steady-state powers may be different from the load-flow conditions. The initialization process is a guaranty for matching the P, Q and V constraints given by the load-flow solution. The initialization procedure reduces the computing time for reaching the steady-state in the time-domain solution.

The controllers in the DEMTP model are divided into slow controllers and fast controllers. The slow controllers are similar to the PSS/E and MEVA cases, with the difference that before they were acting directly on the generator/converter model and now their outputs are the references for the fast controllers. The fast controllers act on the PWM device.

The fundamental frequency of the current injected in the rotor of the asynchronous machine is given by the slip for the system frequency. When this current component is injected into the rotor, the result is a perfect initialization. In the contrary case an initialization transient will occur when harmonics are present in the injected current. This fact translates into a flux transient. The time constant of this phenomenon is limited to 0.5 s, which is the minimum time to reach the steady state condition. Due to this limitation, during the initialization process the integrators are closed during the short period of 0.5 s. This strategy has the effect of accelerate the convergence of the electric variables to their values corresponding to the load flow solution.

The following equations are programmed in the auxiliary script to help in the initialization task. P is the total active power generated in W, Q is the total reactive power generated in vars, V is the voltage (line-to-neutral) in V, θ is the voltage phase angle in degrees, r_S is the stator resistance in pu, X_S is the stator reactance in pu, X_r is

the magnetisation inductance in pu, r_r is the rotor resistance in pu, X_r is the rotor reactance in pu, s is the initial slip of ASM in pu, V_n is the rated terminal voltage in V, S_n is the rated complex power in VA, P_s is the active power generated by the stator of the asynchronous machine, Q_s is the reactive power generated or absorbed by the stator of the asynchronous machine, P_c is the active power output by the grid side converter, Q_c is the active power output by the grid side converter. Then

$$Z_{base} = \frac{V_n{}^2}{S_n} \tag{5.16}$$

$$Z_s = (r_s + j\,X_s)\,Z_{base} \tag{5.17}$$

$$Z_r = (\frac{r_r}{s} + j\,X_r)\,Z_{base} \tag{5.18}$$

$$Z_m = (j\,X_m)\,Z_{base} \tag{5.19}$$

$$P_s = \frac{P}{1-s} \tag{5.20}$$

$$Q_s = Q \tag{5.21}$$

$$\overrightarrow{S_s} = -(P_s + j\,Q_s) \tag{5.22}$$

$$\overrightarrow{V_s} = \sqrt{2}\,V\,e^{j\theta} \tag{5.23}$$

$$\overrightarrow{I_s} = conj(\frac{\overrightarrow{S_s}}{1.5\overrightarrow{V_s}}) \tag{5.24}$$

$$\overrightarrow{V_m} = \overrightarrow{V_s} - Z_s\overrightarrow{I_s} \tag{5.25}$$

$$\overrightarrow{I_r} = \frac{\overrightarrow{V_m} - Z_m\overrightarrow{I_s}}{Z_m} \tag{5.26}$$

$$\overrightarrow{V_r} = (\overrightarrow{V_m} + Z_r\overrightarrow{I_r})\,s \tag{5.27}$$

$$P_r = P_s\,s \tag{5.28}$$

$$\overrightarrow{S_c} = P_r + j\,0 \tag{5.29}$$

$$\overrightarrow{I_c} = conj(\frac{\overrightarrow{S_c}}{1.5\overrightarrow{V_s}}) \tag{5.30}$$

Using $\theta = \omega.t$ and Park's transformation

$$\begin{bmatrix} v_{d_r} \\ v_{q_r} \\ v_{o_r} \end{bmatrix} = P_{dqo} \begin{bmatrix} v_{a_r} \\ v_{b_r} \\ v_{c_r} \end{bmatrix} \tag{5.31}$$

$$\begin{bmatrix} i_{d_r} \\ i_{q_r} \\ i_{o_r} \end{bmatrix} = P_{dqo} \begin{bmatrix} i_{a_r} \\ i_{b_r} \\ i_{c_r} \end{bmatrix} \tag{5.32}$$

$$\begin{bmatrix} i_{d_c} \\ i_{q_c} \\ i_{o_c} \end{bmatrix} = P_{dqo} \begin{bmatrix} i_{a_c} \\ i_{b_c} \\ i_{c_c} \end{bmatrix} \tag{5.33}$$

where v_{d_r} is the d component of the rotor voltage, v_{q_r} is the q component of the rotor voltage, i_{d_r} is the d component of the rotor current, i_{q_r} is the q component of the rotor current, i_{d_c} is the d component of grid side converter current and i_{q_c} is the q component of grid side converter current. These last three equations give the reference values to the controllers on the rotor side and grid side.

5.1.9 MVEMTP DFIG model

The alternative between the MEVA model and the DEMTP model is the MVEMTP. This model approach only changes the dc link of the DEMTP model with control sources keeping both the slow and fast controls used in the DEMTP model. The IGBT bridges are eliminated. The dc link block is shown in Figure 136.

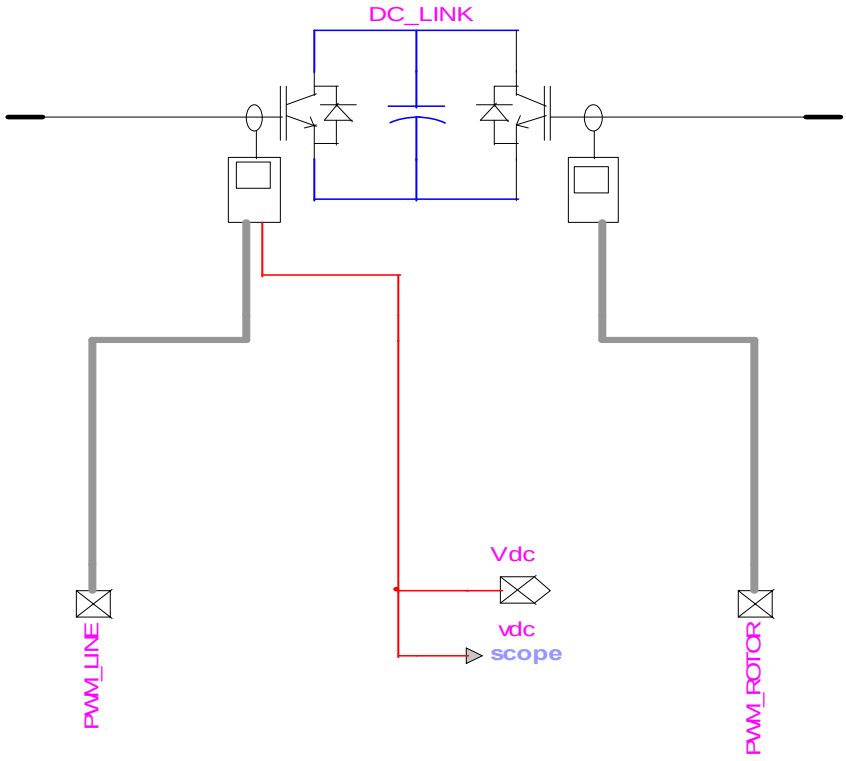

Figure 136: DC link block, MVEMTP model

Figure 137 shows the controlled sources [25][26] connected on the line side and rotor side.

The control signals of the sources are generated from the PWM implementation, (Figure 132), by suppressing the comparison part shown in Figure 138, and adding a gain to change from pu values to physical values.

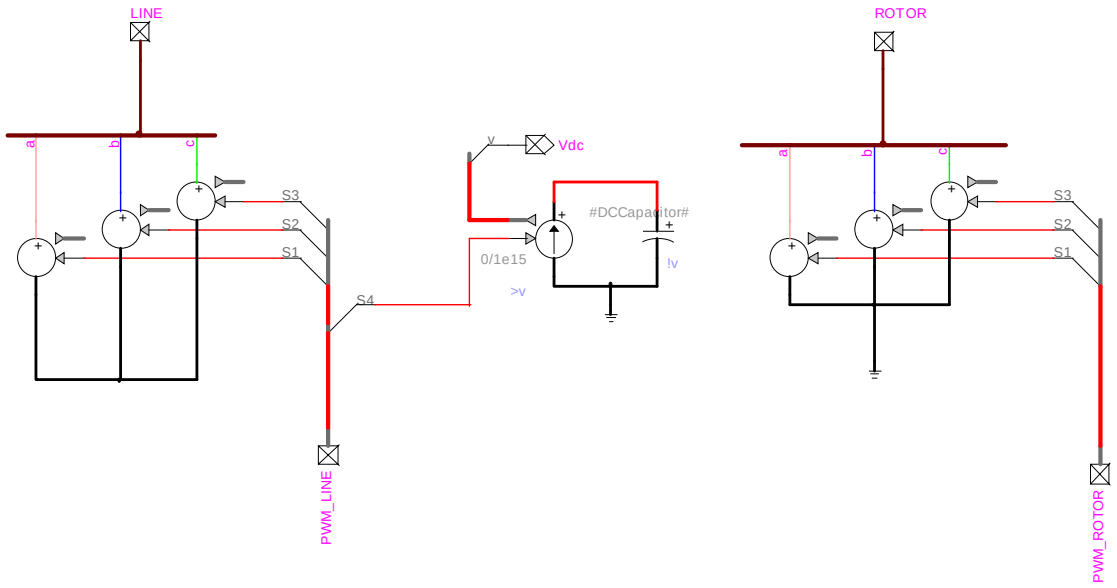

Figure 137: Controlled sources of DC link, MVEMTP model

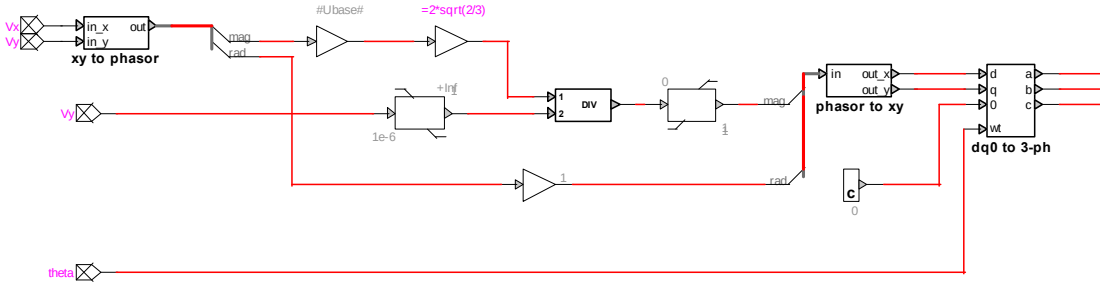

Figure 138: Control signals, in pu.

Neglecting the converter losses, the direct voltage v_{dc} on the main capacitor C terminal is obtained according to equations (5.34) and (5.35). The current source i_{dc} is controlled with the equation (5.34).

$$i_{dc} = \frac{P_{line} - P_{rotor}}{v_{dc}} \tag{5.34}$$

$$v_{dc} = \frac{1}{C}\int_{0}^{t} i_{dc}\, dt + v_{dc_{ini}} \tag{5.35}$$

where P_{line} is the active power measured on the line side, P_{rotor} is the active power measured on the rotor side and $v_{dc_{ini}}$ is the initial value of the direct voltage.

The MEVA model only considers in its response the fundamental component of the electrical variables, in addition the wind speed must be approximately constant and equal to the mean value. It cannot contain higher frequencies. The advantage of the MVEMTP modeling approach in comparison with MEVA model is that it admits a variable wind speed with increased computation time. In consequence the voltage evaluation with absence of harmonic component due to the real wind speed measured or the wind speed extended model, develop in the section 5.1.10, may be calculated.

The DEMTP model includes all the harmonics in its response due to the IGBT bridges controlled by the PWM method. The MVEMTP model considers in its response only the fundamental component on the converter side. It is limited to lower frequency transients. On the other hand this modeling approach saves significantly on computation time with a good match of results. The MEVA model is the fastest and gives the best computational performance.

5.1.10 Extended Wind model

This section is complementary to the wind model section 2.2. The extended wind model is essential for obtaining realistic simulations for the power fluctuations during the continuous operation of a wind farm. The wind model combines the stochastic effects caused by the turbulence and deterministic effects caused by the tower shadow.

The stochastic part includes the coherence between the wind speeds at different wind turbines in a wind farm as well as the effects of rotational sampling, which is known [27] to move energy to multiples (3P) of the rotor speed from the lower frequencies. The wind farm scale model may include the effects of wakes from the wind turbines, by means of the modification of the wind speed and turbulence intensity.

Equivalent Wind

Active and reactive power fluctuations generated by the wind turbines cause voltage fluctuations or flicker. Active power fluctuation may be caused by terrain

roughness effect, tower shadow effect (3P), wind turbulence, wake of the towers and fluctuations in the control system

Except for control system fluctuations, the other effects may be included in the equivalent wind speed model. Equivalent wind speed produced by our model takes into account four main effects: mean wind speed, tower shadow, turbulence and wake.

Mean wind speed

The wind power equation considers that the wind speed distribution on the rotor area is constant. In reality wind speed profiles result in different wind speeds at the blades nearest to the ground level compared to those at the top of the blade travel, which in turn produce corresponding flow and power effect on the entire rotor at the same instant. For wind speeds that lie in the operational range of the turbine and exceed about 4m/s, the wind speed at a given height can be found from the relation [28].

$$v_w(h)=v_{10}(\frac{h}{h_{10}})^a \tag{5.36}$$

Where a is the Hellman exponent, where 0.14<a<0.17; v_{10} is the wind speed for a height of h10 m; h_{10} is the height of 10 m. The mean wind speed is measured for 10 m and it is converted from its measuring level to the wind turbine hub level.

Tower shadow

Towers are obstacles to the free wind and modify the wind flow. When the rotor blade crosses the tower, a drop in the aerodynamic torque is occurred. The variation in the power or torque can be found from the performance characteristic [29]

$$M=M_u-\frac{1}{z}[M_o(z.\omega_w t)] \tag{5.37}$$

where the M_u represents the undisturbed wind distribution at the rotor and M_o is the oscillating component. The effect on the shaft is inversely proportional on the number of blades z and has a recurrence frequency $z.\omega_w$.

Turbulence

Turbulence decreases the possibility of using the energy in the wind effectively for a wind turbine. The turbulence effect may be described by means of the Kaimal spectrum, $K(f)$ [27]

$$\frac{f.K(f)}{\sigma^2} = \frac{\frac{f.XL}{Uo}}{(1+1.5\cdot(\frac{f.XL}{Uo}))^{5/3}} \tag{5.38}$$

where $K(f)$ is the spectral density function, f is the frequency of the turbulence, σ is the standard deviation, XL is the turbulence length scale and Uo is the average wind speed, all in the upwind direction.

The length scale is dependent on the surface roughness, z0, as well as the height above ground, z. For the wind speed longitudinal component the standard deviation σ is approximately constant with height. The standard deviation depends on the turbulence intensity and the average wind speed, it is given by $I = \sigma / Uo$.

Wake Effect

Since a wind turbine generates electricity from the energy in the wind, the wind leaving the turbine must have a lower energy content than the wind arriving in front of the turbine. In fact, there will be a wake behind the turbine, a long trail of wind which is quite turbulent and slowed down, when compared to the wind arriving in front of the turbine. In the the wake effect, each wind turbine will slow down the wind behind it as it pulls energy out of the wind and converts it to electricity. Typically, energy loss from the Park Effect will be somewhere around 5 per cent **[30]**.

5.1.11 Power quality parameters

This section defines the power quality parameters such as total harmonic distortion, instantaneous flicker level, short term flicker and the flicker meter function. These concepts are use to test the model with fast wind speed variation.

The currently existing power quality standard for wind turbines, issued by the International Electrotechnical Commission (IEC), IEC61400-21[31], defines the parameters that are characteristic of the wind turbine behavior in terms of the quality of power and also provides recommendations to carry out measurements and assess the power quality characteristics of grid connected wind turbines.

Two parameters are of remarkable importance: the flicker and the harmonic distortion.

Voltage fluctuations.

Active power fluctuations generated by the wind turbines cause voltage fluctuations or flicker. Turbulence and tower shadow effect are the reasons for these fluctuations. Measurements of the short duration flicker sensation (Pst) [32] has be performed inside the turbulence intensity range of 8-16%.The short duration flicker sensation is limited to Pst<=1. The Pst is based on observation times of ten minutes. However other norms demand a reduced observation time. To evaluate the Pst a flicker meter was developed in EMTP-RV.

Total harmonic distortion (THD).

The THD will be calculated directly using a probe included in EMTP-RV. The harmonic distortion limit for the voltage is THD <=8% .

Flicker meter.

The dependency between voltage fluctuation and flicker level must simulate a combining effect of human eye's response to light, response characteristic of luminescent device and type of voltage fluctuation. The most popular flicker meter corresponds to UIE standard [33].

The whole measuring chain is a sequential combination of 5 blocks, the block 1 is a normalizing transducer (voltage adapter); the block 2 is the demodulator in the form of squaring transducer and low pass filter with cut-off frequency 35 Hz; the block 3 is a

weighting filter in accordance with UIE rule; the block 4 is a squaring transducer, low pass filter whose time constant equals to 300 ms; the block 5 is a statistic process.

The flicker meter input $\Delta V / V$ may be obtained by means of a demodulation process or measuring the $\Delta V / V$ at the collector bus using the relation

$$\frac{\Delta V}{V} = r\,\Delta P + x\,\Delta Q \tag{5.39}$$

Where r (resistance) and x (inductance) are known from the grid data and the active and reactive powers are measured and expressed in pu.

The flicker meter is represented by a voltage adapter block and three block more where each name block is according with its function.

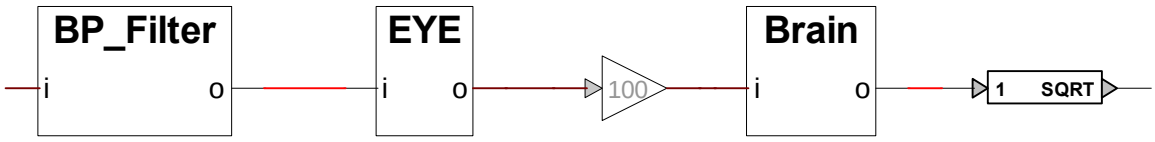

Figure 139. : Flicker meter blocks

In the case of short term flicker evaluation, the action of the fifth block can be performed after the simulation has finished through the previous storage of IF points (IFL is Instantaneous Flicker level). After that, using the process indicated in the standard [33] we calculate the percentile and finally with the following equation to calculate the short term flicker Pst

$$Pst=\sqrt{0.0314P_{0.1}+0.0525P_1+0.0657P_3+0.28P_{10}+0.08P_{50}} \tag{5.40}$$

The percentile notation used in the standards is slightly confusing, since the percentiles Pi correspond to percentage of samples for which levels are exceeded rather than to cumulative numbers of samples at lower levels. For example, $P_{0.1}$ corresponds to the level exceeded by 0.1% of the example. This level is more conventionally referred to as the percentile 99.9. The curves of IFL and PST values are obtained running a statistical process.

5.1.12 MEVA, MVEMTP and DEMTP Comparison

This section compares the mean value models MEVA and MVEMTP with the detailed DEMTP model of DFIG.

The MEVA model is the faster model approach but has limitations in the maximal time step, due to accuracy to calculate its phasors in the time domain solution. For the MEVA DFIG case the maximum time step is 250 μs. This maximum allows to maintain accuracy in the steady state condition and during a fault event (see Figure 143 to Figure 150) . This model may be used for electromechanical transient studies with large frequency variations and voltage variations, such as islanding studies (see Figure 151 to Figure 156). The main limitations in this approach are the neglected flux dynamics of the generator and the absence of the dc link. This model not may be used for power quality studies such as flicker and harmonic. The MEVA model operates with wind variation such as gust or ramp with good results but when a real time series of wind speed is modeled the results are not sufficiently accurate. Then it is preferred to use the model with only constant wind speed. The absence of the dc link model makes it impossible to represent the crowbar simulation. The voltage protection acts tripping the model during heavy faults on the ac side, no dc protection is included.

The DEMTP model has a typical time step of 20 μs to 50 μs. It has been found that the MEVA model is at least 15 times faster than the DEMTP model. Its typical time-step is near 200 μs.

The MVEMTP modeling approach is the second fastest approach. This modeling approach includes a dc link model replacing the switching elements by controlled sources, as a consequence it is possible to trigger the crow bar protection, see Figure 186. The possibility to run with variable wind speed (see Figure 179) make it possible to perform flicker studies, but the absence of harmonic production makes it impossible to study harmonic distortion (see Figure 181) . It has been found that when compared to the DEMTP model, the MVEMTP model is at least 7 times faster. The typical MVEMTP time-step is near 100 μs.

The DEMTP model is taken as reference to all the studies specially for fast transients. The following studies are presented: total harmonic distortion (see Figure 163); insulation coordination (see Figure 158), protection setting studies, (see Figure 169) and flicker of short duration (see Figure 165 and Figure 166).

5.1.13 DFIG DEMTP model tests

This section presents several benchmarks to test specific aspects of the DFIG modelling. The tests are described below.

- Test 1, initialization: for comparing the CPU timing with and without initialization method.
- Test 2, combines modelling: for showing the similarities in the dynamic behaviour between the MEVA and DEMTP modelling approaches as in the radial benchmark as in islanding scenario.
- Test 3, power Quality: a DEMTP model including a wind speed model with the ability to simulate turbulence and tower shadow effects with the objective of calculating total harmonic distortion and flicker level.
- Test 4, full scale park: a wind speed model that includes wake effect and random initial blade angle together with four equivalent machines for wind park representation were used to evaluate the differences in the flicker and harmonic results.
- Test 5, fast transient: the transient analysis for reproducing the finest details that could have influence on the development of the overvoltage phenomenon. The results of the analysis will be used to evaluate a strategy for limiting the overvoltage phenomenon.
- Test 6, performance coefficient C_p comparison: it shows the similarities in the dynamic behaviour before and after fault between two equivalent machines with the DEMTP model. Three C_p matrix representations are compared. The polynomial version is contributed in this thesis and it is the most efficient.

- Test 7, mean value comparison: using the same radial benchmark of Test 2, but with different nominal terminal voltages and separated simulation, it shows the similarities in the dynamic behaviour between the MVEMTP and DEMTP modelling approaches considering variable wind speed during the simulation.

5.1.13.1 Test 1, initialization

The correct initialization of the reference voltages and currents of the power electronics controls allows an important gain of computing time. To show the advantage of the method of initialization of the reference sources, a computationally intensive benchmark, a wind park section with 16 machines (DFIG) was simulated. The benchmark includes an equivalent system of 230 kV, a Zig-Zag grounding transformer, the substation transformer 230kV/34.5kV of 125 MVA Xcc=11.75% with saturation curve, an underground cable distribution grid in 34.5kV of 29 km of length, 16 DFIG generators of 1.5MW with their unit transformers of 34.5kV/0.575kV of 1.75MVA Xcc=5.7% with saturation and ZnO arresters on the 34.5kV side.

This benchmark, shown in Figure 140, was used to evaluate the overvoltage produced after the main switch opens due to a single phase to ground fault near the wind generator number 8. When the main switch opens, it leaves the distribution system in neutral isolated condition, triggering a ferroresonance phenomena between the cable grid and the transformer unit nonlinear inductance.

The minimum total simulation time is 3 s: 1 s is needed to reach the steady state condition and at least 2 s of simulation are needed after the fault condition. In the simulation of a wind farm section with 16 machines, with a required time step of 10μsec, each second of simulation (Intel reference processor) consumes 2.4 hours.

A reduction of the simulation time period to reach the steady state condition from 5-8 s to 0.5-1 s delivers a gain of 10 in computing time. This time gain becomes more important and significant when individual machines are represented with the DEMTP model.

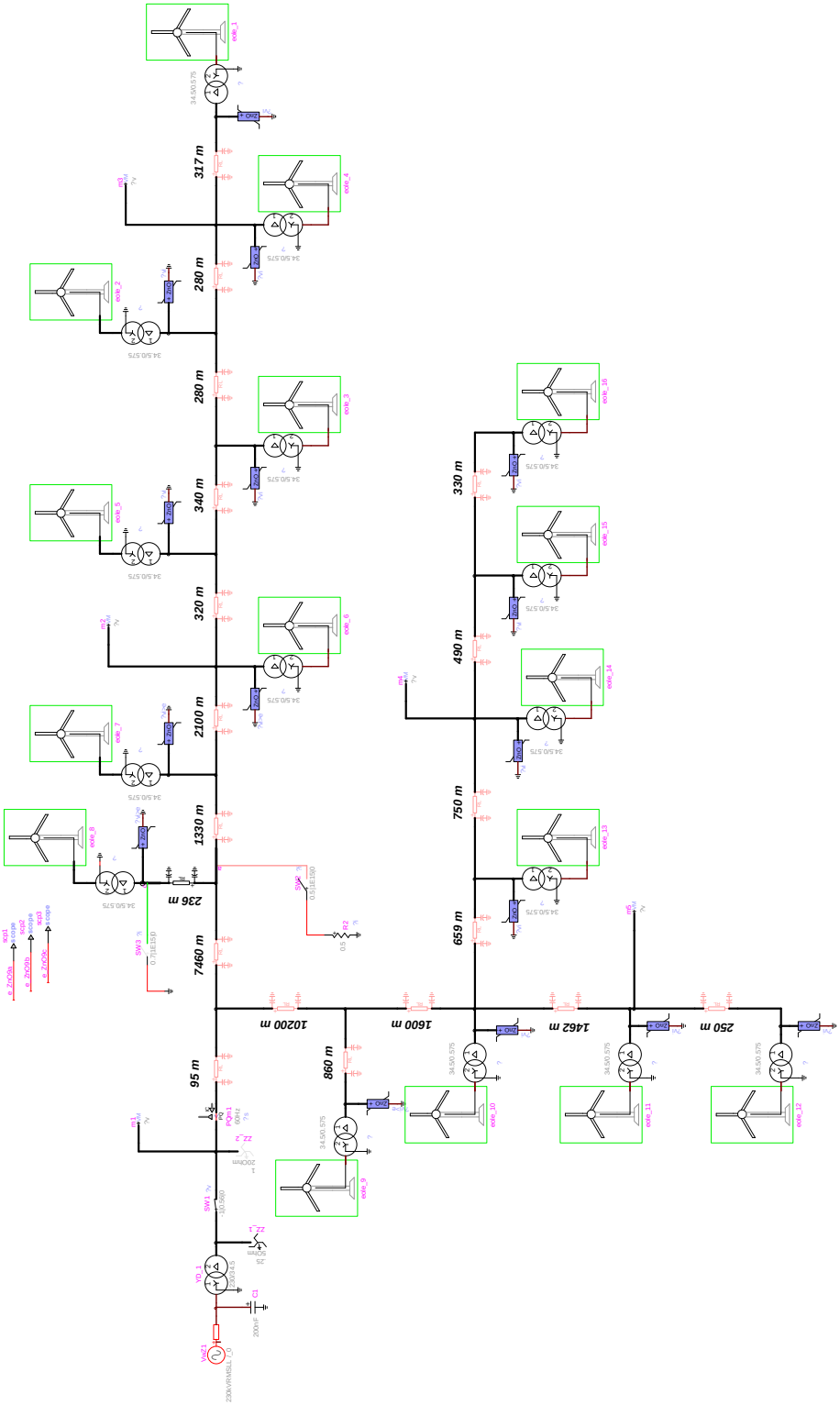

Figure 140: Benchmark of 16 WECs

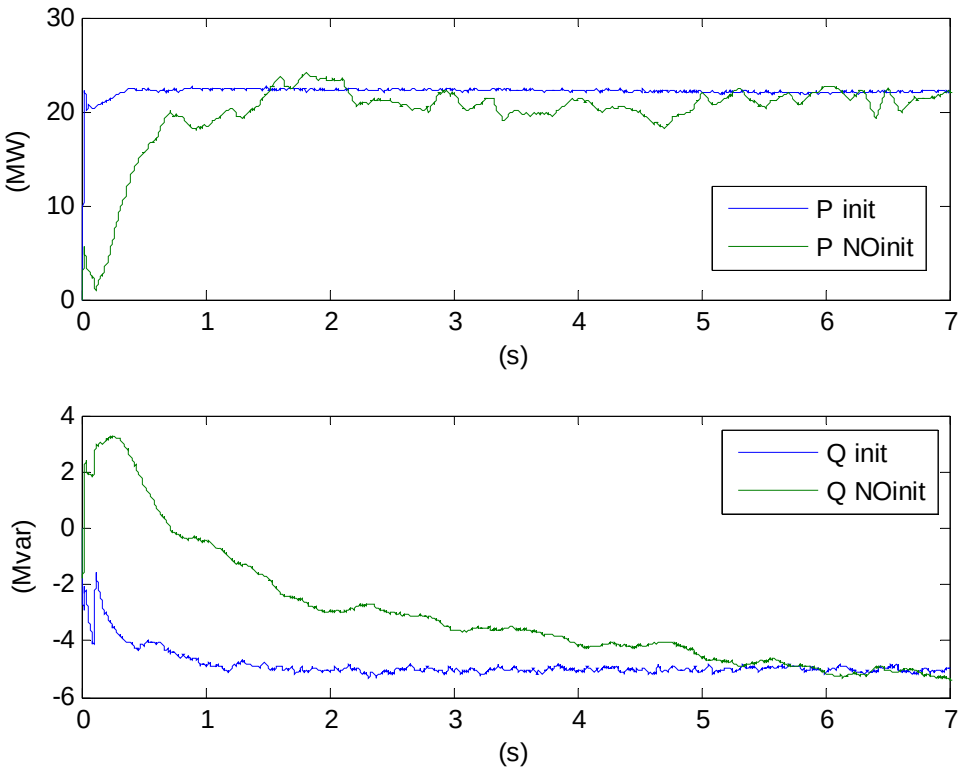

Figure 141: Results with and without initialization

5.1.13.2 Test 2, combined modelling

To test the combined model for a small perturbation, a three phase fault and islanding event were applied to two benchmarks, the radial benchmark shown in Figure 142 and the islanding benchmark shown in Figure 151.

The radial benchmark represents a wind farm wit by two equivalent generators (DFIG) of 10 machines as shown in Figure 142. The benchmark includes the transformer with 6% of short circuit impedance in its self base, the cable collector with 2% of impedance in 100 MVA base, the station transformer of 10% of short circuit impedance in its self base and the system equivalent with 10% of short circuit impedance in its self base.

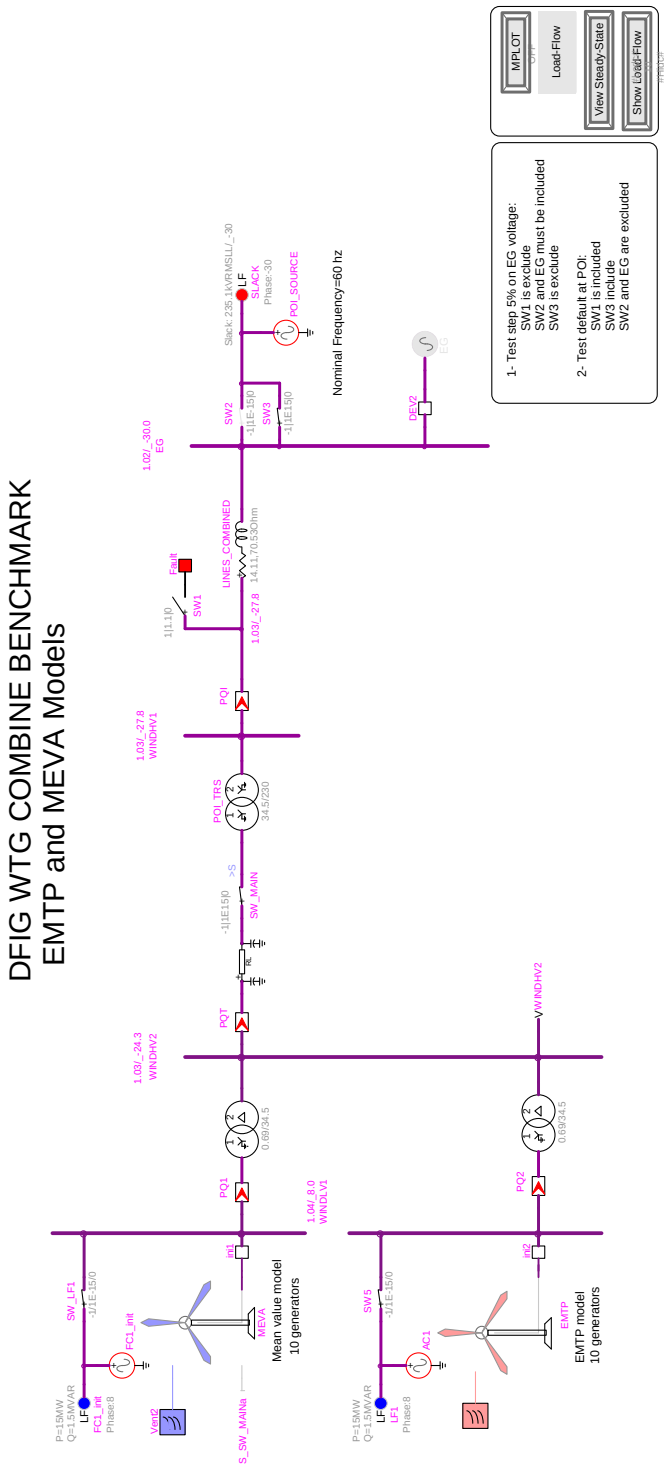

Figure 142: Combined MEVA and DEMTP models for DFIG benchmark

The benchmark shown in Figure 142 was used to test the model by applying a small perturbation and a three phase fault event.

- Test A, small perturbation: a change of ±5% on the terminal voltage of the equivalent was applied with the objective of obtaining a linear response of the controls.
- Test B, three phase fault: at the interconnection point, a three-phase fault with a fault impedance applied during 100 ms to obtain the voltage drop below 0.7 pu at the terminal and out of the linear range of the converter operation.

A change of ±5% on the terminal voltage of the network equivalent was applied with the objective of obtain a linear response of the controls for MEVA and DEMTP models with limited mismatch between results.

The voltage step was applied to the Grid voltage bus EG. At the beginning the WTG Terminal voltage tracks the grid voltage but finally the WTG Terminal voltage is controlled in its reference value (see Figure 143).

A response to the change of ±5% on the terminal voltage of the equivalent allows to compare reactive power outputs of MEVA and DEMTP models. Both responses match well with limited differences in the reactive power values. It is observed that the differences are small and increase near the new steady state.

The Figure 144 shows the reactive power of the WTGs measured at PQ1 and PQ2, raises when the voltage step lowers and drops when the voltage step lowers but it does not reach neither the maximum limit nor the minimum limit of the reactive power.

The active power are compared next. Both response matches well with limited differences in the active power values. The mechanical power remains constant since the wind is constant. In consequence the active power produced by the WTGs, will remain constant in the final steady-state after perturbation. This trend is shown in Figure 145.

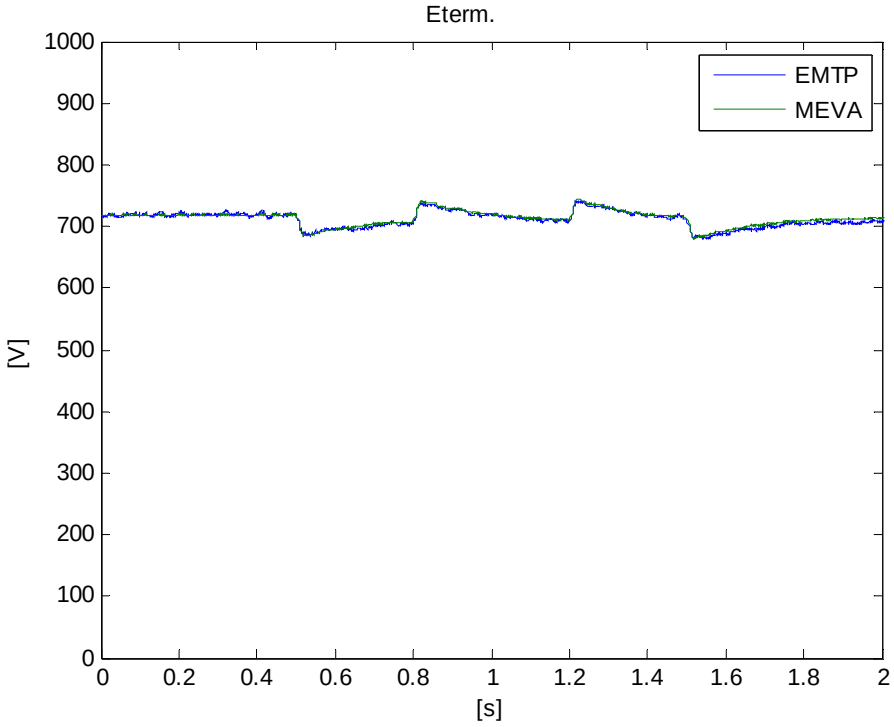

Figure 143: Voltage, small perturbation, Test A.

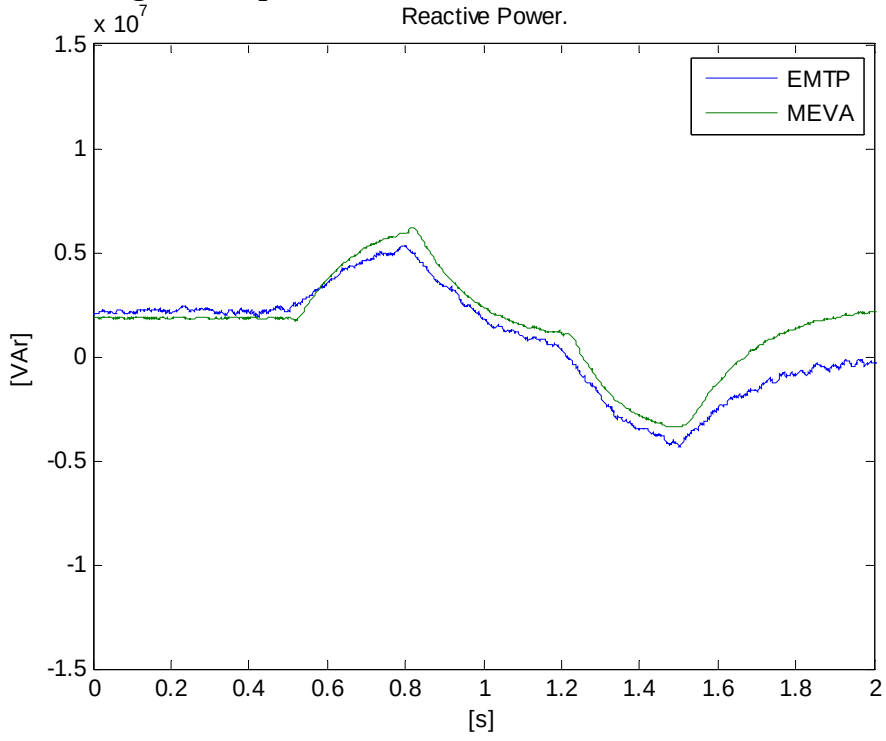

Figure 144: Reactive power, Test A.

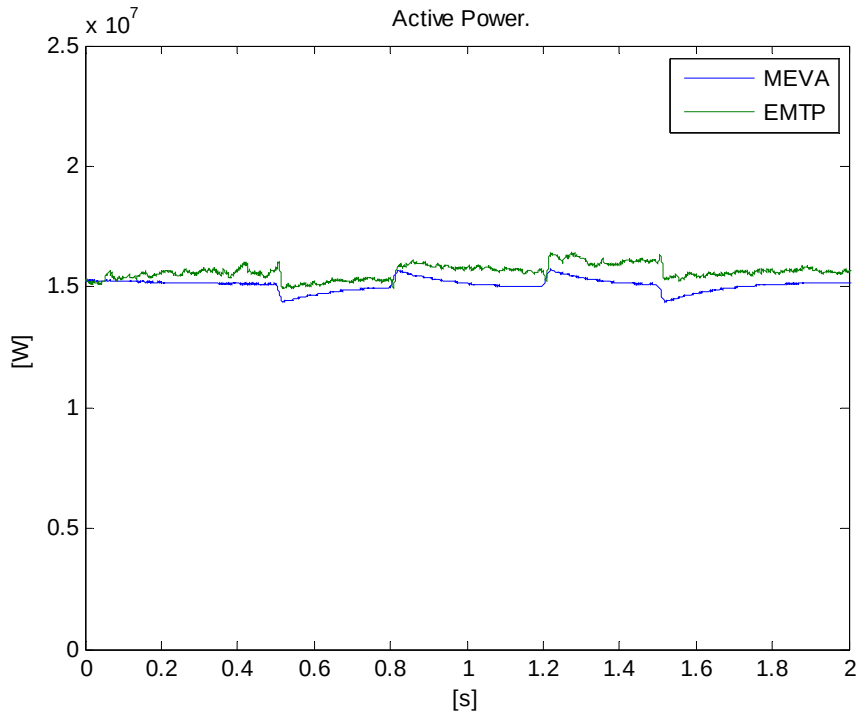

Figure 145: Active power, Test A.

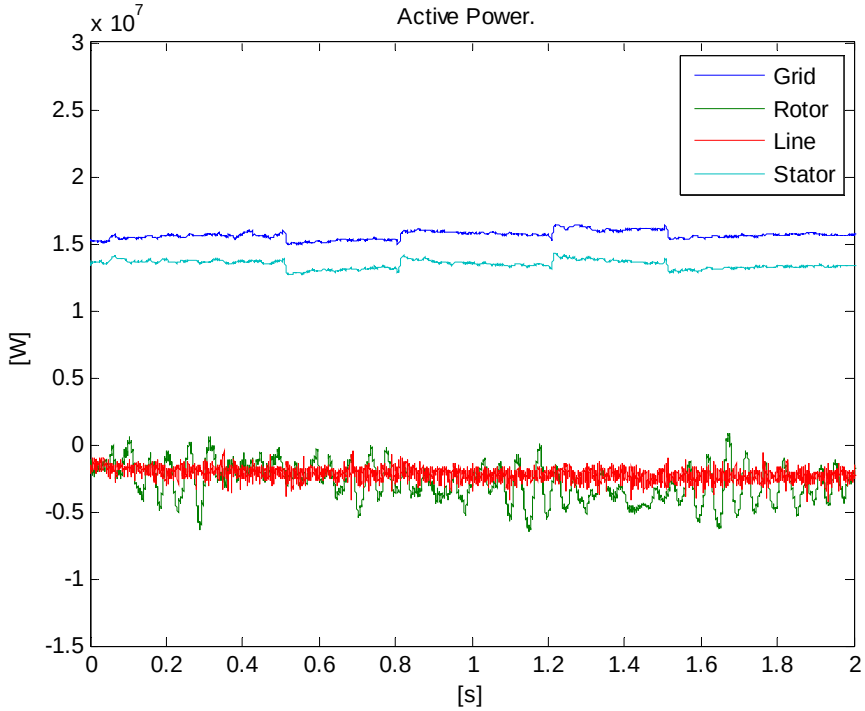

Figure 146: Active power DEMTP model: Grid, Rotor (inst), Line (inst) and Stator, Test A.

The last Figure 146 shows the Grid, Rotor, Line and Stator active powers. The negative values indicate power direction entering the converter.

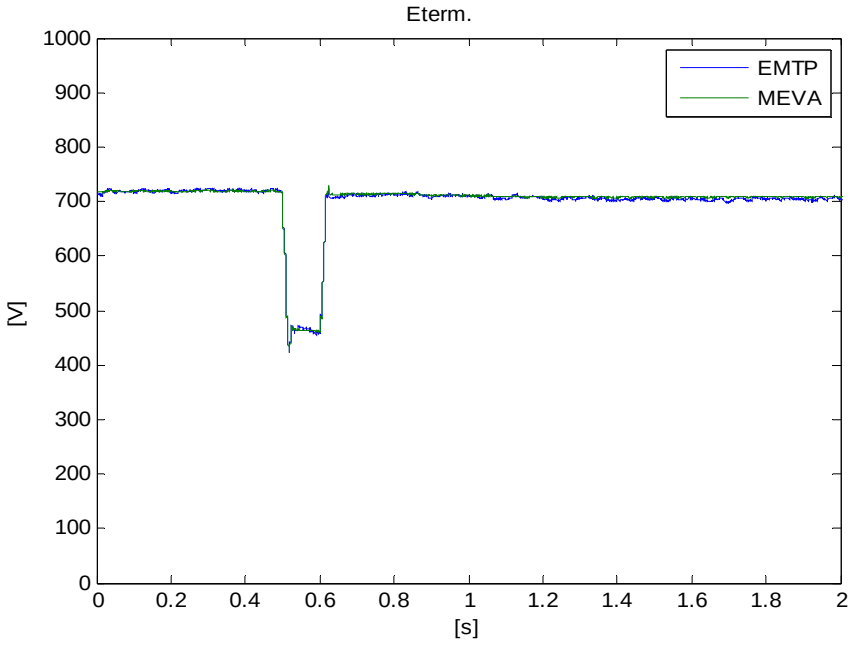

Figure 147: Voltage, Test B

As response of the three phase fault with fault impedance at the interconnection point, the terminal voltage of the DFIG drops near 0.65 pu during the time of fault. This is shown for both DEMTP and MEVA models in Figure 147. After the fault was cleared the terminal voltage remains controlled.

The reactive power contributions to the fault are compared in Figure 148. Both response matches well with limited differences in the reactive power values. It is observed that the differences are small during the variation and increase near the new steady state.

The active power comparisons for Test B are shown in Figure 149. The significant mismatch between both waveforms is shown during the fault duration, as a consequence of converter non linearity in the DEMTP model. This mismatch will be compared with the result obtained in the MVEMTP model where the simplification only reaches to the dc link keeping the other model components identical to the DEMTP model.

The active powers for the three phase fault with a fault impedance are shown in Figure 150.

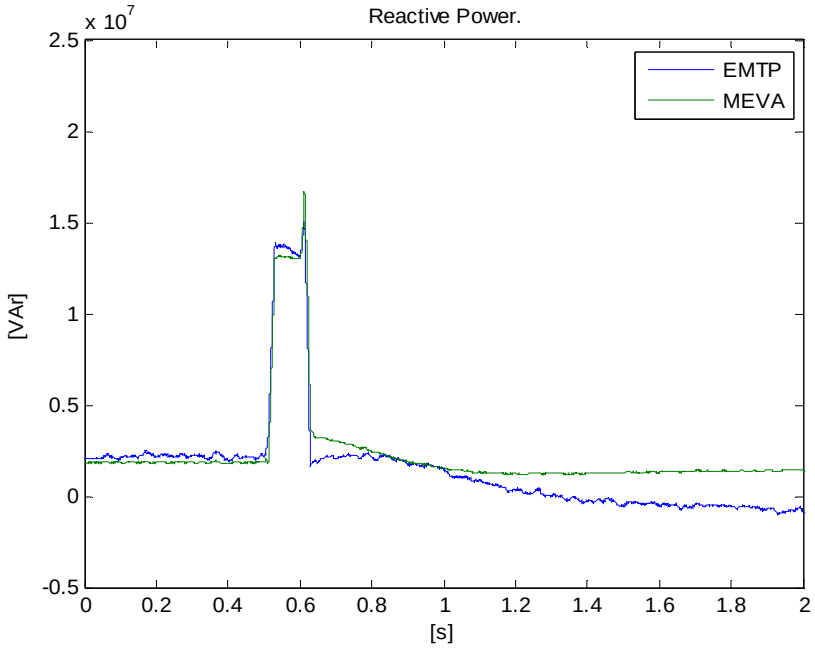

Figure 148: Reactive power, Test B

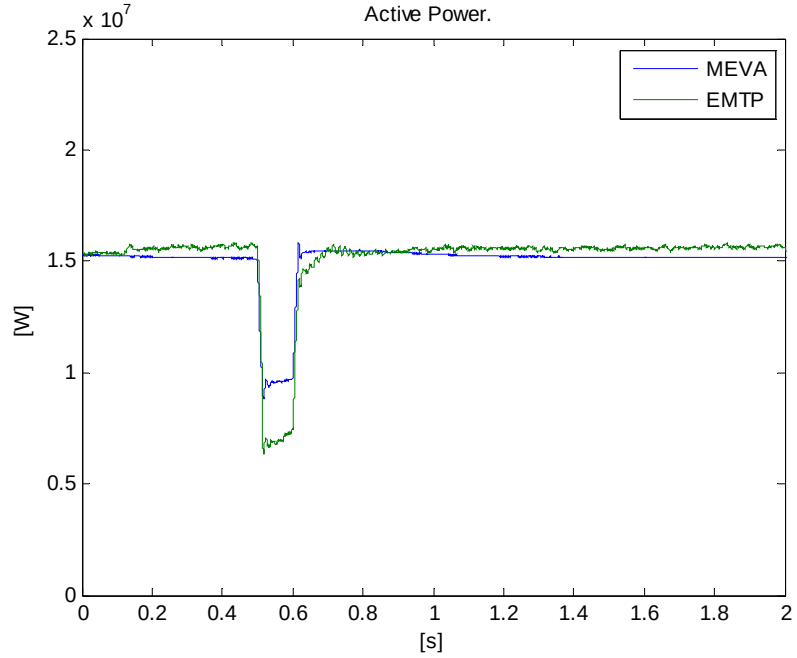

Figure 149: Active power, Test B

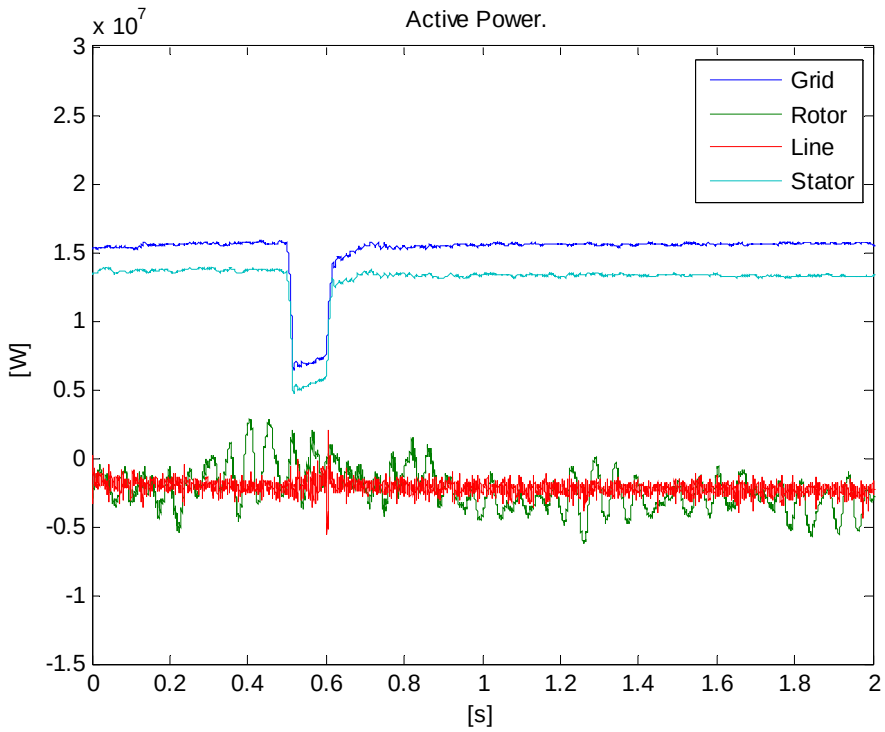

Figure 150: Active power DEMTP model, Test B: Grid, Rotor (inst), Line (inst) and Stator, Test B.

The numerical stability limit in the MEVA model is for a time-step of 2380 µs but using this time step creates an inacceptable error in both the steady state conditions and during the fault period. In consequence it must be reduced to match with results obtained with a DEMTP model in same scenario. This target is reached with a time step of 250 µs or lower. There is no sufficient gain in precision when using lesser values.

The time step used in the above simulations was 20µs for the DEMTP model and 250µs for the MEVA model. The CPU time after 2 s of simulation time are 10 s and 153 s respectively. That results into an acceleration factor of 15.3 times.

The Test C is an islanding event generated by a three phase fault and tripping the line 104-125. The islanding benchmark shown in Figure 151 was used to test the combined model with an importing islanding scenario. There are six synchronous machines with exciter and prime mover; an equivalent WTGs of 15MW with DEMTP model and others of similar power with the MEVA model, three voltage levels of 315

kV, 33kV, 13.2kV and 0.69kV, two power system areas linked by a 300 km line, system light load condition with 450 MW and import area condition of 28 MW. A realistic scenario of light load condition with a local generation of 145 MW, power imported of 28MW and a wind power penetration of 20% was considered.

To test the PLL performance for the MEVA model, an important frequency and voltage variation is needed. These variations are associated with an islanding event when the isolated area has a high degree of WTG penetration and with an import condition.

As a response of the islanding event, Figure 152 shows the active power outputs of MEVA and DEMTP models. The wind farms do not contribute to the frequency and their active power outputs remain unchanged. All the active power contributions are produced by the conventional generators (see Figure 155).

The reactive power comparisons are shown in Figure 153 with a good match.

The terminal voltages of MEVA and DEMTP models in the stable island with wind power generator are shown in Figure 154.

As response of the islanding event it is shown in that the active power outputs of conventional generation G4, G5 and G6 must rise (see Figure 155).

The frequency excursion on the island with conventional generation is shown in Figure 156.

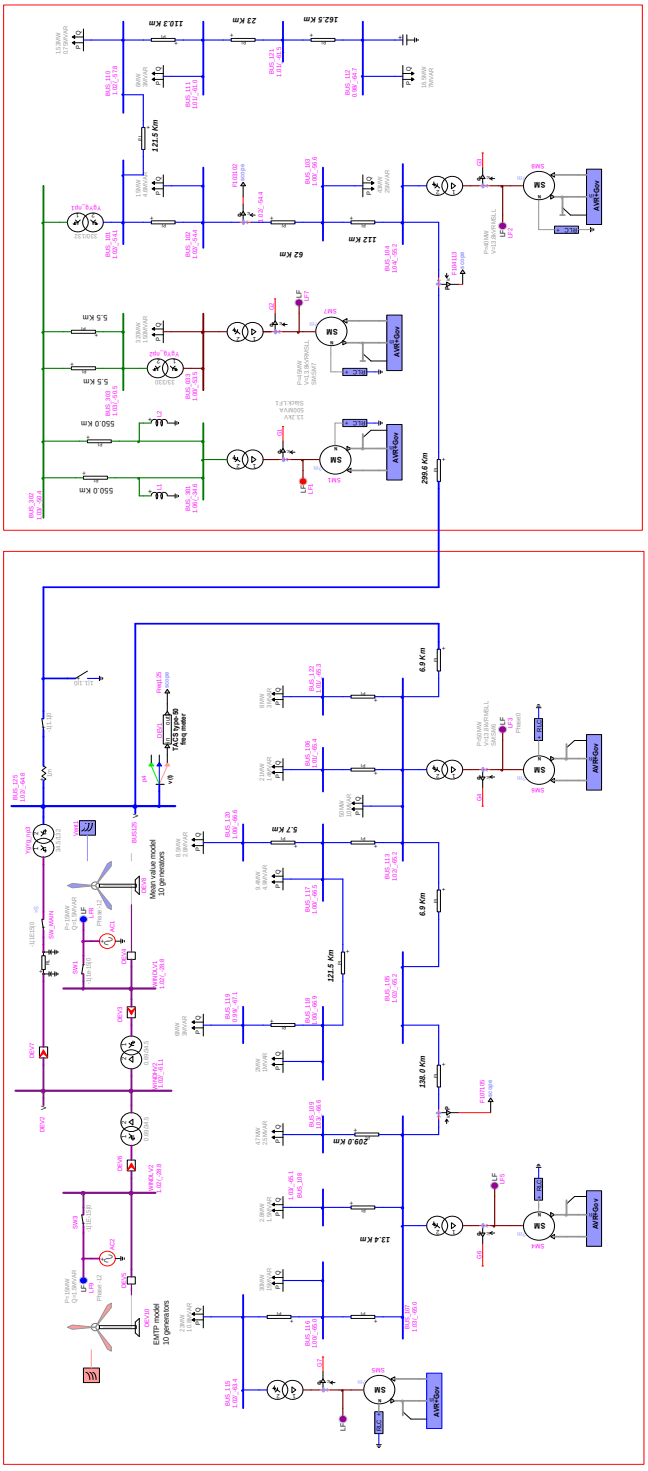

Figure 151: Islanding benchmark, Test C

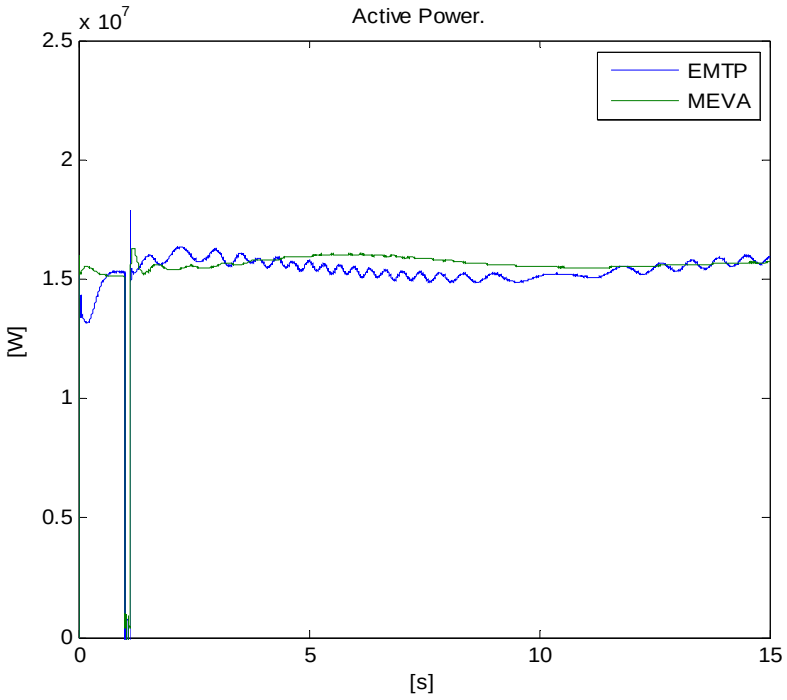

Figure 152: Active power of WTG, Test C

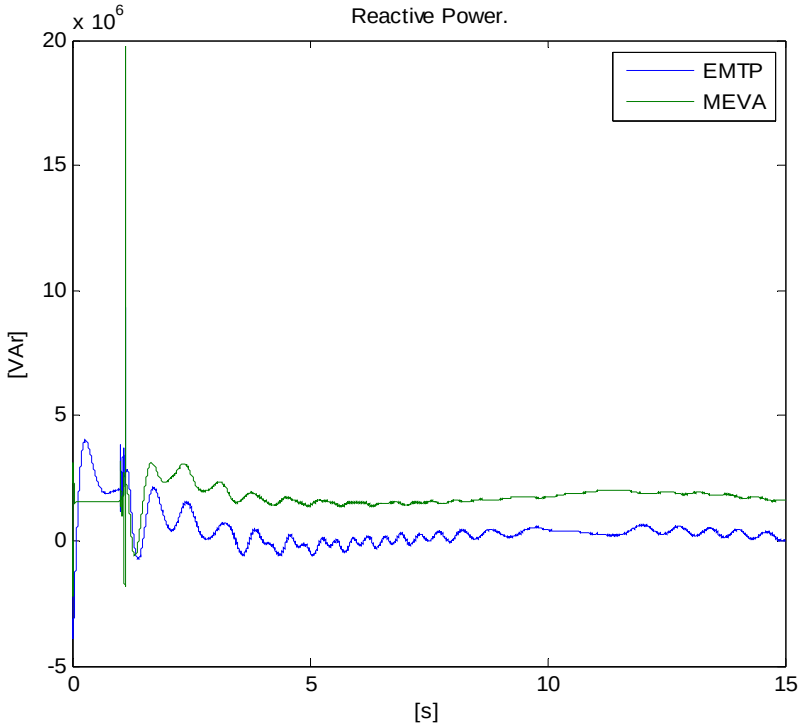

Figure 153: Reactive power of WTGs, Test C

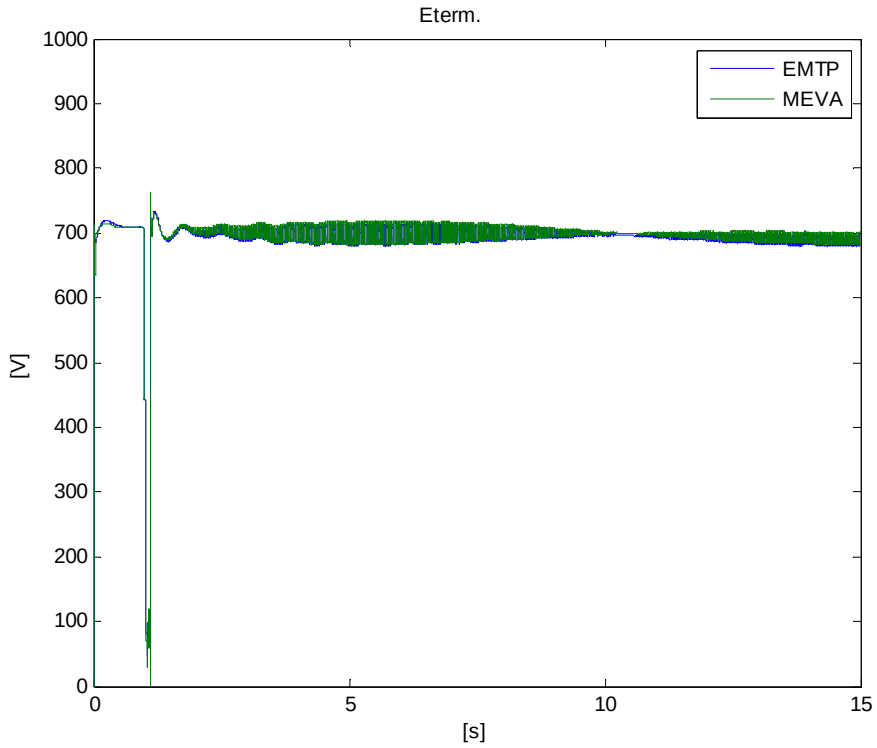

Figure 154: Terminal voltage, Test C

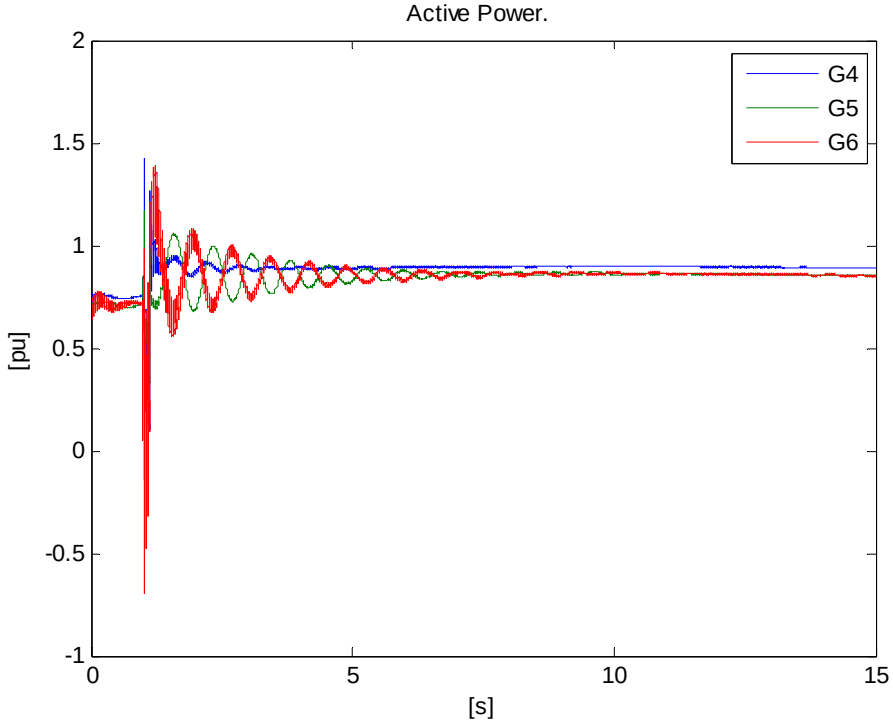

Figure 155: Conventional generation into the island, Test C

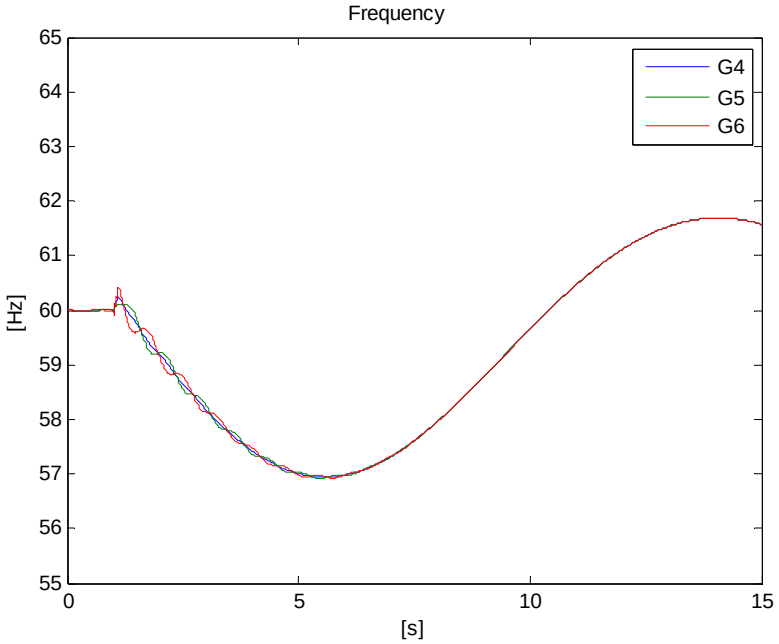

Figure 156: Island frequency, Test C

5.1.13.3 Test 3, Power Quality

The benchmark of Figure 157 represents a wind farm integrated by only one equivalent generator for 20 DFIG type generators. The unique machine representation is pessimist, and could be known as a superior limit of the Pst and THD, since the negative effect of the wind perturbation and harmonic amplitude are added directly. A full scale wind farm representation could be considered as a more realistic condition, due to the compensation effect that is considered with the multiple machine representation.

The unique machine test results in a Pst overestimation of 36% taking as reference the full scale test. The Pst of unique machine is 0.42896 while the full scale is 0.31519.

The benchmark includes a transformer with 6% of short circuit impedance in its self base, the cable collector with 2% of impedance on 100 MVA base, the station transformer of 10% of short circuit impedance on its self base and the system equivalent with a 10% of short circuit impedance on its self base.

With the target to consider the influence on the power quality parameters THD and Pst defined in the section 5.1.11, a special wind speed model is used and includes the wind turbulence effect defined in [30], the 3P effect and drop of torque produced by the blade passing in front of the tower. These effects were explained in the section 5.1.10.

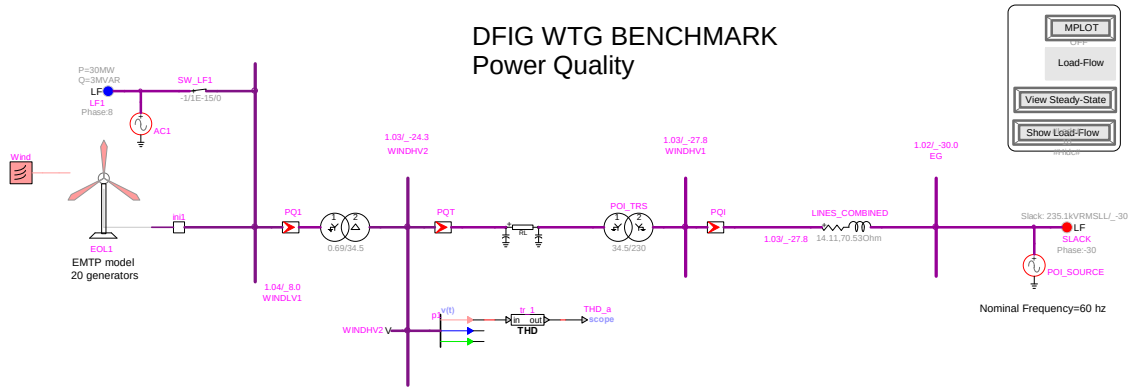

Figure 157: Power Quality DFIG benchmark, DEMTP model

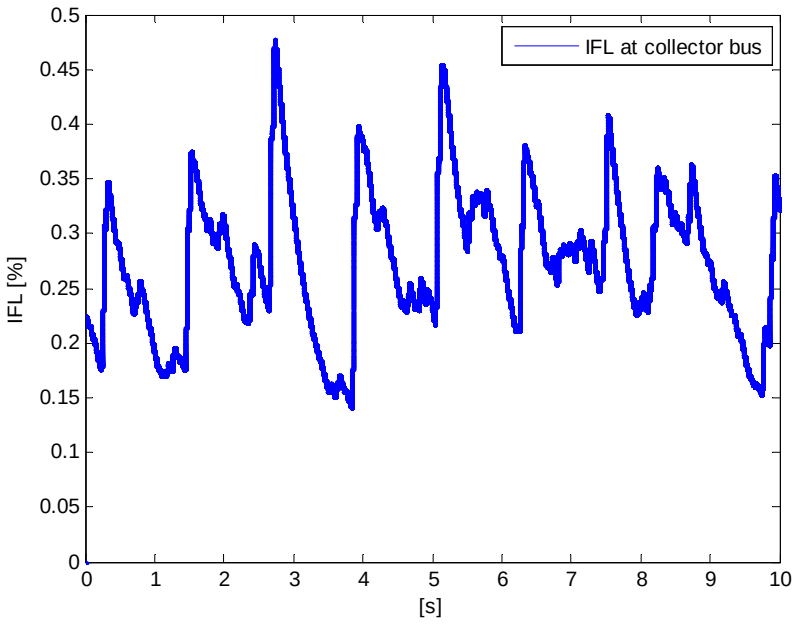

Figure 158: IFL computation at collector bus for

From the points obtained from Figure 158 to for IFL it is possible to use equation (5.40) to calculate Pst shown in Figure 159. The mechanical torque results of the application of the wind speed waveform are shown in Figure 160.

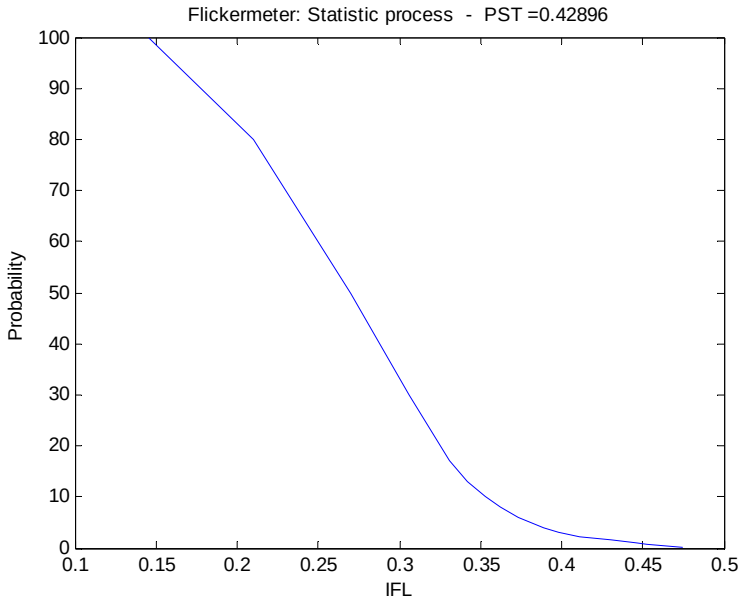

Figure 159: Pst computation at collector bus

The corresponding wind speed is given in Figure 161. Figure 162 shows the active power output variations at the collector bus.

Figure 163 shows the THD measured at the collector bus.

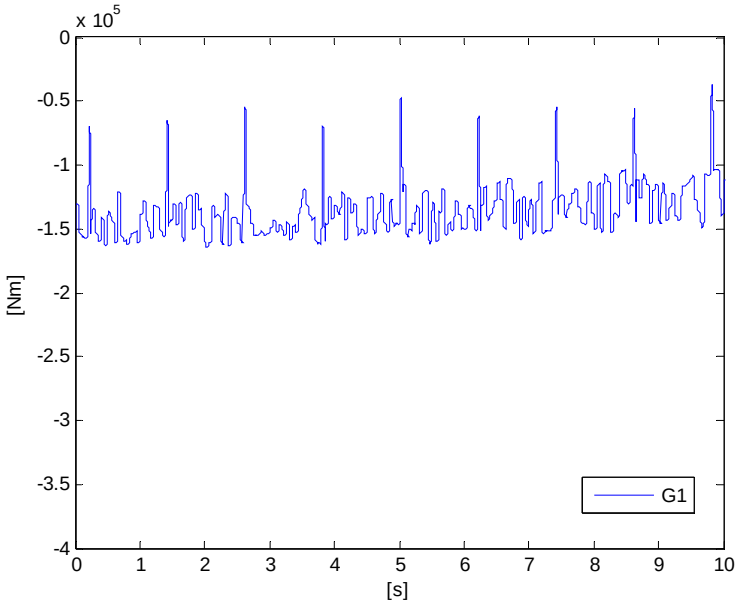

Figure 160: Torque resulting from wind speed fluctuations

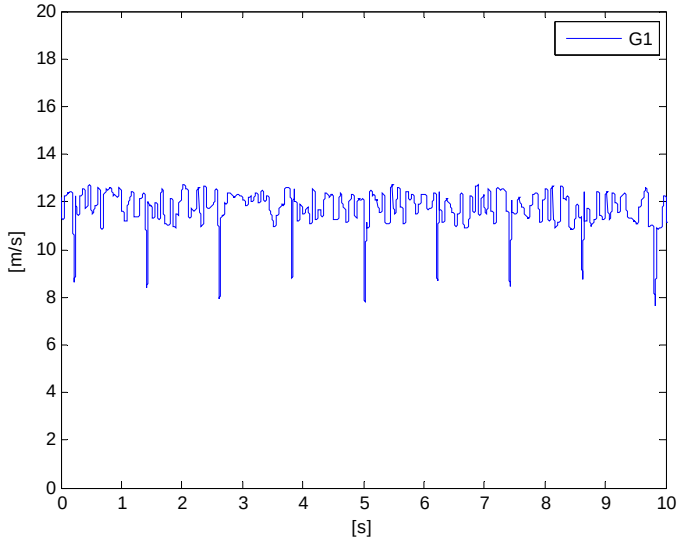

Figure 161: Wind speed variations

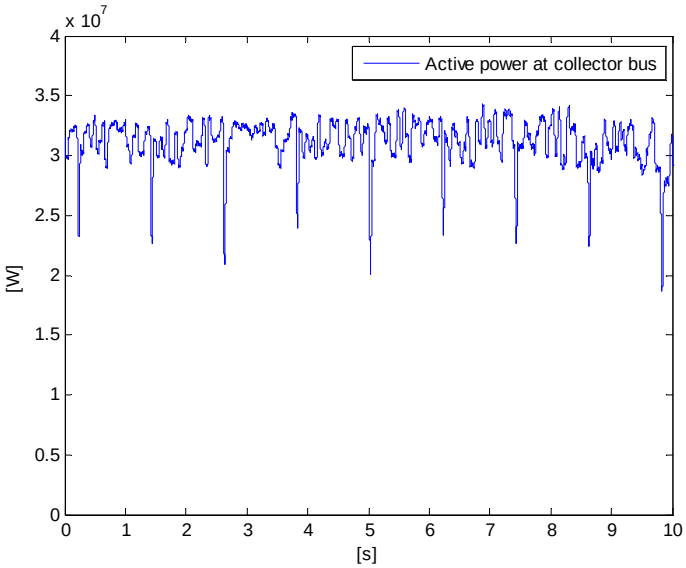

Figure 162: Active power variations at the collector bus for wind fluctuations

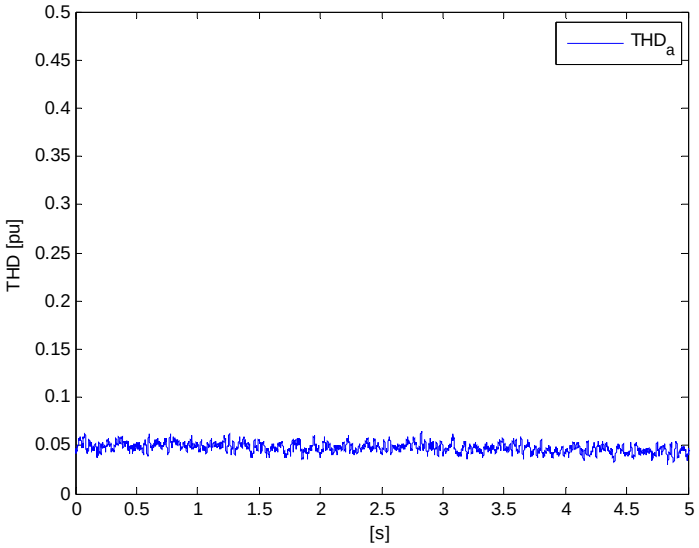

Figure 163: THD computation at the collector bus

5.1.13.4 Test 4, Full scale

The benchmark has 3 voltage levels, 230kV, 34.5kV and 0.69kV. The constant voltage source in 230kV and all the WTG of the wind farm are connected to the collector bus by the unit transformer of 5% Zcc.

The DFIG EMTP detailed model, include the converter detailed with IGBT bridge and fast controllers. Additionally the blocks to represent turbulence, tower shadow, wake effect and terrain roughness effect were included.

The benchmark was built considering a minimal short circuit power relation, equal to 5. Habitual wtg manufacture consider in its installation short circuit power relation equal to 50 in relation with the wind farm project.

The flicker measure point is the collector bus, it is the worst point because of P, Q, R and X have the values that more contribute to the ΔV/V.

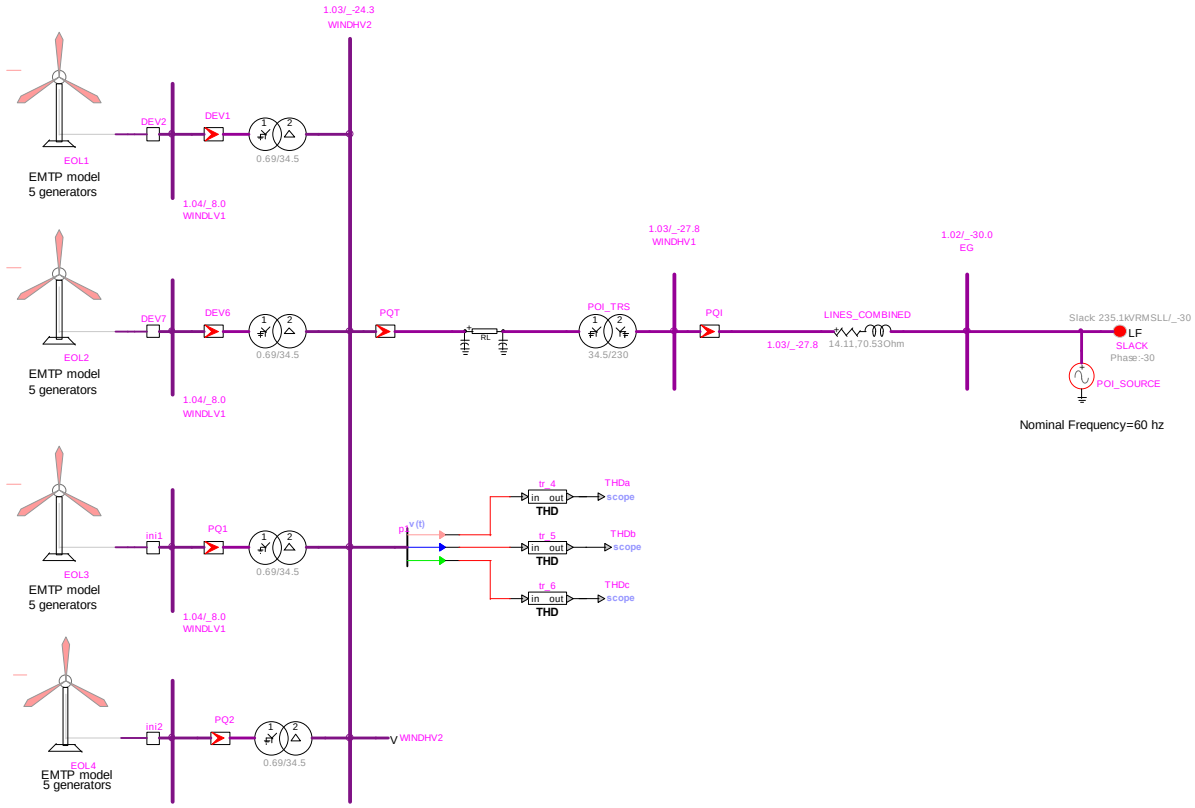

Figure 164: Benchmark to harmonic and flicker simulations

The values of the R and X from the fix 230 kV equivalent source to the measure point are 0.05 and 0.53 pu respectively, taken as Sbase=150MVA. Once obtain the time variation $\Delta V/V$, it will be filtered according the process descript in the IEC norm about flicker to get the IFL and finally a statistic analysis of IFL will be require to determine the Pst value. The period of time used in the Pst in each simulation isn't according with the IEC norm, but the Pst continue being a good indication of the flicker of short duration rank.

The simulation considers the following characteristics:

Real wind turbulence and Kaimal turbulence of 10%

Random initial angle to deterministic shadow tower effect

Drop of torque of 30% (shadow tower effect).

Drop of torque duration 50 ms.

Wind speed travel time to the next wind turbine line of 10 s.

Decay of the magnitude of the longitudinal component 5% (wake effect).

To consider in a random way the initial blade angle with the tower an uniform distribution was used. This model considers that the 120 mechanical degree are divided in 10 different position shift 12 degree each one. Zero degree or 120 degree represents a division.

The Figure 165 shows the instantaneous flicker level, IFL, obtains to the output of flickermeter block diagram of the Figure 139. After 10 second of time simulation with the application of the variable wind speed considering the full scale wind conditions.

From the point obtains from the Figure 165 to the instantaneous flicker level, IFL, using the statistic process to calculate the percentile demanded in the equation (5.40) finally the short term flicker, Pst, is obtained to the full scale case.

The Figure 167 shows mechanical torque applied to the four turbines results of the application of wind speed wave form considering the turbulence and 3P effect components and random initial angle of blades.

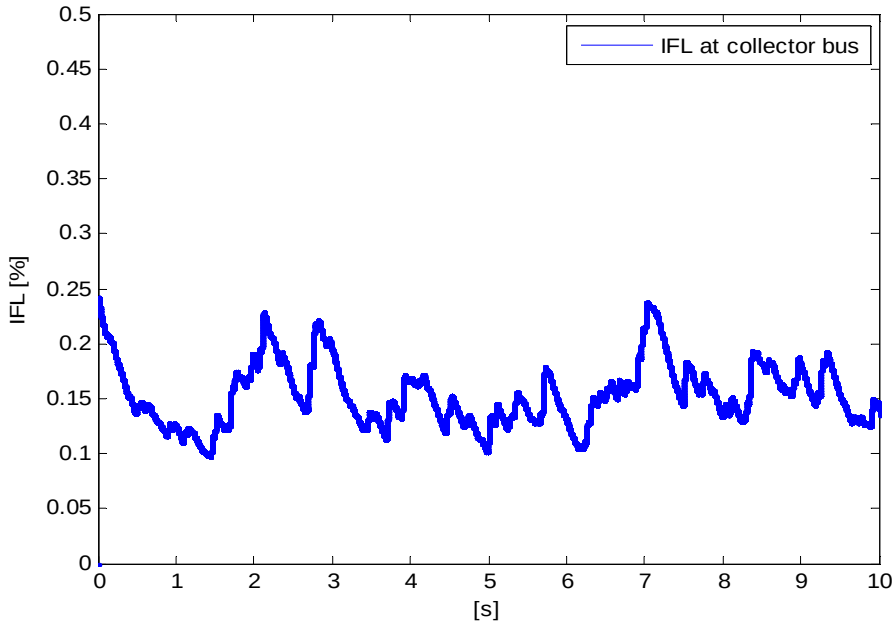

Figure 165: IFL

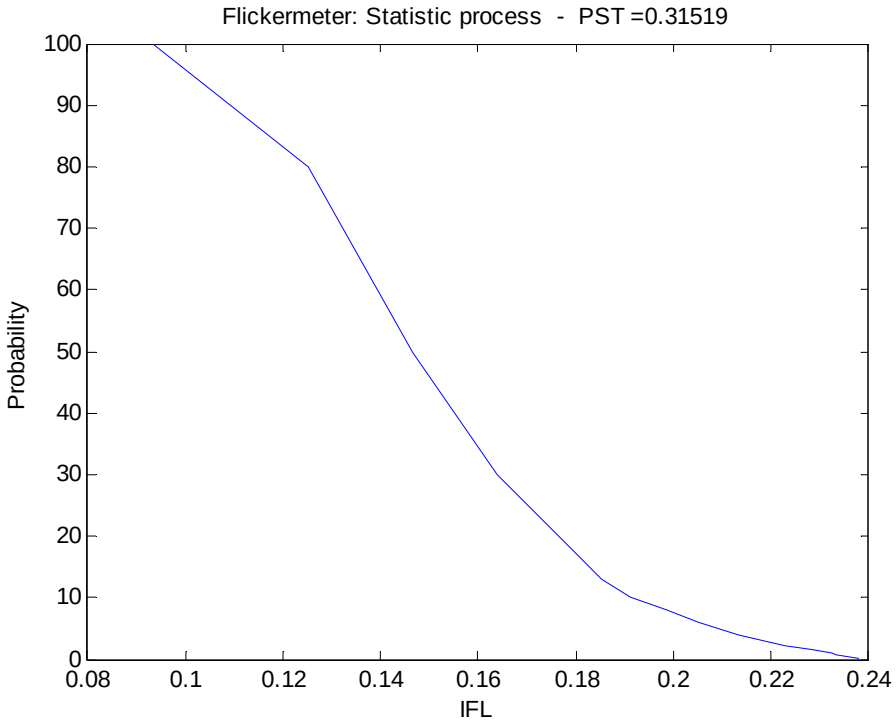

Figure 166: Pst

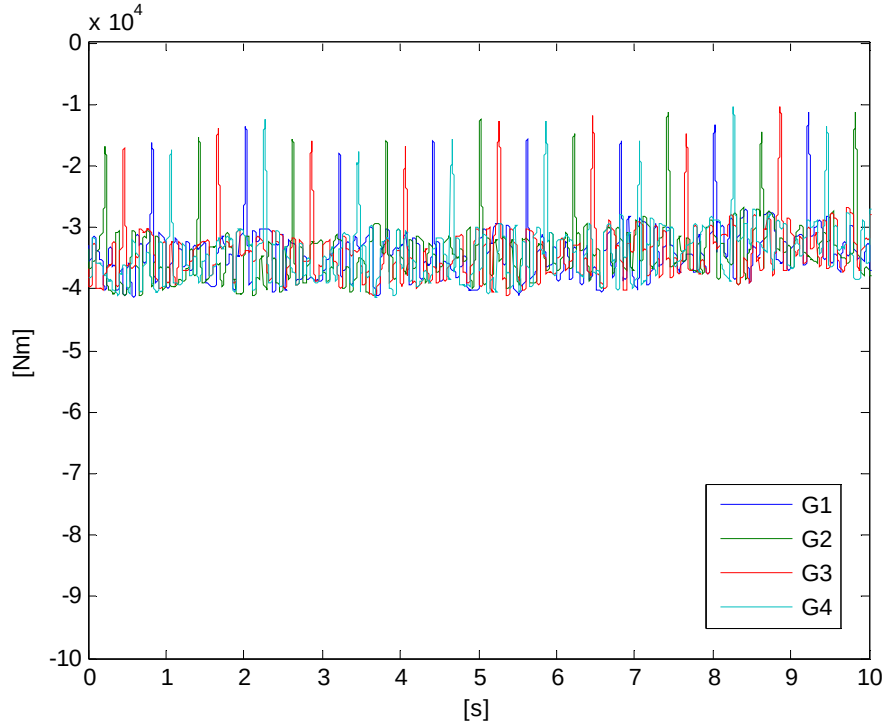

Figure 167: Torque

5.1.13.5 Test 5, Fast transient

A wind farm is a microgrid with equipment capable of generating a wide variety of transient phenomenon. A special focus for research is the synergy of phenomenon due to the particular topology of the microgrid and the distributed generation (DG).

The transient analysis allows to reproduce to the finest details overvoltage conditions. The results of the analysis will be used to evaluate strategies for more efficient overvoltage limitation. Overvoltages can damage equipment and are an important factor in power system analysis and design.

Figure 168 shows an actual wind farm section which has been represented using the EMTP-RV. The DEMTP model is used for all WTGs. All modeling details for components are included for switching transient analysis. If key components, such as surge arresters, are not modeled correctly, overvoltage calculations will contain important errors.

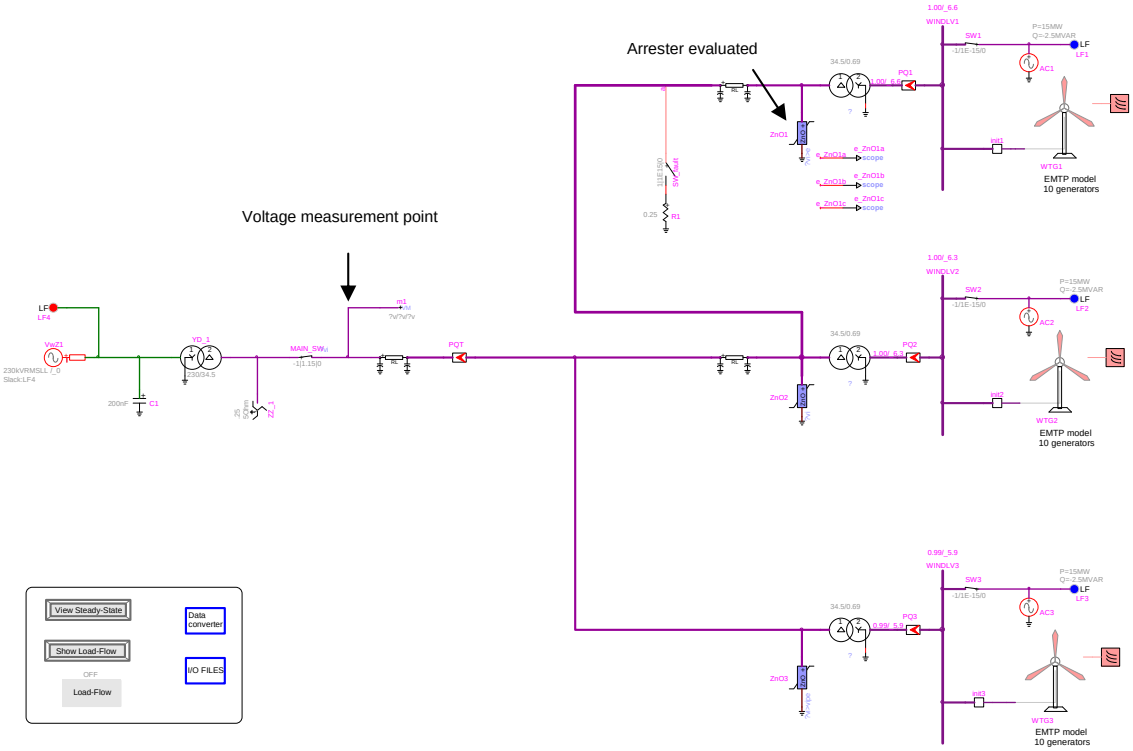

Figure 168: Fast transient DFIG benchmark

The main network components are: an equivalent system of 230 kV, a Zig-Zag grounding transformer, the substation transformer 230kV/34.5kV of 125 MVA Xcc=11.75%, underground cable distribution grid in 34.5kV, 3 double-fed asynchronous generator of 15 MW with unit transformers of 34.5kV/0.69kV of 17.5MVA Xcc=5.7% and ZnO Arresters on the 34.5kV side. The arrester has a TOV 36.3 kV to 10 s and the energy absorption capability is 7 kJ/kV.

The connection group of the substation transformer has influence on the grounding on the 230kV and 34.5 kV sides and consequently on the overvoltages. On the delta side of the substation transformer a grounding transformer is connected to the west switch terminal with the mission of detecting the ground fault and limiting the associated overvoltage.

The unit transformer connection has its influence on the grounding on the 34.5 kV side and harmonic pollution. The delta winding traps harmonic multiples of three times the fundamental frequency.

Finally, the arrester on the 34.5 kV side has decisive influence on the overvoltage reached on the delta side of the unit transformers.

The overvoltages are due to the feed-back of the wind generators over an isolated neutral grid during a fault condition. A ground fault on the cable grid triggers a series resonance phenomenon among the zero sequence capacitances of 34.5 kV cables with the induction machine and the transformer impedances.

The arrester absorbed energy is shown in Figure 172. The trip operation, by means of the over voltage protection, prevents an early arrester destruction, the arrester should be destroyed in several seconds if the overvoltage condition is maintained.

The overvoltage is particularly severe in the DFIG machines because of the increase of the external impedance. In the wound machine the presence of the power electronic circuit makes the increased impedance seen from the stator. The rise of the impedance seen from the stator creates a Ferro resonance. The Ferro resonance is a phenomenon of series resonance associated to a very high voltage across the elements

of the series LC circuit when it is exciting at or near its natural frequency. The inductance involved in this phenomenon has an iron core.

Ferroresonance overvoltages can occur on the wye-delta transformer of a wind generator. They are related to the transformer size and length of lateral cable.

Three alternative solution to the overvoltage problem were considered: change the arresters, add additional grounding transformer installation on the fault side or add a high speed grounding switch after the main switch opens.

In the author's opinion the best solution is the high speed grounding switch. It is a technique widely used in high voltage lines and now begins to be recommended to the distribution level. Another positive aspect is its minimum cost alternative.

Figure 169 shows the terminal voltage waveform on the DFIG side of the switch, and the trip signal of the protection of crowbar and overvoltage after the main switch opens.

The Figure 170 shows that the active and reactive powers are null after the voltage protection trips.

The overvoltages shown in Figure 171 are due to the feed-back of the wind generators over an isolated neutral grid during the fault condition.

The arrester energies are shown in Figure 172 remains within the limits. The generator trip operation, by means of the overvoltage protection, prevents arrester destruction. The arrester should be destructed in the case of no operation of protection system.

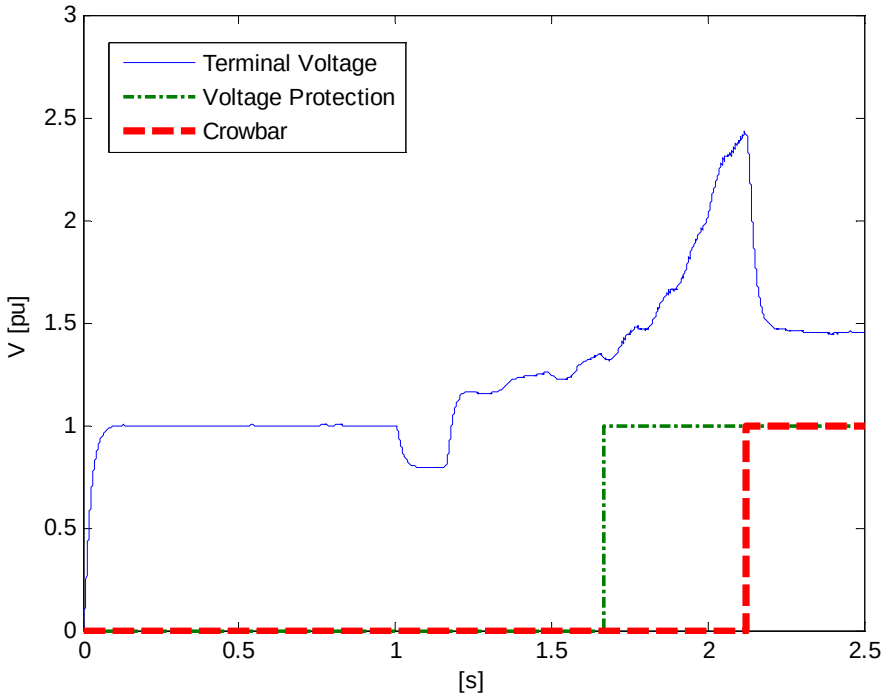

Figure 169: Terminal voltage and protection signals

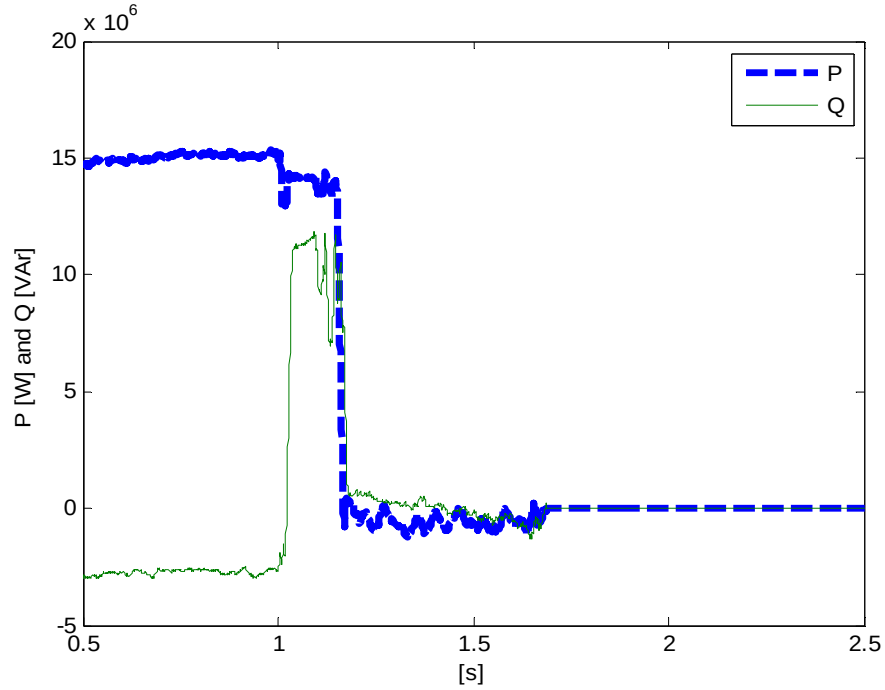

Figure 170: Active and reactive powers

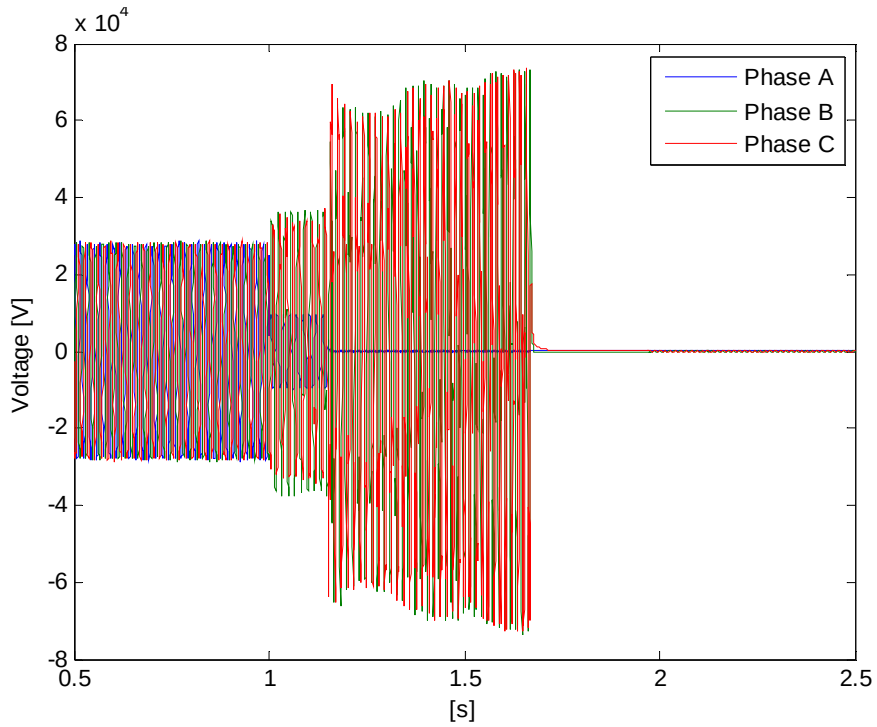

Figure 171: Voltage at point m1

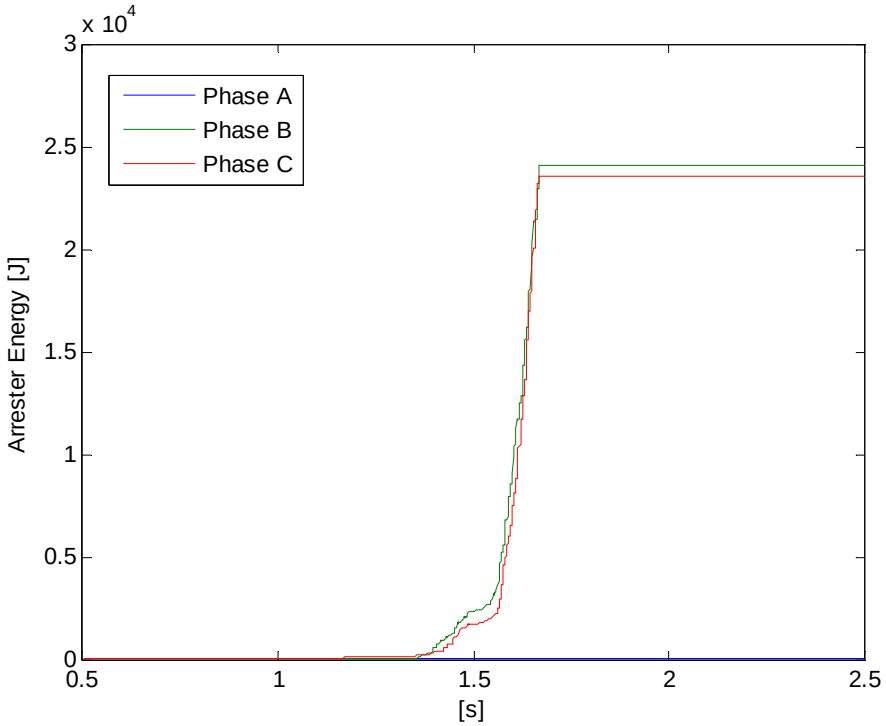

Figure 172: Arrester evaluated Energy

5.1.13.6 Test 6, Performance coefficient comparison

The benchmark represents a wind farm integrated by two equivalent generators (DFIG) of 10 machines (see Figure 173). The benchmark includes a transformer with 6% of short circuit impedance in its self base, the cable collector with 2% of impedance in 100 MVA of base, the station transformer of 10% of short circuit impedance in its self base and the system equivalent with 10% of short circuit impedance in its self base

The Figure 174 shows a fault event and differences in the active power output when different performance coefficient representations are used. The different performances between matrix representation and polynomial representation are little and more evident with regard to general transcendent function representation. In the last case the mismatch is 5%.

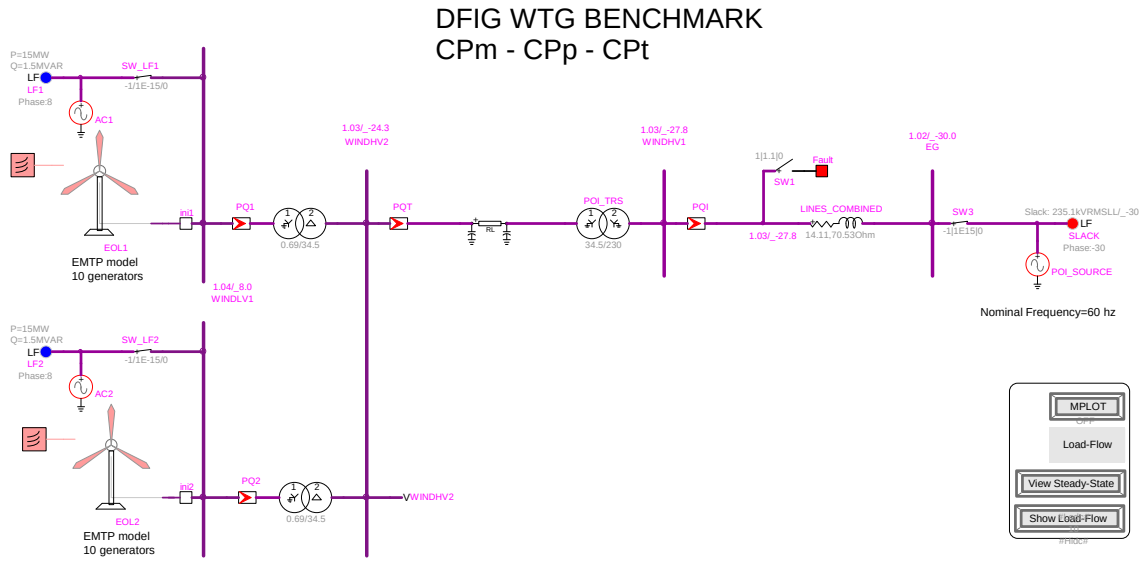

Figure 173: Performance coefficient DFIG benchmark

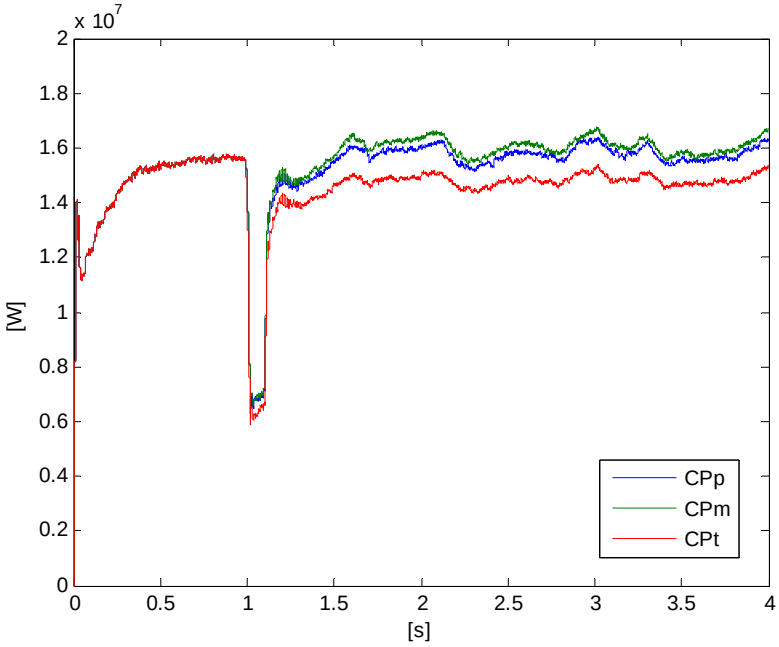

Figure 174: Active power comparison

5.1.13.7 Test 7, MVEMTP and DEMTP comparisons

The benchmark represented in Figure 175 is a single 1.5 MW machine with a terminal voltage of 575 V. The rest of the benchmark data is the same as the benchmark in Test 2.

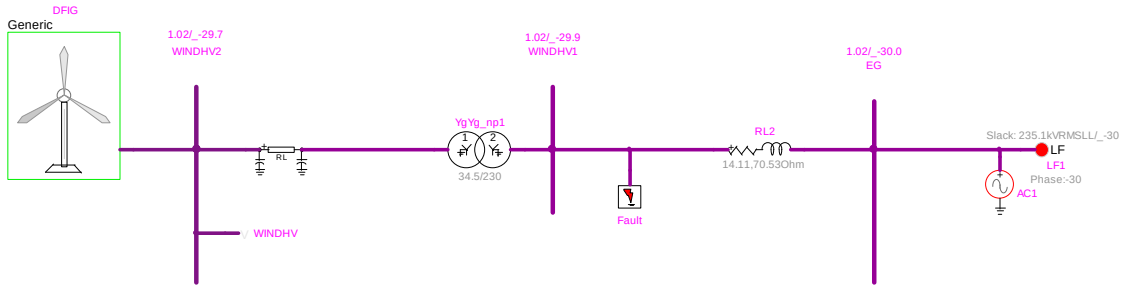

Figure 175: Mean value benchmark

The following tests of the DFIG WTG were performed:

- Test A: variable wind speed without fault.

- Test B: three phase fault and variable wind speed. At the interconnection point, a three-phase fault with a fault impedance id applied during 100 ms to obtain a terminal voltage drop of 0.5 pu and to operate out of linear range of converter. The wind speed is considered variable according to real measurements.

The active power movement, shows in Figure 176 , is according to the wind speed variation in Figure 179. The reactive power comparison is given in Figure 177. The transient variation of the reactive power shown in Figure 177 is related to the variation of the terminal voltage of the Figure 178.

Figure 179 shows the wind speed variation applied to the turbine.

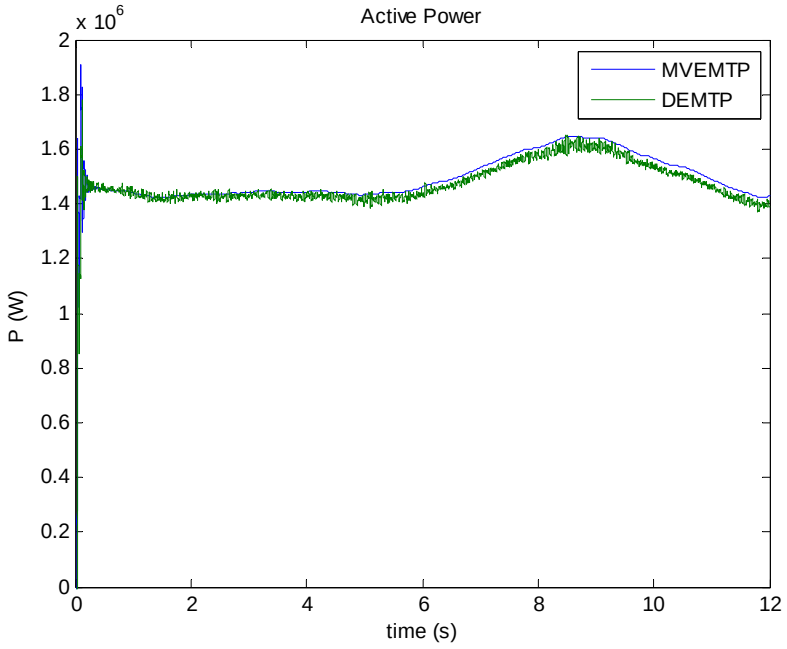

Figure 176: Active power of DFIG DEMTP and MVEMTP models, Test A

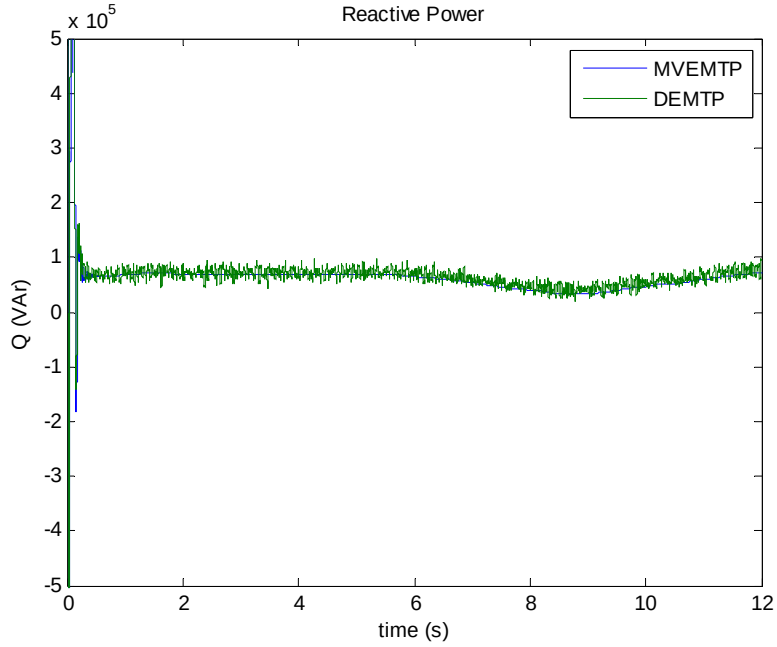

Figure 177: Reactive power of DFIG DEMTP and MVEMTP, Test A

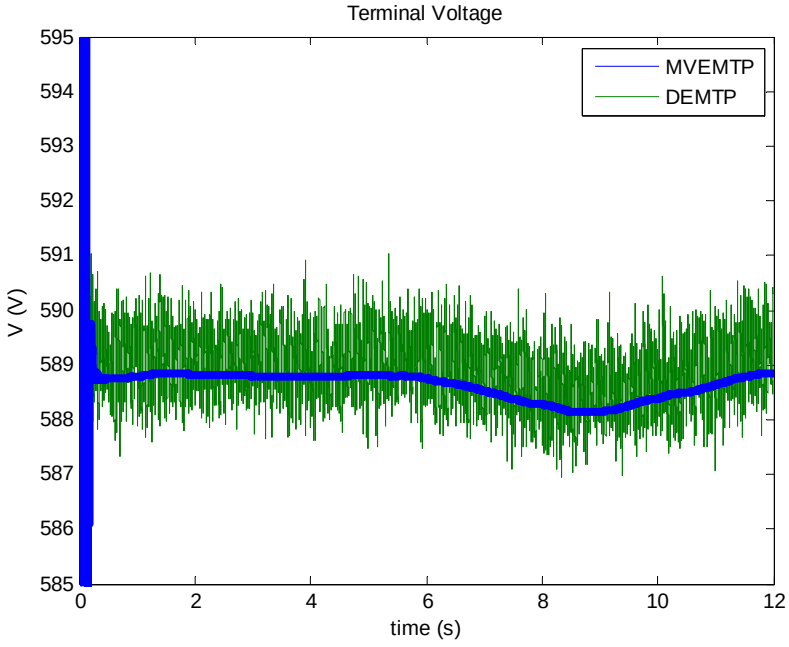

Figure 178: Terminal voltage of DFIG DEMTP and MVEMTP, Test A

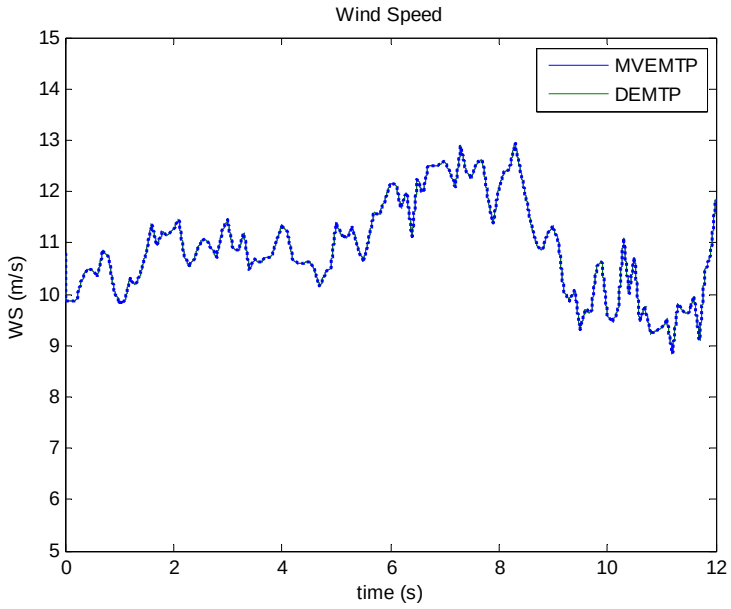

Figure 179: Wind speed applied to DFIG DEMTP and MVEMTP, Test A

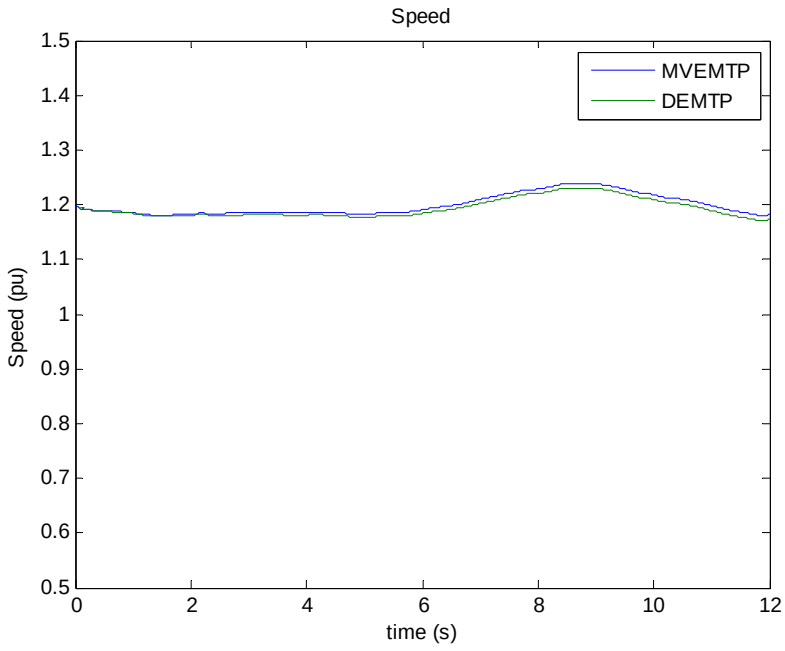

Figure 180: Speed in pu of DFIG DEMTP and MVEMTP, Test A

The speed variation, shown in Figure 180 is is according to the wind speed variation in Figure 179.

The DC link voltage shown in Figure 181 compares the responses obtained with the DEMTP and MVEMTP models. The MVEMTP model does not represent harmonics.

According to the previous figures the simulation results obtained using the MVEMTP approach match with those of the DEMTP model. The step time used in the simulation was 20μs for the DEMTP model and 100μs for MVEMTP model. The CPU times after 12 s of simulation were 930 s and 120 s respectively. That results into a factor of 7.75 times.

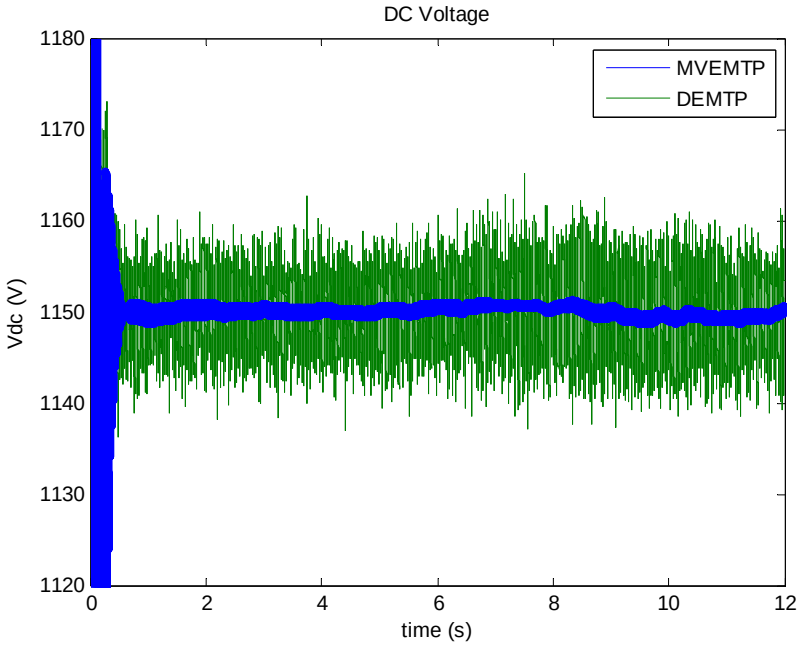

Figure 181: DC link voltage of DFIG DEMTP and MVEMTP, Test A

The active powers, shown in the Figure 182, track the voltage drop waveform. The mismatch during the fault obtained with the MVEMTP model has a better performance than the MEVA model that shows an improvement during the fault operation of the converter model in MVEMTP approach. The mismatch shown in the Figure 182 during the fault could be consequence of the IGBT model in the DEMTP approach. The IGBT is modeled according to the diagram of Figure 126. It is a combination of an ideal controlled switch, nonlinear resistance for the classical diode equation and a snubber

(RLC branch). The snubber and the nonlinear resistance have shown their influence in the converter losses.

The Figure 183 shows that the differences in the reactive power are very small during all the simulation time. As a response to the three fault with a fault impedance at the interconnection point, the terminal voltage of the DFIG drops to 0.5 pu during the time of fault, is shown in Figure 184. After the fault was cleared the terminal voltage remains controlled.

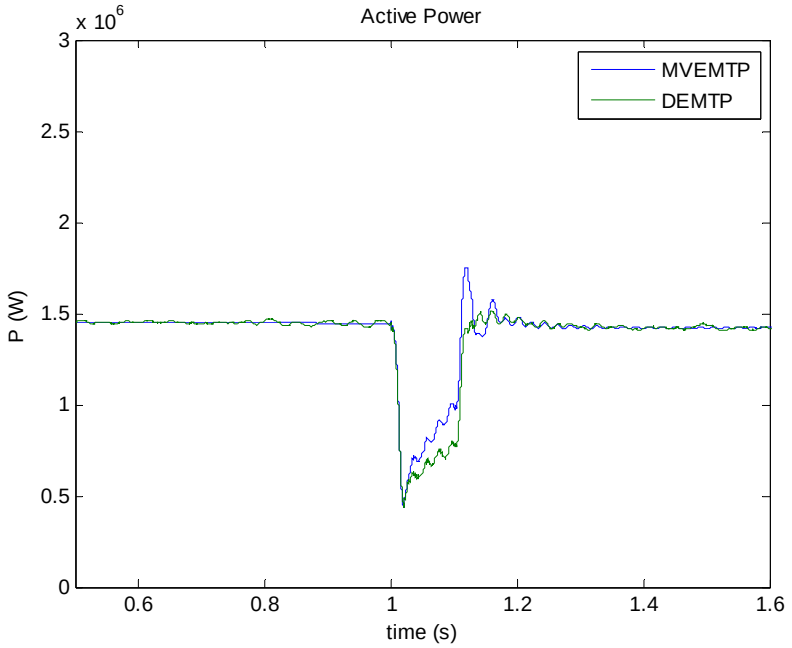

Figure 182: Active powers of DFIG DEMTP and MVEMTP models, Test B

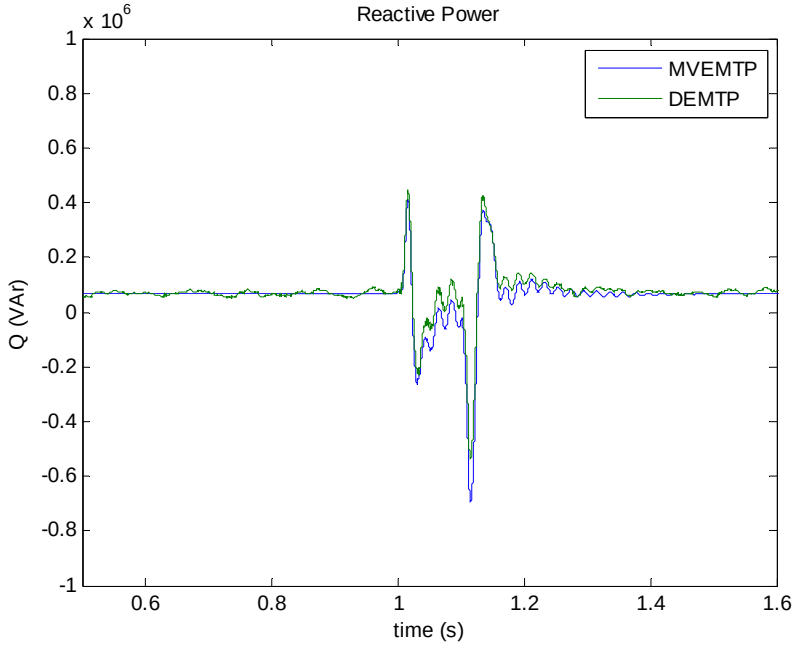

Figure 183: Reactive power of DFIG DEMTP and MVEMTP models, Test B

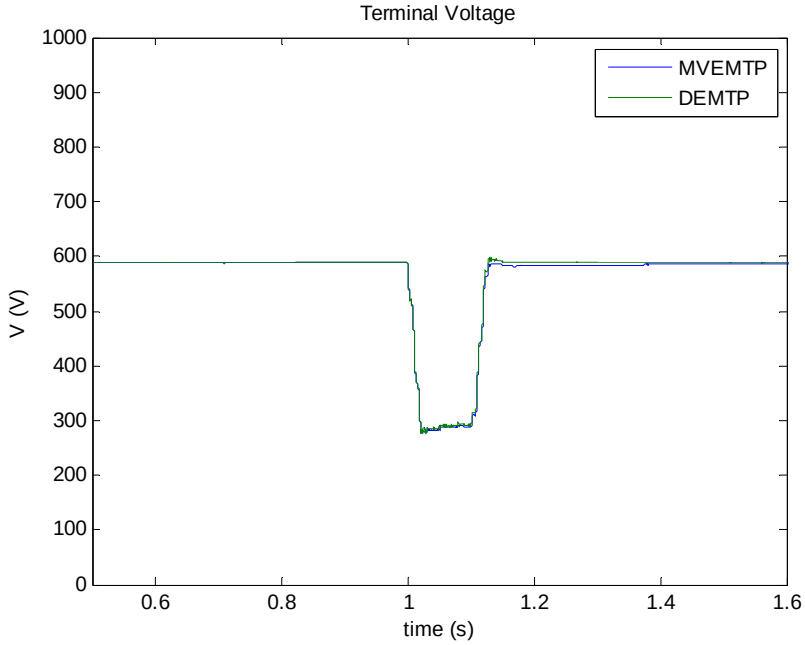

Figure 184: Terminal voltages with DEMTP and MVEMTP models, Test B

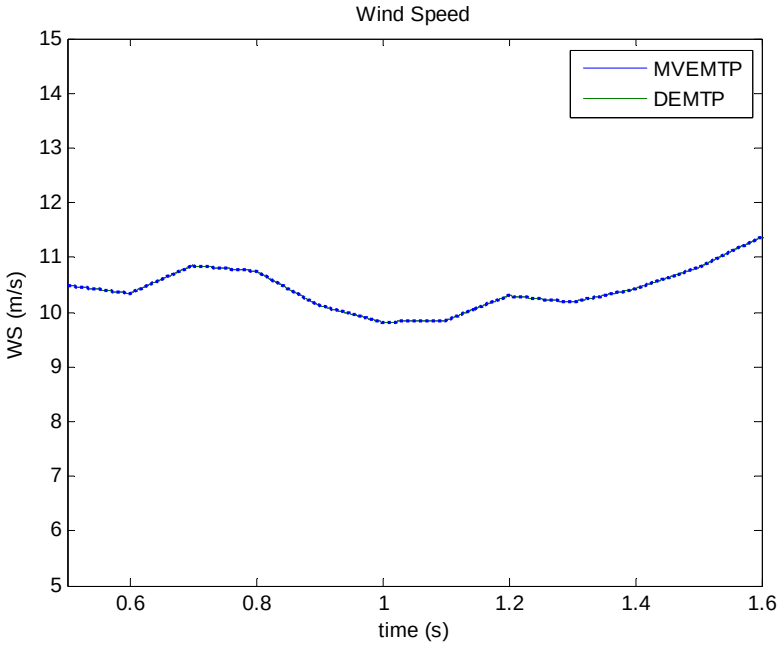

Figure 185: Wind speed applied to DFIG DEMTP and MVEMTP, Test B

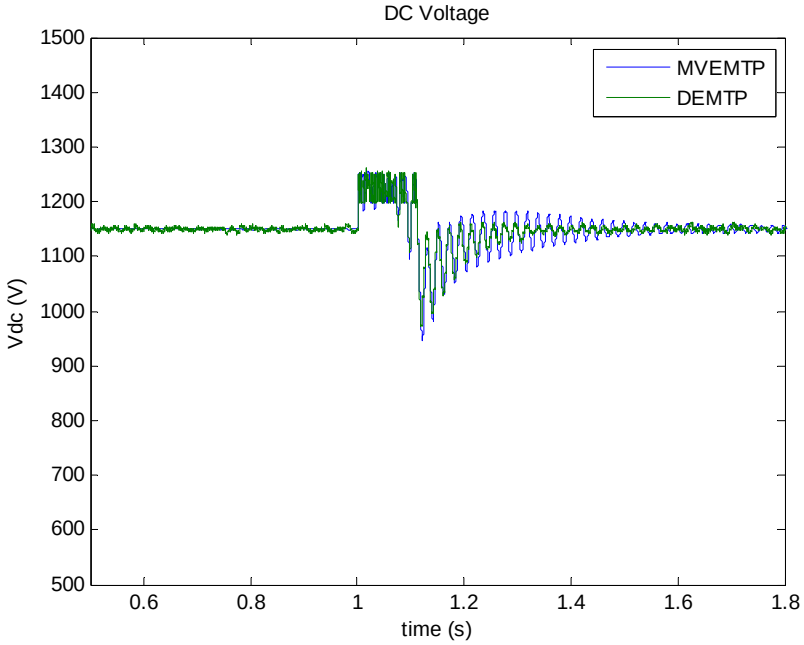

Figure 186: DC link voltage, DEMTP and MVEMTP models, Test B.

The DC link voltage shown in Figure 186 compares the responses obtain with the DEMTP and MVEMTP models. Once again the overall match in responses between these two modeling approaches is very good.

The time-step used in the simulation was 20μs for the DEMTP model and 100μs for the MVEMTP model. The CPU times after 2 s of simulation were 21 s and 153 s respectively. That results into a factor of 7.28 times.

5.2 EMTP-RV FC

The FC (Full Converter) WTG model presented in this section is an EMTP-type model implemented in EMTP-RV. The model can be initialized and connected to any EMTP-RV network. It consists of a detailed synchronous generator with a converter connected between the grid and the stator of the machine. This model is based on the vector control theory that admits to decouple the active and reactive powers controlling the voltage and current of the dc link.

The active power is determined from the controls associated to the mechanical equation of the WTG. The reactive component is associated to the voltage control at the WTG terminals or the reactive power constraints.

5.2.1 Model usage

The top level view of the FC WTG with its initialization devices is shown in Figure 187. The FC_WTG device is a subnetwork with several subnetworks for its various modeling functions and control systems.

Almost all parameters of the device can be modified through its mask. There are two external interfacings points (pins). The right pin is a 3-phase pin allowing to connect the FC_WTG device to a 3-phase network. The left pin is used for providing the random variation of the wind speed. The mean wind speed is found inside the top level mask as a parameter. Each FC_WTG device can represent one or more generators a include an entire wind park.

Since the model must be initialized it is need to perform a load flow solution followed by a steady-state solution. In EMTP-RV this is achieved using separate layers of components for the different solution modules. As show in Figure 187 each FC_WTG device is paired with a Load-Flow constraint device (LF device) and a ideal voltage source. The LF device is used in the Load-Flow solution layer. It provides the PQ constraints of the FC_WTG. The LF device is used in the load flow solution and

together with other LF devices, it allows calculation the Load-Flow solution phasor for the complete network.

The steady-state and the following time-domain solution can be started from the Load-Flow solution. The procedure is similar to the one used for the DFIG model presented in the previous section (see also Figure 187 and Figure 188). The initialization script was developed in the section 5.1.8.

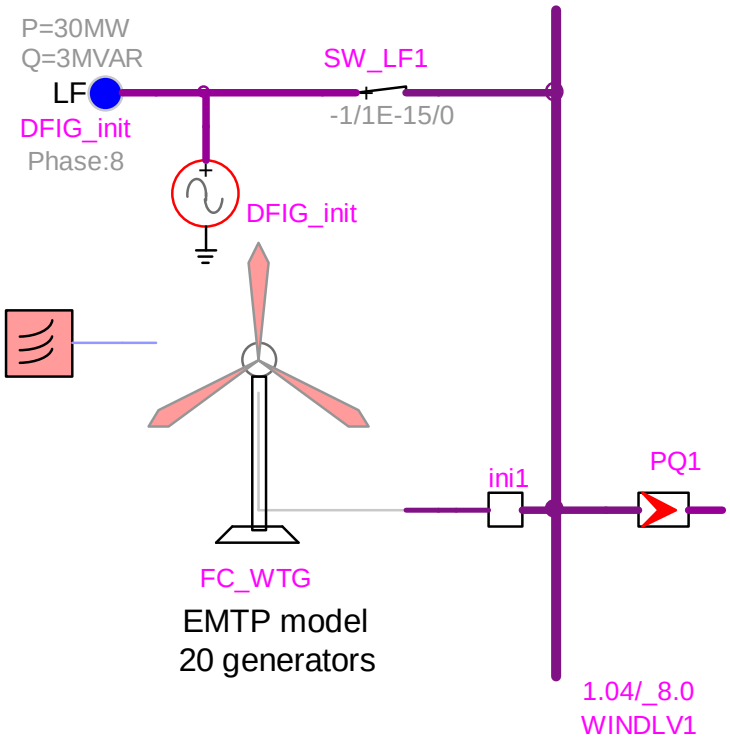

Figure 187: Top level device view of the FC_WTG

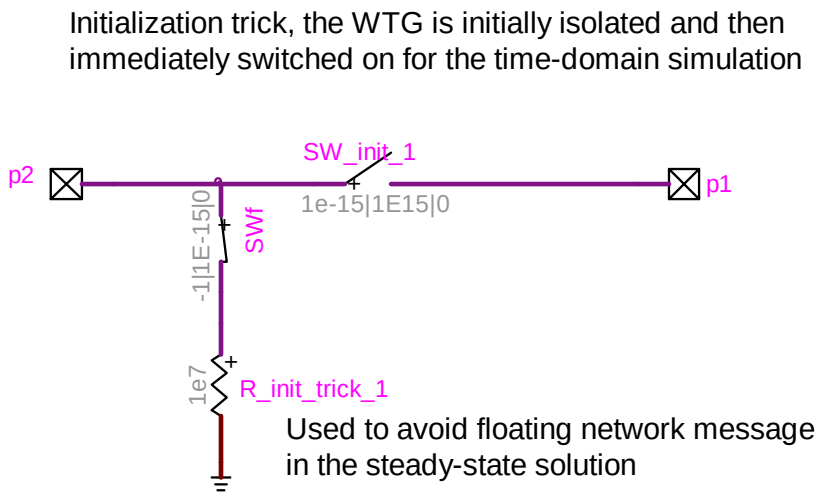

Figure 188: Initialization switches for connecting the WTG in the time-domain solution

5.2.2 Top level circuit

The top level circuit of the FC_WTG shown in Figure 189. It is composed of functional blocks for various model sections.

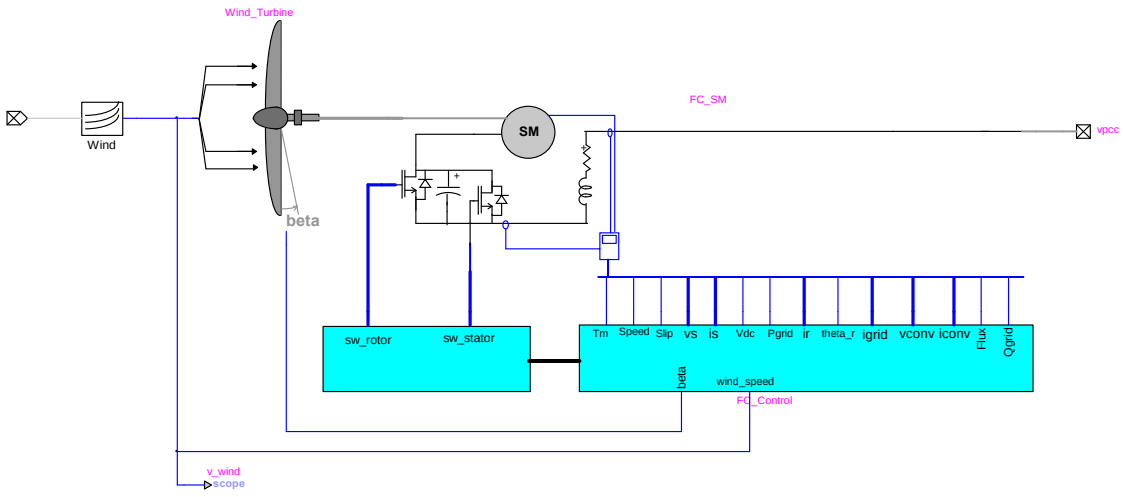

Figure 189: Top level circuit block of the FC_WTG.

DEMTP modelling approach shares the same PSS/E model blocks defined in the CHAPTER 2. The references are:

- for the wind block see section 2.2,

- For the mechanical turbine model, see the section 2.1.2.3,
- for the pitch control, see the section 2.3.4,
- for the rotor model, see the section 2.5.1,
- for the reactive control, see the section 2.7,
- for the torque and power controls, see the section 2.6,
- for the protection block model, see the section 2.8.

The FC DEMTP model includes additional components described below.

5.2.2.1 FC_SM

The full converter utilizes a synchronous generator with an ac-dc-ac converter between the generator and the grid. The wind generator arrangements are shown in Figure 190.

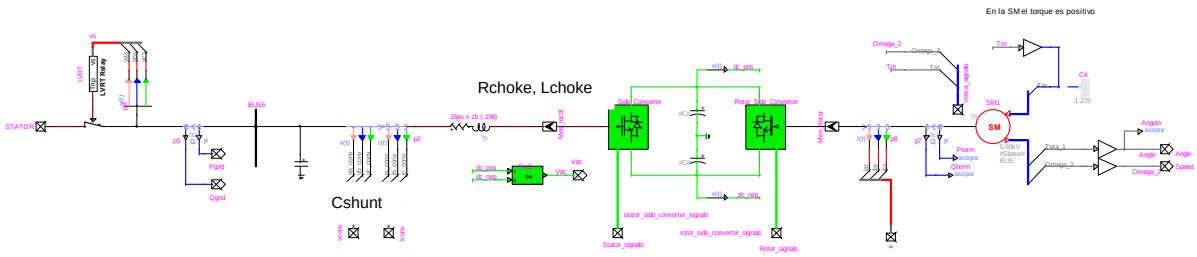

Figure 190.: Top level circuit block

5.2.3 FC Control

Essentially the FC model has the same slow controls as the DFIG EMTP model. The main difference in the line side is that the output of slow control, current IPcmd and IQcmd, based on the FC MEVA model (Figure 94), are used as reference current fast controller of the Figure 135. In this way id_ref=IPcmd and iq_ref=IQcmd.

The other important difference in the generator side is that the reference angle used in the firing control is the rotor machine angle. In the absence of slip angle in the synchronous machine, the fast controller on the generator side was modified, since no rotation is necessary now. The final controller configuration is shown in Figure 191.

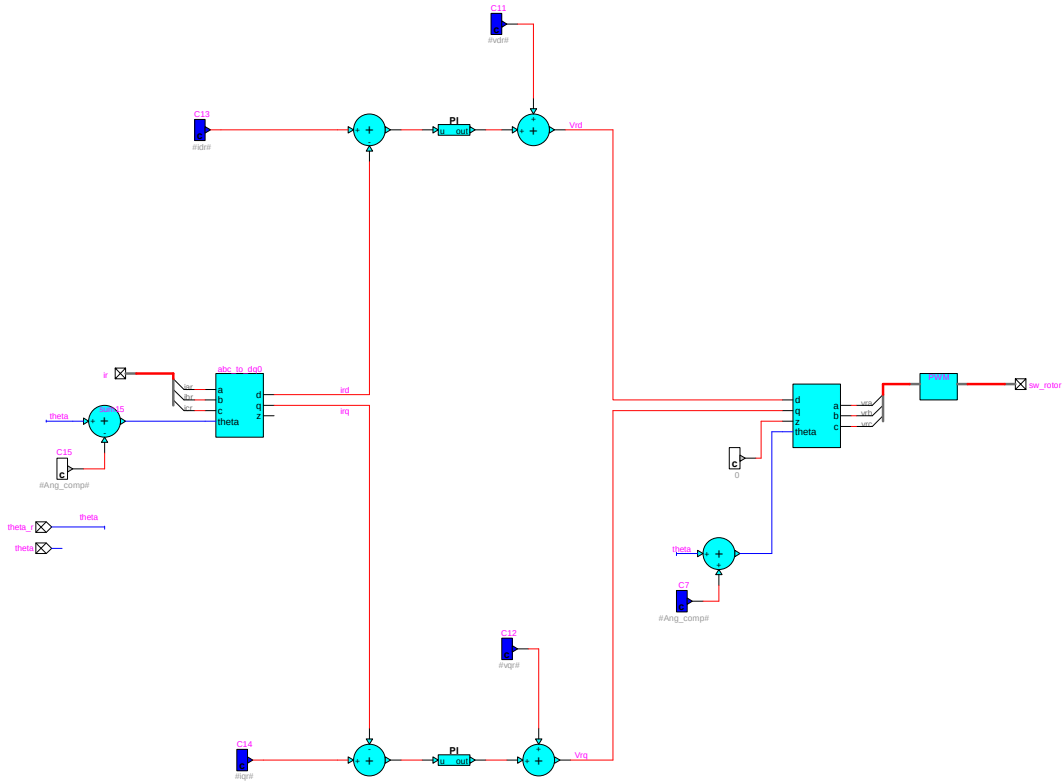

Figure 191: Converter control generator side

5.2.4 FC DEMTP model tests

The benchmark used here represents a wind farm. The equivalent generator has 20 machines. The benchmark includes a transformer with 6% of short circuit impedance in its self base , the cable collector with 2% of impedance in 100 MVA of base, the station transformer of 10% of short circuit impedance in its self base and a system equivalent with 10% of short circuit impedance in its self base.

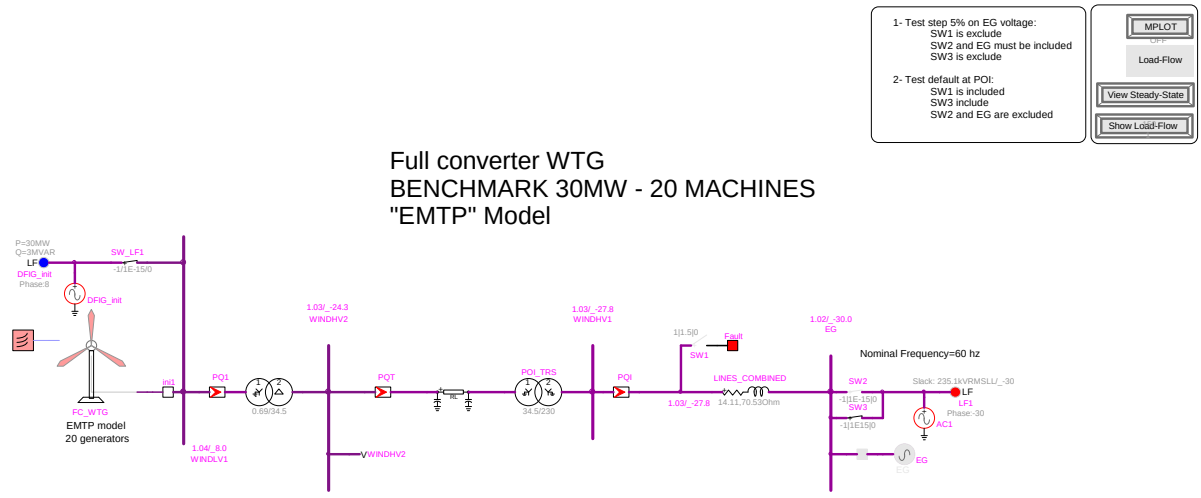

Figure 192: Benchmark 30 MW, FC DEMTP model.

The following tests were performed:

- Test A, variable wind speed without fault
- Test B, heavy fault at the interconnection point,
- Test C, zero power ramp down.
- Test D, light fault at the interconnection point without reactive current limiter.

The above tests demonstrate the correct behaviour of the model.

The tests B, C and D were simulated with a constant wind speed of 11.57 m/s. In Test 4 the reactive current limiter is disconnected to show the linear response of the model.

Figure 193 shows active power outputs without fault with wind speed variation. Figure 194 shows the reactive power output with only wind speed variation. The terminal voltage is not perturbated. Figure 195 shows the mechanical speed variation. The measured (realistic) wind waveform is the one shown in Figure 196.

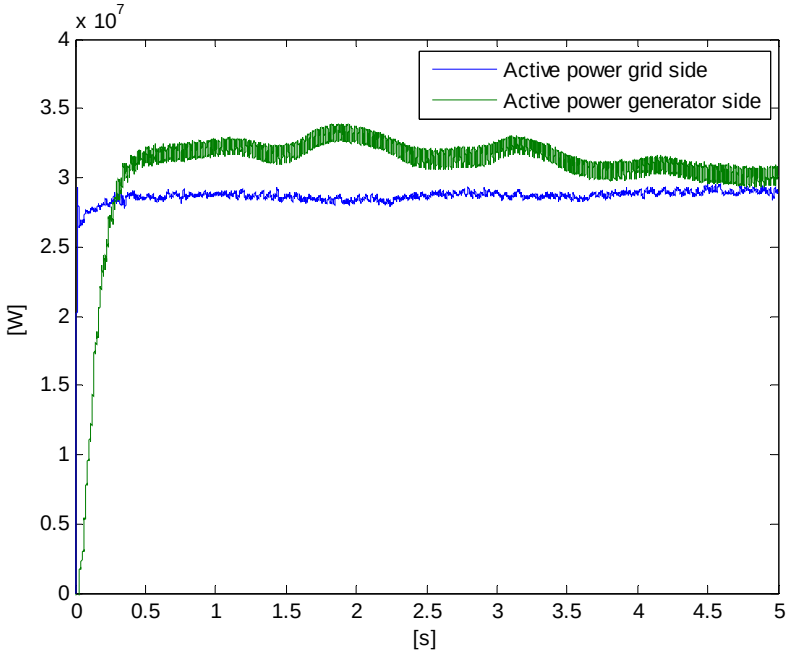

Figure 193: Active powers FC DEMTP model, Test A

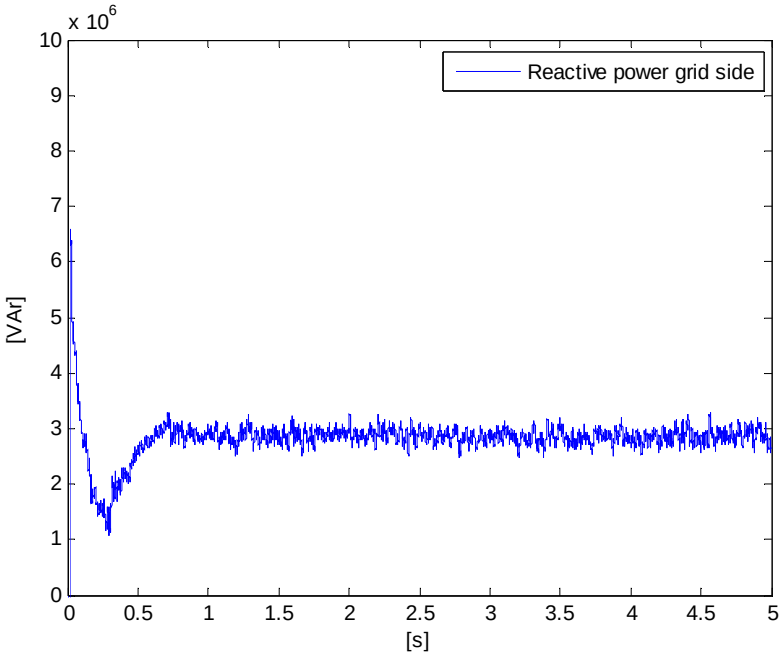

Figure 194: Reactive power, Test A

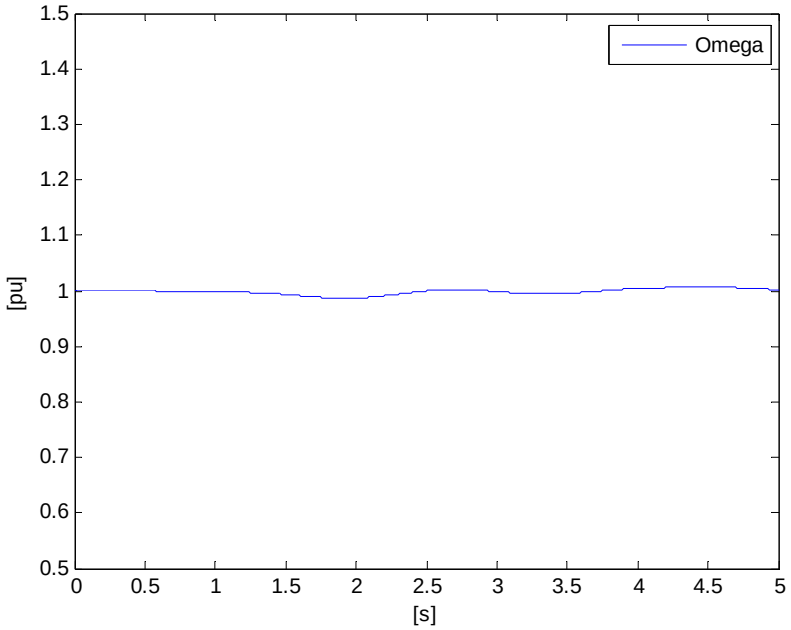

Figure 195: Machine speed, Omega in pu, Test A

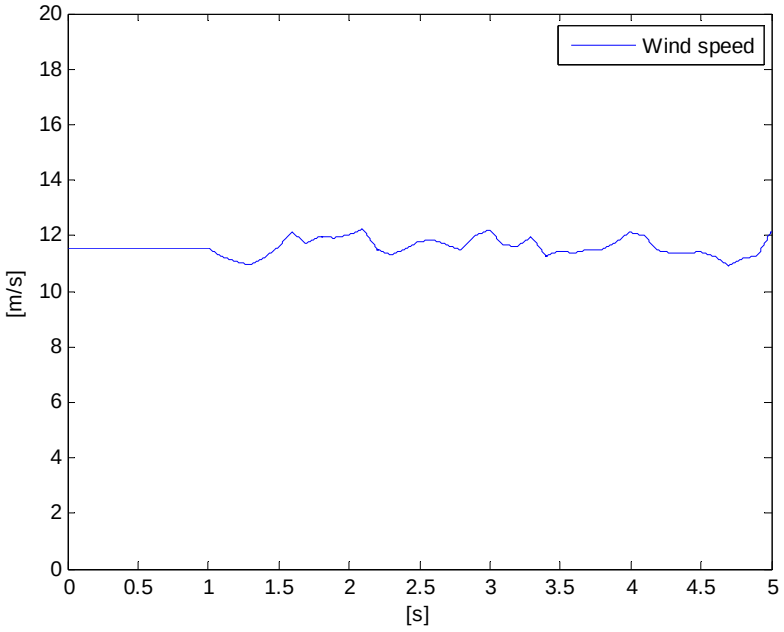

Figure 196: Wind speed in m/s, Test A

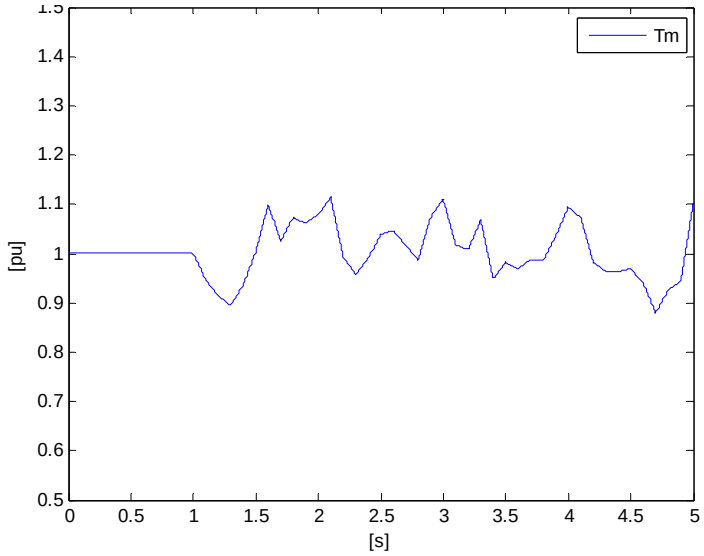

Figure 197: Torque in pu, Test A

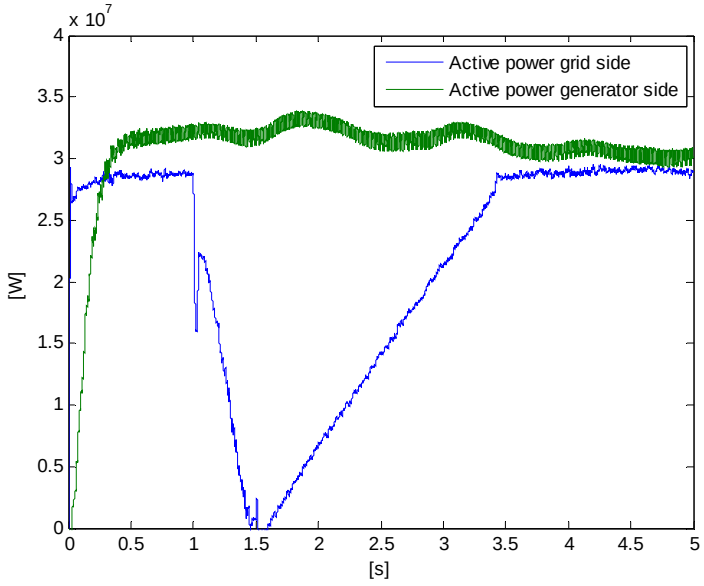

Figure 198: Active powers, Test B

Figure 198 shows the response to the heavy fault at the bus WINDHV1. The power logic was activated during the heavy fault event. Figure 199 shows the reactive power output variation. Figure 200 shows that the fault has been applied at 1 s, the terminal voltage drops to 0.5 pu, while the voltage at the bus WINDHV1 drops to approximately

0.15 pu during 0.5 s. The mechanical speed variation due to the application of wind speed variation is the same that in the Test A.

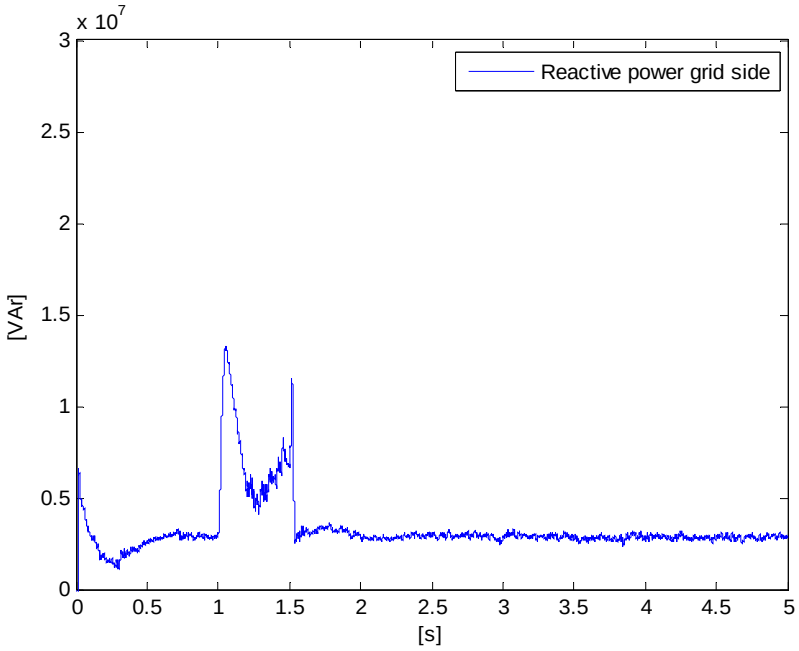

Figure 199: Reactive power, Test B

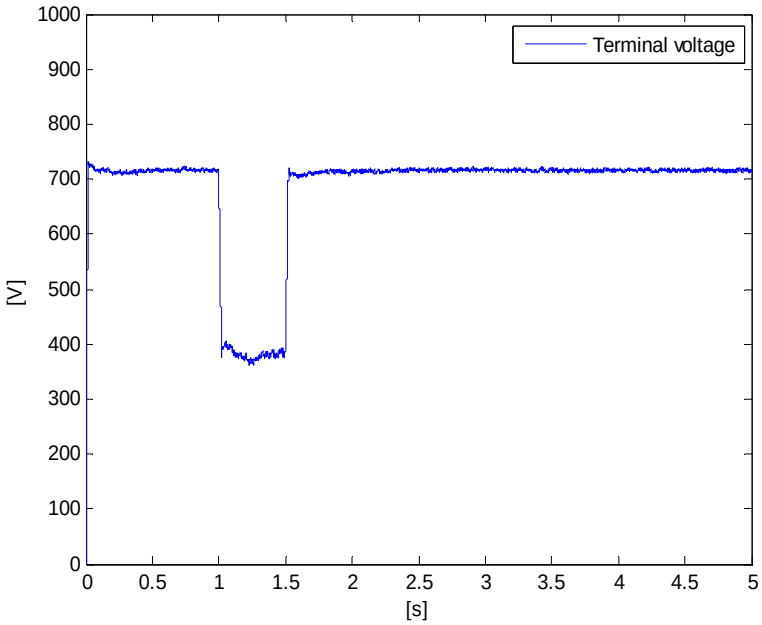

Figure 200: Terminal voltage, Test B

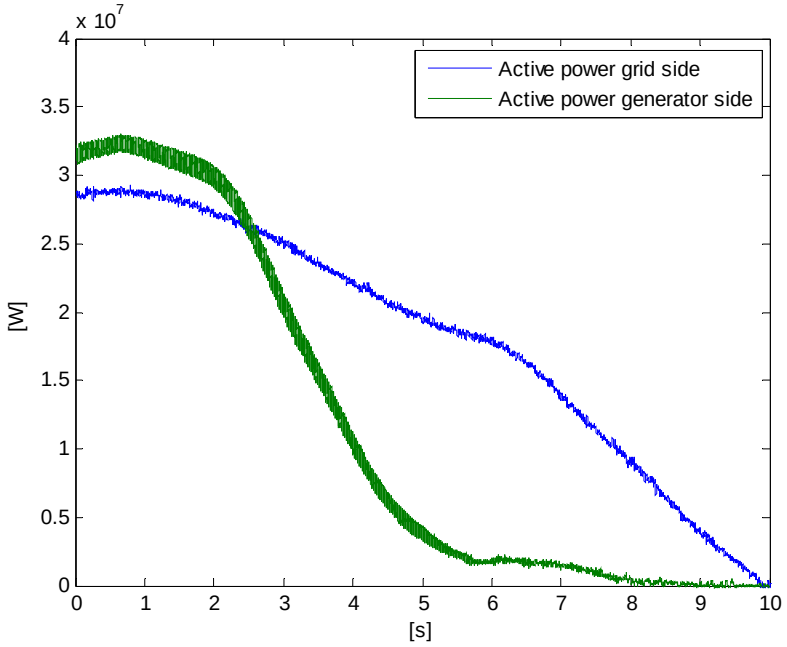

Figure 201: Active power from the generator side of FC WTG, Test C.

Figure 201 shows the behaviour for decreasing wind speed ramp of the active power output. The turbine decreases its speed at 10 second, the rotor speed, the electrical power and mechanical power are null.

The Figure 202 shows the behaviour to decreasing wind speed ramp of the reactive power output. While the electrical power changes to zero, the reactive power remains with its initial value.

The decreasing wind speed ramp doesn't change the terminal voltage. While the electrical power decreases to null, the voltage remains without changes.

The Figure 203 shows the behaviour to decreasing wind speed ramp of the mechanical speed.

The Figure 204 shows the behaviour to decreasing wind speed ramp

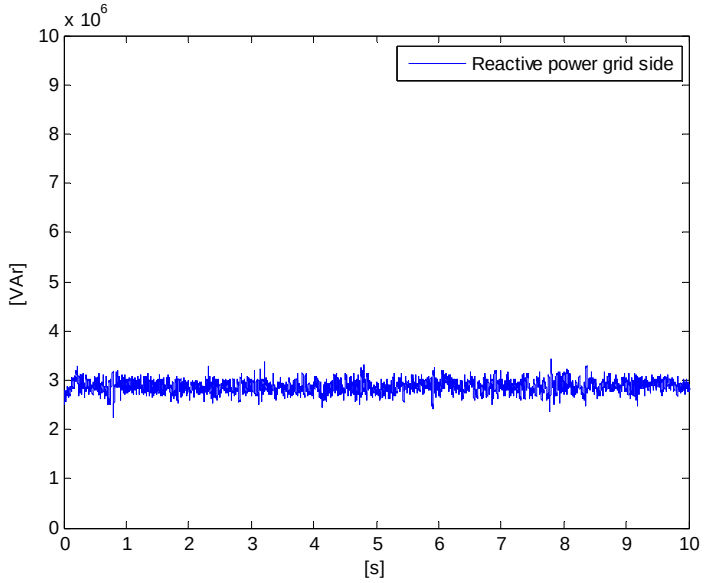

Figure 202: Reactive power, Test C

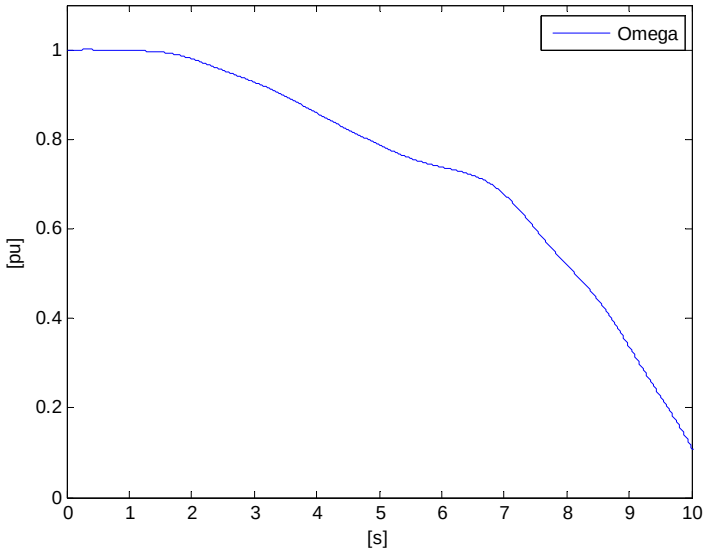

Figure 203: Omega in pu, Test C

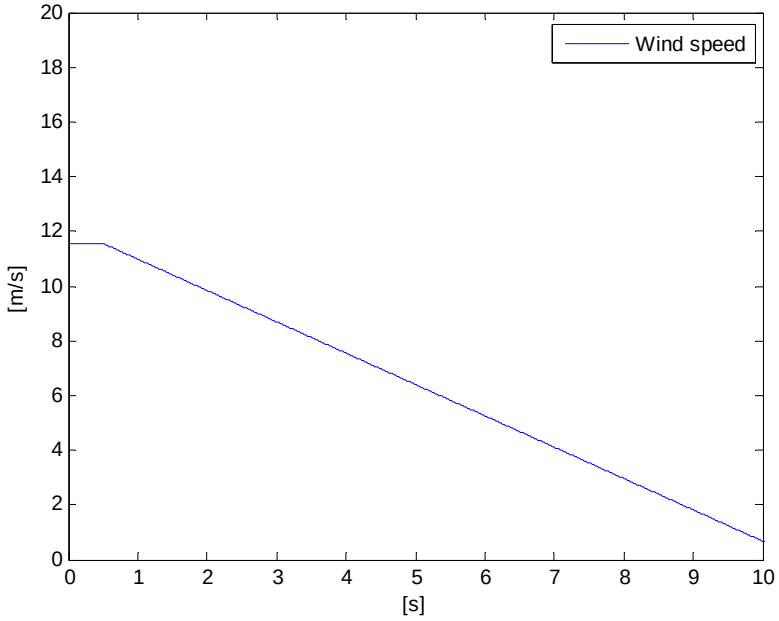

Figure 204: Wind speed in m/s, Test C

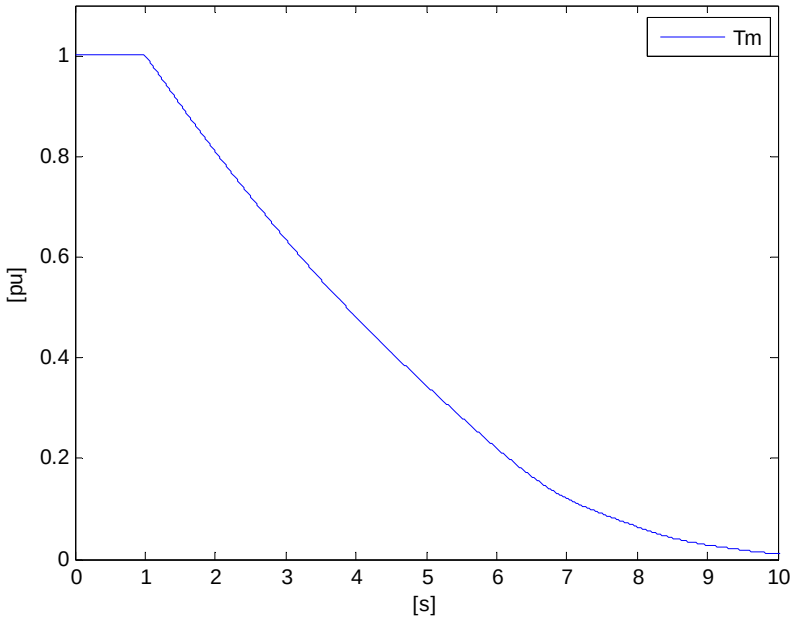

Figure 205: Torque, in pu, Test C

The Figure 205 shows the behaviour to decreasing wind speed ramp of the mechanical torque output.

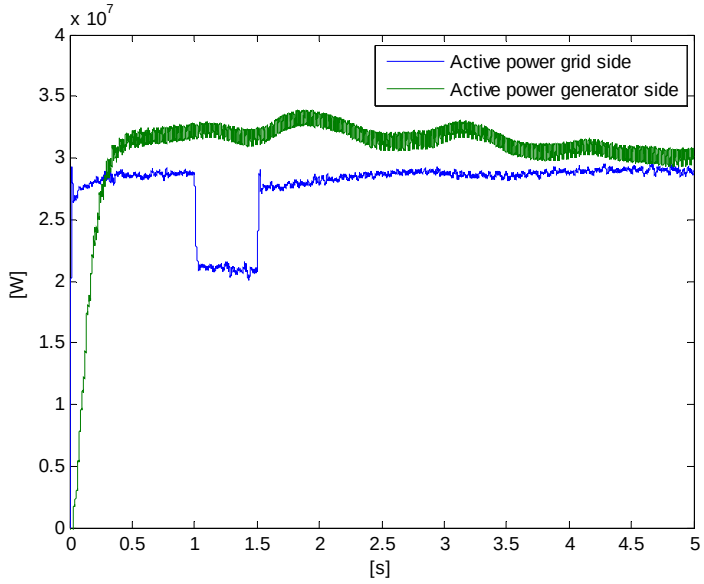

Figure 206: Active power from the generator side of FC WTG, Test D.

The Figure 206 shows the active power output as response to the light fault at bus POI. The power logic is not activated in light fault events.

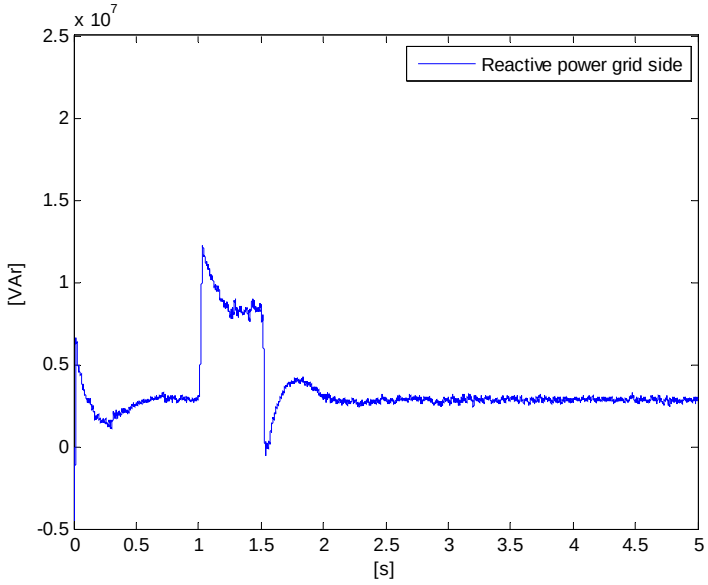

Figure 207: Reactive power at terminal of FC WTG, Test D.

The Figure 207 shows reactive power output of FC with light fault and wind speed variation

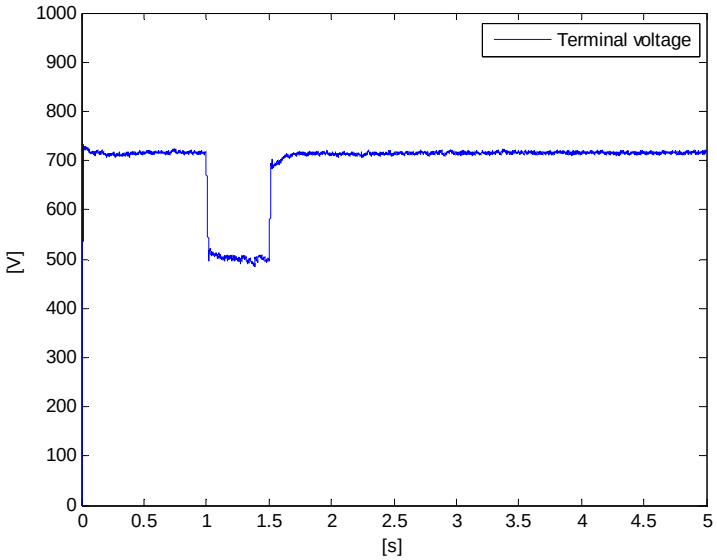

Figure 208: Voltage at terminal of FC WTG, Test D.

The Figure 208 shows the terminal voltage when the fault has been applied at 1 second, the terminal voltage drops to 0.75 pu while the voltage at POI bus fell approximately 0.7 pu during 0.5 seconds.

The wind speed modeled applied to the turbine is the same that Test A, in consequence, the mechanical torque applied is the same.

The above simulation results demonstrate the correct performance of the FC model presented in the thesis.

Conclusion

The integration of wind farms into existing power systems requires to conduct extensive studies on operational conditions, protection and control. Such studies are conducted with modern simulation tools and using numerical models. Wind farms can impact on power system stability. The interaction between wind farms and the power grid can cause various transients in the grid and the wind farm. This implies a wide spectrum of frequencies in the related transient waveforms. The phenomenon ranges from electromechanical to electromagnetic transients.

The traditional approach in power systems is to use phasor domain tools for studying electromechanical transients and time-domain tools for studying electromagnetic transients. Phasor domain tools, such as PSS/E make the assumption that the involved transients are of low frequency and calculate the dynamic phasors using a steady-state network solution. Such tools are targeting mainly the study of electromechanical transients for large scale systems where frequency perturbations are strongly coupled. Performance is achieved through various simplifications, but as shown in this thesis such simplifications have a significant impact on the precision of the models specially when involving unbalanced conditions, harmonics and power electronics based component. Modern wind generators are based on power electronics.

The simulation of electromagnetic transients encompasses the simulation of electromechanical, but deteriorates computational performance. This thesis proposed solutions to optimize precision and performance through a single environment for the simulation of all types of transients. This is a new research trend and it is expected to impact on the simulation and analysis technology of modern power systems by providing the most efficient and precise simulation models.

The first difficulty level and an important constituent of this work is the development of wind generator models. This task, as such, requires significant efforts. This thesis delivers several models and benchmarks based on realistic wind generator

and wind farm models. It contributes significantly to this research in this field. The models allow studying electromechanical transients, power quality problems, overvoltage and undervoltage conditions and electromagnetic transients in general. The benchmarks are realistic and can be reused for conducting research on mitigation and protection techniques in addition to new control algorithms for wind generators. Aggregation or individual wind generators can be used to model complete wind parks.

On the second level this thesis contributed the unified simulation of wind generators using the time-domain approach and circuit based power system representation. This approach allows studying wind generators for a wide range of frequencies with optimized precision and performance. It also eliminates limitations and approximations used in traditional packages for electromechanical transients.

The development of a basic first model in a stability type package (PSS/E) has been used to demonstrate limitations and establish the development of a mean value model (MEVA) in an EMTP-type package (EMTP-RV). This model is a new realization that can perform in a multiphase circuit based environment. It has been demonstrated that this type of model can be combined with a detailed (DEMTP) modeling approach in the same system study. The MEVA modeling is applicable for the study of slow (or electromechanical) transients. It benefits from the time-domain capabilities of EMTP-RV and can use reduced time-steps as compared to a stability type package. It, however, allows using significantly larger time-steps than the DEMTP modeling approach and provides a significant increase in computational speed. The MEVA approach has been demonstrated for both FC and DFIG wind generator technologies.

The detailed IGBT based modeling approach DEMTP has been used to create two models, FC and DFIG technologies. A byproduct is the development of another mean value modeling approach (MVEMTP). It is more precise than the MEVA approach, but requires smaller time-steps and becomes slower. It eliminates the IGBT models through controlled sources which imitate the effects of switch commutations.

The mean value models are more appropriate for slower transients and provide sufficient precision for network side events. The detailed modeling offered by the

DEMTP approach offers the ultimate precision and it has been demonstrated that the establishment of an appropriate initialization method allows to reduce dramatically the computational effort spent during the decay of natural startup transients.

This thesis has also contributed to the correction of various problems related to wind generator models, such as PLL performance in the PSS/E model. This thesis also proposed an alternative to the performance coefficient matrix representation for increased accuracy.

The advanced benchmarks delivered in this thesis constitute an important basis for further research in the field of wind farm integration into power systems. They can be used for research on mitigation techniques for overvoltage and undervoltage studies and for studying various electromagnetic and electromechanical transients in the general sense.

The future research will take into account the improvement of the following items:

1. Improvements to the MEVA model for extending its application range
2. Improvements to converter models in DEMPT
3. Improvements to MVEMTP approach for better dc side representation

REFERENCES

[1] PSS/E, http://www.energy.siemens.com

[2] J. Mahseredjian, “Simulation des transitoires électromagnétiques dans les réseaux électriques”, Éditions Les Techniques de l’Ingénieur, Dossier No.D4130, Réseaux électriques et applications.

[3] J. Mahseredjian, S. Dennetière, L. Dubé, B. Khodabakhchian and L. Gérin-Lajoie, “On a new approach for the simulation of transients in power systems”, Proceedings of International Conference on Power Systems Transients, IPST 2005 in Montréal, June 19th-23rd, 2005.

[4] EMTP-RV, http://www.emtp.com

[5] OPAL-RT, http://www.opal-rt.com/

[6] J.G. Slootweg, H. Polinder, W.L. Kling, “Initialization of Wind Turbine Models in Power System Dynamics Simulations”, IEEE Porto Power Tech Conference, September 10-13, 2001, Porto, PT.

[7] S. Chiniforoosh, J. Jatskevich, A. Yazdani, V. Sood, V. Dinavahi, J. A. Martinez, and A. Ramirez, "Definitions and Applications of Dynamic Average Models for Analysis of Power Systems", IEEE Transactions on power delivery, Vol. 25, No. 4, October 2010.

[8] Richard Gagnon et all, "Large-Scale Real-Time Simulation of Wind Power Plants into Hydro-Québec Power Systems", http://www.windintegrationworkshop.org

[9] C. Abbey, J. Morneau, J. Mahseredjian, and G. Joos, “Modeling requirements for transient stability studies for wind parks,” in Proc. IEEE Power Eng. Soc. General Meeting, Jun. 2006, pp. 1–6.

[10] Albert Betz, , “Das Maximum der theoretisch möglichen Ausnutzung des Windes durch Windmotoren”, 20 septembre 1920.

[11] Rajesh Saiju, Gunter Arnold, Siegfried Heier, “Voltage dips compensation by wind farm(s) equipped with power converters as decoupling element” University of Kassel, Institute of Electrical Engineering Electrical Power Supply System.

[12] Matlab, http://www.mathworks.com/products/matlab/

[13] J. G. Slootweg, S. W. H. de Haan, H. Polinder, and W. L. Kling, “General model for representing variable speed wind turbines in power system dynamics simulations,” IEEE Trans. Power Syst., vol. 18, no. 1, pp. 144–151, Feb. 2003.

[14] J. G. Slootweg, S. W. H. de Haan, H. Polinder, and W. L. Kling, “Modeling new generation and storage technologies in power system dynamics simulations,” in Proc. IEEE Power Eng. Soc. Summer Meeting, Jul. 2002, vol. 2, pp. 868–873.

[15] N. Hatziargyriou (ed.), “Modeling new forms of generation and storage”, Paris: Cigré Technical Brochure CE/SC 38.01.10, Paris, 2001.

[16] P. Kundur "Power System Stability and Control" EPRI. Mc Graw-Hill. 1994.

[17] J. Morren, S. W. H. de Haan, P. Bauer, J. Pierik, and J. Bozelie, “Comparison of complete and reduced models of a wind turbine with doubly-fed induction generator,” in Proc. 10 Eur. Conf. Power Electronics and Applications, Sep. 2003, pp. 1–10.

[18] Yuriy Kazachkoff, Steve Stapleton, "Modeling wind farm for power system stability studies", Power Technologies News letter issue 95, April 2004.

[19] J. G. Slootweg, H. Polinder, and W. L. Kling, “Representing wind turbine electrical generating systems in fundamental frequency simulations,” IEEE Trans. Energy Convers., vol. 18, no. 4, pp. 516–524, Dec. 2003.

[20] Transmission provider technical requirements for the connection of power plants to the Hydro-Québec transmission system. Direction planification des actifs. March 2006.

[21] Dynamic Modeling of GE 1.5 and 3.6 Wind Turbine-Generators; Prepared by: Nicholas W. Miller, William W. Price, Juan J. Sanchez-Gasca; October 27, 2003, Version 3.0; GE-Power Systems Energy Consulting; Copyright 2002 General Electric Company, U.S.A.

[22] GH Bladed, http://www.garradhassan.com/products/ghbladed

[23] J. V. Sarlashkar, F. L. Alvarado and J. Mahseredjian, "Interfacing time domain and phasor domain simulations," UPEC 1996, Iraklio, Crete, September 18-20, 1996.

[24] N. Mohan, W. P. Robbin, and T. Undeland, Power Electronics: Converters, Applications, and Design, 2nd ed. New York: Wiley, 1995.

[25] V. Akhmatov, H. Knudsena, A.H. Nielsenb, "Advanced simulation of windmills in the electric power supply", Electrical Power and Energy Systems 22 (2000) 421–434

[26] Akhmatov, V., "Variable-speed wind turbines with doubly-fed induction generators part III: model with the back-to-back converters", Wind Engineering, Vol. 27, No. 2, 2003.

[27] P.M. Anderson, A. Bose, "Stability simulation of wind turbine systems", IEEE Transactions on Power Apparatus and Systems, v.102, n.12, Dec. 1983, pp.3791-3795

[28] Heier, Siegfried (2005). Grid Integration of Wind Energy Conversion Systems. Chichester: John Wiley & Sons

[29] Dale S. L. Dolan, *Student Member, IEEE*, and Peter W. Lehn, *Senior Member,* "Simulation Model of Wind Turbine 3p Torque Oscillations due to Wind Shear and Tower Shadow" IEEE TRANSACTIONS ON ENERGY CONVERSION, VOL. 21, NO. 3, SEPTEMBER 2006

[30] Danish wind industry association. www.windpower.org

[31] IEC61400-21,"Measurement and assessment of power quality characteristics of grid connected wind turbines"

[32] IEC868-0, Flickermeter, Evaluation of flicker severity

[33] IEC868, Flickermeter, Functional and design specifications

APPENDIX A

Benchmark data

Benchmark 1: data files Load Flow and dynamics.

RAW FILE : TEST.RAW

```
0,   100.00          / PSS/E-30.1    WED, DEC 13 2006  19:45
TEST GRID

  1000,'            ', 230.0000,3,     0.000,     0.000,   1,   1,1.02000,   0.0000,   1
  1001,'            ', 230.0000,1,     0.000,     0.000,   1,   1,1.02753,  10.8054,   1
  1500,'            ',  34.5000,1,     0.000,     0.000,   1,   1,1.02569,  16.1307,   1
  1501,'            ',  34.5000,1,     0.000,     0.000,   1,   1,1.03631,  17.6990,   1
  1601,'            ',   0.6900,2,     0.000,     0.000,   1,   1,1.04000,  20.3227,   1
0 / END OF BUS DATA, BEGIN LOAD DATA
0 / END OF LOAD DATA, BEGIN GENERATOR DATA
  1000,'1 ',   -28.289,     7.352,   100.000,   -30.000,1.02000,     0,   100.000,
0.00000,   0.00100,   0.00000,   0.00000,1.00000,1,  100.0,   100.000,  -100.000,
1,1.0000
  1601,'1 ',    29.640,     2.986,     9.860,   -14.520,1.04000,     0,    33.000,
0.00000,   0.80000,   0.00000,   0.00000,1.00000,1,  100.0,    30.000,     0.000,
1,1.0000
0 / END OF GENERATOR DATA, BEGIN BRANCH DATA
  1000,   1001,'1 ',   0.13300,   0.66000,   0.00000,   30.00,   30.00,   30.00,
0.00000,  0.00000,  0.00000,  0.00000,1,   0.00,   1,1.0000
  1500,   1501,'1 ',   0.03300,   0.10000,   0.00000,   30.00,   30.00,   30.00,
0.00000,  0.00000,  0.00000,  0.00000,1,   0.00,   1,1.0000
0 / END OF BRANCH DATA, BEGIN TRANSFORMER DATA
  1500,  1001,     0,'1 ',1,1,1,   0.00000,   0.00000,1,'            ',1,   1,1.0000
   0.00000,   0.33300,   100.00
1.00000,   0.000,   0.000,   100.00,   100.00,   100.00, 0,      0, 1.10000, 0.90000,
1.10000, 0.90000,  33, 0, 0.00000, 0.00000
1.00000,   0.000
  1601,  1501,     0,'1 ',1,1,1,   0.00000,   0.00000,1,'            ',1,   1,1.0000
   0.00000,   0.16650,   100.00
1.00000,   0.000,   0.000,    30.00,    30.00,    30.00, 0,      0, 1.10000, 0.90000,
1.10000, 0.90000,  33, 0, 0.00000, 0.00000
1.00000,   0.000
0 / END OF TRANSFORMER DATA, BEGIN AREA DATA
   1,  1000,     0.000,     0.000,'            '
0 / END OF AREA DATA, BEGIN TWO-TERMINAL DC DATA
0 / END OF TWO-TERMINAL DC DATA, BEGIN VSC DC LINE DATA
0 / END OF VSC DC LINE DATA, BEGIN SWITCHED SHUNT DATA
0 / END OF SWITCHED SHUNT DATA, BEGIN IMPEDANCE CORRECTION DATA
0 / END OF IMPEDANCE CORRECTION DATA, BEGIN MULTI-TERMINAL DC DATA
0 / END OF MULTI-TERMINAL DC DATA, BEGIN MULTI-SECTION LINE DATA
0 / END OF MULTI-SECTION LINE DATA, BEGIN ZONE DATA
0 / END OF ZONE DATA, BEGIN INTER-AREA TRANSFER DATA
0 / END OF INTER-AREA TRANSFER DATA, BEGIN OWNER DATA
0 / END OF OWNER DATA, BEGIN FACTS DEVICE DATA
0 / END OF FACTS DEVICE DATA
```

DYRE FILE : TEST.DYR

```
  1000 'GENCLS'  1     50.0  0.0/
  1601    'USRMDL'  1 'FUWI' 1 0 0 68 17 29
  0.8     0.87    0.0     0.02    0.02    2.0     0.1     -0.1    1.0     0.05
```

```
  3.0     0.60    1.01    0.09    0.296   -0.436  1.11    0.      0.45    -0.45
  5.0     0.1     0.9     1.1     40.     -0.5    0.4     0.0     0.05    1
  1.000   5.00    3.00    101.0   106.0   3.00    3.400   1.520   5.19    2
  0       12.0    4.0     29.0    0.0     0.0     1.225   35.00   90.0    1800.
  1500.   1.67    0.3     150.    25.     3.00    30.0    0.      29.     -9.
  9.      0.91      8.990000 -0.0038732  14.000000  -0.194950   0.898204   0.090481/
```

Benchmark 2 data file. Load Flow and dynamics

```
RAW FILE :

0,   100.00          / PSS/E-30.1    THU, JAN 03 2008  14:21
RéSEAU éQUIVALENT
ANALYSE DES MODèLES D'éOLIENNES
  1000,'SWING       ', 315.0000,3,     0.000,     0.000,   1,   1,1.00000,   0.0000,   1
  1001,'TR_HT01     ', 315.0000,1,     0.000,     0.000,   1,   1,0.99127,  29.2419,   1
  1500,'TR_MT01     ',  34.5000,1,     0.000,    60.000,   1,   1,1.00000,  39.6771,   1
  1501,'EOLMT01     ',  34.5000,1,     0.000,     0.000,   1,   1,1.02290,  42.3696,   1
  1502,'EOLMT02     ',  34.5000,1,     0.000,     0.000,   1,   1,1.02290,  42.3696,   1
  1503,'EOLMT03     ',  34.5000,1,     0.000,     0.000,   1,   1,1.02290,  42.3696,   1
  1504,'EOLMT04     ',  34.5000,1,     0.000,     0.000,   1,   1,1.02290,  42.3696,   1
  1505,'EOLMT05     ',  34.5000,1,     0.000,     0.000,   1,   1,1.02291,  42.3695,   1
  1510,'TR_MT02     ',  34.5000,1,     0.000,    60.000,   1,   1,1.00000,  39.6771,   1
  1511,'EOLMT06     ',  34.5000,1,     0.000,     0.000,   1,   1,1.02290,  42.3696,   1
  1512,'EOLMT07     ',  34.5000,1,     0.000,     0.000,   1,   1,1.02290,  42.3696,   1
  1513,'EOLMT08     ',  34.5000,1,     0.000,     0.000,   1,   1,1.02290,  42.3696,   1
  1514,'EOLMT09     ',  34.5000,1,     0.000,     0.000,   1,   1,1.02290,  42.3696,   1
  1515,'EOLMT10     ',  34.5000,1,     0.000,     0.000,   1,   1,1.02291,  42.3695,   1
  1520,'TR_MT03     ',  34.5000,1,     0.000,    60.000,   1,   1,1.00000,  39.6771,   1
  1521,'EOLMT11     ',  34.5000,1,     0.000,     0.000,   1,   1,1.02290,  42.3696,   1
  1522,'EOLMT12     ',  34.5000,1,     0.000,     0.000,   1,   1,1.02290,  42.3696,   1
  1523,'EOLMT13     ',  34.5000,1,     0.000,     0.000,   1,   1,1.02290,  42.3696,   1
  1524,'EOLMT14     ',  34.5000,1,     0.000,     0.000,   1,   1,1.02290,  42.3696,   1
  1525,'EOLMT15     ',  34.5000,1,     0.000,     0.000,   1,   1,1.02291,  42.3695,   1
  1600,'EOLBT       ',   0.6900,2,     0.000,     0.000,   1,   1,1.02994,  45.4188,   1
  1601,'EOLBT01     ',   0.6900,2,     0.000,     0.000,   1,   1,1.02994,  45.4188,   1
  1602,'EOLBT02     ',   0.6900,2,     0.000,     0.000,   1,   1,1.02994,  45.4188,   1
  1603,'EOLBT03     ',   0.6900,2,     0.000,     0.000,   1,   1,1.02994,  45.4188,   1
  1604,'EOLBT04     ',   0.6900,2,     0.000,     0.000,   1,   1,1.02994,  45.4188,   1
  1605,'EOLBT05     ',   0.6900,2,     0.000,     0.000,   1,   1,1.02994,  45.4188,   1
  1606,'EOLBT06     ',   0.6900,2,     0.000,     0.000,   1,   1,1.02994,  45.4188,   1
  1607,'EOLBT07     ',   0.6900,2,     0.000,     0.000,   1,   1,1.02994,  45.4188,   1
  1608,'EOLBT08     ',   0.6900,2,     0.000,     0.000,   1,   1,1.02994,  45.4188,   1
  1609,'EOLBT09     ',   0.6900,2,     0.000,     0.000,   1,   1,1.02994,  45.4188,   1
  1610,'EOLBT10     ',   0.6900,2,     0.000,     0.000,   1,   1,1.02994,  45.4188,   1
  1611,'EOLBT11     ',   0.6900,2,     0.000,     0.000,   1,   1,1.02994,  45.4188,   1
  1612,'EOLBT12     ',   0.6900,2,     0.000,     0.000,   1,   1,1.02994,  45.4188,   1
  1613,'EOLBT13     ',   0.6900,2,     0.000,     0.000,   1,   1,1.02994,  45.4188,   1
  1614,'EOLBT14     ',   0.6900,2,     0.000,     0.000,   1,   1,1.02994,  45.4188,   1
  1615,'EOLBT15     ',   0.6900,2,     0.000,     0.000,   1,   1,1.02994,  45.4188,   1
0 / END OF BUS DATA, BEGIN LOAD DATA
  1000,'1 ',1,  15, 102, 27965.000,  5592.000,     0.000,     0.000,     0.000,
0.000,   1
0 / END OF LOAD DATA, BEGIN GENERATOR DATA
  1000,'1 ', 27483.660,  5736.683,  9999.000, -9999.000,1.00000,     0, 27865.000,
0.00000,   0.18000,   0.00000,   0.00000,1.00000,1,  100.0,  1000.000, -1000.000,
1,1.0000
  1600,'1 ',   499.000,    67.649,   165.000,  -242.400,1.00000,  1510,   551.000,
0.00000,   0.80000,   0.00000,   0.00000,1.00000,1,  100.0,   500.000,     0.000,
1,1.0000
  1601,'1 ',    33.000,    10.846,    10.846,   -15.972,1.00000,  1500,    36.300,
0.00000,   0.80000,   0.00000,   0.00000,1.00000,0,  100.0,    33.000,     0.000,
1,1.0000
```

```
  1602,'1 ',    33.000,     9.415,    10.846,   -15.972,1.00000,  1500,    36.300,
0.00000,   0.80000,   0.00000,   0.00000,1.00000,0,  100.0,    33.000,     0.000,
1,1.0000
  1603,'1 ',    33.000,     3.451,    10.846,   -15.972,1.00000,  1500,    36.300,
0.00000,   0.80000,   0.00000,   0.00000,1.00000,0,  100.0,    33.000,     0.000,
1,1.0000
  1604,'1 ',    33.000,     3.451,    10.846,   -15.972,1.00000,  1500,    36.300,
0.00000,   0.80000,   0.00000,   0.00000,1.00000,0,  100.0,    33.000,     0.000,
1,1.0000
  1605,'1 ',    34.500,     3.451,    11.339,   -16.698,1.00000,  1500,    37.950,
0.00000,   0.80000,   0.00000,   0.00000,1.00000,0,  100.0,    34.500,     0.000,
1,1.0000
  1606,'1 ',    33.000,     0.000,    10.846,   -15.972,1.00000,  1510,    36.300,
0.00000,   0.80000,   0.00000,   0.00000,1.00000,0,  100.0,    33.000,     0.000,
1,1.0000
  1607,'1 ',    33.000,   -18.492,    10.846,   -15.972,1.00000,  1510,    36.300,
0.00000,   0.80000,   0.00000,   0.00000,1.00000,0,  100.0,    33.000,     0.000,
1,1.0000
  1608,'1 ',    33.000,   -18.492,    10.846,   -15.972,1.00000,  1510,    36.300,
0.00000,   0.80000,   0.00000,   0.00000,1.00000,0,  100.0,    33.000,     0.000,
1,1.0000
  1609,'1 ',    33.000,   -51.236,    10.846,   -15.972,1.00000,  1510,    36.300,
0.00000,   0.80000,   0.00000,   0.00000,1.00000,0,  100.0,    33.000,     0.000,
1,1.0000
  1610,'1 ',    34.500,   -51.236,    11.339,   -16.698,1.00000,  1510,    37.950,
0.00000,   0.80000,   0.00000,   0.00000,1.00000,0,  100.0,    34.500,     0.000,
1,1.0000
  1611,'1 ',    33.000,     0.000,    10.846,   -15.972,1.00000,  1520,    36.300,
0.00000,   0.80000,   0.00000,   0.00000,1.00000,0,  100.0,    33.000,     0.000,
1,1.0000
  1612,'1 ',    33.000,   -32.756,    10.846,   -15.972,1.00000,  1520,    36.300,
0.00000,   0.80000,   0.00000,   0.00000,1.00000,0,  100.0,    33.000,     0.000,
1,1.0000
  1613,'1 ',    33.000,   -32.756,    10.846,   -15.972,1.00000,  1520,    36.300,
0.00000,   0.80000,   0.00000,   0.00000,1.00000,0,  100.0,    33.000,     0.000,
1,1.0000
  1614,'1 ',    33.000,   -32.756,    10.846,   -15.972,1.00000,  1520,    36.300,
0.00000,   0.80000,   0.00000,   0.00000,1.00000,0,  100.0,    33.000,     0.000,
1,1.0000
  1615,'1 ',    34.500,  -142.488,    11.339,   -16.698,1.00000,  1520,    37.950,
0.00000,   0.80000,   0.00000,   0.00000,1.00000,0,  100.0,    34.500,     0.000,
1,1.0000
0 / END OF GENERATOR DATA, BEGIN BRANCH DATA
  1000,   1001,'1 ',   0.00200,   0.10000,   0.00000,  500.00,  500.00,  500.00,
0.00000,  0.00000,  0.00000,  0.00000,1,  20.00,   1,1.0000
  1500,   1501,'1 ',   0.06060,   0.15150,   0.00660,   35.00,   35.00,   35.00,
0.00000,  0.00000,  0.00000,  0.00000,1, 999.00,   1,1.0000
  1500,   1502,'1 ',   0.06060,   0.15150,   0.00660,   35.00,   35.00,   35.00,
0.00000,  0.00000,  0.00000,  0.00000,1, 999.00,   1,1.0000
  1500,   1503,'1 ',   0.06060,   0.15150,   0.00660,   35.00,   35.00,   35.00,
0.00000,  0.00000,  0.00000,  0.00000,1, 999.00,   1,1.0000
  1500,   1504,'1 ',   0.06060,   0.15150,   0.00660,   35.00,   35.00,   35.00,
0.00000,  0.00000,  0.00000,  0.00000,1, 999.00,   1,1.0000
  1500,   1505,'1 ',   0.05800,   0.14490,   0.00690,   35.00,   35.00,   35.00,
0.00000,  0.00000,  0.00000,  0.00000,1, 999.00,   1,1.0000
  1510,   1511,'1 ',   0.06060,   0.15150,   0.00660,   35.00,   35.00,   35.00,
0.00000,  0.00000,  0.00000,  0.00000,1, 999.00,   1,1.0000
  1510,   1512,'1 ',   0.06060,   0.15150,   0.00660,   35.00,   35.00,   35.00,
0.00000,  0.00000,  0.00000,  0.00000,1, 999.00,   1,1.0000
  1510,   1513,'1 ',   0.06060,   0.15150,   0.00660,   35.00,   35.00,   35.00,
0.00000,  0.00000,  0.00000,  0.00000,1, 999.00,   1,1.0000
  1510,   1514,'1 ',   0.06060,   0.15150,   0.00660,   35.00,   35.00,   35.00,
0.00000,  0.00000,  0.00000,  0.00000,1, 999.00,   1,1.0000
  1510,   1515,'1 ',   0.05800,   0.14490,   0.00690,   35.00,   35.00,   35.00,
0.00000,  0.00000,  0.00000,  0.00000,1, 999.00,   1,1.0000
```

```
  1520,   1521,'1 ',   0.06060,   0.15150,   0.00660,   35.00,   35.00,   35.00,
0.00000,  0.00000,  0.00000,  0.00000,1, 999.00,   1,1.0000
  1520,   1522,'1 ',   0.06060,   0.15150,   0.00660,   35.00,   35.00,   35.00,
0.00000,  0.00000,  0.00000,  0.00000,1, 999.00,   1,1.0000
  1520,   1523,'1 ',   0.06060,   0.15150,   0.00660,   35.00,   35.00,   35.00,
0.00000,  0.00000,  0.00000,  0.00000,1, 999.00,   1,1.0000
  1520,   1524,'1 ',   0.06060,   0.15150,   0.00660,   35.00,   35.00,   35.00,
0.00000,  0.00000,  0.00000,  0.00000,1, 999.00,   1,1.0000
  1520,   1525,'1 ',   0.05800,   0.14490,   0.00690,   35.00,   35.00,   35.00,
0.00000,  0.00000,  0.00000,  0.00000,1, 999.00,   1,1.0000
  1600,   1601,'1 ',   0.00000,   0.00010,   0.00000,   35.00,    0.00,    0.00,
0.00000,  0.00000,  0.00000,  0.00000,1,   0.00,   1,1.0000
  1600,   1602,'1 ',   0.00000,   0.00010,   0.00000,   35.00,    0.00,    0.00,
0.00000,  0.00000,  0.00000,  0.00000,1,   0.00,   1,1.0000
  1600,   1603,'1 ',   0.00000,   0.00010,   0.00000,   35.00,    0.00,    0.00,
0.00000,  0.00000,  0.00000,  0.00000,1,   0.00,   1,1.0000
  1600,   1604,'1 ',   0.00000,   0.00010,   0.00000,   35.00,    0.00,    0.00,
0.00000,  0.00000,  0.00000,  0.00000,1,   0.00,   1,1.0000
  1600,   1605,'1 ',   0.00000,   0.00010,   0.00000,   35.00,    0.00,    0.00,
0.00000,  0.00000,  0.00000,  0.00000,1,   0.00,   1,1.0000
  1600,   1606,'1 ',   0.00000,   0.00010,   0.00000,   35.00,    0.00,    0.00,
0.00000,  0.00000,  0.00000,  0.00000,1,   0.00,   1,1.0000
  1600,   1607,'1 ',   0.00000,   0.00010,   0.00000,   35.00,    0.00,    0.00,
0.00000,  0.00000,  0.00000,  0.00000,1,   0.00,   1,1.0000
  1600,   1608,'1 ',   0.00000,   0.00010,   0.00000,   35.00,    0.00,    0.00,
0.00000,  0.00000,  0.00000,  0.00000,1,   0.00,   1,1.0000
  1600,   1609,'1 ',   0.00000,   0.00010,   0.00000,   35.00,    0.00,    0.00,
0.00000,  0.00000,  0.00000,  0.00000,1,   0.00,   1,1.0000
  1600,   1610,'1 ',   0.00000,   0.00010,   0.00000,   35.00,    0.00,    0.00,
0.00000,  0.00000,  0.00000,  0.00000,1,   0.00,   1,1.0000
  1600,   1611,'1 ',   0.00000,   0.00010,   0.00000,   35.00,    0.00,    0.00,
0.00000,  0.00000,  0.00000,  0.00000,1,   0.00,   1,1.0000
  1600,   1612,'1 ',   0.00000,   0.00010,   0.00000,   35.00,    0.00,    0.00,
0.00000,  0.00000,  0.00000,  0.00000,1,   0.00,   1,1.0000
  1600,   1613,'1 ',   0.00000,   0.00010,   0.00000,   35.00,    0.00,    0.00,
0.00000,  0.00000,  0.00000,  0.00000,1,   0.00,   1,1.0000
  1600,   1614,'1 ',   0.00000,   0.00010,   0.00000,   35.00,    0.00,    0.00,
0.00000,  0.00000,  0.00000,  0.00000,1,   0.00,   1,1.0000
  1600,   1615,'1 ',   0.00000,   0.00010,   0.00000,   35.00,    0.00,    0.00,
0.00000,  0.00000,  0.00000,  0.00000,1,   0.00,   1,1.0000
0 / END OF BRANCH DATA, BEGIN TRANSFORMER DATA
  1001,  1500,     0,'1 ',1,2,1,   0.00000,   0.00000,2,'            ',1,   1,1.0000
   0.00370,   0.14760,   140.00
1.05625,   0.000,   0.000,   140.00,   140.00,   140.00, 1,   1001, 1.15000, 0.85000,
1.02000, 0.98000,  17, 0, 0.00000, 0.00000
1.00000,   0.000
  1001,  1510,     0,'1 ',1,2,1,   0.00000,   0.00000,2,'            ',1,   1,1.0000
   0.00370,   0.14760,   140.00
1.05625,   0.000,   0.000,   140.00,   140.00,   140.00, 1,   1001, 1.15000, 0.85000,
1.02000, 0.98000,  17, 0, 0.00000, 0.00000
1.00000,   0.000
  1001,  1520,     0,'1 ',1,2,1,   0.00000,   0.00000,2,'            ',1,   1,1.0000
   0.00370,   0.14760,   140.00
1.05625,   0.000,   0.000,   140.00,   140.00,   140.00, 1,   1001, 1.15000, 0.85000,
1.02000, 0.98000,  17, 0, 0.00000, 0.00000
1.00000,   0.000
  1501,  1601,     0,'1 ',1,2,1,   0.00000,   0.00000,2,'            ',1,   1,1.0000
   0.00120,   0.06000,    35.20
1.00000,   0.000,   0.000,    35.20,    35.20,    35.20, 0,      0, 1.15000, 0.85000,
1.02000, 0.98000,  17, 0, 0.00000, 0.00000
1.00000,   0.000
  1502,  1602,     0,'1 ',1,2,1,   0.00000,   0.00000,2,'            ',1,   1,1.0000
   0.00120,   0.06000,    35.20
1.00000,   0.000,   0.000,    35.20,    35.20,    35.20, 0,      0, 1.15000, 0.85000,
1.02000, 0.98000,  17, 0, 0.00000, 0.00000
1.00000,   0.000
```

```
  1503,  1603,     0,'1 ',1,2,1,   0.00000,   0.00000,2,'            ',1,   1,1.0000
   0.00120,   0.06000,    35.20
1.00000,   0.000,   0.000,    35.20,    35.20,    35.20, 0,      0, 1.15000, 0.85000,
1.02000, 0.98000,  17, 0, 0.00000, 0.00000
1.00000,   0.000
  1504,  1604,     0,'1 ',1,2,1,   0.00000,   0.00000,2,'            ',1,   1,1.0000
   0.00120,   0.06000,    35.20
1.00000,   0.000,   0.000,    35.20,    35.20,    35.20, 0,      0, 1.15000, 0.85000,
1.02000, 0.98000,  17, 0, 0.00000, 0.00000
1.00000,   0.000
  1505,  1605,     0,'1 ',1,2,1,   0.00000,   0.00000,2,'            ',1,   1,1.0000
   0.00120,   0.06000,    36.80
1.00000,   0.000,   0.000,    36.80,    36.80,    36.80, 0,      0, 1.15000, 0.85000,
1.02000, 0.98000,  17, 0, 0.00000, 0.00000
1.00000,   0.000
  1511,  1606,     0,'1 ',1,2,1,   0.00000,   0.00000,2,'            ',1,   1,1.0000
   0.00120,   0.06000,    35.20
1.00000,   0.000,   0.000,    35.20,    35.20,    35.20, 0,      0, 1.15000, 0.85000,
1.02000, 0.98000,  17, 0, 0.00000, 0.00000
1.00000,   0.000
  1512,  1607,     0,'1 ',1,2,1,   0.00000,   0.00000,2,'            ',1,   1,1.0000
   0.00120,   0.06000,    35.20
1.00000,   0.000,   0.000,    35.20,    35.20,    35.20, 0,      0, 1.15000, 0.85000,
1.02000, 0.98000,  17, 0, 0.00000, 0.00000
1.00000,   0.000
  1513,  1608,     0,'1 ',1,2,1,   0.00000,   0.00000,2,'            ',1,   1,1.0000
   0.00120,   0.06000,    35.20
1.00000,   0.000,   0.000,    35.20,    35.20,    35.20, 0,      0, 1.15000, 0.85000,
1.02000, 0.98000,  17, 0, 0.00000, 0.00000
1.00000,   0.000
  1514,  1609,     0,'1 ',1,2,1,   0.00000,   0.00000,2,'            ',1,   1,1.0000
   0.00120,   0.06000,    35.20
1.00000,   0.000,   0.000,    35.20,    35.20,    35.20, 0,      0, 1.15000, 0.85000,
1.02000, 0.98000,  17, 0, 0.00000, 0.00000
1.00000,   0.000
  1515,  1610,     0,'1 ',1,2,1,   0.00000,   0.00000,2,'            ',1,   1,1.0000
   0.00120,   0.06000,    36.80
1.00000,   0.000,   0.000,    36.80,    36.80,    36.80, 0,      0, 1.15000, 0.85000,
1.02000, 0.98000,  17, 0, 0.00000, 0.00000
1.00000,   0.000
  1521,  1611,     0,'1 ',1,2,1,   0.00000,   0.00000,2,'            ',1,   1,1.0000
   0.00120,   0.06000,    35.20
1.00000,   0.000,   0.000,    35.20,    35.20,    35.20, 0,      0, 1.15000, 0.85000,
1.02000, 0.98000,  17, 0, 0.00000, 0.00000
1.00000,   0.000
  1522,  1612,     0,'1 ',1,2,1,   0.00000,   0.00000,2,'            ',1,   1,1.0000
   0.00120,   0.06000,    35.20
1.00000,   0.000,   0.000,    35.20,    35.20,    35.20, 0,      0, 1.15000, 0.85000,
1.02000, 0.98000,  17, 0, 0.00000, 0.00000
1.00000,   0.000
  1523,  1613,     0,'1 ',1,2,1,   0.00000,   0.00000,2,'            ',1,   1,1.0000
   0.00120,   0.06000,    35.20
1.00000,   0.000,   0.000,    35.20,    35.20,    35.20, 0,      0, 1.15000, 0.85000,
1.02000, 0.98000,  17, 0, 0.00000, 0.00000
1.00000,   0.000
  1524,  1614,     0,'1 ',1,2,1,   0.00000,   0.00000,2,'            ',1,   1,1.0000
   0.00120,   0.06000,    35.20
1.00000,   0.000,   0.000,    35.20,    35.20,    35.20, 0,      0, 1.15000, 0.85000,
1.02000, 0.98000,  17, 0, 0.00000, 0.00000
1.00000,   0.000
  1525,  1615,     0,'1 ',1,2,1,   0.00000,   0.00000,2,'            ',1,   1,1.0000
   0.00120,   0.06000,    36.80
1.00000,   0.000,   0.000,    36.80,    36.80,    36.80, 0,      0, 1.15000, 0.85000,
1.02000, 0.98000,  17, 0, 0.00000, 0.00000
1.00000,   0.000
0 / END OF TRANSFORMER DATA, BEGIN AREA DATA
```

```
0 / END OF AREA DATA, BEGIN TWO-TERMINAL DC DATA
0 / END OF TWO-TERMINAL DC DATA, BEGIN VSC DC LINE DATA
0 / END OF VSC DC LINE DATA, BEGIN SWITCHED SHUNT DATA
0 / END OF SWITCHED SHUNT DATA, BEGIN IMPEDANCE CORRECTION DATA
0 / END OF IMPEDANCE CORRECTION DATA, BEGIN MULTI-TERMINAL DC DATA
0 / END OF MULTI-TERMINAL DC DATA, BEGIN MULTI-SECTION LINE DATA
0 / END OF MULTI-SECTION LINE DATA, BEGIN ZONE DATA
0 / END OF ZONE DATA, BEGIN INTER-AREA TRANSFER DATA
0 / END OF INTER-AREA TRANSFER DATA, BEGIN OWNER DATA
0 / END OF OWNER DATA, BEGIN FACTS DEVICE DATA
0 / END OF FACTS DEVICE DATA
```

DYRE FILE :

```
1000 'GENSAL'  1
       7.4100   0.0700   0.0700   3.1000   0.0000   1.0270
       0.5590   0.3400   0.1800   0.1500   0.0860   0.2930   /
1600    'USRMDL'  1 'FUWI' 1 0 0 68 17 29
0.8     0.87    0.0     0.02    0.02    2.0     99      -99     1.0     0.05
3.0     0.60    1.01    0.09    0.296   -0.436  1.11    1.      0.45    -0.45
5.0     0.05    0.95    1.05    0.001   -0.07   0.07    0.0     0.05    1
61.000  65.00   1.00    101.0   106.0   1.00    3.400   1.520   5.19    2
1       12.0    4.0     29.0    0.0     0.0     1.225   35.00   90.0    1800.
1500.   1.67    0.3     150.    25.     3.00    30.0    0.      29.     -9.
9.      0.91      4.631300 -0.0081631  12.000000  -0.194950   0.905626   0.122774/
0 'USRMDL' 0 'LOVOLT' 8 0 2 3 0 5 1600     1  0.00    0.15    0.08    /
0 'USRMDL' 0 'LOVOLT' 8 0 2 3 0 5 1600     1  0.01    0.175   0.08    /
0 'USRMDL' 0 'LOVOLT' 8 0 2 3 0 5 1600     1  0.03    0.25    0.08    /
0 'USRMDL' 0 'LOVOLT' 8 0 2 3 0 5 1600     1  0.10    0.5     0.08    /
0 'USRMDL' 0 'LOVOLT' 8 0 2 3 0 5 1600     1  0.14    0.625   0.08    /
0 'USRMDL' 0 'LOVOLT' 8 0 2 3 0 5 1600     1  0.16    0.7     0.08    /
0 'USRMDL' 0 'LOVOLT' 8 0 2 3 0 5 1600     1  0.25    1.0     0.08    /
0 'USRMDL' 0 'LOVOLT' 8 0 2 3 0 5 1600     1  0.75    2.0     0.08    /
0 'USRMDL' 0 'LOVOLT' 8 0 2 3 0 5 1600     1  0.85    30.     0.08    /
0 'USRMDL' 0 'HIVOLT' 8 0 2 3 0 5 1600     1  1.15    300.    0.08    /
0 'USRMDL' 0 'HIVOLT' 8 0 2 3 0 5 1600     1  1.20    30.0    0.08    /
0 'USRMDL' 0 'HIVOLT' 8 0 2 3 0 5 1600     1  1.25    2.0     0.08    /
0 'USRMDL' 0 'HIVOLT' 8 0 2 3 0 5 1600     1  1.40    0.10    0.08    /
0 'USRMDL' 0 'HIVOLT' 8 0 2 3 0 5 1600     1  1.80    0.03    0.08    /
0 'USRMDL' 0 'LOFREQ' 8 0 2 3 0 5 1600     1  55.5    0.35    0.08    /
0 'USRMDL' 0 'LOFREQ' 8 0 2 3 0 5 1600     1  56.5     2.     0.08    /
0 'USRMDL' 0 'LOFREQ' 8 0 2 3 0 5 1600     1  57.0    10.     0.08    /
0 'USRMDL' 0 'LOFREQ' 8 0 2 3 0 5 1600     1  57.5    90.     0.08    /
0 'USRMDL' 0 'LOFREQ' 8 0 2 3 0 5 1600     1  58.5    660.    0.08    /
0 'USRMDL' 0 'HIFREQ' 8 0 2 3 0 5 1600     1  61.5    660.    0.08    /
[0]    'USRMDL' 0 'HIFREQ' 8 0 2 3 0 5 1600    1  61.7    90.    0.08    /
```

APPENDIX B

DFIG MEVA Benchmark data

Wind generator number	20 machines of 1.67MVA
Transformer unit ratio; power	0.69 kV/34.5 kV; 35 MVA
Transformer unit impedance	5.5%
Transformer unit connection	YnD
Feeder impedance	R=0.0793Ω; XL=0.238Ω; YC=33.5μS
Substation transformer ratio; power	34.5 kV / 230 kV; 50 MVA
Substation transformer impedance	10%
Substation transformer connection	YnYn
Grid short circuit impedance	Rcc=14.11Ω, Xcc=70.53Ω

APPENDIX C

FC MEVA Benchmark data

Wind generators number	7,3,10 machines of 1.67MVA
Transformer unit ratio; power	0.69 kV/34.5 kV; 31, 9 and 30 MVA
Transformer unit impedance	6.0%
Transformer unit connection	YnD
Feeder impedance	R=0.0793Ω; XL=0.238Ω; YC=33.5μS
Substation transformer ratio; power	34.5 kV / 230 kV; 50 MVA
Substation transformer impedance	10%
Substation transformer connection	YnYn
Grid short circuit impedance	Rcc=100.76Ω, Xcc=251.9Ω